Durham E-Theses

Characterisation of the MacA/MacB/TolC tripartite pump that confers resistance to macrolides in E. coli

Lin, Hong-Ting

How to cite:

Lin, Hong-Ting (2008) *Characterisation of the MacA/MacB/TolC tripartite pump that confers resistance to macrolides in E. coli*, Durham theses, Durham University. Available at Durham E-Theses Online: http://etheses.dur.ac.uk/2273/

Use policy

Characterisation of the MacA/MacB/TolC tripartite pump that confers resistance to macrolides in *E. coli*

By

Hong-Ting Lin M.Sc.

A thesis submitted for the degree of Doctor of Philosophy

In

The School of Biological and Biomedical Sciences

Centre for Infectious Diseases
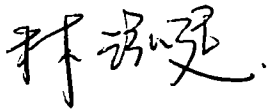
University of Durham

November 2008

Declaration of Originality

I, Hong-Ting Lin, declare that this thesis is my own work except where stated by citation or statement and has not been submitted for other qualifications at any other university or other institute of education.

The copyright of this thesis rests with the author. No quotation or information derived from it may be published in any format without the prior written consent of the author. All consented information derived from this thesis must be acknowledged.

Hong Ting Lin

November 2008

Acknowledgements

My deepest gratitude goes to my supervisor Prof. Adrian R. Walmsley for providing me with the opportunity to study for this PhD. Not only his dedication but all the training and resources he offered have made this thesis complete and it has been a pleasure to work under his supervision.

Many thanks to all my Durham colleagues: Dr. Gary Sharples, Paul Denny, Paul Yeo, DiJun Du, Ines Borges-Walmsley, Kennith McKeegan, Daling Chen, Fiona and Steve for their invaluable scientific directions; together with Li Zhang, Helen Frankish, Teresa Massam-Wu, Bing Zhang, Simon Padbury, Diane Hart, JungWoo Yang, Thamarai Janganan and Nicky Pan for their scientific and personal advice. Particular thanks go to the members of the Biochemistry department in Cambridge University; Dr. Ben Luisi, Vass, Zbigniew and Xue-Yuan; Nelson of the Chemistry department, and Dr. Hendrik van Veen and Saroj of the Pharmocology department in Cambridge for their sound judgements and help on protein crystallization.

Finally, I am indebted to my parents, family, friends and my beloved, Chen-Ju for their perpetual patience, encouragement and support. My little boys, Jing-Huan and Sing-Rung always bring me priceless joy.

Abstract

Gram-negative bacteria possess tripartite pumps, composed of a membrane fusion protein (MFP), an inner membrane protein (IMP) and an outer membrane protein (OMP), to transport drugs across the inner and outer membranes. The plasmid encoding MacA, MacB and TolC confers resistance to the macrolide erythromycin in the host *E. coli* cell Kam3, indicating the three proteins are assembled and actively functional. MFPs are believed to have an important role in the stabilizing the pump complex; intriguingly, we found that the MFP MacA not only interacts directly with the IMP MacB and the OMP TolC, but regulates the function of MacB, apparently increasing its affinity for both ATP and erythromycin. As MacB hydrolyzes ATP there is a burst in phosphate production that is symptomatic of the reaction being rate-limited by product release; but the burst disappeared in the presence of MacA. Since MacA caused only a marginal increase in the k_{cat}, but a significant decrease in the K_m, for the steady-state ATPase activity, this suggests that the disappearance of the phosphate burst is due to a decrease in the rate of hydrolysis, rather than an increase in the rate of product release. This kinetic behaviour indicates that MacA promotes and stabilizes the ATP-binding form of the transporter. MacA regulates the activity of MacB via its β-strand domain since *S. aureus* MacA, which lacks the coiled coil structure that is present in *E. coli* MacA and believed to be involved in the interaction with TolC, was able to abolish the Pi burst catalysed by MacB, in direct analogy with the effect of *E. coli* MacA on MacB. Analytical ultracentrifugation, mass spectrometry and atomic force microscopy indicated that MacB forms dimers, in analogy to ABC-transporters that require a pair of NBDs to bind ATP. Our data suggests a direct role for MacA in facilitating the delivery of drugs by MacB to TolC: by enhancing the binding of drugs to MacB and stabilizing the reorientation of MacB to the outward-facing conformation.

Abstract

Gram-negative bacteria possess tripartite pumps, composed of a membrane fusion protein (MFP), an inner membrane protein (IMP) and an outer membrane protein (OMP), to transport drugs across the inner and outer membranes. The plasmid encoding MacA, MacB and TolC confers resistance to the macrolide erythromycin in the host *E. coli* cell Kam3, indicating the three proteins are assembled and actively functional. MFPs are believed to have an important role in the stabilizing the pump complex; intriguingly, we found that the MFP MacA not only interacts directly with the IMP MacB and the OMP TolC, but regulates the function of MacB, apparently increasing its affinity for both ATP and erythromycin. As MacB hydrolyzes ATP there is a burst in phosphate production that is symptomatic of the reaction being rate-limited by product release; but the burst disappeared in the presence of MacA. Since MacA caused only a marginal increase in the k_{cat}, but a significant decrease in the K_m, for the steady-state ATPase activity, this suggests that the disappearance of the phosphate burst is due to a decrease in the rate of hydrolysis, rather than an increase in the rate of product release. This kinetic behaviour indicates that MacA promotes and stabilizes the ATP-binding form of the transporter. MacA regulates the activity of MacB via its β-strand domain since *S. aureus* MacA, which lacks the coiled coil structure that is present in *E. coli* MacA and believed to be involved in the interaction with TolC, was able to abolish the Pi burst catalysed by MacB, in direct analogy with the effect of *E. coli* MacA on MacB. Analytical ultracentrifugation, mass spectrometry and atomic force microscopy indicated that MacB forms dimers, in analogy to ABC-transporters that require a pair of NBDs to bind ATP. Our data suggests a direct role for MacA in facilitating the delivery of drugs by MacB to TolC: by enhancing the binding of drugs to MacB and stabilizing the reorientation of MacB to the outward-facing conformation.

Abbreviations

ABC	ATP-binding cassette
ADP	Adenosine diphosphate
AFM	Atomic force microscope
AMP-PNP	β, γ-imidoadenosine 5'-triphosphate tetralithium salt
AMS	4-acetoamide-4'-maleimidylstilbene-2, 2'-disulfonic acid
AUC	Analytical ultracentrifugation
ATP	Adenosine triphosphate
CCCP	Cyanide-M-chlorophenyl hydrazone
CD	Circular dichroism
DDM	n-dodecyl-β-D-maltopyranoside
DLS	Dynamic light scattering
DME	Drug-metabolite efflux
DNA	Deoxyribonucleic acid
EM	Electron microscope
ES	Electro-spray
FTIR	Fourier transform infrared spectroscopy
k_{cat}	Catalytic constant
K_m	Michaelis constant
IPTG	Isopropyl-ß-D-thiogalactopyranoside
IMP	Inner membrane protein
MALDI	Matrix-assisted laser desorption/ionization
MATE	Multi and toxic compound extrusion
MDR	Multidrug resistance
MESG	2-amino-6-mercapto-7-methylpurine riboside

MFP	Membrane fusion protein
MFS	Major facilitator superfamily
MIANS	2-(4'-maleimidoanilino) naphthalene-6-sulfonic acid
MOPS	4-Morpholinepropanesulfonic acid
MS	Mass spectrometry
NBD	Nucleotide binding domain
NEM	N-ethyl maleimide
NRMSD	Normalized root mean squared deviation
OMP	Outer membrane protein
PCR	Polymerase chain reaction
P-gp	P-glycoprotein
Pi	Inorganic phosphate
RE	Restriction enzyme
RND	Resistance-nodulation-cell division
SBP	Substrate binding protein
SD	Shine Dalgarno
SEC	Size exclusion chromatography
SMR	Small multidrug resistance family
TM	Transmembrane
TMD	Transmembrane domain
TPP^+	Tetraphenylphosphonium
V_{max}	Maximun Velocity

Contents

Figures and Tables

Chapter one: Introduction

Membrane transporters are involved in the translocation of drugs and antibiotics, uptake of nutrients, protein secretion, toxin production, photosynthesis and many other vital functions in all organisms (Henderson, 1998). Such membrane proteins are notoriously difficult to study due to their hydrophobicity and low expression levels. These difficulties can explain that whilst membranes proteins account for 30% of all cells proteins, only around 160 membrane proteins structures have been solved, whereas the structures of over 8,000 soluble proteins have been solved (Michel, 2006; White, 2008) .

Multidrug transporters, as implied by the name, confer resistance to multiple drugs by pumping them out of cells, decreasing the intracellular concentration of the drug to subtoxic levels (Borges-Walmsley, 2003). It therefore not only leads to prolonged and more complicated treatments but also an increase in the cost of diagnoses and cures. Recent progress in sequencing of microbial genomes and protein crystallography provide opportunities to identify novel antibacterial targets for the new development of drugs. To prevent and control infectious diseases caused by the multidrug-resistant bacteria, more research into multidrug transporters, which are recognized as a major contributor to multidrug resistance, are urgently required.

The MacB protein, an ATP binding casstte (ABC) macrolide antibiotic resistance transporter from *E. coli* (Kobayashi *et al.*, 2001), was studied in order to determine its biochemical and structural properties. Our interest was in determining the mechanism of regulation of the ATPase activity of MacB by MacA and the function of the tripartite complex pump: MacA/MacB/TolC. The ABC transporter MacB was easier to investigate than other pumps, such as those belonging to the RND family in terms of its interaction with MacA due its ATPase characteristic. Importantly, an understanding of the MacA/MacB/TolC system may give us more understanding of type I secretion systems in bacteria, such as the HlyB/HlyD/TolC system, where HlyB is an ABC transporter (Thanabalu *et al.*, 1998).

In the Type I secretion system, a continuous channel is formed by the assembly of multiple proteins into a complex that spans the inner, outer membranes and periplasmic region. The mechanisms of the type II and type V secretion systems are

characterized by a two-step process that involves periplasmic intermediates. The type III secretion system was mediated by approximately 20 proteins and it is sec-independent. The type IV secretion system is involved in genetic exchange, transfer of DNA (Gerlach and Hensel, 2007).

1.1 Antibiotics

Antibiotics, which literally means "against life", were originally produced by bacteria or fungi. They are used to attack the specific agent causing the infection, hence helping the infected host to eliminate the infection. However, extensive use of antibiotics has raised a serious public health problem due to multidrug resistance, in which bacteria become resistant to multi-antibiotics.A common clinical problem in patients with infectious diseases as well as in patients with cancer, multidrug resistance, a phenomenon which enable a disease-causing prokaryotic or eukaryotic microorganisms to resist distinct drugs of a wide variety of structure and function targeted at eliminating the organism. The efflux of drugs by the multidrug transporter p-glycoprotein is one of the principal ways for multidrug resistance.

To combat diseases caused by multidrug resistant bacteria, we need to learn more about the physiology of pathogens to aid in designing new drugs and extend the life of antibiotics (Alanis *et al.*, 2005).

1.1.1 Target of antibiotics

Antibiotics are usually classified on the basis of their chemical structures and modes of action. The main classes of antibiotics inhibit four classical targets: (a) cell wall biosynthesis, (b) protein biosynthesis, (c) DNA and RNA biosynthesis, and (d) other targets, such as cytoplasmic membrane biosynthesis.

Inhibition of bacterial cell wall biosynthesis

β-lactam antibiotics, such as penicillin, penicillin G and amoxicillin, can inhibit the formation of peptidoglycan crosslinkings in the bacterial cell wall. The β-lactam (Figure 1.1) moiety of penicillin binds to the transpeptidase that links the peptidoglycan molecules in bacteria, weakening the cell wall of the bacteria, that can lead to cell cytolysis (Spratt and Cromie, 1988).
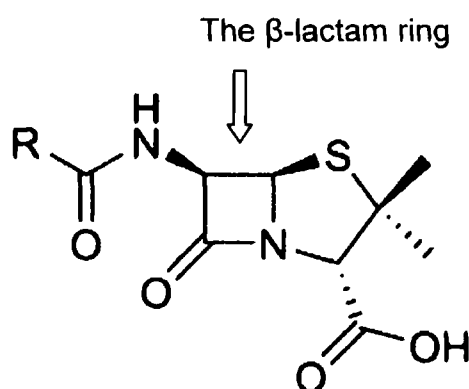
The β-lactam ring

Figure 1.1   **Penicillin core structure;** with the β-lactam ring indicated.

Inhibition of protein biosynthesis

There are a large number of steps involved in protein synthesis, and many kinds of antibiotics are used to bind to bacteria ribosome and block protein synthesis. This action is mainly bacteriostatic, but can also be bactericidal at higher concentrations. Bacteriostatic antiobiotics interfere with bacterial growth, while bactericidal antiobiotics kill bacteria. These two actions are accomplished by different mechanisms. Bactericidal actions can disrupt bacterial cell wall or plasma membrane, and bacteriostatic actions can interfere with protein synthesis, nucleic acid synthesis, or other vital metabolic processes, which may become bactericidal when the bacteria

deplete some essential materials, such as ATP, a main energy source for the majority of cellular functions.

For example, aminoglycosides and tetracyclines can interact with the 30S subunit of the bacterial ribosome; macrolides (Figure 1.2) and chloramphenicol can bind to the 50S subunit of the bacterial ribosome, therefore inhibiting translocation of tRNA (Brodersen *et al.*, 2000; Katz and Ashley, 2005).
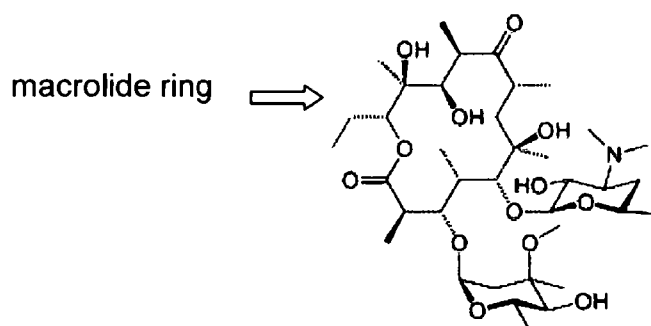
macrolide ring

Figure 1.2   **Core structure of erythromycin**. A first generation macrolide, with the macrolide ring indicated upper left.

Inhibition of DNA and RNA biosynthesis

DNA replication is an essential process for all organisms. On the premise that eukaryotic cells do not contain DNA gyrase or topoisomerase IV, quinolone and fluoroquinolones antibiotics such as norfloxacin are used to inhibit the DNA gyrase or the topoisomerase IV enzyme to stop DNA replication and transcription, therefore actively killing bacteria (Li, 2005). Rifampicin inhibits RNA polymerase by binding to the β subunit of RNA polymerase, thus preventing transcription of mRNA and its subsequent translation into proteins (Campbell *et al.*, 2001).

Other targets

The current generation sulfa drug sulfamethoxazole is used in combination with trimethoprim and each drug inhibits distinct steps in folic acid metabolism (Huovinen, 2001).

Antimicrobial peptides, secreted from both gram-positive and gram-negative bacterial, have been classified within the bacteriocins. Most antimicrobial peptides

such as nisin can attack cytoplasmic membranes, permeabilize target membranes, eventually leading to cell death (Hancock and Chapple, 1999).

1.1.2 Antibiotic resistance

Antimicrobial resistance is a growing problem in the world. For instance, the first case of antimicrobial resistance occurred in the late 1930s and 1940s, soon after the introduction of the first antibiotic classes, sulfonamides and penicillins (Alekshun and Levy, 2007). Common bacteria, such as strains of *S. aureus*, became resistant to these classes of antibiotics. In 2002, a report indicated that strains of Group A *Streptococcus* are becoming resistant to macrolides and spreading outside the hospital, causing community-acquired infections (Martin *et al.*, 2002).

The major mechanisms of antibiotic resistance are as follows:

Avoiding accumulation of antibiotics

The prevention of antibiotic action is by either increasing the efflux or decreasing the influx of antibiotics across biological membranes. Cells having mutant TolC, R367H or R390C, show hypersensitivity to drugs, which is presumably caused by having TolC tunnel open, which allow more antibiotics entered the cell than were expelled (Augustus *et al.*, 2004).

Drugs are pumped out by multidrug transporters faster than they can diffuse across membranes, so the drug level inside can be kept low, at levels that are much less effective. Multidrug transporters present in both gram-positive and gram-negative bacteria confer resistance to a wide variety of drugs and this is now recognized as a major mechanism for multidrug resistance in bacteria (Alekshun and Levy, 2007).

Destruction of antibiotics by either modification or hydrolysis

Enzymatic inactivation of antibiotics is a major mechanism of resistance in pathogenic bacteria to natural antibiotics such as β-lactams, aminoglycosides and chloramphenicol (Walsh, 2000). The classic case is the hydrolysis of the four-

membered β-lactam ring in penicillins by β-lactamases from resistant bacteria, resulting in the inactivation of the antibiotics.

Modification of the drug target

The antibiotic mechanism of target alternation is by modification of the normal target so that it does not bind the antibiotics. As previously stated, erythromycin can bind to the 50S subunit of the bacterial ribosome to inhibit the translocation of tRNA. The methyl transferase enzyme Erm can methylate a specific adenine residue of the 23S RNA component of the ribosome without the interference of protein biosynthesis and lower the affinity of the macrolides for the RNA (Walsh, 2000).

1.2 Multidrug transporters

ABC transporter   **Secondary active transporter**
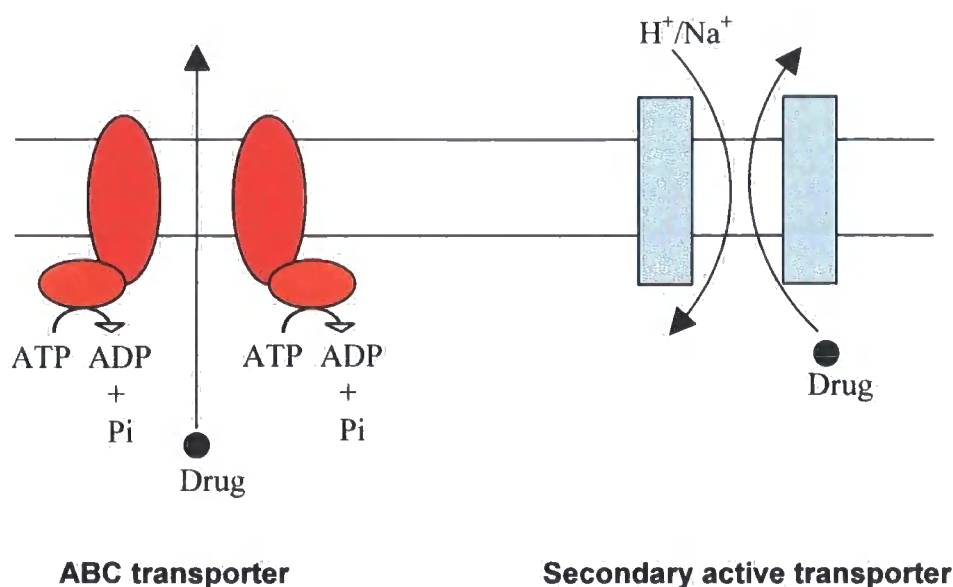
Figure 1.3   ABC and secondary active transporters

The efflux of cytotoxic compounds out of cells by transmembrane proteins is one of the most important mechanisms for drug resistance in prokaryotes and eukaryotes (Borges-Walmsley *et al*, 2003). Most multidrug transporters have been divided into two groups by their energy requirements: those membrane transporters belonging to ATP binding Cassette (ABC) transporters which can couple transport to the hydrolysis of ATP; and secondary active transporter, which can use the potential energy of the electrochemical gradients of H^+ or Na^+ across the membrane (Figure 1.3).

1.2.1 Powerful multidrug transporters: What are they?

Secondary active transporters have been categorized into several families by their sequence similarities: these include the Resistance-Nodulation-cell Division (RND) family, the Major Facilitator (MF) superfamily, the Small Multidrug Resistance (SMR) family, the Multi and Toxic Compound Extrusion (MATE) family and the Drug-Metabolite Efflux (DME) family; while the DME family has only recently been described and are not well characterized, they are believed to have some similarity to the SMR family (Jack *et al.*, 2001).

1.2.1 Secondary active transporters

MF family

The MF transporters form the largest family of the secondary active transporters (Figure 1.4) (Saidijam *et al,* 2006), and these MF family proteins transport drugs, ions, sugars sugar-phosphates, nucleosides, amino acids, and peptides.

In 1998, transport proteins from eukarya, archaea and bacteria were categorized on the basis of their molecular phylogeny (Saijijam *et al.,* 2006) and transport proteins for each organism are classified on the basis of their energy coupling mechanism, protein phylogenic family and substrate specificity. Drug efflux proteins fall into five classes, where MF and ABC superfamily are the the largest families among them.

MF transporters are typically 400 to 600 amino acids long and arranged into 12 trans-membrane α-helices (Figure 1.5), with a large cytoplasmic loop between helices six and seven (Saier *et al.,* 1999). A smaller number of these transporters have 14 trans-membrane α-helices, such as the *S. aureus* tetracycline and divalent cation transporters TetA(K) (Ginn *et al.,* 1997) and QacA, respectively (Paulsen *et al.,* 1996).
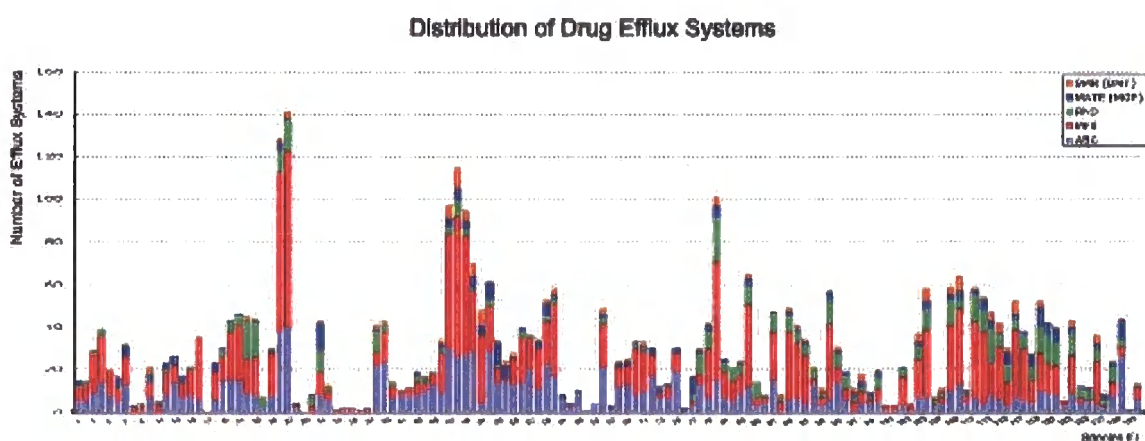
Figure 1.4 **Distribution of putative drug efflux systems in different microorganisms.** The colors signify as follows from the bottom: light blue, ABC; red, MFS; green, RND; dark blue, MATE; and orange, SMR. See ref. Saidijam *et al.,* 2006 for more formation.

MdfA

MdfA, a 410 residue protein arranged into 12 transmembrane helices (Figure 1.5) (Adler *et al.* 2004; Adler and Bibi, 2002), confers resistance to a remarkably diverse group of cytotoxic compounds, including cationic, zwitterionic and uncharged substrates (Edgar and Bibi, 1997; Nishino and Yamaguchi, 2001; Lewinson *et al.*, 2006).
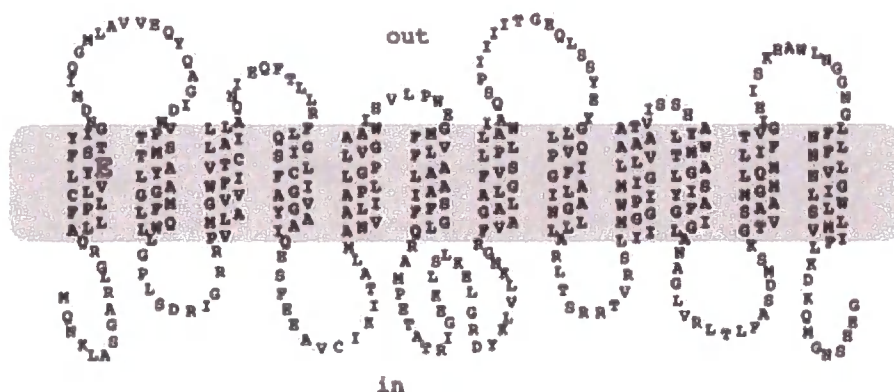
Figure 1.5   Secondary structure model of MdfA (Adler *et al.*, 2004)

Early studies revealed that the charged residue located in the transmemembrane domain, Glu^{26} in helices 1, is important in substrate recognition (Edgar and Bibi, 1999). Replacement of Glu^{26} with the positively charged residue lysine eliminated the resistance against the positively charged drug ethidium bromide, but retained the resistance to chloramphenicol. Interestingly, when Glu^{26} was replaced by the negatively charged residue aspartate, chloramphenicol recognition and transport greatly decreased; however, resistance against lipophilic cations remained. In addition, mutagenesis studies revealed many second site mutations that restored the function of inactive E26 mutants in chloramphenicol. Several of them were differentially affected by different substrates, suggesting different drugs may interact with different regions of the pocket (Adler and Bibi, 2004). A similar observation was made using direct binding studies, which showed positively charged drugs competed with the cationic compound tetraphenylphosphonium (TPP^{+}) in binding to MdfA, whereas some zwitterionic drugs did not. Besides, the neutral drug chloramphenicol stimulated the binding of TPP^{+} by increasing its affinity for MdfA, implying that the two drugs could simultaneously bind to two distinct sites (Lewinson and Bibi, 2001).

EmrD

The MF family transporter EmrD structure was reported and the transport mechanism was proposed in 2006 (Yin *et al.*, 2006). EmrD was first identified as an efflux pump transporting uncouplers of oxidative phosphorylation such as cyanide-M-chlorophenyl hydrazone (CCCP) (Naroditskaya *et al.*, 1993), but subsequently reported to be able to export a broad spectrum of hydrophobic compounds (Nishino and Yamaguchi, 2001). The topology of EmrD is shown in figure 1.6a; EmrD has 12 transmembrane α helices and its N- and C- termini are located in the cytoplasm. As illustrated in figure 1.6b H3, H6, H9 and H12 face away from the interior and are not involved in the pore formation; on other hand, the four central helices H1, H4, H7, H10 and the four lateral helices H2, H5, H8, H11 surround a central cavity, which consists mostly of hydrophobic residues, allowing transportation of lipophilic compounds. Among them are the two pairs of stacked aromatic groups, Tyr^{52}/Tyr^{56} and Trp^{300}/Phe^{249}, which could be involved in substrate binding. In Bmr, a close homolog of EmrD, two phenylalanines have been implicated in substrate recognition. Yin *et al* in 2006 proposed that two long helical regions, (H4/L4-5/H5 and H10/L10-11/ H11), and H1, located on the cytoplasmic side, could serve as a selectivity filter. A potential mechanism for drug transport is that CCCP can enter the central cavity, either through the membrane leaflet or cytoplasm, and is recognized by the long helical filter region, and is subsequently bound by hydrophobic residues in the cavity (Figure 1.6c).

(a)
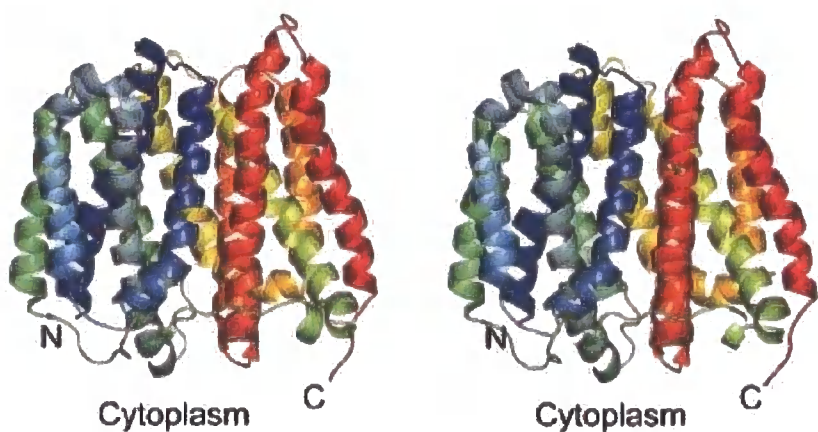
(b)
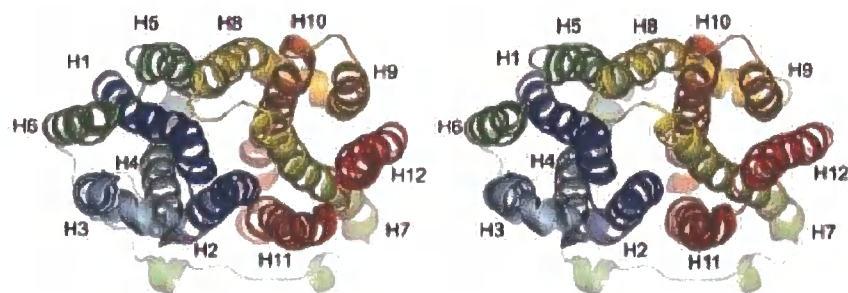
(c)
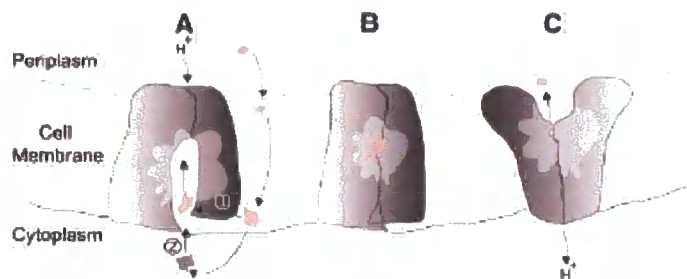
Figure 1.6   **The structure of EmrD by ribbon presentation**. (a) Side view of the
EmrD. (b) Top view of the EmrD. (c) The proposed mechanism of the
EmrD transporter (Yin *et al.*, 2006).

SMR family

The smallest multidrug transporters belong to the SMR family, which are around 100 amino acids long. The SMR family transporters extrude various drugs in exchange for protons, conferring bacteria resistance to these compounds (Yerushalmi et al., 1995; Schuldiner et al., 2001).

EmrE
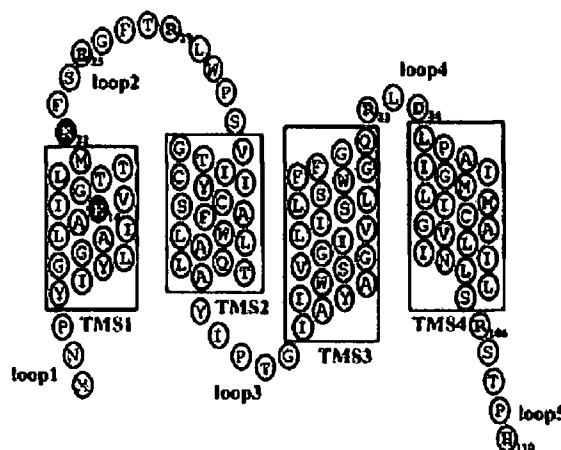
Figure 1.7 **Secondary structure model of EmrE-His.** Putative transmembrane domains are shown in boxes connected by hydrophilic segements. Charged residues are highlighted and the ones conserved in EmrE homologs are shown with black circles (Yerushalmi and Schuldiner, 2000).

The best studied SMR transporter EmrE from *E. coli*, which confers resistance to ethidium bromide and methyl viologen, is putatively arranged into four transmembrane α helices (Figure 1.7) (Yerushalmi et al., 1995; Yerushalmi and Schuldiner, 2000; Ninio et al., 2004). Cysteine scanning mutagenesis and FTIR experiments indicated that EmrE is composed of a tightly packed bundle of α-helices without any continuous aqueous domains, implying substrates are transported through a hydrophobic pathway in the protein (Mordoch et al., 1999; Arkin et al., 1996). Further study on the identity of amino acid residues in the substrate binding and transportation pathway have been provided by site-directed mutagenesis and biochemical experiments. Seven of the eight charged amino acids located in putative loops of EmrE can be replaced with either cysteine or other amino acids bearing the same charge without significant change on transport activity. The other charged amino

acid Glu[14], a carboxylic residue conserved in all EmrE homologs, located in the first putative transmembrane domain is essential for substrate binding and efflux of the drug TPP[+] (Yerushalmi and Schuldiner, 2000). In addition, further data exploring the drug binding domain indicated that some aromatic residues from transmembrane domain 2 and 3 form part of the binding site (Sharoni et al., 2005).

Although the oligomeric state in vivo is still under dispute, the minimal functional unit for substrate binding is a dimer (Butler et al., 2004; Ubarretxena-Belandia et al., 2003). The EmrE-detergent complex was extracted from membranes in a form that retains the ability to bind the drug TPP[+] in a 3 to 1 molar ratio (Muth et al., 2000), which may be due to some inactive monomer. A projection structure of EmrE at 7.0 Å resolution 2D crystals showed the repetitive unit in the crystal comprised of eight α-helices arranged in an asymmetric manner, indicating the minimal functional unit for EmrE was a dimer (Figure 1.8a) (Tate et al., 2001). When TPP[+] binds to EmrE in the 2D crystals, a small conformational change occurs that is shown to be mainly due to the movement of a single α-helix (Tate et al., 2003). The recent X-ray EmrE-TPP[+] strucuture revealed another characteristic in the EmrE structure, dual topology (Chen et al., 2007). In this structure, the SeMet sites are related by a pseudo-twofold rotational axis running along the dimmer interface parallel with the membrane plane. Conserved Glu[14] point toward the binding chamber and appear well placed to form ionic contacts with the positively charged TPP molecular (Figure 1.8b). As illustrated in 1.8c, it shows the Se sites in the first transmembrane helices (residues 21 and 21*) are located pseudo-symmetrically on opposite sides of the bilayer. This feature indicates that the X-ray structure of the EmrE-TPP[+] is an antiparallel dimer.

This EmrE structure is consistent with some biochemical data; for example, the membrane-embedded glutamate (E[14]) is involved in substrate binding and translocation; the conserved Trp[63] in the third transmembrane helix has been identified as an essential residue that is involved with binding of the substrate and protein activity (Elbaz et al., 2005); in the same helix, Tyr[60] is also essential for activity; Tyr[40] is conserved in the EmrE branch of the SMR family, and its replacement has an effect on the specificity of the transporter to substrates (Soskine et al., 2004; Sharoni et al., 2005). Tryptophan residues may play several roles in intergral membrane proteins. For example, tryptophan residues can maintain interactions between a protein and its substrate using hydrophobic stacking interactions (Vazquez-Ibar et al., 2003); they

may also participate in cation/π interactions between protein and their ligands (Zacharias and Dougherty, 2002); moreover, the locations of tryptophan resides of membrane proteins tend to be at the ends of transmemrbane α-helices (Arkin and Brunger, 1998), reflecting the amphipathic nature of a tryptophan residue that has the ability to form hydrogen bonds, as well as to exhibit hydrophobic character.

The proposed mechanism of transport involves the binding of TPP$^+$ by the two membrane-embedded Glu^{14} residues located in transmembrane domain 1 (Figure 1.8d). The substrate enters EmrE either from the inner leaflet of the cytoplasmic membrane or directly from the cytoplasm. The binding site, occupied by the substrate, triggers a conformational change so that it becomes accessible to the other face of the membrane. The direct binding of protons to both Glu^{14} residues induces the release of substrate at the periplasmic surface. The chamber where TPP$^+$ binds is sealed at the top by helix H; the creation of an opening on the opposite side of the membrane from the chamber entrance would require the move of this helix, whilst the proximity of helices G and F could mean they move as a group.

(a)

(b)

(c)

(d)
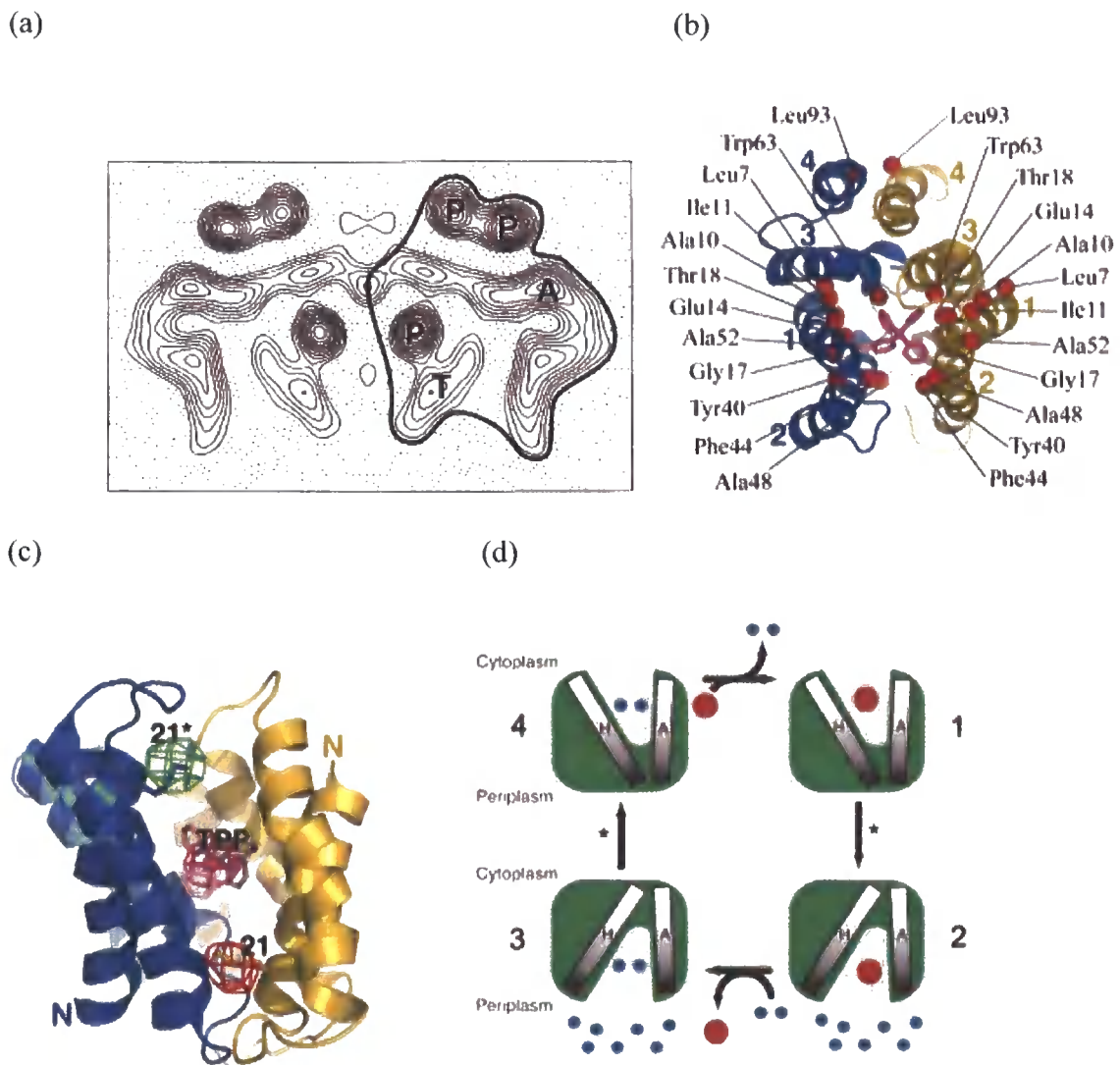
Figure 1.8   **Structure of EmrE**. (a) Projection map of EmrE at 7.0 Å resolution. The interpretation of each mark are as follows: P, an α-helix nearly perpendicular to the membrane plane; T, probably a single α-helix tilted with respect to the membrane normal; A, an arc of probably for tilted α helices (Tate *et al.*, 2001). (b) Top view of the EmrE-TPP$^+$ structure, with transmembrane helices labeled. Red spheres represent the residues that have been implicated in substrate binding and transport by biochemical and mutagenesis studies (Chen *et al.*, 2007). (c) Front view of the EmrE-TPP$^+$ structure, with two SeMet markers. (d) The proposed mechanism of transport by EmrE (Ubarretxena-Belandia *et al.*, 2003).

RND family

RND transporters can be found in all three kingdoms of life, Eukarya, Acrhaea and Eubacteria. RND transporters are composed typically of 1000 amino acid residues and are much larger than other secondary active transporters (Borges-Walmsley *et al.*, 2003). A characteristic feature of the topology of RND transporters is the presence of 2 large periplasmic loops between transmembrane helices 1 and 2 and 7 and 8. Since the N-terminal halves of RND transporters are homologous to the C-terminal halves, this suggests that these transporters have arisen by gene duplication.

AcrB

AcrB, the best studied member of the RND family, is a multidrug transporter that confers resistance to a wide range of antibiotics; including tetracycline, chloramphenicol, β-lactams, novobiocin, fusidic acid, nalidixic acid, and fluoroquinolones; the detergent SDS and Triton X-100; various cationic dyes, disinfectants, and even solvents (Poole, 2001).

The first crystal structure of AcrB was obtained at 3.5 Å resolution. The three protomers are fixed symmetrically by the crystal packing force (Murakami *et al.*, 2002). The appearance of the AcrB trimer is like a jellyfish with a three-fold symmetry axis perpendicular to the membrane plane. It comprises a periplasmic headpiece and a transmembrane region with approximate dimensions of 70 Å by 50 Å, respectively. The AcrB structure contains three domains: the transmembrane (TM) domain, the porter domain and the TolC docking domain (Figure 1.9a). The porter domain is composed of four subdomains, PN1, PN2, PC1 and PC2 for each protomer. PN1 and PN2 locate between TM1 and TM2 and PC1 and PC2 locate between TM7 and TM8. Each subdomain contains two characteristic β-strand-α-helix-β-strand motifs. These four subdomains are packed with their β-sheets surrounding a substrate binding pocket (Figure 1.9b).

More recently, the structure of new crystal forms of AcrB have been determined in which each protomer adopts a different conformation (Murakami *et al.*, 2006; Seeger M. *et al.*, 2006), leading to a rotating pump mechanism.

(a)

(b)
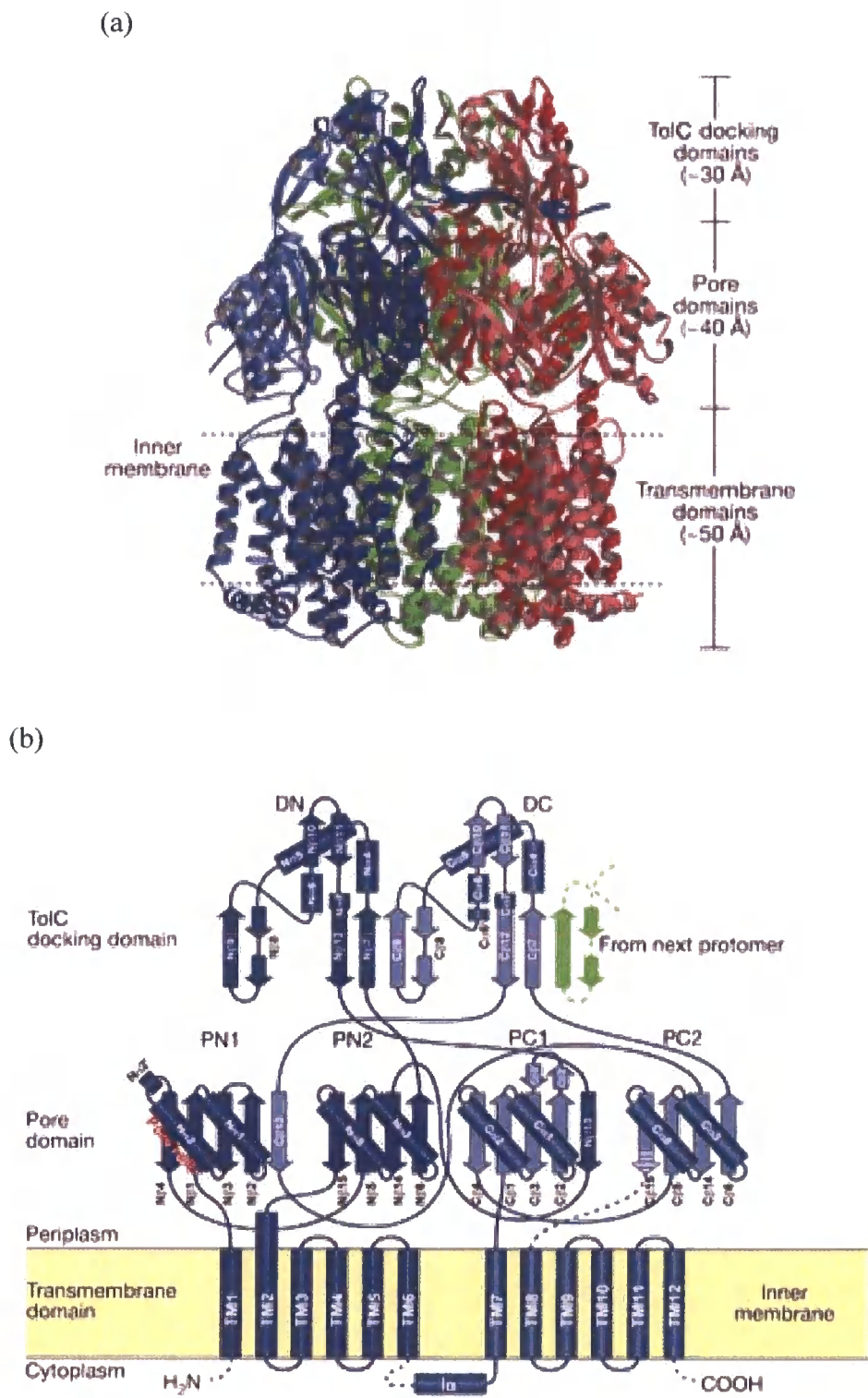
Figure 1.9   **AcrB structure.** (a) The side view of the AcrB structure in ribbon representation. (b) The topology diagram of the protomer (Murakami *et al*., 2002).

Bound minocycline was observed in one of the three protomers at the distal end of the pocket, between the β-sheets of PN2 and PC1 (Figure 1.10a). The substrate binding pocket is rich in aromatic amino acid residues which may interact with the drug molecule by hydrophobic or aromatic-aromatic interactions. It has been shown that two different sets of amino acid can interact with different drugs, indicating different sets of residues are used for binding of different kinds of substrates.

If we compare the protomer involved in extrusion to the one involved in binding drugs, an asymmetric difference can be recognized (Sennhauser et al., 2007; Das et al., 2007; Seeger et al., 2008). PN2 and PC1 are moved back towards PN1 and PC2 in the extrusion protomers, making the pocket too small to bind substrates. The inclined central helix (Figure 1.10a) from the extrusion protomer fills the possible "exit gap" between PN1 and PN2 in the binding protomer and creates a space between PN1 and PN2 in the extrusion protomer opening to the top funnel. Based on the different conformations of the three protomers of AcrB, a three step, (access, binding and extrusion), mechanism was proposed (Figure 1.11). In the access state, the vestibule is open to the periplasm, but the binding pocket is shrunken, making it impossible for substrates to have access to the vestibule. In the binding state, the vestibule is kept open and the binding pocket is expanded for substrate binding. At this stage, exit from the binding site is blocked by the inclined central helix from the extrusion protomer. Final, in the extrusion state, the squeezing of the binding pocket pushes the bound drugs out via the top funnel. Theses protomer conformation can be expected to be coupled with proton translocation across the membrane. Asp^{407}, Asp^{408} and Lys^{940} in transmembrane helices have been identified as essential amino acid residues for AcrB function and are probably involved in proton translocation. In the access and binding protomers, Lys^{940} of TM10 is coordinated by salt bridges with Asp^{407} and Asp^{408} of TM4. In contrast, Lys^{940} in the extrusion protomer is turned towards Thr^{978} of TM11 and this causes movement of TM4 and TM10 (Figure 1.10b). Site mutagenesis and drug susceptibility studies have also shown that Thr^{978} is essential for drug transport (Takatsuka and Nikaido, 2006). Unfortunately, how the twisting of these transmembrane helices causes the movement of the subdomains and the central α-helix inclination is still unclear.

(a) (b)
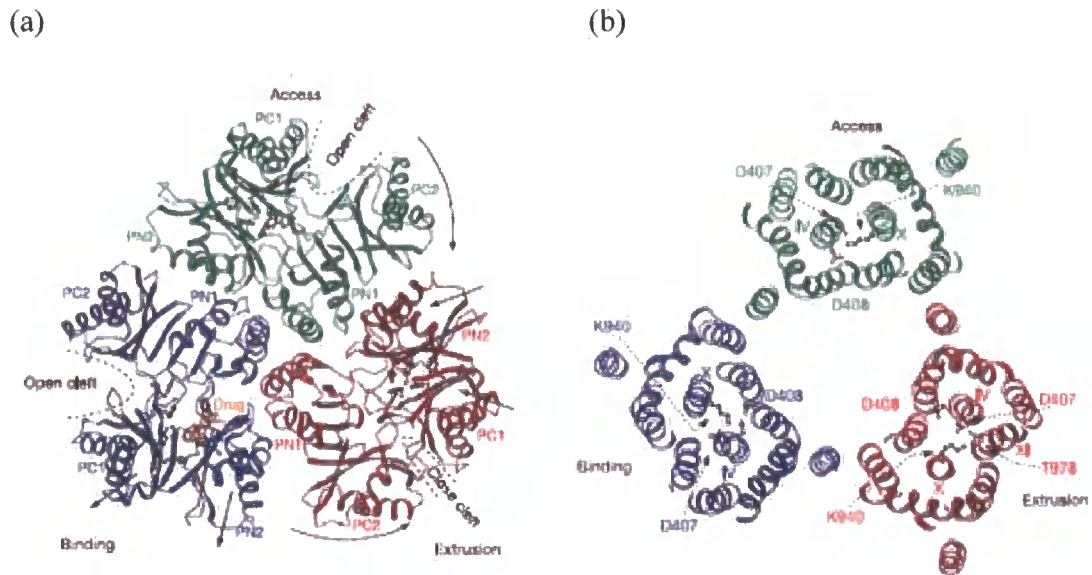
Figure 1.10   The asymmetric crystal structure of AcrB-minocycline complex. (a) Cut view of the porter domain from the distal side of the cell. The bound minocycline molecule is colored in orange. (b) The bottom view of the AcrB transmembrane domain structure from the periplasmic side (Murakami *et al*., 2006).
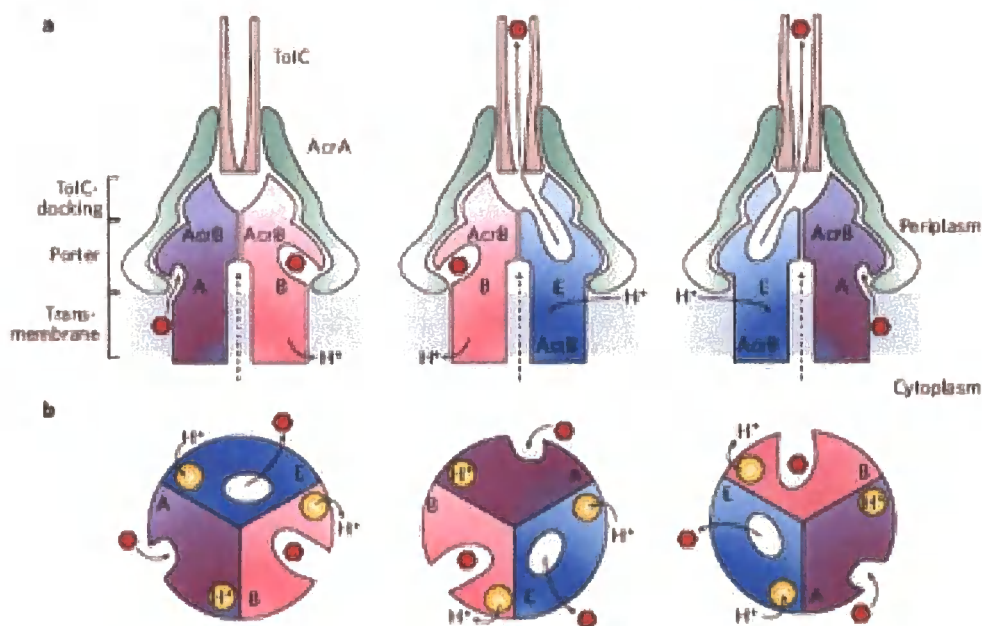
Figure 1.11   Schematic illustration of the proposed transporter mechanism. A, B and E represents the Access, Binding and Extrusion conformation respectively. (a) Side view of the proposed tripartite efflux pump AcrA-AcrB-TolC. (b) The proposed conformational change mechanism of three protomers of AcrB in a transport cycle (Schuldiner, 2006).

MATE family

MATE transporters can be found in all three kingdoms of life, Eukarya, Archaea and Eubacteria. In bacteria, these transporters are around 450 amino acids long and putatively arranged into 12 transmembrane α-helices (Figure 1.12) (Singh *et al.*, 2006). Based on the similar size and topology, MATE transporters were once suggested to be members of the MF family; however, they have no similarity in protein sequence with MF transporters (Brown *et al.*, 1999), such as the five-residue motif (RXGRR), located between TM2 and TM3. (Pao *et al.*, 1998)
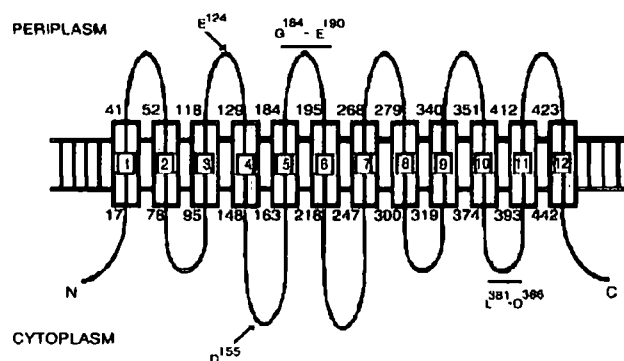
Figure 1.12   **Putative topology of NorM**, with the 12 transmembrane helices boxed (Singh *et al.*, 2006).

NorM

Of all multidrug transporters, our knowledge of the MATE transporters is most rudimentary because they have had little study. NorM, a Na^+/multidrug anti-porter, first found in *V. parahaemolyticus*, confers resistance to hydrophilic fluoroquinolone such as norfloxacin, ciprofloxacin and ethidium bromide, is the best characterized MATE transporter (Morita *et al.*, 1998). The topology of NorM from *V. cholerae* originally predicted by the algorithm HMMTOP was validated by fusing C-terminal truncations of NorM to either the TEM β-lactamase or chloramphenicol acetyltransferase (CAT) reporter (Figure 1.12). These studies indicated that NorM has 12 transmembrane domains and both the N- and C-terminal ends are located in the cytoplasm. In addition, some residues located on the hydrophilic loops are suggested to be involved in norfloxacin efflux (Singh *et al.*, 2006). Mutagenesis experiments indicated that the acidic amino acid residues Asp^{32}, Glu^{251}, and Asp^{367}, highly conserved in cluster 1 MATE transporters, located on the putative transmembrane domains 1, 7 and 10 of NorM, are involved in Na^+-dependent drug transport process (Otsuka *et al.*, 2005).

1.2.2 ABC transporters

1.2.2.1 What are they?

ATP binding Cassette (ABC) transporters can couple ATP (Adenosine 5'-triphosphate) hydrolysis to transport of a tremendous variety of substrates including drugs, vitamins, peptides, polysaccharides, ions, sugars, lipids and even proteins across cellular membranes in all organisms (Higgins, 1992; Hollenstein *et al.*, 2007).

ABC transporters have been conserved across the three kingdoms of Archaea, Eubacteria and Eukarya. Their ubiquitous distribution and primordial origin reflect the fundamental requirement of cellular homeostasis to import and concentrate essential nutrients, expel toxins acquired from the environment, and produce metabolic by-products. The report of the complete genome sequence of *E. coli* K-12 identified 80 ABC proteins, equals to 5% of the genome. In humans, ABC transporters can be grouped into seven different subfamilies (A, B, C, D, E, F, G) (Tatusov *et al*, 1997).

In humans, P-glycoprotein (p-gp) in the plasma membrane is probably the best studied ABC drug efflux transporter. It can transport a wide of substrates; including a number of drugs, such as the anti-cancer drugs doxorubicin and daunorubicin that are applied in therapeutic applications. MRP1, which localizes to the basolateral membrane of epithelial cells, was first identified in a cell line and shown to confer resistance to a range of anti-cancer drugs, such as anthracyclines (Cole *et al*, 1994; Evers *et al*, 1996).

ABC importers mediate the uptake of essential nutrients, whereas ABC exporters expel diverse substrates (Figure 1.13). The ABC exporter is formed by the transmembrane domains (TMD) and the nucleotide binding domains (NBD). In most cases, P-gp for example (Figure 1.13a), a single polypeptide includes the four domains, forming a TMD-NBD-TMD-NBD structure. On the other hand, the LmrA, a multidrug efflux pump, needs two polypeptides to form the functional unit.

Unlike ABC exporters, the ABC importers require the additional soluble protein substrate-binding-protein (SBP) to bind the substrate and deliver it to the translocator in the membrane. In many cases, each domain of ABC importers is present as a separate polypeptide, giving a total of five unique proteins (Figure 1.13b), such as the maltose importer $MalEFGK_2$ and vitamin B12 importer $BtuC_2D_2F$.

The membrane-bound complex importer MalFGK$_2$ from *E. coli*, with the help from MalE, a soluble periplasmic receptor, can mediate the uptake of the nutrient maltose from the periplasm across the membrane into the cytoplasm (Diederichs *et al.*, 2000). Some ABC transporters in bacteria are around 35% identical to the P-gp and the region of homology extends from the nucleotide binding domains to the transmembrane domains, thus suggesting these ABC transporters not only have similar sequences but may transport similar substrates. LmrA, a multidrug efflux pump, from *L. lactis*, confers resistance to drugs and antibiotics and has been found to functionally substitute for human P-gp when expressed in lung fibroblast cells (van Veen *et al.*, 1998). In addition, the ABC pump Sav1866 from *S. aureus* also shows significant sequence similarity to P-gp. The structure of the Sav1866-ADP complex has been determined and can be helpful in understanding the substrate recognition and transportation process (Dawson and Locher, 2006).

(a) ABC exporters

| P-glycoprotein *Homo sapiens* | Sav1866 *S. aureus* | LmrA *L. lactis* | DrrAB *S. peucetius* |

(b) ABC Importers

| Mal *E. coli* | Btu *E. coli* | Mod *A. fulgidus* |
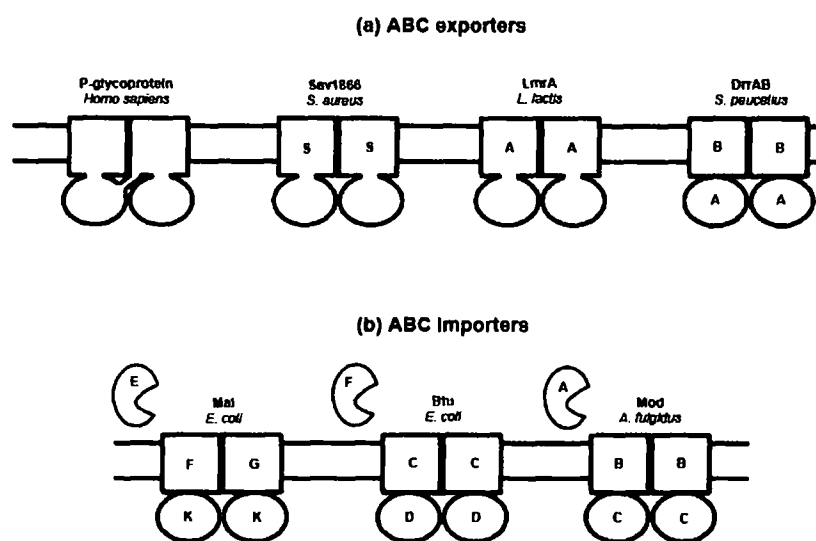
Figure 1.13 **The topology of different ABC transporters.** TMDs are represented by squares, NBDs are represented by circles, and substrate binding proteins with ABC importers are represented by pac-men.

1.2.2.2 Human diseases associated with ABC transporter

Drugs are pumped out by ABC transporters faster than they can diffuse across membranes, so the drug level inside is kept low and is much less effective, causing problems with chemotherapeutic treatments. Besides, there are approximately 50 known ABC transporters in humans and there are currently 13 genetic diseases associated with defects in 14 of these transporters. A few human diseases related to ABC transporters are described as follows (Gottesman and Ambudkar, 2001).

Cancer

Multidrug resistance (MDR) means cells have a cross-resistance phenotype against several unrelated drugs which differ in structure and target specificities. Resistance to chemotherapy is a common clinical problem in patients with cancer, and cellular resistance to drugs is a major reason for treatment failure. The MDR phenotype was first described as P-gp mediated for cancer cell, but cancer cells can be MDR without the involvement of P-gp (Lage, 2003). The Alterations in the signal-transduction pathways can abolish the function of drugs that accelerate programmed cell death. For example, a mutated, inactive p53 that is no longer able to trigger apoptosis after the detection of DNA damage caused by drugs (Hannun, 1997; Lowe *et al.*, 1993).

AIDS

Human immunodeficiency virus (HIV), which causes acquired immune deficiency syndrome (AIDS), has been studied for more than a decade. However, it can not be eradicated from infected patients partially due to multidrug resistance (Huisman *et al.*, 2000). The ABC transporter P-gp is known to efflux a number of drugs that includes the human immunodeficiency virus protease inhibitor. A report indicated that overexpression of p-gp can protect cell lines from the cytotoxic effects of high concentrations of phosphatidylinositol (PI) (Choo *et al.*, 2000). *In vivo*, pharmacological inhibition of the accumulation of PIs in brain and testes of mice (Choo *et al.*, 2000) and p-gp knockout mice also demonstrated an increased antiretroviral drug saquinavir accumulation in the brain (Washington *et al.*, 2000).

Surprisingly, growing evidence suggests that p-gp may also affect replication of enveloped viruses (Owen *et al.*, 2005). A report showed that p-gp overexpression can block insertion of the influenza virus fusion protein into the plasma membrane, inhibiting the membrane fusion and infectivity of the influenza virus (Raviv *et al.*, 2000).

Cystic fibrosis

Malfunctional ABC transporters can also cause diseases. The cystic fibrosis transmembrane conductance regulator (CFTR) is a cAMP-activated chloride channel, which creates sweat, digestive juices, and mucus, is expressed in the epithelia of the lung, intestine, pancreas and other tissues (Verkman *et al.*, 2006). Mutations, such as the most common mutation ΔF508, in CFTR can cause cystic fibrosis (CF), a hereditary disease, where defective epithelial cell fluid transport produces chromic lung infection and deterioration of lung function, pancreatic insufficiency and male infertility.

1.3 The structure and mechanism of ATP-binding cassette transporters

1.3.1 Conserved domains and motifs

So far, each ABC transporter has been discovered to consist of four domains: two nucleotide binding domains (NBD) that serve as engines, where ATP can be hydrolyzed, coupling hydrolysis to active transport; and two transmembrane domains (TMD) that are believed to constitute the transport pathway.

NBD in ABC transporters

Many crystals of isolated NBDs are available, yielding detailed information about the overall structures of the nucleotide-binding sites (Davidson and Chen, 2004). Generally, the NBDs can be divided into two sub-domains: a RecA-like sub-domain and a helical sub-domain, the latter being specific for ABC transporters. The RecA-like fold is characterized by a central β-sheet flanked by α-helices and can be found in a broad subclass of topologically homologues including RecA, DNA and RNA helicases, F1-ATP synthase, DNA repair enzymes and ABC transporters (Ye *et al.*, 2004).

Many conserved motifs, involved in ATP binding and hydrolysis or facilitating crucial interfaces in the assembled transporter (Higgins *et al.*, 2004), can be recognized in the NBDs of ABC transporters (Figure 1.14) and will be described as follows:

Walker A and Walker B

The Walker A (Walker *et al.*, 1982), also known as the P-loop, and Walker B motifs, present in many ATP-binding proteins and are not specific to ABC transporters. The highly conserved Walker A motif (G-X-X-G-X-G-K-S/T, where X represents any amino acid) is located after β-strand 3 and before the α-helix, and is involved in the coordination of the phosphates of ATP during the hydrolysis reaction. The less conserved Walker B motif (O-O-O-O-D-E, where O represents a hydrophobic amino acid) located on β-strand 7 provides a conserved aspartate that coordinates the Mg^{2+} ion in the nucleotide-binding site through H_2O. The last residue, a glutamate, in the Walker B motif arranges the nucleophilic attack on ATP via a water molecule and mutation of this residue leads to loss of ATPase activity (Moody *et al.*, 2002; Smith *et al.*, 2002). Zaitseva *et al.* suggested that residue H662 may interact with the γ-

phosphate moiety of ATP and water molecule 90, which forms hydrogen bonds to H662, E631, and via water molecule 109 to Q550, could serve as the catalytic water since a slight movement would be sufficient to put it in a proper orientation for attack of the scissile bond.

Signature sequence

The signature sequence, also known as the LSGGQ motif and C-loop, located at the joint point between the helical domain and the Walker B motif, binds to ATP, and is the motif that distinguishes ABC proteins from other nucleotide-binding proteins (Davidson, 2002). Mutations in the signature sequence inhibit ATPase activity (Schmees *et al.*, 1999; Bakos *et al.*, 1997) and structural studies indicated the motif contacts the nucleotide in the ATP-bound state (Smith *et al.*, 2002; Chen *et al.*, 2003; Dawson and Locher, 2006; Dawson and Locher, 2007).

Q-loop

The Q-loop, also known as the γ-phosphate linker, following β-strand 6, contains a glutamine that can form hydrogen bonds with the Mg^{2+} and the attacking H_2O. Verdon and co-workers (Verdon *et al.*, 2003), on the basis of the strucutre of the ABC-ATPase GlcV, proposed that the role of the conserved Q-loop glutamine residue, and its interaction with Mg^{2+}, is to keep the two ABC subdomains in close contact to each other. For example, mutations in the conserved glutamine in the Q-loop of MalK had only marginally reduced the ATPase activity but led to defective transporters when they interated in the membrane protein complex.

H motif

A conserved histidine in the H motif, located before α-helix 7, is believed to serve as a linchpin in ATP hydrolysis (Zaitseva *et al.*, 2005). Chen and co-workers found that the H motif residue (His^{192}) not only forms a hydrogen bond with the γ-phosphate but is also involved in direct protein-protein interactions across the dimer interface in the ATP-bound MalK dimer (Chen *et al.*, 2003). Mutations of the conserved histidine in HisP (His^{211}) (Shyamala *et al.*, 1991), MalK (His^{192}) (Davidson and Sharma, 1997) and HlyB (H^{662}) (Zaitseva *et al.*, 2004) resulted in a substantive decrease in the steady-state ATPase activities of these proteins.

D-loop

The D-loop is located between the Walker B motif and α-helix 5 and contributes in the contact interface between the two NBDs. In the closed form of Malk, the conserved Asp^{165} in the D-loop was found to form a hydrogen bond with Ser^{38} in the Walker A motif of the other subunit (Chen *et al.*, 2003)

A-loop

The A-loop, a highly conserved aromatic residue approxmately 25 amino acids upstream of the Walker A motif, is essential for ATP-binding (Ambudkar *et al.*, 2006). The structure of GlcV indicated that a phenylalanine residue is involved in the recognition of the adenine base (Verdon *et al,* 2003). Similarly, it was shown that a tyrosine reside interacts with the adenine ring of ATP in the HlyB-NBD structure (Zaitseva *et al.*, 2005). Mutagenesis studies also indicated that ATP hydrolysis was abolished when Tyr^{16} was mutated to cysteine in the histidine permease (Shyamala *et al.*, 1991).
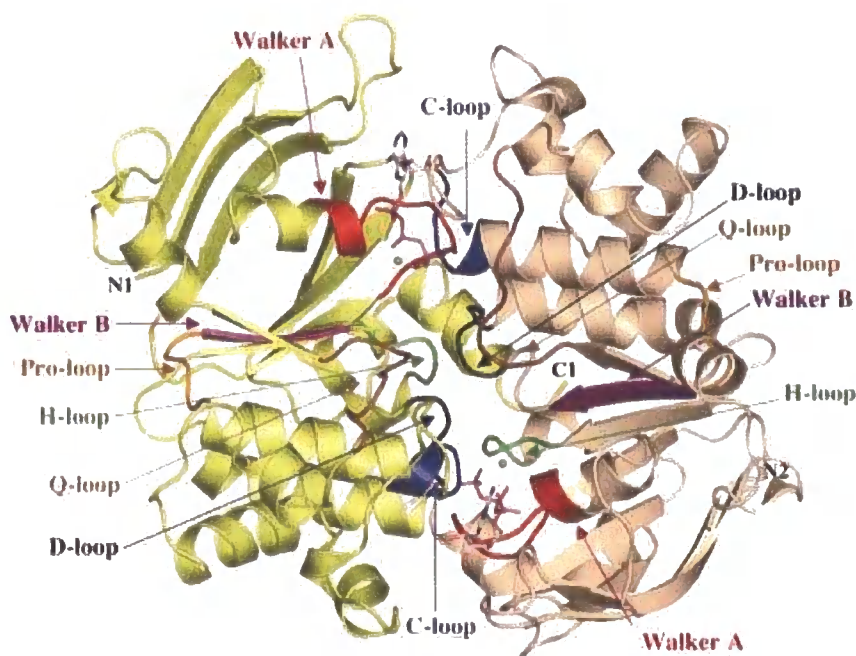
Figure 1.14   **The conserved motifs in NBDs of ABC transporters.** Crystal structure of the Hlyb-NBD dimer with bound ATP/Mg^{2+} (Zaitseva *et al.*, 2005). ATP (stick representation) and Mg^{2+} (green spheres) are sandwiched at the interface of the two monomers.

TMD in ABC transporters

The TMDs create the channel that substrates pass through during translocation. Unlike the NBDs, the TMDs are poorly conserved. The TMDs of ABC transporters are diverse in primary sequence, length, and the number of transmembrane helices, reflecting the large diversity of substrates transported. Characteristically, ABC importers have between 10 and 20 transmembrane helices; while ABC exporters tend to form the two-times-six α-helix structure, making a total of 12 transmembrane helices per functional unit (Figure 1.15). However, this is not always the case. For example, P-gp and CFTR are functional as a single polypeptide that includes all four domains (Sheppard and Welsh, 1999; Loo and Clarke, 1995); whilst the ABC transporter MacB from *E. coli* is predicted to have a topology consisting of four transmembrane helices; which will be described further below (Kabayashi *et al.*, 2003).
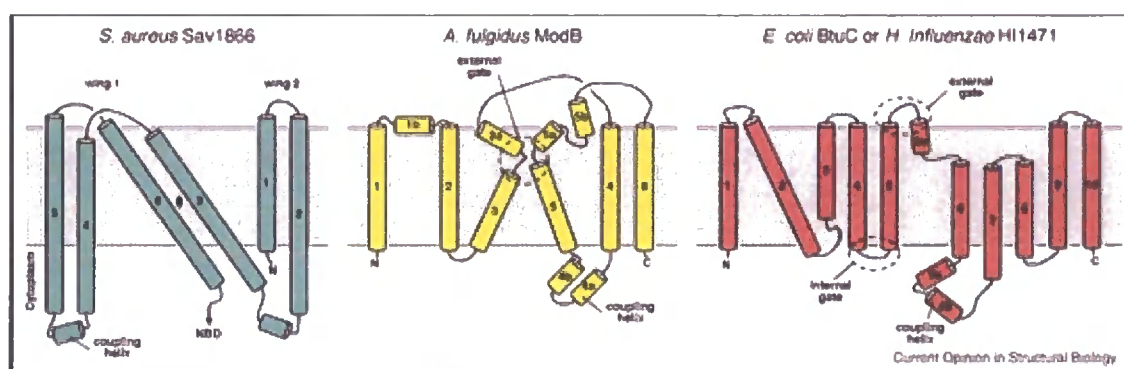
Figure 1.15   **Illustration of the TMDs topology of ABC transporters**. Sav1866 is shown in green, ModB is shown in yellow and BtuC, HI1471 are in red (Hollenstein *et al.*, 2007).

1.3.2 Structures of ABC transporters

So far there are five complete ABC transporter structures that have been determined: the importers BtuCD, from *E. coli*, HI1470/1, from *H. influenzae* and $ModB_2C_2A$ from *A. fulgidus*, and the exporter Sav1866, from *S. aureus* and MsbA. The four domains of the importers are on separate polypeptides and form a complex of homodimeric NBDs and TMDs (the structure of the periplasmic binding protein ModA is also shown in the $ModB_2C_2A$ structure) whereas Sav1866 is a half transporter with one NBD and one TMD on each polypeptide (Locher *et al.*, 2002; Pinkett *et al.*, 2007; Hollenstein *et al.*, 2007; Dawson and Locher, 2006; Ward *et al.*, 2007).

Sav1866

Sav1866 is a multidrug ABC transporter from *S. aureus*. When reconstituted into liposomes, Sav1866 ATPase activity can be stimulated by the anti-cancer drugs doxorubicin, vinblastine and the fluorescent dye Hoechst 33342 (Dawson and Locher, 2006), indicative of communication between the substrate binding site, in the TMD, and the cytoplasmic NBDs.

The Sav1866 structure is the first determined for an ABC exporter (Dawson and Locher, 2006). The Sav1866 transporter (Figure 1.16) is a 120 Å long, 65 Å wide and 55 Å deep homodimer and each polypeptide is composed of two domains: an N-terminal TMD (amino acid residues 1–320) and a C-terminal NBD (residues 337–578). Conserved ATP-binding and hydrolysis motifs, which are exposed at the interface, can be observed in the structure, revealing a "head-to-tail" arrangement. The electron density map indicated that the two bound ADP molecules were sandwiched at the NBD-NBD interface, in contact with the Walker A motif of one NBD and the ABC signature motif of the other.

Each Sav1866 subunit has 6 transmembrane helices, making a full transporter with 12 transmembrane helices. Bundles of transmembrane helices are divided into two wings that point away from one another towards the cell exterior, providing an outward-facing conformation in the crystal (Figure 1.16). Interestingly, each wing is composed of helices 1 and 2 from one subunit and helices 3 to 6 from the other. A large cavity was observed in the interface of the two TMDs, which is exposed to the

extracellular space. The cavity features a hydrophilic surface, lined primarily with polar and charged amino-acid side chains from helices 2 to 5, in the inner leaflet.

(a)   (b)

(c)

Figure 1.16   Sav1866 structure by ribbon representation. (a) Side view of the Sav1866 structure with subunits colored in yellow and green. (b) Stereo view rotated with respect to "(a)" by 90° around the vertical axis. (c) Close-up view of the interfaces between NBDs and TMDs of Sav1866. One subunit is colored in green ribbon representation and other is in yellow coil representation (Dawson and Locher, 2006).

The transmembrane helices are extended beyond the lipid bilayer by short extracellular loops (ECLs) and long cytoplasmic loops (ICLs), which protrude 25 Å into the cytoplasm. ICLs 1 and 2, which connected helix 2 and 3, and 4 and 5, respectively, both contain short helices, known as "coupling helices", and are orientated approximately parallel to the membrane of the shared interface formed by the TMDs (figure 1.16c). Surprisingly, coupling helix 1 contacts both subunits whereas coupling helix 2 contacts only the other, indicating that the ICLs of Sav1866 primarily contact the NBD of the opposite unit. In contrast, the TMDs of the ABC importer BtuCD contact only on NBD, resulting in a large gap at the center of the four protein domains (Locher et al., 2002). Residues around the conserved Q loops from the NBDs participate in the NBD-TMD contact interface and those residues can also be observed in the ABC importer BtuCD. In the BtuCD structure, residues around the Q loop dominate the interface between BtuC and BtuD. Side chains making specific contacts to the L loop of BtuC are located in helices H2, H3 of BtuD. Elements involved in ATP-binding and hydrolysis may be coupled to the conformation of the L loop from the membrane-spanning subunit and vice versa.

In the Sav1866, two prominent exceptions which wer not observed in the BtuCD include the conserved residues Tyr^{391} and Glu^{473}. The residue Glu^{473} contacts both ICLs and is found to be part of a previously unrecognized sequence motif (EVGERG), only conserved in ABC exporters. This newly-discovered specific sequence motif, called the X-loop, may indicate that ABC importers and exporters have diverse coupling mechanisms (Dawson and Locher, 2006).

Nucleotide-bound structures of MsbA provide another example of the outward-facing conformation of an ABC transporter (Figure 1.17). The electron-density maps of the MsbA-AMPPNP complex showed a conformation similar to the homologous Sav1866-ADP complex (Ward et al., 2007). Each monomer of MsbA has six transmembrane helices, forming a full transporter of 12 transmembrane helices. Similar to the Sav1866 strucutre, each wing of the MsbA full transporter is composed of helices 1 and 2 from one subunit and helices 3 to 6 from the other. In this study, the structural evidence arising from three MsbA structures, the nucleotide boud, open apo and closed apo forms, indicated that MsbA can undergo a large range of motions between the apo and nucleotide-bound states. This proposal will be described in the following sections.
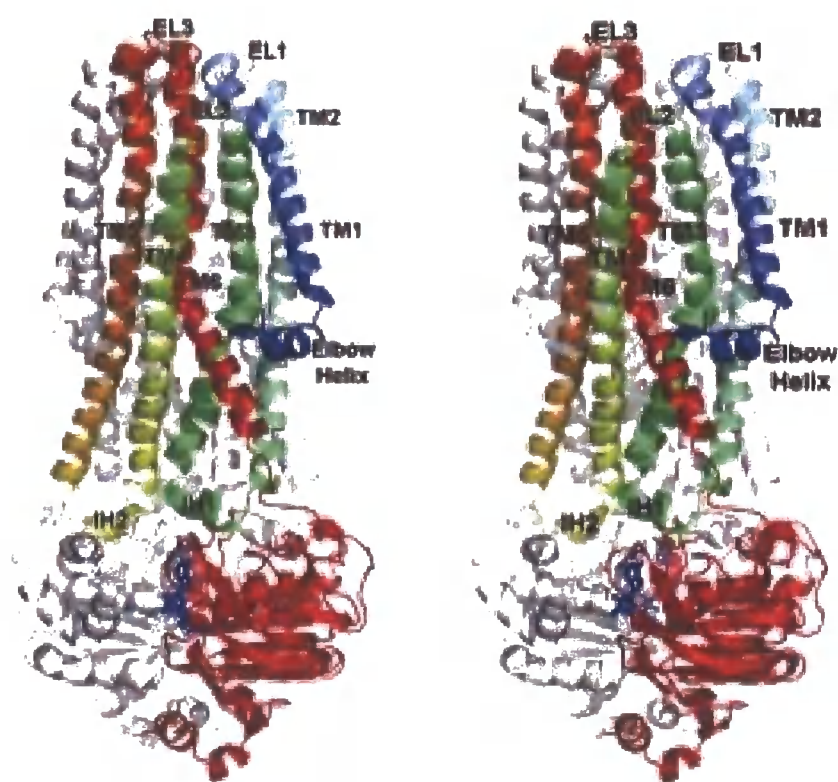
Figure 1.17   The stereoview of the nucleotide-bound MsbA structure. One monomer is colored with a rainbow gradient (N to C terminus, blue to red), and the other is white. The AMP-PNP molecule is displayed as blue sticks.

ModB₂C₂A

The ModB$_2$C$_2$A is an archaeal molybdate ABC importer from *A. fulgidus*. This full-size transporter is composed of two NBDs (ModC) and two TMDs (ModB) that interact with a periplasmic binding protein (ModA). The structure of the complex has been determined to a resolution of 3.1 Å using X-ray crystallography (Hollenstein *et al.*, 2007) (Figure 1.18a). In the crystal, a single binding protein ModA, with bound tungstate, is attached to the external side of ModB$_2$. Each ModB subunit has 6 transmembrane helices, making a full tranporter of 12 transmembrane helices. The twelve helices provide an inward-facing conformation, which is wide open to the cytoplasm. The nucleotide free ModC subunits reveal an open conformation, which contrasts with the "closed conformation" for the NBDs of Sav1866-ADP.

The ModB subunits form a large cavity, possibly representing the translocation pathway, shielded from the lipid bilayer and only accessible form the cytoplasm. The cavity opens to the cytoplasmic space, narrows down towards the external membrane boundary and is separated from the extracytoplasmic space by a closed gate below the interface with the binding protein ModA (Figure 1.18b). The gate is formed by the joining of four protein stretches (gate regions), two from each ModB subunit. Gate region 1 and 2 are located in transmembrane helices 3 and 5 respectively. In addition, the phenyl rings of the conserved Phe[200], in transmembrane helix 5, from the two ModB subunits are within van der Waals distance, implying their involvement in gating (Figure 1.18c).

An "head-to-tail" arrangement between the P loops and the ABC signature motifs was observed in the two ModC subunits. Not surprisingly, a gap was observed between the ATP-binding motifs of the nucleotide-free NBDs, indicating a so called "open conformation" of NBDs. The observation of the spacing between the Walker A motif and the ABC signature sequence is consistent with the biochemical studies of Mal ABC importers in which the solvent accessibility to the fluorescently labelled ATP binding sites is increased in the absence of ATP (Mannering *et al.*, 2001). In this study, Cys[40], in the Walker A motif of MalK, was labelled with 2-(4'-maleimidoanilino) naphthalene-6-sulfonic acid (MIANS) in order to observe the conformational changes in the Malk subunit.

The ModB-ModC interface is believed to transmit conformational changes, coupling ATP binding and hydrolysis to substrate transport. Similar to the Sav1866

structure, the residues around the Q-loop of ModC are involved in the ModB-ModC interfac. The ModB residues involved in the ModB-ModC interface are located on the short cytoplasmic helices 4a and 4b, with 4a providing the bulk of the contacts. Similar coupling helices have been found in the structures of the exporter Sav1866 and importers BtuCD and HI1470/71. However, the sequence similarities between the coupling helices are limited, although their position suggests a role in coupling ATP binding and hydrolysis to transport.

(a)

(b)

(c)
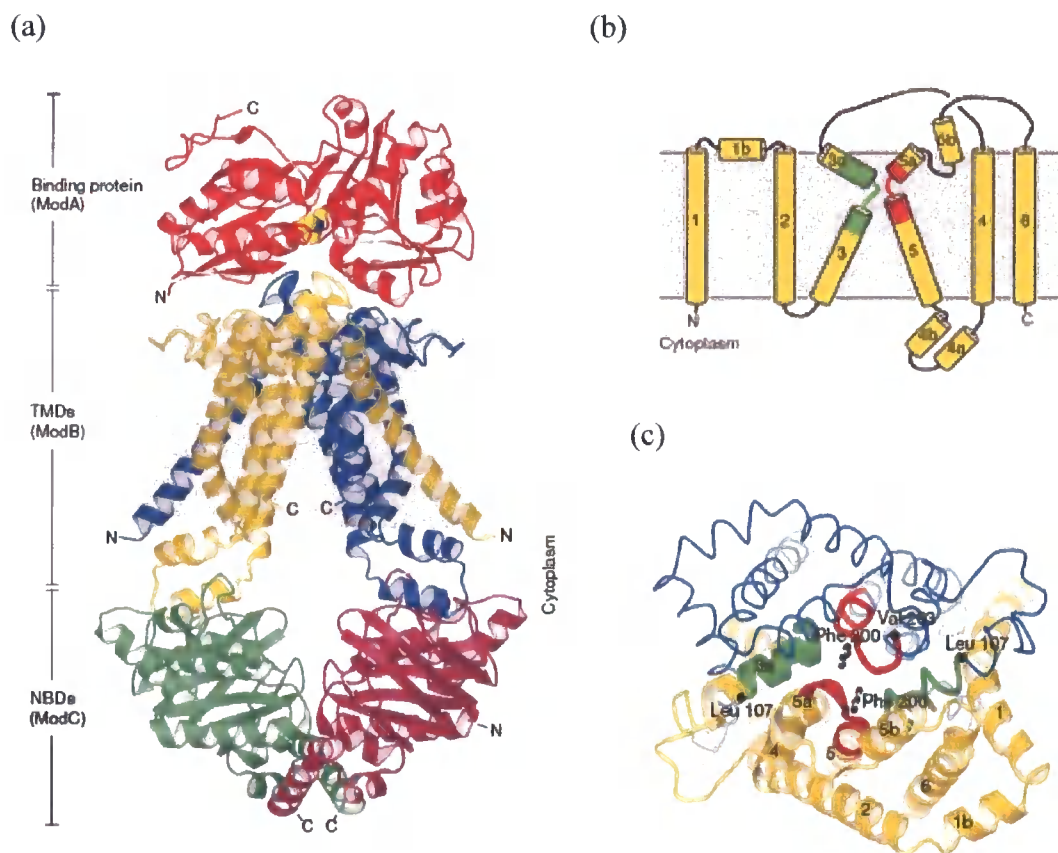
Figure 1.18   **The structure of the ABC transporter ModB$_2$C$_2$A.**   (a) The ModB subunits are in yellow and blue, the ModC subunits are in green and pink, the substrate binding protein ModA is in red, and with bound tungstate in van der Waals representation (yellow and blue spheres). The grey box indicates the possible location of the lipid bilayer on the basis of the hydrophobicity of the protein surface. (b) Topology of the ModB subunit. The conserved gated regions are colored in green and red. (c) Top view of transmembrane ModB subunits, with one subunit in yellow ribbon representation and the other in blue backbone trace (Hollenstein *et al.*, 2007).

1.3.3 Conformational changes in NBDs

The Sav1866 and $ModB_2C_2A$ structures are indicative of the "closed conformation" and "open conformation" of the NBDs respectively. The idea is drawn from comparison of the nucleotide-free-MalK and ATP-bound-MalK structures, in which it was possible to observe major conformational changes in the NBDs as ATP was bound, which has been likened to the action of a pair of tweezers (Figure 1.19). The distance between the two His[89] on the Q-loop moved from the closed form to the semi-open or open conformations by 9 or 25 Å respectively (Chen *et al.*, 2003; Oldham *et al.*, 2007).

In addition to the movement of the whole NBDs, a hinge rotation of the helical subdomain relative to the RecA-like subdomain can be observed in the MalK structures. The difference can be found not only in different NBD structures but in the same protein crystallized in different crystal lattices and even between molecules in the same lattice (Chen *et al.*, 2003). Interesting, the orientation of the helical subdomains are the same among the three ATP-bound structures: HisP, MalK and MJ0796, suggesting the helical subdomain has unique orientation in the presence of γ-phosphate. The flexibility of the helical subdomain was only observed in the NBD structures in the absence of the γ-phosphate of ATP, suggesting an important mechanistic role for this movement. When the helical subdomain is tilted away from the RecA-like subdomain, as in the nucleotide-free conformation, the two NBDs are unable to come into close enough contact to form the ATP-bound dimer. This rotation of the helical subdomain could also be coupled with ATP binding and hydrolysis and the characteristic flexibility may be important in adjusting the size of the opening of the translocation pathway for various sizes of substrates. This can also be found in full size ABC transporters by comparing the NBD structures from Sav1866 (closed form) and $ModB_2C_2A$ (open form). A difference can be observed in the $ModC_2$ dimer in the withdrawal of the helical subdomain from the interface with the opposite NBD, combined with a slight outward tilt. Also, several lines of biochemical evidence indicated that the association and dissociation of NBDs plays an important role in transport. The E171Q mutant of MJ0796 eliminated hydrolysis and stabilized the ATP-bound dimer (Smith *et al.*, 2002). Addition of ATP enhanced disulfide-crosslinking between cysteines introduced at position 85 in the Q-loops of the MalK subunits (Hunke *et al.*, 2000).
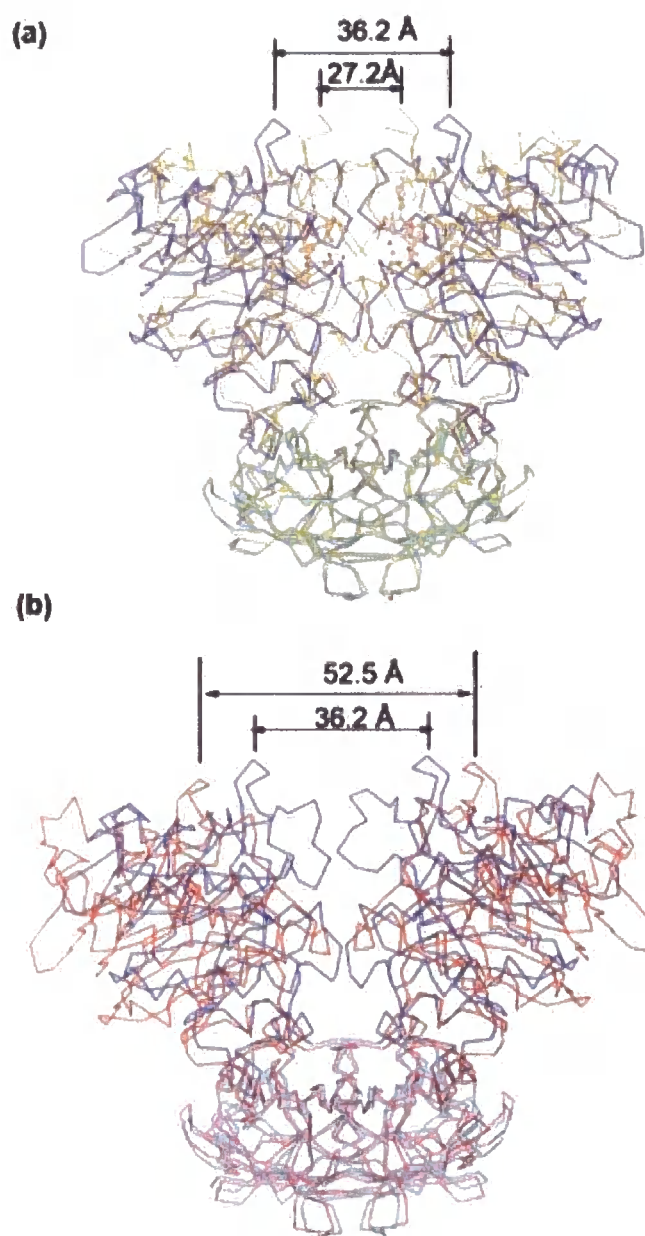
Figure 1.19 **Comparison of two MalK structures,** where closed form MalK with bound ATP is in yellow and semi-open form MalK without bound ATP is in blue (Chen *et al.*, 2003).

1.3.4 Mechanisms for coupling of hydrolysis to transport

That the binding of ATP triggers the NBDs to dimerize has been described in the previous section. Two models for the transport mechanism, based on the Sav1866 and $ModB_2C_2A$ structures, and MsbA structures, will be described below.

A transport mechanism based on the Sav1866 and $ModB_2C_2A$ structures
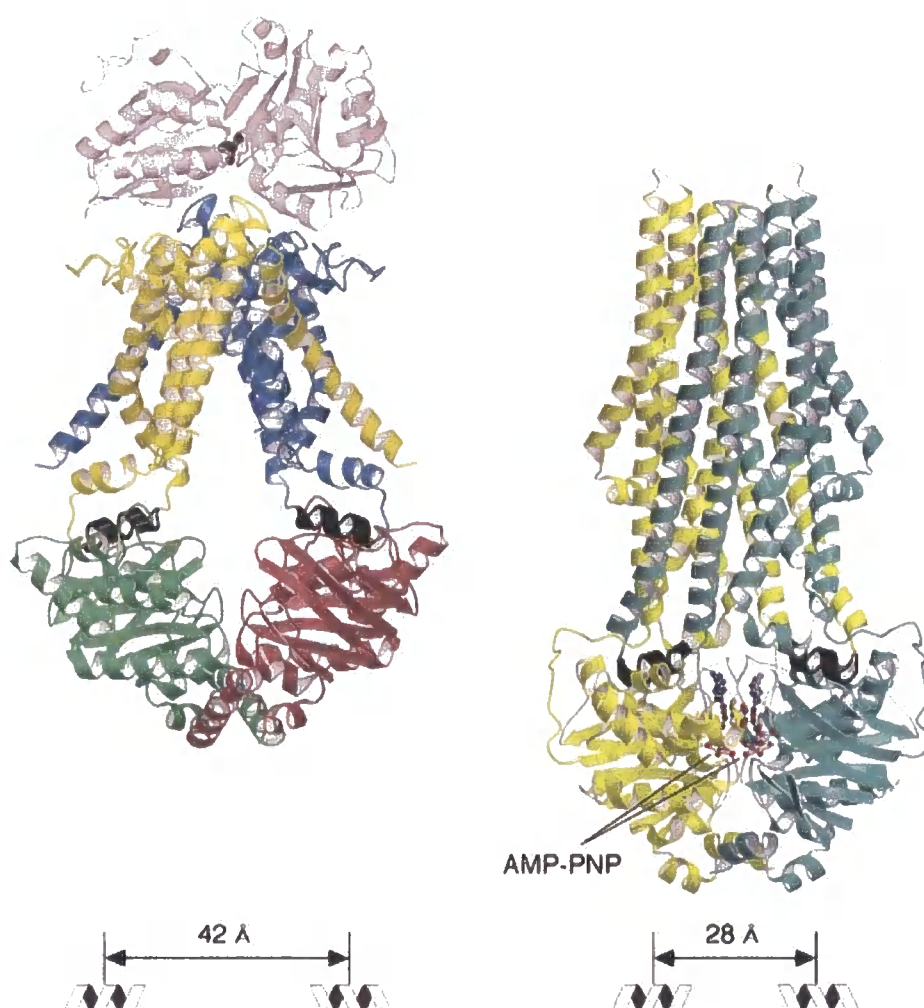
Figure 1.20 **Conformational changes triggered by ATP**. The structure of $ModB_2C_2A$ indicates an inward-facing conformation and the Sav1866 structure indicates an outward-facing conformation The black helices are the coupling helices from the TMDs (Hollenstein *et al.*, 2007).

A mechanism for ABC transporters has been proposed on the basis of the structures of the two full size ABC transporters, Sav1866 and ModB₂C₂A (Hollenstein *et al.*, 2007) (Figure 1.20), where Sav1866 represents the "closed form" of the NBDs and the "outward-facing" conformation of the TMDs whilst ModB₂C₂A represents the "open form" of the NBDs and the "inward-facing" conformation of the TMDs. In the Sav1866 structure, the distance between the coupling helices is decreased by 10-15 Å when compared with the nucleotide-free structure for ModB₂C₂A. ABC importers may now accept substrates from their cognate binding proteins and ABC exporters may extrude bound drugs to the environment by presenting a cavity of low affinity to the extracellular medium (Loo and Clarke, 2005). The hydrolysis of ATP, and the subsequent release of ADP and inorganic phosphate, may return the transporter to an inward-facing conformation. ABC importers may now release their substrates into the cytoplasm, whereas ABC exporters may recruit new substrates into their high-affinity binding sites.

A transport mechanism based on the structures of three conformations of MsbA

Ward and co-workers (Ward *et al.*, 2007) provided structural evidence, arising from different conformational states for MsbA, showing that MsbA can undergo a large range of motions between the apo and nucleotide-bound states (Figure 1.22a).

The conformational changes between difference MsbA structures are most noticeable when monomers from each state are aligned using transmembrane helices 1, 2, 3, and 6 (Figure 1.21). Comparison of the apo structures reveals that TM4/TM5/IH2 can pivot around 30° about a hinge formed by EL2/EL3 in a rigid-body motion with nearly conserved NBD alignment. In apo structures, this hinge creates an inward-facing conformation between TM3/TM6 and TM4/TM5 (Figure 1.21). Interestingly, although the NBDs were closed in the apo state, an ATP sandwich structure was not observed (Figure 1.22). In addition, the P-loops of opposing monomers are positioned next to one another (Figure 1.22c).

The transition from the closed apo conformation to the nucleotide-bound conformation can be accounted for by two motions. Firstly, there is a 10° pivot about the hinge, EL2/EL3 (Figure 1.21), bringing the NBDs closer together. Secondly, the NBDs form an ATP sandwich by tilting the TM4/TM5 pair around 20° out of plane

(relative to the first motion) about that pivot point centered along its length. Since TM3/TM6 are connected to TM4/TM5 via EL2 and EL3, the formation of the NBD sandwich pulls TM3/TM away from TM1/TM2 (Figure 1.22ab). An outward opening is created between TM3/TM6 and TM1/TM2, which is different from the inward opening created between TM3/TM6 and TM4/TM5. The conformational changes (Figure 1.21 and 1.22) in the NBDs cause a rearrangement of the packing of TMDs, switching access to the internal chamber from the inner to the outer leaflet of the bilayer. The large inward-facing opening may serve an important role in transport because the open and closed apo structures can accommodate substrates from the inner leaflet or the cytoplasm. Substrate binding to the inward-facing conformation may lead to the closure the TMDs and then rearrangement of the NBD, allowing the formation of an ATP sandwich conformation.
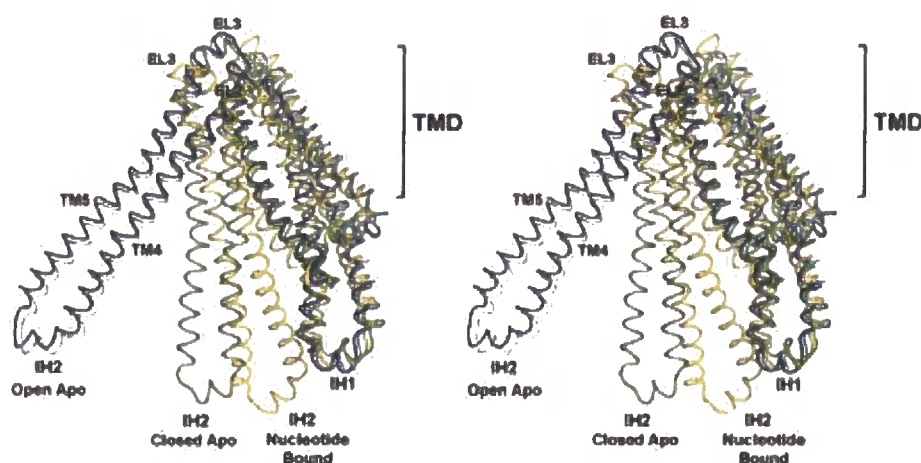
Figure 1.21 **Comparison of the MsbA monomers**. The stereoview of the conformational changes within the MsbA monomer illustrates the mobility of the TM4/TM5/IL2. Monomers are aligned on transmembrane helices 1, 2, 3 and 6. Two apo open MsbA monomers that differ in the relative positioning of TM4/TM5/IH2 are shown in blue and cyan. The apo closed MsbA is colored in green and the nucleotide-bound MsbA is in yellow (Ward *et al.*, 2007).
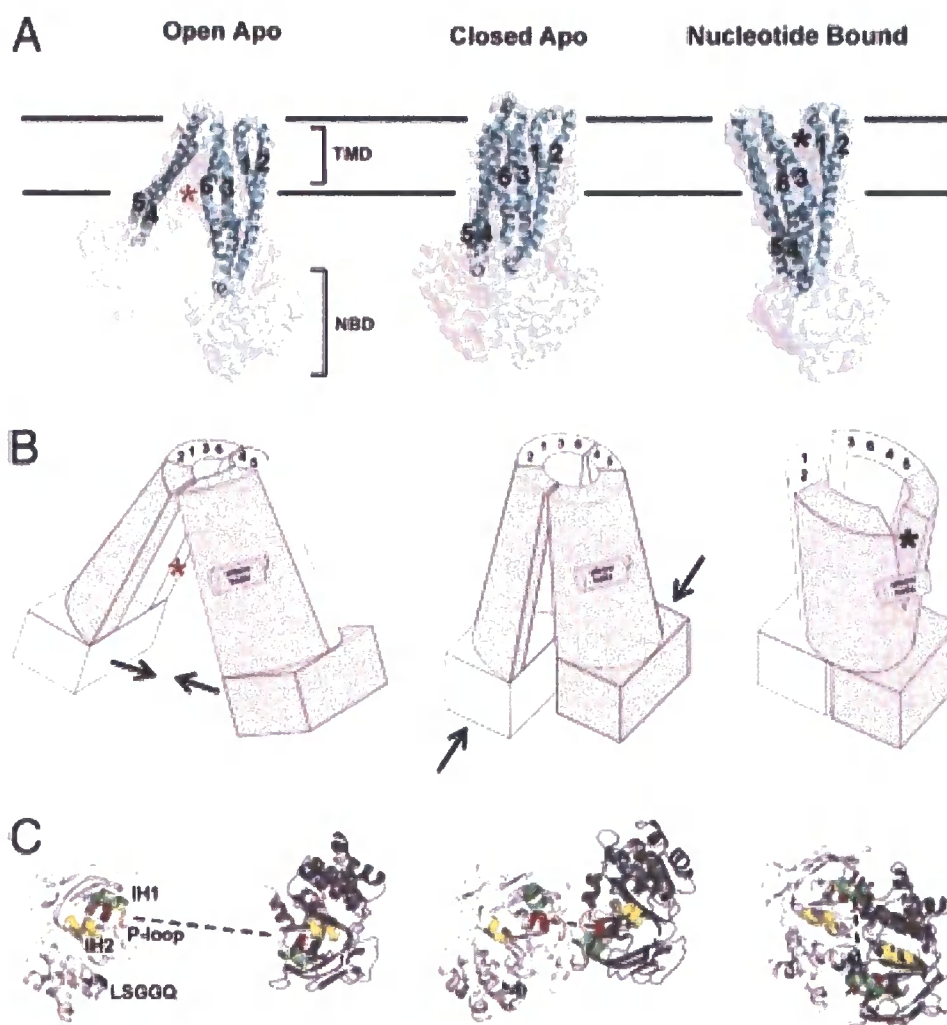
Figure 1.22   Conformational changes in MsbA. (a) Conformational changes in the open apo, closed apo and nucleotide-bound MsbA. (b) Model of the conformations changes. The arrows illustrate the motions required to go to the next state. (c) Top view of the NBDs. One monomer is colored in white and the other in gray (Ward *et al.*, 2007).

1.4 Tripartite multidrug efflux pumps in gram-negative bacteria

Antibiotic resistance due to multidrug transporters is a growing problem in the world; to combat them, more research into the transport mechanism and structures of efflux pumps is necessary. Gram-negative bacteria possesse tripartite complex pumps which are composed of an inner membrane protein, a periplasmic protein and an outer membrane protein, which work together to confer multidrug resistance. Recent studies have brought a better understanding of tripartite drug efflux pumps, particularity, AcrA/AcrB/TolC in *E. coli* and MexA/MexB/OprM in *P. aeruginosa*. The determination of the structures of the three components, AcrA, AcrB and TolC, provide us with clues to the function and mechanism of these tripartite efflux complexes (Koronakis *et al.*, 2000; Mikolosko *et al.*, 2006; Murakami *et al.*, 2002).

TolC structure

TolC, a multifunctional outer membrane protein, is involved in type I secretion of toxins and proteases and plays an important role in antibiotic efflux. It can export haemolysin by a substrate-induced transient interaction with the ABC transporter HlyB and the membrane fusion protein HlyD (Thanabalu *et al.*, 1998). On the other hand, the *in vivo* disulfide cross-linking between AcrB and TolC may suggest that the AcrA/AcrB/TolC efflux complex appears to be independent for the drug substrates and is assembled constitutively (Touzé *et al.*, 2004).

The TolC structure has been solved by X-ray crystallography (Koronakis *et al.*, 2000), indicating that three TolC protomers assemble to form a 140 Å long channel spanning the outer membrane and periplasmic space (Figure 1.23a). The TolC molecule is composed of three domains: a β-barrel domain, an α-helical domain, and a mixed α/β-domain which forms a strap around the middle section of the helical barrel (Figure 1.23b). The α-helical barrel domain of trimeric TolC forms a cylinder of 100 Å in length and 35 Å internal diameter, which makes a mostly solvent-filled inner volume of roughly 43,000 Å^3, one of the largest known in a protein structure. The upper end of the TolC structure is open, providing wide solvent access, while the lower end of the structure is closed by dense packing of 12 tunnel-forming α helices (Figure 1.23a).
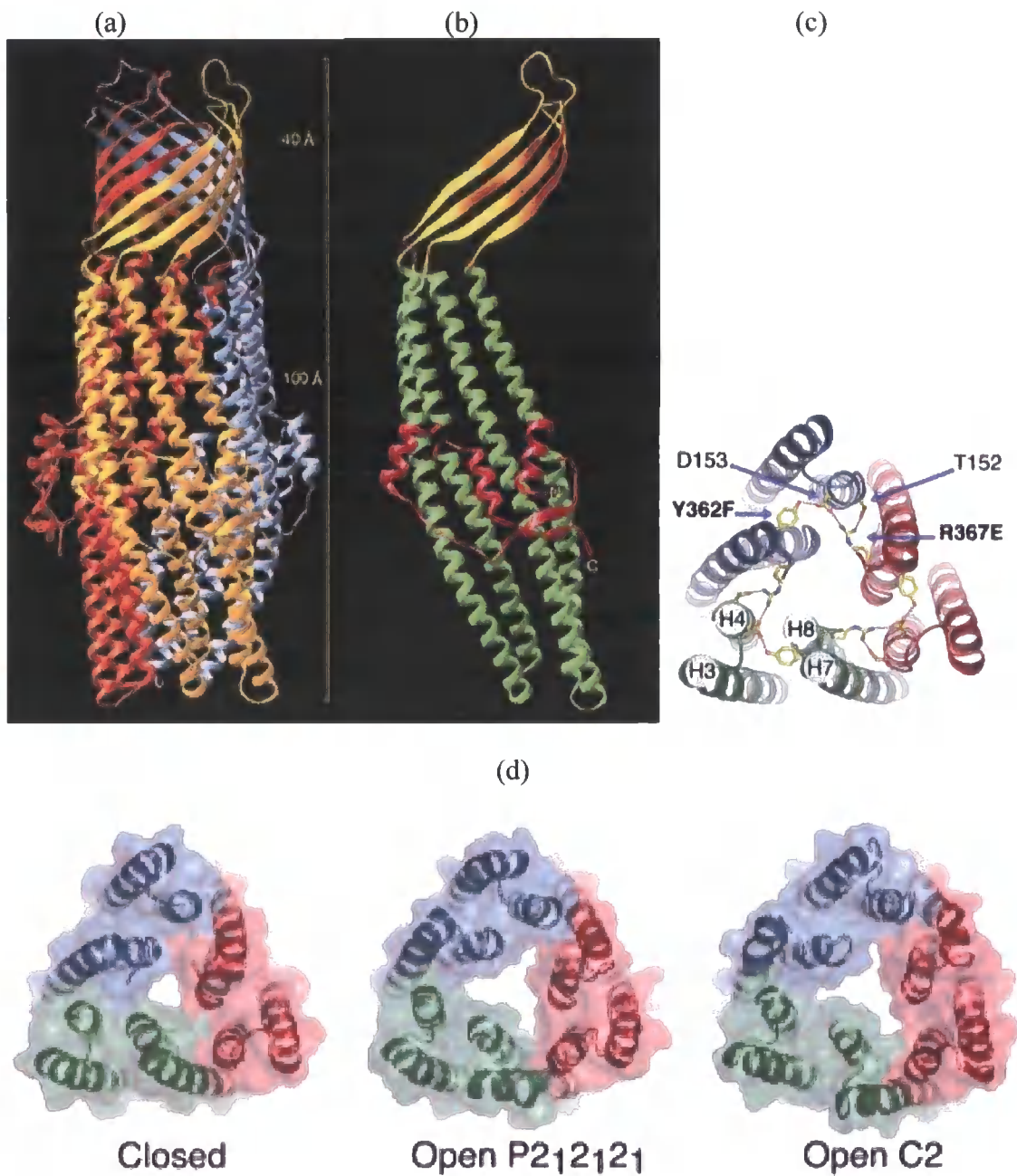
Figure 1.23 **The structure of outer membrane protein TolC.** (a) The Side view of the TolC by a ribbon representation where three protomers are colored in red, yellow and blue. (b) TolC monomer by a ribbon representation where the β-barrel domain is in yellow, the α-helix domain is in green and the equatorial domain is in red (Koronakis *et al.*, 2000). (c) A scheme of the mutations to stabilize channel opening of TolC. (d) The bottom view of the open and closed TolC structures (Bavro *et al.*, 2008).

TolC must undergo a conformational change to open the entrance for translocation since it is too small for the substrates to enter the channel (Figure 1.23c). The disruption of the hydrogen bond between amino acid residue D^{153} and Y^{362} and the salt bridge between the D^{153} and R^{367} of TolC increase the conductance in lipid bilayers, enlarging the low end entrance (Figure 1.23c) (Andersen et al., 2002). The translocation of polypeptide substrate is prohibited by introducing disulphide bonds to constrain the entrance coiled coils in the close state (Eswaran et al., 2003), further supporting the proposal that the transition to the open state TolC is accomplished by the re-arrangements of the entrance helices.

Bavro and co-workers determined two TolC structures in its partially open state (Bavro et al., 2008). Previous report indicated that the disruption of the hydrogen bond between amino acid residue D^{153} and Y^{362} and the salt bridge between the D^{153} and R^{367} of TolC can enlarge the TolC periplasmic entrance (Andersen et al., 2002). The structure of the double mutant (Y362F and R367E) of TolC was solved in two crystallin forms at 3.2 and 3.3 Å resolution (Figure 1.23d). The crystal structures of the double mutant showed that three of the six pairs of colied coils move radially outward from the central in comparison of the closed state form, repacking the helices and partially opening the channel (Figure 1.23d). It was found that the greatest conformational changes occur in the H7/H8 helices; the H3/H4 helices are comparatively static and are like a stator around which the H7/H8 swings. Although the movements of the helices in the double mutant TolC strucutre enable the opening for passage of molecules pas the distal tip of TolC, the second aperature is still closed, suggesting that a further conformational change is required for greater channel opening.

AcrA structure

The membrane fusion protein AcrA is a component of the tripartite multidrug efflux pump AcrA/AcrB/TolC in *E.coli*. AcrA has been shown to interact with both AcrB and TolC, which suggests that AcrA serves as a scaffold in the tripartite efflux pump (Touze *et al.*, 2004; Tikhonova *et al.*, 2004). In addition, AcrA may also function in the opening of the periplasmic end of TolC channel (Bavro *et al.*, 2008). The crystal structure of a 28 kDa core of AcrA (residues 45-312) was shown to be comprised of an α-helical hairpin domain, a lipoyl domain and a β-barrel domain (Figure 1.24a). Indeed, it is closely related to the structure of the membrane fusion protein MexA from *P. aeruginosa* (Higgins *et al.*, 2004; Mikolosko *et al.*, 2006). Interestingly, in the lattice in the AcrA crystal, each α-helical hairpin of the four monomers has a different orientation (Figure 1.24b), which is not observed in the MexA structure. The difference in orientation of the α-helical hairpin of AcrA stems from an effective hinge, located between the α-helical hairpin and lipoyl domain, composed of residues 99-106 in α-helix 1 and residues 169-173 in α-helix 2.

In contrast to AcrB and TolC, which form trimers, the oligomeric state of AcrA is uncertain. In the crystals, AcrA are seen to form a dimer through extensive contacts involving the α-helical hairpins as well as adjoining lipoyl and β-barrel domains. On the other hand, AcrA was monomeric in solution and was found to be trimeric when crosslinked *in vivo* by DSG, which has a short spacer arm (7.7 Å) (Eswaran *et al.*, 2004; Zgurskaya and Nikaido, 2000).
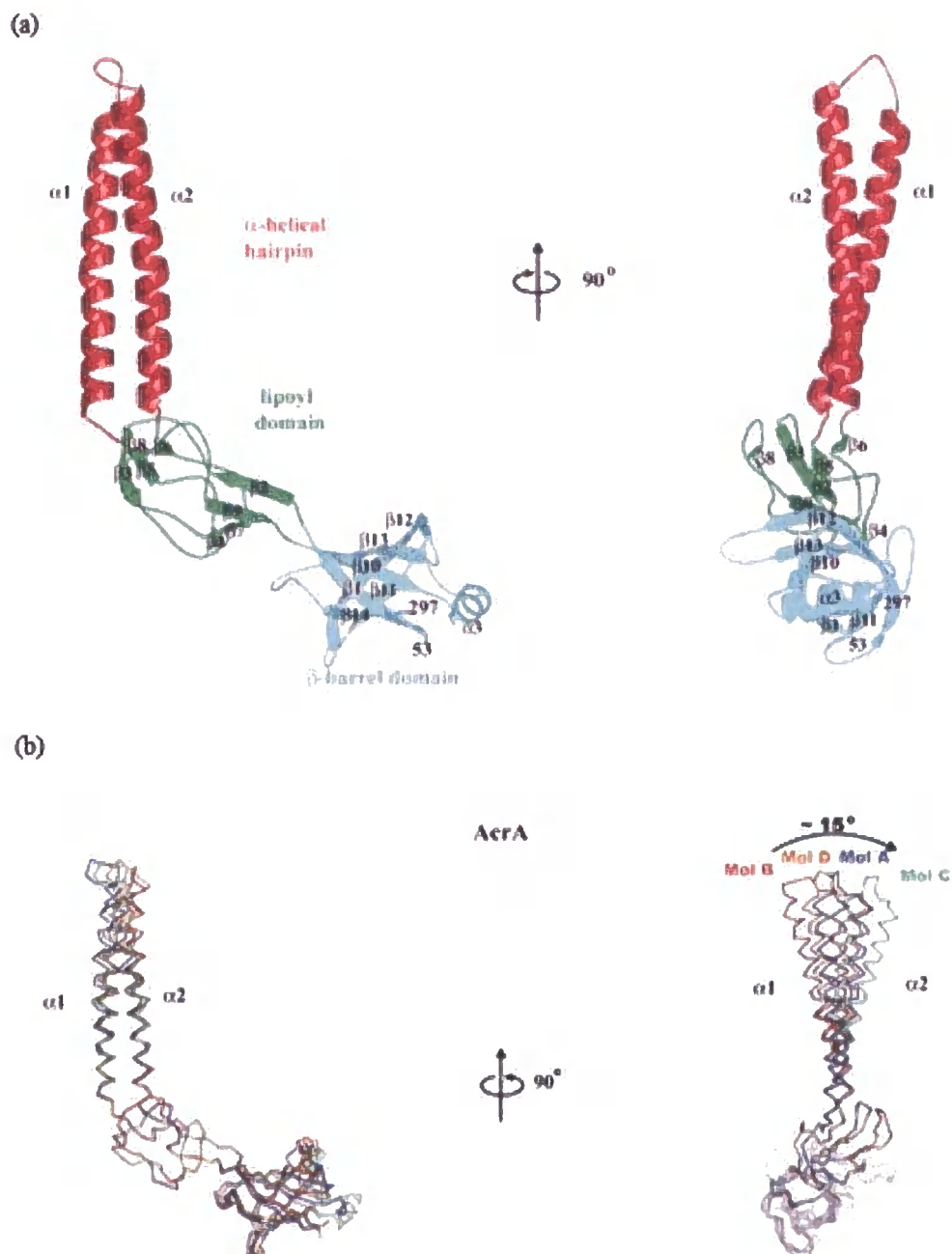
Figure 1.24 **Structure of AcrA.** (a) Ribbon representation of the crystal structure of AcrA (residues 45-312) monomer, with the α-helical hairpin domain in red, lipoyl domain in green and β-barrel domain in cyan. (b) Four conformations of AcrA in the crystal show the conformational flexibility of the α-helical hairpin (Mikolosko *et al.*, 2006).

The AcrB/AcrA/TolC complex pumps

TolC is a homotrimeric outer membrane protein that comprises an outer-membrane β-barrel, prolonged by a 100 Å α-helical transperiplasmic tunnel. The TolC extracellular exit channel is constitutively open, with a pore diameter of 35 Å, but the periplasmic domain channel entrance was restrained by coiled-coil α-helices. Andersen and co-workers proposed an iris-like transition to the open state based on the realignment of the inner coils on the outer ones (Anderson et al., 2002). The inner membrane protein AcrB, known as being trimeric, consists of a transmembrane domain at its bottom and a huge periplasmic domain on top. The top docking domain forms a funnel, with about a 30 Å internal diameter that is consistent with that of the TolC conduit. The sum of the periplasmic length of AcrB and TolC is about 170 Å, which is enough to cross the periplasmic space (Koronakis et al., 2000; Murakami et al., 2002). Moreover, the length and topology of the periplasmic domains of both TolC and AcrB suggests that the two interact directly (Tamura et al., 2005). Substrates might access the AcrB central cavity from the periplasm through the AcrB lateral vestibules for transport to the cell exterior.

AcrA and TolC in E. coli have been found to form a stable intermembrane multidrug efflux complex with or without the substrate (Eswaran et al., 2004; Tikhonova and Zgurskaya, 2004). The AcrA-AcrB complex was identified upon purification from cell membranes after stabilization by in vivo crosslinking in the absence of TolC (Zgurskaya and Nikaido, 2000). Moreover, AcrA was found to be crosslinked with AcrB and TolC individually in vivo, and microcalorimetry studies demonstrated energetically favourable interactions of AcrA with both purified AcrB and TolC (Touzé et al., 2004). AcrB can also be isolated as a complex with TolC by in vivo crosslinking; however, isothermal titration calorimetry did not detect an interaction between the purified AcrB and TolC proteins, suggesting AcrA may serve a scaffold to stabilize the complex in vivo (Eswaran et al., 2004).

The AcrB and TolC crystals structures indicated that the 70-Å- and 100-Å-long periplasmic domains of AcrB and TolC would come into close proximity (Murakami et al., 2002; Koronakis et al., 2000). The interaction between the apex of AcrB and the bottom of TolC was then revealed by in vivo disulfide crosslinking between AcrB and TolC without a crosslinking agent (Tamura et al., 2005). Domain swapping and crosslinking experiments suggest that the C-terminal region of AcrA is required for the

interaction with AcrB (Elkins and Nikaido, 2003; Touzé *et al.*, 2004). The crystal strucutures of AcrA and TolC (Mikolosko *et al.*, 2006; Koronakis *et al.*, 2000; Federici *et al.*, 2004) suggested that the AcrA hairpin and the TolC lower α-helical domain could be involved in complex assembly; a proposal that has been proven by hairpin domain swapping (Stegmeier *et al.*, 2006; Eda *et al.*, 2006).

Although AcrA, AcrB and TolC are proven to form a stable tripartite efflux pump in *E. colli*, some critical points about how the complex works are still uncertain. Touzé (Touzé *et al.*, 2004) suggested the complex is assembled constantly since the assembly occurred independently of the presence of the substrate. Besides, it is estimated that around 500 toxic ethidium molecules are exported every second by each MexA/MexB/OprM pump in *P. aeruginosa* (Narita *et al.*, 2003). On the other hand, Tamura suggested that there is not enough TolC, a multifunctional protein, to form permanent complexes with AcrB and AcrA, although the assembly is substrate independent (Tamura *et al.*, 2005). Instead, he proposed two possibilities: (1) transient complex formation is simply substrate independent; or (2) an unknown intrinsic substrate which facilitates complex formation has not been discovered. As discussed in the previous section, we still do not know how TolC undergoes the conformational change from the close to open state during substrate transportation. Since there is no obvious conformational change in the TolC docking domain of AcrB during the translocation cycle, Murakami (Murakami *et al.*, 2006) proposed the conformational change caused by proton translocation and drug binding may be transmitted, via AcrA, to TolC, thus causing opening of the TolC periplasmic channel. In this case, the AcrA α-helical hairpin may be involved in the opening TolC, via its conformational flexibility (Mikolosko *et al.*, 2006).

Unlike trimeric AcrB and TolC, our knowledge of how many AcrA fit into the tripartite pump remains uncertain. A complex model, based on homology modelling and molecular docking, was proposed (Fernandez-Recio *et al.*, 2004). In this model the lipoyl domain of AcrA docks into the AcrB clefts, whilst three AcrA fit simultaneously into the interprotomer grooves of AcrB and the open state of TolC, so that the predicted protomer stoichiometry is 1:1:1 for the MFP: IMP: OMP components of the tripartite pump (Figure 1.25). In that case, the conformational change caused by proton translocation and drug binding may be transmitted through AcrA via a mutual pushing and pulling movement at the cleft (Murakami *et al.*, 2006), consistent with a recent

report showing the cleft flexibility of AcrB is essential for the pump function (Takasuka and Nikaido, 2007). A recent study also suggested that there is only a single binding site on the TolC protomer (Lobedanz *et al.*, 2007); however, by using *in vivo* crosslinking to map the extent of intermolecular contacts, it showed that AcrA contacted the intramolecular groove between the inner and outer entrance coils of TolC H7/H8/H3 which is different from the contacts with the groove by helices H3/H4/H7 in the previous model.

(a)   (b)
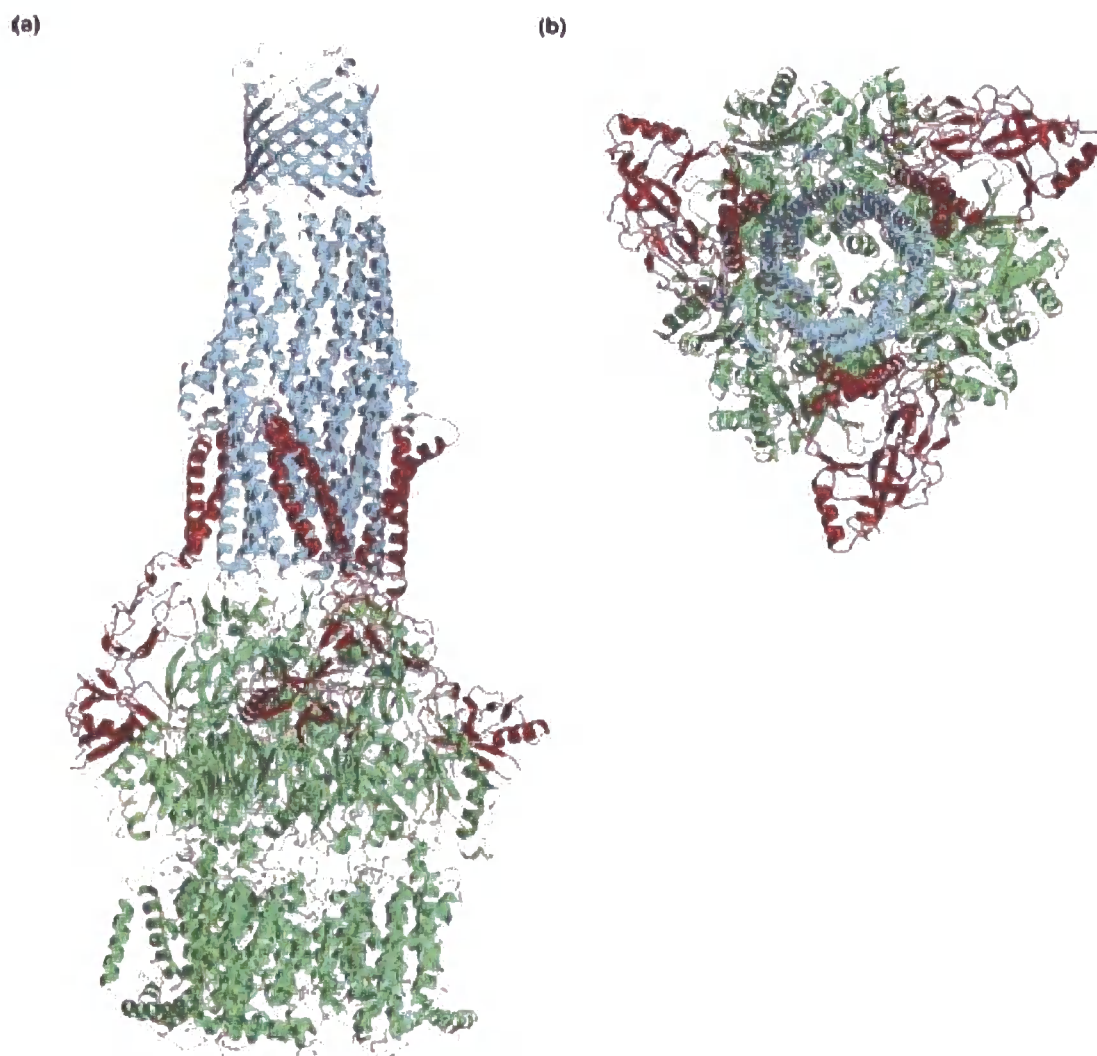
Figure 1.25   **Two sides of view of the assembled tripartite efflux pump model** consisted of AcrA (red), AcrB (green) and TolC (blue). (a) Side view of the complex. (b) Top view of the complex (Fernandez-Recio *et al.*, 2004).

Another model of the tripartite complex predicted a stoichiometry of 3:1:1 for the MFP: IMP: OMP components of the tripartite pump (Figure 1.26) (Higgins *et al.*, 2004). The modelled ring of nine MexA (AcrA homologue) is sufficiently large to form a sheath around the open state TolC and AcrB, stabilizing the complex and making a conduit that spans the entire periplasm. This sheath model may be crucial for MF transporters, without a periplasmic domain, as a scaffold to interact with outer membrane proteins. Isothermal titration calorimetry data indicated the AcrA-AcrB and AcrA-TolC bindings are concentration dependent (Touzé *et al.*, 2004); moreover, it suggested that there would be enough space on each protomer TolC to accommodate up to three membrane fusion proteins (Mikolosko *et al.*, 2006; Higgins *et al.*, 2004).
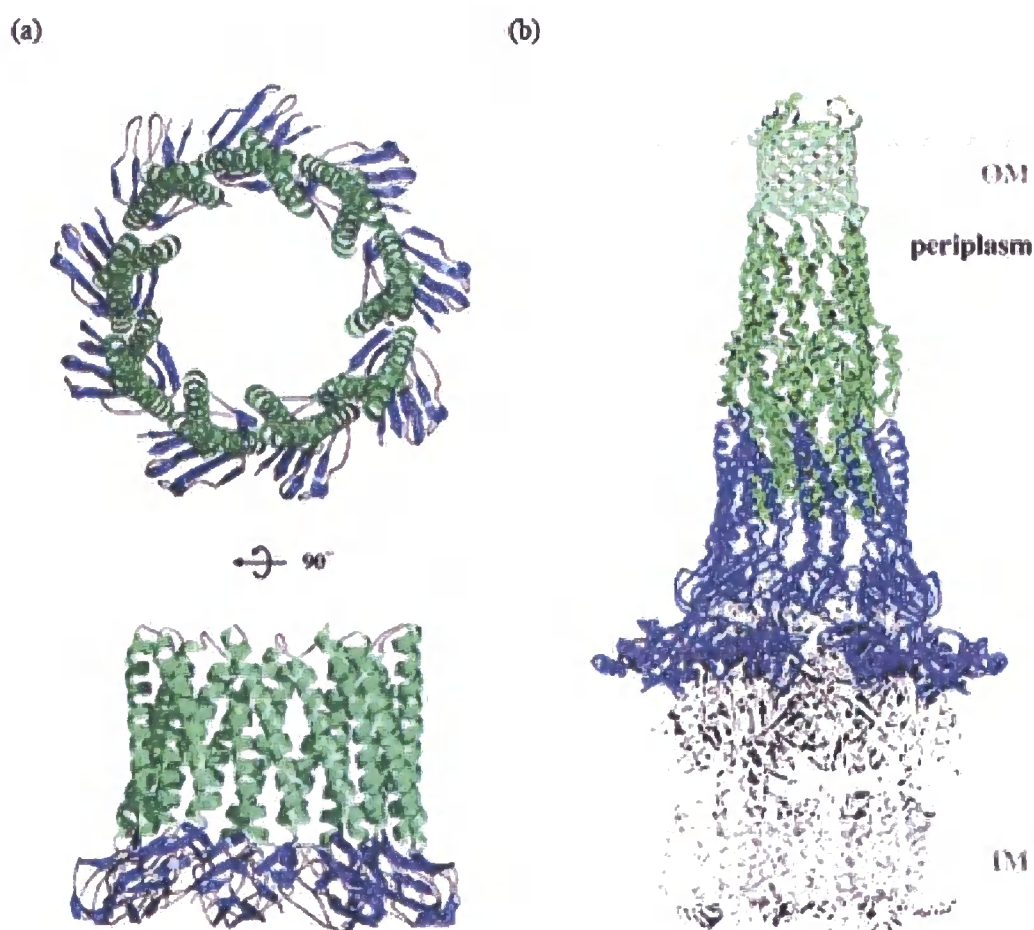
Figure 1.26   The model of the tripartite efflux pump. (a) Two perpendicular views of the nine MexA molecules forming like a ring structure where the α-helices hairpin are in green and the β-strands of the lipoyl domains are in blue. (b) The side view of the complex consisted of AcrA (blue), AcrB (white) and TolC (green) (Higgins *et al.*, 2004).

1.5 What is known about the MacA/MacB/TolC tripartite complex pump

The ABC transporter MacB was first found to confer MacA and TolC dependent resistance to macrolides in *E. coli* cells (Kobayashi *et al.*, 2001). By drug susceptibility test, Kobayashi and co-workers established that *E. coli* strain Kam3 cells (*ΔAcrAB*), harboring a plasmid encoding MacAB had an obvious enchancement in their resistance to macrolides, such as erythromycin, clarithromycin, oleandomycin and azithromycin. Furthermore, Kam3 cells transformed with a plasmid encoding MacAB were found to take up less [^{14}C] erythromycin than ones without MacAB, suggesting active efflux of erythromycin out of the cells. A homologue of the MacA-MacB ABC transporter of *E. coli* was identified in *N. gonorrhoeae* (Rouquette-Loughlin *et al.*, 2005); furthermore, Rouquette and co-workers indicated that *E. coli* cells JMZ120 (*ΔAcrAB*) harboring a plasmid encoding MacAB have higher resistance to erythromycin and azithromycin.

It is predicated, by secondary structure analysis, that MacB putatively has four transmembrane helices, and there is a large periplasmic loop between the transmembrane helix 1 and 2; the NBD domain is located on the N terminal side of the polypeptide and the TMD domain is on the C terminal side. The MacB topology was determined by systematically replacing residues with cysteines and testing for the [^{14}C] NEM binding (Figure 1.27) (Kobayashi *et al.*, 2003). MacA share a sequence identity of 21.3%, and similarity of 38.7% to its homologous protein *E. coli* AcrA, which comprised of an α-helical hairpin domain, a lipoyl domain and a β-barrel domain in its truncated form.

During the course of our study, another revealed that co-reconstitution of MacA and MacB into proteoliposomes increased the steady-state ATPase activity of MacB, suggesting that the MFP as not only serves a scaffold, for assembly of the tripartite complex, but also has a functional role (Tikhonova *et al.*, 2007). We have established that the periplasmic β-strand domain of MacA interacts with the periplasmic domain of MacB to modulate the ATPase activity of its cytoplasmic NBD. Our data suggests that this interaction promotes and stabilizes a conformation of MacB in which the substrate-binding site is outward-facing. This is concomitant with an increase in the resistance of cells to erythromycin that indicates that antibiotic

extrusion is stimulated. This suggests that MacA has a direct role in controlling the pump action to facilitate the transfer of substrates across the inner-membrane.
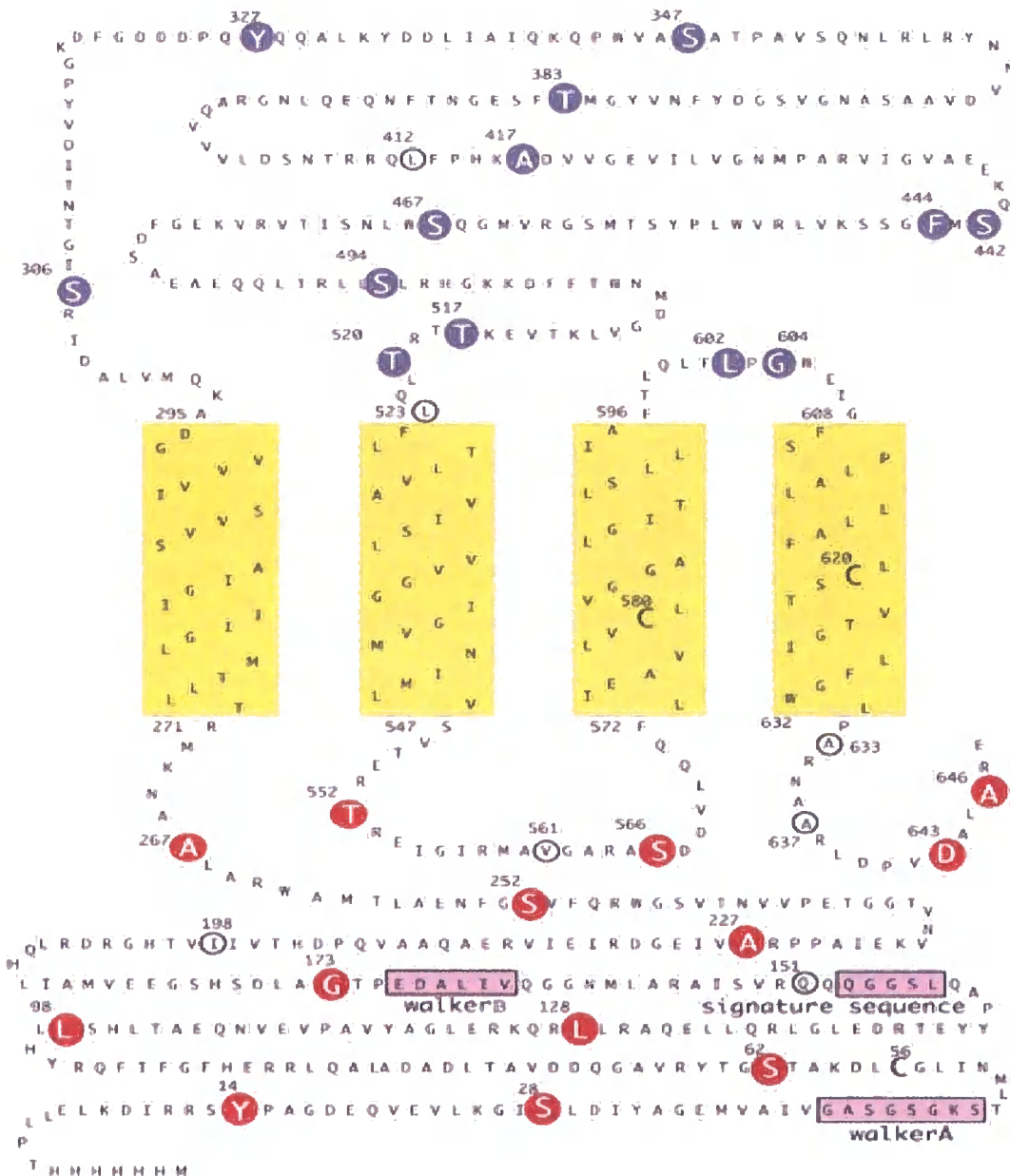
Figure 1.27 **Topology of ABC transporter MacB from E. coli.** Nucleotide binding motifs are boxed in pink squares and the putative transmembrane helices are boxed in yellow squares. Cys[56], replaced by Ala, and the other two intrinsic cysteins are shown in blod letters. NEM labelings which was completely or largely blocked, and not affected by AMS were shown in blue ovals and red ovals, respectively. [14C] NEM which was not reacted regardless of pretreatment or not with AMS was shown in open circles (Kobayashi *et al.*, 2003).

Chapter two: Material and methods

2.1 Web and computer resources

The nucleotide sequences of *E. coli* macB, *macA* and *tolC* were obtained from the National Center for Biotechnology Information (NCBI, www.ncbi.nlm.nih.gov). The Vector NTI Advance 10 (Invitrogen) was used for the design and analysis of oligonucleotides, and for the alignments of DNA and protein sequences for comparison. Protein secondary structures were predicted by Jpred from the University of Dundee (www.compbio.dundee.ac.uk/~www-jpred/). The Dichroweb at Birbeck College (www.cryst.bbk.ac.uk/cdweb/html/home.html) was used as an online Circular Dichroism (CD) data analysis program. The Research Collaboratory for Structural Bioinformatics protein data bank (RCSB, www.rcsb.org/pdb/home/home.do) was used as a source for protein structures.

2.2 Media and antibiotics

Luria-Bertani (LB) medium was used in molecular cloning. *E. coli* cells harboring plasmid(s) were grown in 2xYT medium at 37°C. The antibiotics carbenicillin (100 µg/ml), kanamycin (30 µg/ml) and inducing agent isopropyl-ß-D-thiogalactopyranoside (IPTG) were added as required. Reagents were of analytical molecular biology grade and sourced from Difco, Melford and Sigma unless otherwise stated.

Luria-Bertani (LB) Medium

NaCl	10g
Trypton	10g
Yeast extract	5g
dH_2O	up to 1L

Mueller-Hinton Medium

	Mueller-Hinton powder	23g
	dH₂O	up to 1L

SOC Medium

	NaCl	0.585g
	KCl	0.1865g
	Trypton	20g
	Yeast extract	5g
	dH₂O	up to 970ml

The above were autoclaved and the following filter sterilised components were added.

	1M MgCl₂	10ml
	1M MgSO4	10ml
	2M Glucose	10ml

2x Yeast Tryptone (2x YT) Medium

	NaCl	5g
	Tryptone	16g
	Yeast extract	10g
	dH₂O	up to 1L

2.3 Bacteria strains, media and vectors

The bacterial strains and plasmids used in this study are listed in Table 2.1 and 2.2. *E. coli* strain Novablue(DE3) was used for blue and white screening of constructs. *E. coli* strain C43(DE3) was used for protein expression, and Kam3(DE3) was used for drug resistance tests.

Plasmid pGEM-T Easy vector (Promega) was used for blue and white screening of transformants in molecular cloning, and plasmids pET28a(+), pET21d(+) and pET21a (Novagen) were used as cloning and expression vectors for *macA*, *macB* and *tolC* individually. pETDuet™-1 was used as cloning vector for *macA*, *macB* and *tolC* for growth curve measurements.

Table 2.1 *E. coli* Strains.

Strains	Genotype	Reference
NovaBlue(DE3)	*end*A1 *hsd*R17 ($r_{k12-}m_{k12+}$) *sup*E44 *thi-1* *rec*A1 *gyr*A96 *rel*A1 *lac* [F'*proA*⁺B⁺ *lacl*^{q}ZΔM15::Tn*10* (Tet^R)]	Novagen
C43(DE3)	*E. coli* B F⁻ *omp* had S (r_B^- m_B^-) *dcm*⁺ Tet^r *gal EndA The[argU ileY leuW Cam^r]*	Miroux and Walker, 1996
Kam3(DE3)	Δ*acrAB*	Morita *et al.*, 1998

Table 2.2 Plasmids.

Plasmid	Description	Reference
pGEM-T Easy	Cloning vector compatible with complementation, Ap^R	Promega
pET21a(+)	T7 promoter expression vector, Ap^R	Novagen
pET21d(+)	T7 promoter expression vector, Ap^R	Novagen
pET28a(+)	T7 promoter expression vector, Km^R	Novagen
pET45b(+)	T7 promoter expression vector, Ap^R	Novagen
pETDuet™-1	T7 promoter expression vector with two cloning site, Ap^R	Novagen
pBAD/gIII	pBR322-derived expression vectors for secreted recombinant protein expression	Invitrogen

2.4 Genetic manipulation

2.4.1 Polymerase chain reaction

Polymerase chain reaction (PCR) was achieved by a Qiagen hotstar taq DNA polymerase kit. All components were mixed gently in a PCR tube (Sarstedt) and then the mixture was divided equally into two tubes (each tube contains 50 μl), which were then transferred to a PCR machine. The reagent recipe used for PCR reactions is as follows.

Reagents	Volume (μl)
dH$_2$O	84.5
10X Buffer	10
dNTPs	2
Primer Forward	1
Primer Reverse	1
Hotstar taq	0.5
DNA template	1
Total	100

Primers were synthesised by Invitrogen Custom Primers, on a 50 nmol scale, and desalted. Stock solutions were prepared to a final concentration of 50 pmol/μl and stored at -20°C. Oligonucleotide primers used in this study are listed in Table 2.3.

Table 2.3   **Oligonucleotide primers.** Oligonucleotide names that end with 'F' and 'R' represent primer pairs. **Bold** sequences indicate restriction endonuclease sites. *Italicised* sequences indicate additional nucleotides inserted to keep target sequence in-frame with the start codon. Underlined sequences indicate stop codons incorporated to prevent addition of vector sequences into the transcription. Dotted underlined indicate Shine-Dalgarno (SD) sequences (Shine and Dalgarno, 1974). Shaded sequences indicate part of the leading sequence on pBAD/gIII which permits secretion of recombinant protein into the periplasmic space (Rapoza and Webster, 1993; Chen *et al.*, 1994)

Primers	Nucleotide sequence (5' to 3')	Application
NdeI-macB Forward	**CAT ATG** ACG CCT TTG CTC GAA TTA AAG GAT	Chapter 3
SacI-stop-macB Reverse	**GAG CTC** <u>TCA</u> CTC TCG TGC CAG AGC ATC TAC	Chapter 3
NcoI-macA Forward	**CCA TGG** *GA* GCA TAT GGA GTA TTC AGA AAA TTT	Chapter 4
NcoI-FD20-macA F	**CCA TGG** *GA* GGA CTG ATT ACG TTA TGG AGA ATT	Chapter 4
XhoI-macA Reverse	**CTC GAG** TTG TGC AGC TCC TGG <u>TTT</u> GGC CTC	Chapter 4
NdeI-tolC Forward	**CAT ATG** AAG AAA TTG CTC CCC ATT CTT ATC	Chapter 4
XhoI-RD43tolC Reverse	**CTC GAG** TTC CGG ATT AGT GGA AAC CGG TTT	Chapter 4
NcoI-TolC Forward	**CCA TGG** *GA* AAG AAA TTG CTC CCC ATT CTT ATC	Chapter 5
EcoRI-MacB Forward	**GAA TTC** *G* ACG CCT TTG CTC GAA TTA AAG GAT	Chapter 5
SalI-stop-MacB Reverse	**GTC GAC** <u>TCA</u> CTC TCG TGC CAG AGC ATC TAC	Chapter 5
SalI-SD-macA Forward	**GTC GAC** GAG GAA TAA TAA ATG GCA TAT GGA GTA TTC AGA AAA	Chapter 5
SalI-SD-gIII Seqence F	**GTC GAC** GAG GAA TAA TAA ATG AAA AAA CTG CTG TTC GCG ATT	Chapter 5
Not1-stop-T7tag-macA Reverse	**GCGG CCGC** <u>TCA</u> ACC CAT TTG CTG TCC ACC AGT CAT GCT AGC CAT TTG TGC AGC TCC TGG TTT GGC CTC ACC AAT CAC CAC TTC ATC GC	Chapter 5

2.4.2 DNA preparation and electrophoresis

DNA purification was accomplished by a QIAGEN QIAquick gel extraction kit and a Promega Wizard® SV 96 Plasmid DNA Purification kit. DNA was then visualized on a 1% agarose gel containing adequate ethidium bromide (Sigma). A 1kb DNA ladder (Invitrogen) allowed estimation of DNA fragment size. The Components of 6X DNA loading buffer and 10X TAE (Tris-acetate-EDTA) agarose gel running buffer are listed as below.

6X DNA loading buffer

Bromophenol Blue	0.25%
Glycerol	30%

10X TAE buffer

Tris Base	48.4g
Glacial acetic acid	10.9g
EDTA	2.92g
dH_2O	up to 1L

2.4.3 Cloning

2.4.3.1 Cloning into pGEM-T easy vectors

The pGEM-T easy vector system (Promega) was adopted for the cloning of PCR products. The pGEM-T Easy vector utilises single 3' thymidine overhangs on either side of the multiple cloning site to clone PCR products possessing complimentary 3' adenosine overhang generated by *Taq* DNA polymerase. The pGEM-T easy vector also contains T7 and SP6 RNA polymerase promoters flanking a multiple cloning region within the coding region for the α-peptide of β-galactosidase. The successful insertion of a target gene inactivated β-galactosidase, which could then be identified as white colonies on LB plates containing 5-bromo-4-chloro-3-indolyl-β-D-galactopyranoside (X-Gal) and IPTG.

After cleanup, the amplified DNA was mixed with pGEM-T easy vector and T4 DNA ligase, and then left overnight at 4℃ for ligation. A detailed recipe for the ligation reaction is as follows.

Reagents	Volume (µl)
2x Ligase buffer	5
PCR product	3
pGEM-T easy vector	1
T4 DNA ligase	1
Total	10

The plasmid was then transformed (see 2.4.4 for details) into *E. coli* Novablue(DE3) for the screening of transformants. Novablue cells harboring plasmids were stored with 20% glycerol at -80℃ until used.

2.4.3.2 Cohesive end DNA cloning

Restriction digestion was performed using the relevant restriction enzymes (Promega) in order to generate insert sequences from pGEM-T easy plasmids and linear overexpression vectors. All reagents were added in order as below and incubated for 3 to 5 hours at 37℃ as needed.

Reagents	Volume (µl)
dH$_2$O	35.2
10X Buffer	8
100X BSA	0.8
Enzyme I	3
Enzyme II	3
Plasmid	30
Total	80

Ligations were carried out using the desired linear insert and vector. T4 DNA ligase HC (Invitrogen) catalyses the ligation of the complimentary ends of DNA fragment and linear vector, generated from digestion with the same restriction enzymes. The insert to vector molar ratio can have a significant effect on the outcome of a ligation and subsequent transformation step. Therefore, insert: vector molar ratios between 2 and 6 were utilized in this study. All components were added in the order listed as follows.

Reagents	Volume (µl)
5x Ligase buffer	4
Insert DNA	variable
Vector DNA	variable
T4 DNA ligase	1
Total	10

The reaction mixture was incubated at 16°C for 90 min and then at 4°C overnight.

2.4.4 Transformation into *E. coli*

For transformation with DNA vectors, *E. coli* competent cells were prepared according to the procedure below. A chemical method for the induction of competence in *E. coli* strains is used for cloning.

1 ml of an overnight culture of the desired bacterial strain was inoculated into 100 ml of media and when the cells had reached an OD_{600} of 0.5, they were cooled on ice for 5 min. The cells were then harvested by centrifuge at 5,000 xg for 5 min at 4°C and the supernatant was discarded. The cell pellet was resuspended in ice-cold TFB1 buffer containing 100 mM rubidium chloride, 50 mM manganese chloride, 30 mM potassium acetate, 10 mM calcium chloride, 15% (v/v) glycerol, pH 5.8, and kept on ice for 90 min. The cells were harvested by centrifuge at 4°C and the supernatant was discarded. The cell pellet was resuspended in 4 ml of ice-cold TFB2 buffer containing 10 mM MOPS, 10 mM rubidium chloride, 75 mM calcium chloride, 15% (v/v) glycerol, pH 6.8, and kept on ice for another 45 min. As described above, cells were

harvested, resuspended one more time in 4 ml ice-cold TFB2. Aliquots of 50 µL were flash frozen in a dry ice/ethanol bath and stored at -80°C.

Another method was applied to make *E. coli* strains, for use in protein expression, competent by using $MgCl_2$ and $CaCl_2$. The desired bacterial strain was grown in 5 ml LB media at 37°C for 5 hours and then placed on ice for 5 min before harvesting by centrifuge at 4°C. The cell pellet was resuspended in 1 ml ice-cold 0.1 M $MgCl_2$ and harvested by centrifugation at 5,000 xg for 6 min. As described above, the cell pellet was resuspended in 1 ml ice-cold 0.1 M $CaCl_2$ and harvested by centrifugation. Cells were then carefully resuspended in 200 µl ice-cold 0.1 M $CaCl_2$, and kept on ice for transformation.

Transformation was performed as follows. Competent cells were kept on ice until thawed. After adding 5 µl of plasmid, the competent cells were then put back on ice for a further 30 min. The cells were treated with a 42°C heat shock for 30~90 sec and placed on ice for another 1~5 min. LB plates, with relevant antibiotics, were used for plating out of cells and incubated at 37°C overnight. Cells harboring the desired plasmids were stored at -80°C until used.

2.4.5 λDE3 Lysogenisation of bacterial strains

A λDE3 Lysogenization Kit (Novagen) was applied for the integration of λDE3 prophage into an *E. coli* host cell chromosome, so that the lysogenized host could be used to express heterologous DNA from T7 expression vectors. Host cells were grown in LB media supplemented with 0.2% maltose and 10 mM $MgSO_4$, at 37°C to an OD_{600} of 0.5, and 1–10 µl host cells were taken to mix with 10^8 of pfu of λDE3, 10^8 pfu of helper phage and 10^8 pfu of selection phage. The mixture was incubated at 37°C for 20 min to allow the phage to adsorb to the host and spread on a LB plate. The plate was then incubated at 37°C overnight for cells to grow.

The presence of the λDE3 prophage in host cells was verified with a T7 phage deletion mutant, T7 tester phage. The T7 tester phage can make large halo-like plaques on authentic λDE3 lysogens in the presence of IPTG, while smaller plaques appear in the absence of inducer. In duplicate tubes, 100 µl of infected host cells, at an OD_{600} of 0.5, were added with 100 µl of T7 tester phage (1×10^3 pfu/ml). The mixtures were incubated at room temperature for 10 min to allow phage to adsorb to host and added

with 3 ml of molten agarose (no warmer than 47°C). The contents of one duplicate were poured out onto a LB plate and other one onto a LB plate with 0.4 mM IPTG. After 4 hours of incubation at 37°C the plates were ready to check.

2.5 Protein overexpression and purification

2L flasks of 2xYT media containing relevant antibiotics were inoculated with 8 ml of pre-incubated cells harboring plasmids and incubated at 37°C. 0.2~0.5 mM IPTG was added when the cells density reached an OD_{600} of 0.5. The temperature was adjusted to 25°C and protein overexpression was allowed to proceed overnight.

Cells were harvested by centrifugation at 4°C and resuspended in buffer containing 20 mM Tris-HCl pH 7.5, 500 mM, 10% (v/v) glycerol. Cell paste was added with a tablet of complete protease inhibitor (Roche) and 1000 units of DNAse I (Sigma) before going through a French press twice for cell lysis. Cell debris was removed by centrifugation at 24,000 xg (JA-20 rotor, Beckman), and cell membranes were isolated by ultracentrifugation at 168,000 xg (Type 50.2 Ti rotor, Beckman). Membranes pellets were resuspended in buffer containing 20 mM Tris-HCl pH 7.5, 20% (v/v) glycerol and stored at -80°C until needed.

2.5.1 Immobilized metal affinity chromatography

Protein-His$_6$ was solublized from cell membranes with Triton X-100 (5% [v/v]) (Promega) or n-dodecyl-β-maltopyranoside (DDM) (1% [w/v]) (Melford) and loaded into a 1 ml Ni^{2+} or Cu^{2+} charged HiTrap chelating column (GE Healthcare) by a peristaltic pump (Williamson) at 4°C . The column was then transferred onto an AKTA 10 purifier (GE Healthcare) for further purification steps. The column was washed with, 15-30 times column volume, Tris-HCl buffer containing a suitable concentration of NaCl and imidazole to strip off contaminants and then eluted in buffer containing Tris-HCl pH 7.5, 500 mM NaCl, 500 mM imidazole or 50 mM L-histidine and 0.2% Triton X-100 or 0.05% DDM to isolate the target protein. PD-10 desalting columns (GE Healthcare) were used for desalting and protein was stored at -80°C for further use.

Used columns were washed with distilled water to dispel salts, and 0.1 M EDTA was applied to strip off metal ions. After being washed thoroughly with

distilled water, the columns were recharged with 0.1 M $NiSO_4$ or $CuSO_4$ and kept at 4°C until needed.

2.5.2 Ion exchange chromatography

Protein extraction was followed by ion-exchange purification using a Hitrap Q column (GE Healthcare). The sample was loaded on an AKTA 10 purifier and a salt gradient (10~100% 500 mM NaCl) was used to generate a separate isolated protein peak. Used columns were washed with Tris buffer containing 1 M NaCl and distilled water in order. Columns were stored with 20% ethanol at 4°C.

2.5.3 Detergent exchange

Purified MacB in Triton X-100 (0.2%) was mounted onto a HiTrap Q column and washed with 10 column volume of Tris Buffer 1 (20 mM Tris-HCl buffer, 10 mM NaCl, 10% glycerol, 0.2% DDM, pH 7.5) to remove the Triton X-100 detergent. The column was then washed with an additional 2 column volume of the Tris-HCl buffer 1 containing 0.05% DDM. MacB-DDM was then eluted out with the Tris-HCl buffer 1 containing 100 mM NaCl, and 0.05% DDM.

2.6 Protein Analysis

2.6.1 Electrophoresis

Recombinant proteins were resolved by SDS-PAGE (sodium dodecyl sulfate polyacrylamide gel electrophoresis) to determine the efficiency of overexpression and purification. Proteins were visualized on NuPAGE pre-cast Bis-Tris polyacrylamide gels and gradient 4-12% or 12% gels which were adopted as appropriate. A NuPAGE LDS Sample Buffer (4X) (Invitrogen) was used in protein sample preparation and a Seeblue pre-stained protein marker (Invitrogen) allowed estimation of the protein molecular weight. The recipes for the MOPS running buffer, stain solution and destain solution were as follows:

<u>10X MOPS running buffer</u>

MOPS	104g
Tris base	61g
SDS	10g
EDTA	3g
dH$_2$O	Bring up to 1 Liter

<u>Stain solution</u>

Methanol	40% (v/v)
Acetic acid	10% (v/v)
Coomassie Brilliant Blue R250	0.1% (w/v)
dH$_2$O	50% (v/v)

<u>Destain solution</u>

Methanol	40% (v/v)
Acetic acid	10% (v/v)
dH$_2$O	50% (v/v)

2.6.2 Protein Assay

Protein concentrations were determined using a Coomassie protein assay kit (Bio-Rad). The assay, based on the method of Bradford, is a Coomassie-binding assay where a differential color change of a dye occurs in response to various concentrations of protein. The absorbance maximum for Coomassie Brilliant Blue G-250 dye shifts from 465 nm to 595 nm when it binds to protein and primarily to basic and aromatic amino acid residues, especially arginine (Compton and Jones, 1985).

Protein was diluted 200, 400 and 800 fold into 800µL dH$_2$O to ensure the protein concentration measured was within the working range of the assay (1.2-10µg/ml). The samples were then added with 200 µl of dye reagent concentrate, mixed well, and left at room temperature for 5 min. The absorbance was measured at 595 nm against a dH$_2$O blank. A calibration curve was generated using bovine serum albumin as a standard, and made by plotting the concentration (µg/µl) against the Abs$_{595}$ and fitting the data by linear regression. Both standard and experimental reactions were performed in triplicate and the concentration of protein was then calculated.

2.6.3 Western blot

Protein samples were run using two SDS-PAGE gels by gel electrophoresis in duplicate, applied as experimental gel and control gel. The proteins on the experimental gel were transferred to a PVDF (Polyvinylidene difluoride) membrane (Millipore) where they were probed with the primary antibody. Mouse monoclonal anti-polyhistidine antibody (Sigma), S•Tag™ monoclonal antibody (Novagen) and T7•Tag® monoclonal antibody (Novagen) are used as primary antibodies as appropriate. The PVDF membrane was then incubated with a second antibody, goat anti-mouse immunoglobulin G AP (alkaline phosphatase) conjugate (Bio-Rad), and protein identified a colorimetric AP conjugate substrate kit (Bio-Rad) so that signal was viewable on a film. All buffers involved in the procedure are listed below:

Transfer buffer

Glycine	29g
Tris base	5.8g
SDS	0.37g
Methanol	20% (v/v)
dH_2O	Bring up to 1 Liter

ELISA Wash buffer

Phosphate stock*	30ml
NaCl	8.76g
Tween 20	0.05% (v/v)
dH_2O	Bring up to 1 Liter

*Phosphate stock

KH_2PO_4	6.465g
K_2HPO_4	35.3g
Adjusted to pH 7.4	
dH_2O	Bring up to 1 Liter

Blocking buffer

ELISA Wash buffer	25ml
BSA (Bovine serum albumin)	0.75g

2.7 Biochemical assays

2.7.1 ATPase activity

The ATPase activity was determined using stopped flow spectrometer (PiStar-180 spectrometer, Applied Photophysics). EnzChek phosphate assay, a Pi quantification assay (Molecular Probes) was adopted in the measurements of protein ATPase activity. When Pi is present, PNP (purine nucleoside phosphorylase) can enzymatically convert MESG substrate (2-amino-6-mercapto-7-methylpurine riboside) into ribose 1-phosphate and 2-amino-6-mercapto-7-methylpurine, which results in a spectrophotometric shift in the maximum absorbance from 330 nm to 360 nm (Webb, 1992). A standard curve was generated, using KH_2PO_4 as a standard, by plotting the phosphate concentration (nmoles) against the A_{360} and fitting the data by linear regression. The reaction components are as follows:

Reagents	Volume (μl)
dH_2O	740μl - x
20X Reaction buffer	50
MESG substrate	200
KH_2PO_4	x
PNP	10
Total	1000

Measurements at A_{360} were recorded continuously when protein and ATP were mixed from two drive syringes. The reaction temperature was controlled at 25°C by a water bath (Jasco). The recipes for the two reservoirs are as follows:

Protein sample syringe reservoir

Reagents	Volume (μl)
dH_2O	740μl - x
20X Reaction buffer	50
MESG substrate	200
PNP	10
Protein (s)	x
Total	1000

<u>Substrate sample syringe reservoir</u>

Reagents	Volume (µl)
dH$_2$O	740µl - y
20X Reaction buffer	50
MESG substrate	200
PNP	10
ATP	y
Total	1000

The data were analyzed by fitting a single exponential plus slope equation:

$$f(x) = a*\exp(-kx) + bx + c$$

Once the a, b, c, k values were determined, the Abs$_{360}$ values were then collected and calculated into Pi concentration. The traces were plotted the phosphate concentration against time using Sigma Plot.

2.7.2 Equilibrium binding of [^{14}C] erythromycin

50 µg of purified protein was incubated with 1, 5 and 10 µM of hot [N-methyl-^{14}C] erythromycin (48.8 mCi/mmol, Perkin Elmer Life sciences, USA) and cold erythromycin for 30 min. The incubation was carried out in glass tubes in a final volume of 500 µl of buffer containing 10 mM Tris-HCl pH 7.4, 0.05% DDM. The samples were incubated at room temperature in the dark for 45 min, and rapidly filtered through 0.22 µM nitrocellulose filters (Whatmann), which were pre-equilibrated overnight in ice-cold wash buffer containing 10 mM Tris-HCl pH 7.4, 150 mM KCl, 5 mM MgCl$_2$. The filters were back-to-back washed once more with 3 ml of ice-cold wash buffer and soaked in scintillation fluid for at least 3 hours until totally dissolved. Subsequently, filter-retained radioactivity was measured by liquid scintillation counting using the scintillant Ultima Gold XR (Perkin Elmer Life Sciences, USA). Non-specific binding to MacB was determined as the amount of [^{14}C] erythromycin bound to half molar quantities of 12 transmembrane helices-containing sugar transporter GalP (Velamakanni *et al.*, 2007), and was less than 30% of total binding.

2.7.3 Pull-down Assay

Pull-down assays were used to determine if there was a physical interaction between two proteins *in vitro*. In a pull-down assay, a tagged bait protein is captured on an immobilized affinity ligand (Ni^{2+} in this study) specific for the tag. The immobilized bait protein can be incubated with putative prey proteins to capture the one that interacts with the bait protein. Membrane pellets containing preyed protein with an S-tag, a 15 residues tag sequence, were dissolved in detergent and mixed with purified bait protein with a polyHis tag. The mixture was loaded into a Ni^{2+} charged Hitrap chelating column (GE Healthcare), so that the bait protein could be immobilised on the column, along with the prey protein if there was an interaction between them. The column was then washed with 15-20 column volumes of 20 mM Tris-HCl buffer containing reasonably high imidazole (75-100 mM) to eliminate any false positive results due to non-specific interactions. The bait-prey complex was eluted with 20 mM Tris-HCl buffer containing 500 mM imidazole; followed by the gel electrophoresis to visualize the bait and prey proteins. A Western blot was carried out using S•Tag monoclonal antibody (Novagen) to probe the prey protein, confirmating its identity. To eliminate false positive non-specific interactions between the prey protein and the column, a control experiment was done in a similar manner without the bait protein.

2.7.4 Protein cross-linking

Crosslinker Dithiobis succinimidyl propionate (DSP) (Figure 2.1) was adopted for crosslinking of MacB. It contains an amine-reactive N-hydroxysuccinimide (NHS) ester at each end of an 8-carbon spacer arm. NHS esters react with primary amines at pH 7-9 to form stable amide bonds, along with release of the N-hydroxysuccinimide leaving group. DMA and DMS (Figure 2.1) belong to homobifunctional imidoester cross-linkers. The imidoester functional group is available for the modification of primary amines and has minimal cross reactivity toward other nucleophilic groups in proteins.
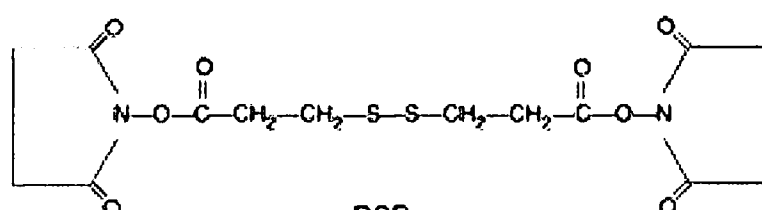
DSP

[Dithiobis(succinimidylpropionate)]

also know as Lomant's Reagent

MW 404.42

Spacer Arm Length 12Å
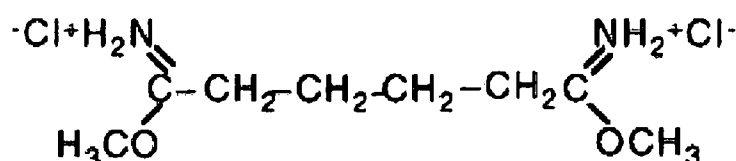
DMA

M.W. 245.15

Spacer Arm 8.6Å
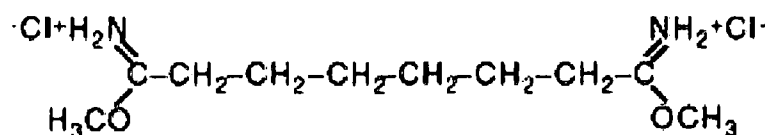
DMS

M.W. 273.20

Spacer Arm 11Å

Figure 2.1   Structures of crosslinkers.

2 mg/ml MacB in buffer containing 50 mM Na$_2$HPO$_4$ pH 7.5, 50 mM NaCl, 10% glycerol was incubated with 1, 2, 10, 20, 50, 100-fold excess of DSP concentration for 30 min at 30°C. To stop the reaction, 1 M Tris-HCl was added to the samples and boiled for 3 min before being analyzed by gel electrophoresis. Pre-stained marker Seeblue (Invitrogen) and bench marker (Invitrogen) were used for estimation of protein molecular weight.

2 mg/ml MacA, 1 mg/ml MacB or MacA-MacB was also crosslinked by 5 mM DMA or DMS individually for 60 min at room temperature, and analyzed in an analogous manner to that for DSP.

2.7.5 Phenol-sulfuric acid colorimetric assay

Detergents are essential for membrane protein isolation and purification. DDM, a glycosidic nonionic detergent, has been used for the membrane proteins manipulated in this study. A rapid, simple and sensitive procedure for the quantification of glycosidic and bile salt-based detergents has been presented (Urbani and Warne, 2005). This method can quantify sugar or cholate moieties by colorimetric reactions with phenol and sulfuric acid, which can be used to quantify DDM. Furfural derivatives are generated when sugars are dehydrated in concentrated sulfuric acid; following a condensation reaction in the presence of phenol, an aromatic molecule, the *p*-semiquinonoid chromogen is formed, which has as visible absorbance at 490 nm. The colorimetric assay was undertaken to quantify the DDM contribution in the MacB-DDM complex via a similar approach to a previous report (Butler *et al*, 2004).

The MacB-DDM complex and processing buffer, 20 mM Tirs HCl, 50 mM NaCl, 10% glycerol, with or without 0.2% DDM, pH 7.5, were collected after a detergent exchange and the buffer with DDM served as blank for correction for the background in absorbance measurements. The MacB concentration was determined as described in section 2.6.2 before assaying, which enable to estimate the total amount of DDM, from MacB-DDM complex and DDM micelles in the buffer, and keep it in the effective range the standard curve (0-60μg in 60μL). The MacB-DDM complex was diluted as necessary into the original purification buffer (Tris-HCl buffer) without DDM to make a final volume of 60μL. The sample was fist mixed with 300 μL phenol (5%, w/v), then 720 μL concentrated sulphuric acid was carefully added and mixed

well by votexing with the tube cap closed. One thing needs to be paid attention to is the strong exothermic reaction that occurs on the addition of concentrated sulfuric acid, during which the temperature can go up to 110-120°C. The mixture was allowed to cool down at room temperature for 20 min and transferred to a cuvette for the absorbance measurements at 490 nm using buffer as a background blank. A standard curve was generated using DDM as a standard, and made by plotting the DDM concentration ($\mu g/60\mu L$) against the Abs_{490}, fitting the data by linear regression. The molar ratio of protein to detergent was then calculated.

2.7.6 Growth curve measurements

In order to test the ability of the proteins to assemble into functional transporters that confer resistance in *E. coli*, drug susceptibility assays were undertaken by measuring cell growth curves in the presence of erythromycin. Cells of *E. coli* strain Kam3(DE3), harboring plasmids or blank vectors, were grown in 2xYT media at 37°C, with shaking at 200 rpm. 0.05-0.1 mM IPTG was added when the cells density reached an OD_{600} of 0.5-0.6. Cells were grown for overnight and diluted into media, incubated with the antibiotic erythromycin at the concentrations of 100 $\mu g/ml$. Cells growth curves were recorded over the next 12 hours. For experiments to measure the loss in growth due to erythromycin, cells were grown for 3 hours in the absence and presence of 50 $\mu g/ml$ erythromycin and the relative growth is the ratio of the OD_{600} values.

2.8 Structural approaches

2.8.1 Dynamic light scattering (DLS)

A Zetasizer Nano instrument (Malvern) was used for DLS analyses in order to determine particle distribution and molecule weight for the MacB protein. The protein was dialyzed against buffer containing 20 mM Tris-HCl pH 7.5, 100 mM NaCl, 1% glycerol, and 0.005% βDDM overnight at 4°C and diluted to a final concentration of 1 mg/ml. The sample was centrifuged at 14,000 xg for 10 min in order to check protein's stability before analysis. The data for the protein sample and buffer itself were recorded at 4°C and 16°C.

2.8.2 Analytical size exclusion chromatography (SEC)

A superdex 200 PC 3.2/30 column (GE Healthcare) was used in this experiment. The column was equilibrated with degassed and filtered buffer containing 20 mM Tris-HCl pH 7.5, 300 mM NaCl, 10% glycerol and 0.05% DDM for 2 column volume. The sample was filtered through a 0.22 μm filter (Millipore) and centrifuged at 14,000 xg for 5 min before loading onto a column. The sample injection was accomplished by using a 100 μl loop and a 1 ml syringe. A high molecular weight gel filtration calibration kit containing aldolase (Mr 158 000), catalase (Mr 232 000), ferritin (Mr 440 000), thyroglobulin (Mr 669 000) and blue dextran 2000 served as standards for estimation of molecular weight of the protein. The used column was washed with distilled water and stored with 20% ethanol at 4°C.

The Mr of protein was calculated from a calibration curve generated by plotting the log values of the Mr of the standards against their gel-phase distribution coefficient values (K_{av}). The K_{av} values were calculated using their elution volumes (V_e), total bed volume of 2.4 ml (V_t) and the void volume (V_o) according to the equation K_{av}= (V_e-V_o)/(V_c-V_o), where V_c represents total column volume.

2.8.3 Analytical ultracentrifugation (AUC)

AUC is one of the most powerful and versatile techniques for the quantitative characterisation of macromolecular associations in solution (Howlett *et al.*, 2006). Sedimentation equilibrium measurements were performed using a Beckman Optima XL-A analytical ultracentrifuge equipped with both absorbance and interference optics,

allowing optical signals to be measured as a function of radial distance. 100 μL of 0.2 mg/ml MacB in buffer 1 (20 mM Tris 8.0 150 mM NaCl, 1% glycerol and 0.006% βDDM) supplemented with 10%, 25% or 50% D_2O was placed in the sample compartment of a epon double-sector centerpiece and 110 μl buffer 1 was placed in the reference compartment. The samples were centrifuged at 10°C and 10,000, 15,000 and 25,000 rpm using an An60-Ti rotor. Scans were acquired using the absorbance optical system 15 hours after the start of the experiment and in 1 hour intervals until equilibrium was attained. The buffer densities and partial specific volume of MacB were calculated using the program SEDNTERP (Laue *et al.*, 1992) and the partial specific volume of βDDM was taken as 0.809 cm^3/g (Peterson *et al.*, 1988). The equilibrium data was analyzed using SEDPHAT (Vistica *et al.*, 2004). Sedimentation velocity measurements have been performed using the same hardware at 55,000 rpm at 10°C. The measurements were performed in buffer 1.

2.8.4 Circular dichroism (CD) spectroscopy

Circular Dichroism (CD) is a valuable technique for examining the structure of proteins in solution (Kelly *et* al., 2005). CD analysis was used to determine the secondary structure compositions of proteins from the peptide bond region in this study. CD spectroscopy and data collection was achieved using a CD spectrometer, with a Xe arc light source (Jasco J-810). It is difficult to make measurements below 180 nm by a conventional CD instrument since the intensity of the radiation falls off in this region; besides, both the N_2 used for purging the sample compartment and H_2O solvent absorb significantly. Protein secondary structure observations by CD spectroscopy occur in the region of 190-260 nm and the absorption is due to the peptide bond. There is a broad but weak signal centred around 220 nm based on n to π transition and a more intense π to π^* transition centred around 190 nm. By determining the CD spectrum in this range, the secondary structure of a protein can be determined.

The priority for CD spectroscopy analysis is to keep the total absorbance of the sample within reasonable bounds in order to avoid excessive noise. The signal/noise ratio for CD is theoretically a maximum when the absorbance is 0.869 (Fasman, 1996). The absorbance of the sample is conveniently monitored by the trace of the High Tension voltage (the voltage applied to the photomultiplier). For reliable data, this

should be less than 700 V, but this value will depend on the particular instrument being used.

The NaCl and imidazole in the protein samples were reduced as much as possible by dialysis to minimize the strong absorbance from the components of the buffer. The spectrum of proteins in 20 mM Tris buffer, 20 mM NaF, pH 7.5 was recorded from 260 nm to 190 nm, six times and averaged; from this average spectrum the baseline spectrum for buffer itself was substracted to get the final spectrum. Data was then input into the online server Dichroweb at Birbeck College (Whitmore and Wallace, 2004) and analyzed by a number of algorithms, including SELCON3, CDSSTR and CONTIN-LL.

2.8.5 Electrospray (ES) mass spectrometry

MacB sample purification and preparation were accomplished as described in section 3.1. Analyses were performed using a nanoflow ES mass spectrometers Q-ToF2 (Micromass) modified for transmission and isolation of high mass ions (Sobott *et al.*, 2002). The following experimental parameters were used to record the mass spectra of 2 mg/ml MacB on the Q-ToF2 instrument: a needle voltage of 1.5 kV and an MCP of 2350 V.

2.8.6 Atomic force microscope (AFM)

MacB sample purification and preparation were accomplished as described in section 3.1. 1 mg/ml MacB in buffer containing 20 mM Tris pH 7.5, 50 mM NaCl, 10% glycerol and 0.05% βDDM was diluted 1000 times to a final concentration of 1 μg/ml, and 45 μl of the sample was allowed to adsorb to freshly cleaved mica. After 10 min incubation, the sample was washed with Milli-Q water and dried under nitrogen. Imaging was performed with a Multimode atomic force microscope (Digital Instruments, Santa Barbara, CA). Samples were imaged in air and experiments were carried out in tapping mode. The silicon cantilevers containing a diamond-like extra tip had a drive frequency of ≈ 300 kHz and a specified spring constant of 40 N/m (MikroMasch, Portland, OR). The applied imaging force was kept as low as possible (target amplitude ≈ 1.6-1.8 V and amplitude set-point ≈ 1.3-1.5 V).

The molecular volumes of the protein particles were determined from particle dimensions based on AFM images. After adsorption of the receptors onto the mica support, the particles adopt the shape of a spherical cap. The heights and half-height radii were measured from multiple cross-sections of the same particle, and the molecular volume was calculated by using the following equation:

$$V_m = (\pi h/6)(3r^2 + h^2) \tag{1}$$

where h is the particle height and r is the radius (Barrera *et al.*, 2005; Schneider *et al.*, 1998).

Molecular volume based on molecular mass was calculated by using the equation

$$V_c = (M_0/N_0)(V_1 + dV_2) \tag{2}$$

where M_0 is the molecular mass, N_0 is Avogadro's number, V_1 and V_2 are the partial specific volumes of particle and water, respectively, and d is the extent of protein hydration (Barrera *et al.*, 2005; Schneider *et al.*, 1998). We used the value of 0.74 cm^3/g for the partial specific volumes of protein, and 0.4 g of water per g of protein for the extent of protein hydration (Grant, 1957). Using automated recognition of proteins (Barrera *et al.*, 2007; Barrera *et al.*, 2008), it was calculated the molecular volume of isolated particles as described above.

2.8.7 Transmission electron microscope (TEM)

MacA and MacB sample purifications and preparations were accomplished as described in section 4.1 and 3.1 respectively. Protein samples in buffer containing 20 mM Tris pH 7.5, 500 mM NaCl, 10% glycerol and 0.2% TX-100 were pipetted onto the carbon-coated side of a grid. After 1 min, filter paper was used to take off excessive liquid without touching the grid. The grid was then negatively stained using 1% uranyl acetate for 30 seconds. Filter paper was used to take off excess liquid without touching the grid. The gird was then examined using a transmission electron microscope instrument (Hitachi).

2.8.8 Crystallization

Crystallization is an important tool for the determination of the structure of biological macromolecules through the use of X-ray diffraction for analyzing the atomic arrangement of crystals. Proteins were initially screened with commercial sparse matrix screens that provided a broad range of parameters to identify good crystallization conditions. Once an initial condition, good for protein crystals to grow, was found, modification of the crystallization conditions was then carried on to obtain crystals that are of X-ray diffraction quality.

2.8.8.1 Sitting drops technique

Crystallization trials were undertaken using the vapour diffusion sitting drop method on Greiner crystallization plates, which have 96 round wells; crystallization conditions were screened automatically using a Cartesian robot. The volume of each screen drop was around 50 nl. After setting up the drops the whole tray was sealed and spun at 1000 xg for 1 min in order to pull the drops into good shape at the bottom of the well. Crystals were grown at 18 °C and their development was monitored intermittent periods by light microscopy.

2.8.8.2 Hanging drops technique

Crystallization trials were carried out using 24-well crystallization plates (Nextal). A droplet of protein solution was mixed with crystallization reagent on a platform inverted over the reservoir in vapor equilibration with the reagent. The initial reagent concentration in the droplet is less than that in the reservoir but will eventually reach equilibrium and settle between the drop and the reservoir when the reservoir pulls water from the droplet in the vapor phase. During this equilibration process, the sample is also concentrated, increasing the relative supersaturation of the sample in the drop. The plates were incubated at 18°C and the droplets were monitored by light microscopy to identify different stages of crystallization.

Chapter three: Determination of the MacB oligomeric state

The ABC transporter MacB has been shown to confer macrolides resistance in the presence of TolC via active drug efflux (Kobayashi *et al.*, 2001). MacB has a topology that consists of one N-terminal cytoplasmic nucleotide binding domain, four transmembrane helices and one large periplasmic loop between the helix 1 and 2. The MacB topology was determined by systematically replacing residues with cysteines and testing for the [^{14}C] NEM binding (Figure 1.27) (Kobayashi *et al.*, 2003)

Most ABC transporter, have been found to consist of four domains: two nucleotide binding domains (NBD) that serve as engines for ATP hydrolysis, which is coupled to active transport, and two transmembrane domains (TMD) that are believed to constitute the transport pathway. The 3D structures of such as Sav1866, MsbA and ModB$_2$C$_2$A are in an agreement with a four domain organization in full-size ABC transporters (Dawson and Locher, 2006; Hollenstein *et al.*, 2007). Well studied ABC exporters such as LmrA, Sav1866 and MsbA are believed to form a full transporter with twelve transmembrane helices; six helices being contributed by each subunit (Borges-Walmsley *et al.*, 2003). After detergent solubilization the ABC transporter BmrA, from *Bacillus subtilis*, was found to be a dimer using analytical ultracentrifugation (Ravaud *et al.*, 2006). Exceptionally, MacB has only "four" transmembrane helices rather than six, leading to the question of MacB's functional oligomeric state. In the tripartite efflux pump AcrA-AcrB-TolC, AcrB and TolC are proven to form trimers, whereas the AcrA oligomeric state is uncertain. MacB confers TolC-dependent macrolide resistance, which might indicate that MacB also forms trimers in order to coordinate TolC.

In this chapter, I report on the development of procedures that provide a good yield and purity of MacB, which has enabled detailed characterisation of its functional and structural states. Size exclusion chromatography (SEC), analytical ultracentrifugation (AUC), electro-spray mass spectrometry and atomic force microscope (AFM) were applied to discover the oligomeric state of MacB when in a detergent-solubilized state.

3.1 MacB-His₆ construction and production

Cells of the *E. coli* strain Novablue, derived from *E. coli* K12, served as the source of chromosomal DNA for the *macA* and *macB* genes. The completed genome of *E. coli* is available from the NCBI database, as a source of sequence information for the genetic manipulation of these genes (section 2.1). A list of primers, vector plasmids and *E. coli* strains used in the study can be found in section 2.3 and 2.4. The *macB* gene of *E. coli* was amplified by PCR, incorporating artificial restriction enzyme sites, suitable for cloning into a chemically inducible expression vector. The detailed methods for the construction can be found in section 2.4, genetic manipulation.

The forward primer, NdeI-macB, and reverse primer, SacI-stop-macB, were designed to incorporate the restriction enzyme (RE) sites, *NdeI* and *SacI*, at the 5' and 3' ends of the amplified *macB*, respectively. Successful PCR amplification of the *macB* sequence was shown to be consistent with the predicted size on an agarose gel (Figure 3.1a). The amplified *macB* gene was extracted and purified from the agarose gel and ligated into the A-T propagation pGEM-T Easy vector. The ligation mixture was then transformed into chemically competent *E. coli* NovaBlue. The pET28a(+) expression vectors and the recombinant pGEM-T Easy vectors were digested with *NdeI* and *SacI* simultaneously, and the digests were then separated by gel electrophoresis. The *macB* gene and linear pET28a were cut out and purified; followed by cohesive end ligation using T4 DNA ligase. The ligation mixture was transformed into chemically competent *E. coli* NovaBlue. Plasmid DNA purified from recombinant colonies was digested with *NdeI* and *SacI* to confirm the presence of inserted DNA (Figure 3.1b).

The pET28a-*mac*B expression construct was transformed into the *E. coli* strain C43(DE3) (Miroux and Walker, 1996) for protein production. The protocols for protein expression and for harvesting cell membranes were as described in section 2.5. The cell membranes were dissolved in 20 mM Tris buffer pH 7.5, 50 mM NaCl, 10 mM imidazole, 1 mM THP, 10% glycerol and 5% Triton X-100 on a rotary shaker overnight.

MacB-His₆ was purified by metal affinity chromatography using HiTrap Cu^{2+} column (section 2.5.1). MacB-His₆ was eluted in buffer containing 20 mM Tris-HCl pH 7.5, 500 mM NaCl, 10% glycerol, 50 mM L-histidine and 0.2% Triton X-100. The buffer was exchanged into 20 mM Tris-HCl pH 7.5, 10 mM NaCl, 10% glycerol, and

0.2% Triton X-100 by using PD-10 columns prior to the second purification by ion exchange chromatography using HiTrap Q column (section 2.5.2).

The efficiency of expression and purification of MacB-His$_6$ was determined by gel electrophoresis (section 2.6.1) (Figure 3.2). The migration of the major protein band (lanes 2 to 8) is between the 51 kDa and 64 kDa of the SeeBlue protein marker (lane 1), which is marginally different from the MacB-His$_6$ calculated molecular weight of 72.97 kDa. The identification of MacB-His$_6$ protein was confirmed by Western blot, as shown in figure 3.2.
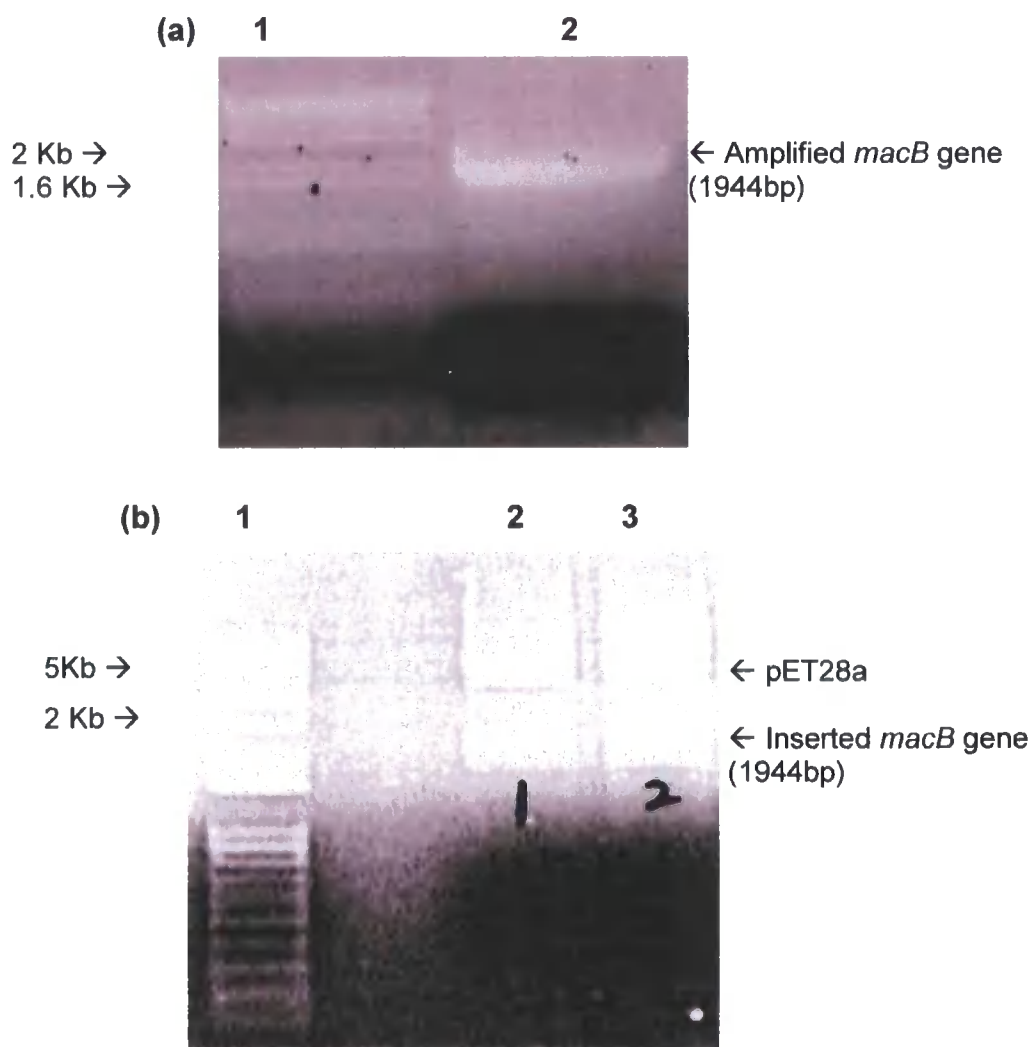
Figure 3.1   **pET28a/macB construction** (a) PCR amplification of *macB* gene from *E.coli* K-12. Lane 1= DNA ladder. Lane 2= the amplified *macB* gene. (b) Restriction enzyme digestion analysis of the pET28a/*macB* plasmid. Lane 1= ladder. Lanes 2-3 indicate the presence of the *macB* gene.
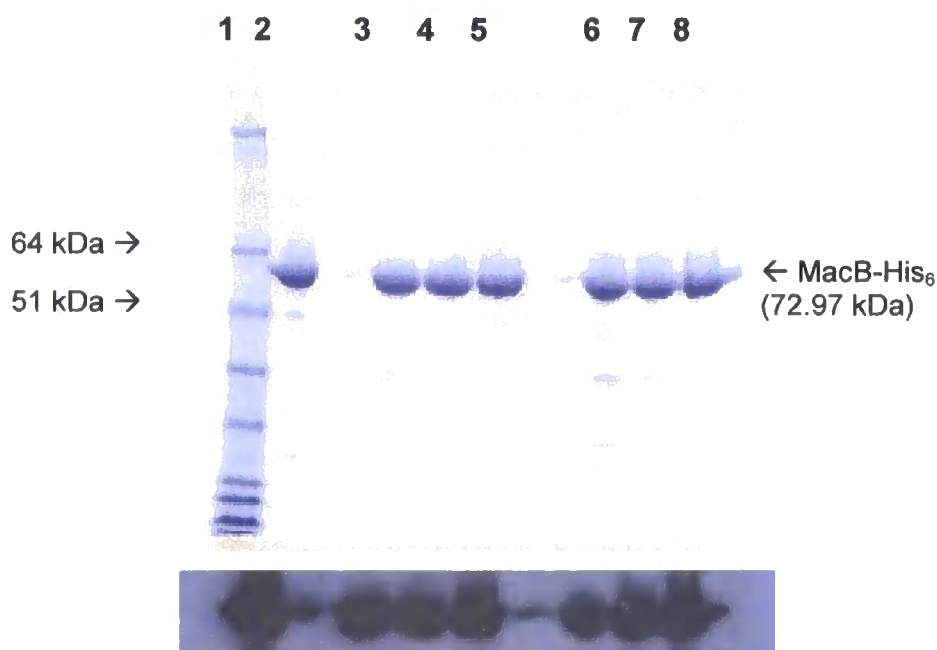
Figure 3.2 **SDS-PAGE of MacB-His₆.** Lane 1= protein molecular weight (M_r) marker. Lanes 2-8 indicate the MacB proteins. The signals for MacB-His₆ were shown on the X-ray film by using Western blot.

3.2 Size exclusion chromatography of MacB

Analytical SEC was used to determine the molecular weight of MacB in order to investigate its oligomeric state. The analysis was performed on an AKTA using a Superdex200PC3.2/30 column as described previously (section 2.8.2). The elution profiles of MacB were monitored using a 280 nm UV detector.

Blue dextran was applied to the column to determine the void volumn (V_0) of the column. The protein molecular mass standards included aldolase, catalase, ferritin and thyroglobin, which were run individually in order to determinate the K_{av} for each stardard (Table 3.1), which was then used to generate a calibration curve ($r^2 > 0.99$) (Figure 3.3).

Standard	Mr (kDa)	Concentration (mg/ml)	V_e (ml)	$K_{av}=(V_c-V_0)/(V_c-V_0)$
Blue dextran	--	2	1.01	--
Aldolase	158	5	1.59	0.42
Catalase	232	5	1.48	0.34
Ferritin	440	2	1.32	0.22
Thyroglobin	669	3	1.18	0.12

Table 3.1   **Generation of the gel-phase distribution coefficient values (K_{av}).**
$(K_{av}) = (V_e-V_0)/(V_c-V_0)$, V_e = elution volume for the protein, V_0 = column void volume and V_c = geometric column volume (2.4 ml).
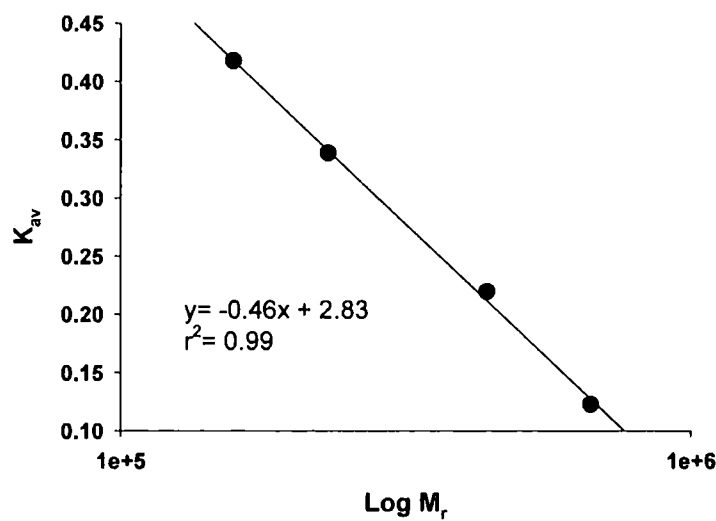
Figure 3.3   **A molecular weitht calibration curve** generated for protein standards on an analytical Superdex 200 PC 3.2/30 gel filtration column.
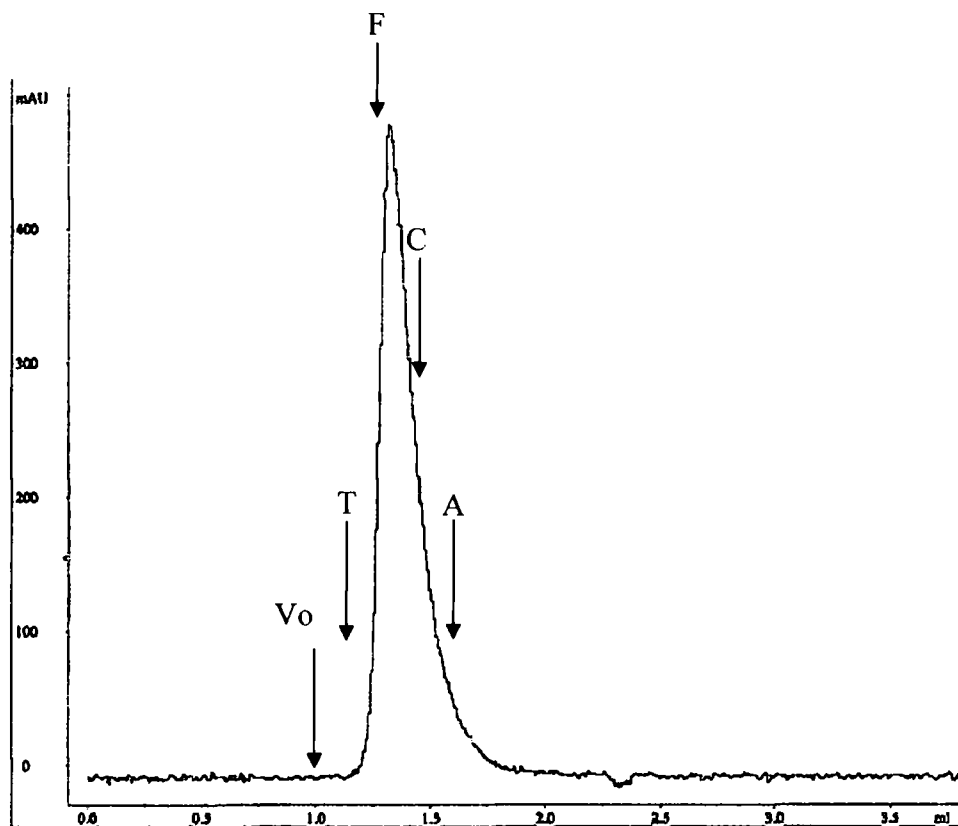
Figure 3.4   **Elution profile of MacB-His$_6$ on the analytical gel filtration column** Superdex 200 PC 3.2/30. V_0 = column void volume obtained by blue dextran, T= thyroglobin (669 kDa), F= ferritin (440 kDa), C= catalase (232 kDa) and A= aldolase (158 kDa).

MacB was first extracted and purified in Triton X-100; however, Triton X-100 absorbed strongly at 280 nm, making it impossible to monitor the MacB elution profile. Thus, MacB-His$_6$ was exchanged into buffer containing Tris-HCl pH 7.5, 300 mM NaCl, 10% glycerol and 0.2% DDM before being analyzed by SEC (section 2.5.3). Using an Enzchek Assay, MacB was confirmed to retain ATPase activity and retained activity after detergent exchange (data not shown). The MacB-His$_6$ was applied to the column and it showed a sharp peak at an elution volume of approximate 1.32 ml (V_e), giving a K_{av} value of 0.223, corresponding to a Mr for the MacB-His$_6$/DDM complex of 415 kDa (Figure 3.4). The average Mr for MacB-His$_6$/DDM complex calculated from 2 runs in the solution is 410 kDa ± 10 kDa.

3.3 Quantification of DDM contribution in MacB/DDM complex

Considering that MacB was in a detergent solubilized state, the detergent could make a significant contribution to the Mr of the protein-detergent complex (Ravaud *et al.*, 2006). In order to determine the contribution of DDM in the MacB/DDM complex, a phenol-sulfuric acid colorimetric assay was applied to quantify the DDM contribution (section 2.7.5). A standard curve containing six points between 0 µg to 20 µg of DDM was produced with a line of best fit ($r^2 > 0.99$) (Figure 3.5).
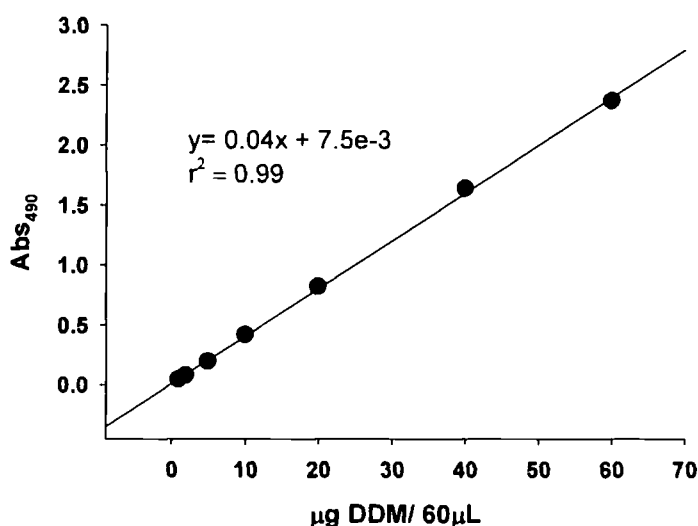
Figure 3.5   Standard curve of DDM quantity by using the colorimetric assay.

A MacB protein sample and its elution buffer were obtained from the same batch used for the SEC analysis in the previous section, and used to determine the quantity of bound DDM using a colorimetric assay. This MacB sample was determined to have concentration of 0.85 mg/ml using coomassie protein assay kit (section 2.6.2). The colorimetric assays were performed in triplicate and two dilutions (1:10 and 1:20) to ensure that the amount of DDM detected was within the range of the standard curve. Using the equation generated from the standard curve, the amount of DDM bound by MacB was determined spectrometrically to be 1.2 g DDM/g MacB (Table 3.2), which is equivalent to a MacB: DDM molar ratio of 1: 171. Ravaud *et al* in 2006 concluded that the ABC transporter BmrA is a dimer in the detergent solubilized state and that the amount of DDM bound by BmrA was about 1.5 g DDM/g BmrA. BmrA consists of six transmembrane α-helices whereas MacB has only four transmembrane α-helices,

suggesting that the DDM: MacB ratio is reasonable. These results indicate that for every MacB molecule, bound DDM adds a further 88 kDa to the Mr of the complex, resulting in the Mr for a MacB monomer, with bound DDM, to be about 161 kDa. However, we should also consider that there would be a quantity of bound lipid, which would make a further contribution to the total Mr of the complex but this is probably less significant (Ravaud et al., 2006). The estimated Mr of 410 kDa for the complex from the SEC analysis suggested that there are at least two MacB protomers in the MacB/DDM/lipid complex, but the Mr of 410 kDa is slightly higher than expected for the dimer. The size estimate from the SEC analysis is on the basis of the radius of gyration. If the particle is elongated, it tends to overestimate the size of the particle. Since MacB has a membrane domain that is sandwiched by cytoplasmic and periplasmic domain it is likely to have an elongated structure.

1 to 10 Dilution (MacB 5.1 µg/60 µL sample volume)					Average MacB: DDM (g/g)
--	Abs_{490} (blank off)	Bound DDM (µg)	Average of bound DDM (µg)	MacB: DDM (g/g)	
1	0.2753	6.73			
2	0.2511	6.12	6.31	1: 1.24	1: 1.2
3	0.2489	6.07			
1 to 20 Dilution (MacB 2.55 µg/60 µL sample volume)					Average MacB: DDM (Molar/Molar)
--	Abs_{490} (blank off)	Bound DDM (µg)	Average amount of DDM (µg)	MacB: DDM (g/g)	
1	0.1277	3.02			
2	0.1201	2.83	3.01	1: 1.18	1: 171
3	0.1411	3.36			

Table 3.2   The MacB/DDM ratio in the protein-detergent complex. Both the g/g and Molar/Molar ratio have been represented.

3.4 Crosslinking of MacB *in vitro*

In order to stabilize the oligomeric state of the detergent solubilized complex, crosslinking experiments were undertaken in collaboration with Dr. Vassiliy N. Bavro at the University of Cambridge.

Since Tris can quench the crosslinking reaction, purified MacB was exchanged into buffer containing 50 mM Na_2HPO_4 pH 7.5, 50 mM NaCl, 10% glycerol and 0.05% DDM prior to crosslinking. The MacB crosslinking *in vitro* was performed using DSP, a crosslinker with 12 Å spacer arms (section 2.7.4), and analyzed by gel electrophoresis. The Mr of the MacB-His$_6$ monomer was predicated to be 72.97 kDa. On the gel, the MacB monomer was located between the 60 and 70 kDa protein makers and the most predominant band, predicated to be the MacB dimer, which was located between the 120 and 160 kDa markers (Figure 3.6a). However, the presence of some higher Mr bands may suggest MacB can also form higher order oligomers or erroneous crosslinking by the long spacer arm crosslinker DSP. In order to confirm the MacB oligomeric state and eliminate the possibility of erroneous crosslinking, the homobifunctional imidoester cross-linkers DMA (8.6 Å spacer arm) and DMS (11 Å spacer arm) were adopted in the MacB crosslinking. MacB dimers were clearly observed, whilst the higher order oligomers had vanished (Figure 3.6b), consistent with MacB forming dimers.
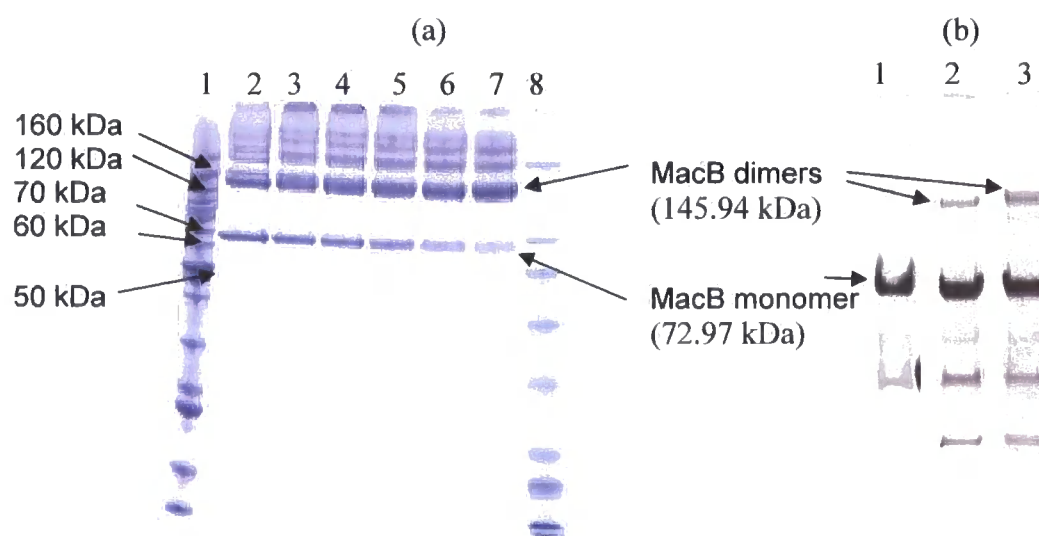
Figure 3.6   **SDS-PAGE of the crosslinked MacB-His$_6$.** (a) MacB was crosslinked with 1, 2, 10, 20, 50, 100 folds (Lane 2-8) of concentration of DSP. (b) MacB was incubated with 5 mM DMA or DMS (Lane 2 and 3) individually.

3.5 AUC analysis of MacB

AUC analysis and data representation were carried out in collaboration with Dr. Martin Montcrieffe and Dr. Vassiliy N. Bavro at the University of Cambridge.

In order to investigate more evidence that MacB is in a dimeric state, a combination of sedimentation equilibrium and sedimentation velocity analyses using analytical untracentrifugation was performed. The MacB was diluted into buffer containing low DDM (just below the CMC [critical micelle concentration]) (Section 2.8.3) in order to minimize the intervention of DDM micelles. The protein was stable in this buffer condition for over a week, allowing several datasets to be collected from the same sample. To determine the detergent contribution in the buoyant mass of the protein-detergent complex, a series of different density buffers were used, which were prepared using different D_2O concentrations (section 2.8.3).

The apparent Mr for MacB was determined from sedimentation equilibrium measurements to be 162.6 kDa (Figure 3.7a), which corresponded to a MacB dimer (The Mr of a MacB monomer is estimated to be 72.97 kDa). Since the equilibrium is only dependent upon the mass as it is calculated by specific buoyancy, buffers with different D_2O concentrations so as to provide different densities were prepared for the experiments in order to negate the detergent contribution in the complex. The idea is basically to create a buffer with the same background buoyancy as the detergent compound so that it is solely the mass of protein that is detected. For technical reasons we could not exactly match the buffer density to that of the DDM; fortunately, we used several different buffer compositions and for each of these we determined the equilibrium mass. Since the protein contribution is constant, it was possible to extrapolate the equilibrium mass to the theoretical point at which the buffer matches the specific density of DDM (Peterson *et al.*, 1988). Sedimentation velocity is shape dependent and a sedimentation coefficient of 6.8 S was generated, which corresponded to a Mr of 160 kDa (Figure 3.7b). The sedimentation velocity, where detergent was taken into account, gave a very similar result to the sedimentation equilibrium, suggesting that few detergent molecules were bound. Our colorimetric data showed that there were 171 molecules of DDM bound to one MacB molecule in the buffer containing 0.2% DDM. However, the DDM in the sample for AUC analysis was much lower at 0.006%, just below the CMC, which may lead to the difference in the data.

(a)
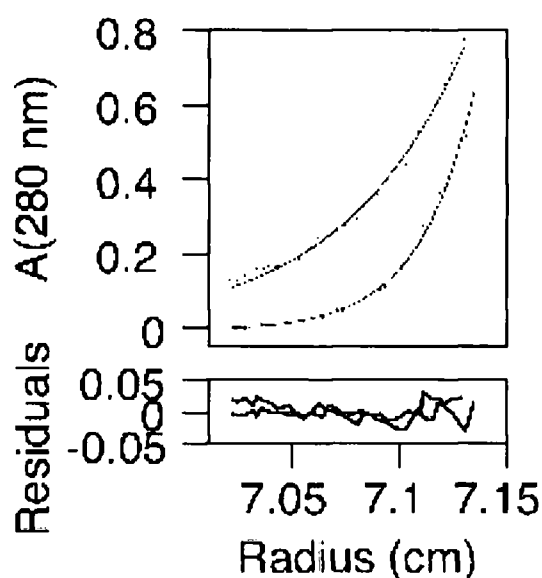
(b)
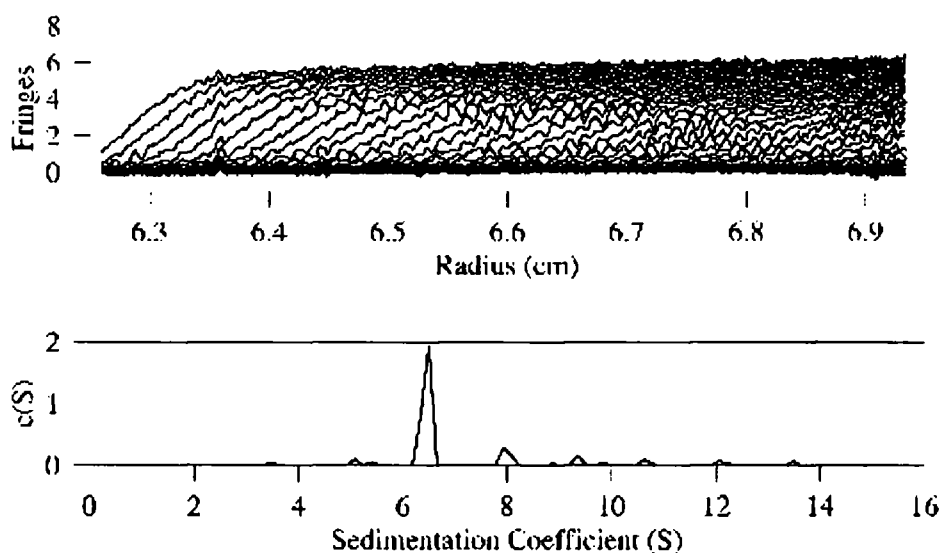
Figure 3.7   **AUC analysis of MacB.** (a) Sedimentation equilibrium profiles of the MacB-DDM. It shows a representative sedimentation equilibrium profile from one of the runs (two different velocities of the same sample). Experimental data (dots) and fitted model (solid line) is shown for each. The bottom panel is the residuals (differences between data and model) after fitting. (b) Sedimentation velocity measurements of the MacB-DDM. Sedimentation velocity profiles of the MacB are consistent with a stable dimer formation.

3.6 Electrospray mass-spectrometry

Electrospray mass-spectrometry experiments and data representation were carried out in collaboration with Dr. Nelson P. Barrera and Dr. Vassiliy N. Bavro at the University of Cambridge.

Electrospray mass-spectrometry was used to determine accurately the Mr of the protein, under conditions that would dissociate the DDM, revealing a peak with a Mr of 145.96 ± 0.02 kDa, which is consistent with a MacB dimer (Figure 3.8). With known mass-to-charge ratio (m/z) and numbers of positive ion, the molecular weight of MacB can be calculated.

The use of mass spectrometry to determine the Mr of membrane proteins is a novel and challenging field and our results are the first, to the best of our knowledge, to report on the determination of the oligomeric state of a native membrane protein from the ABC transporter family.
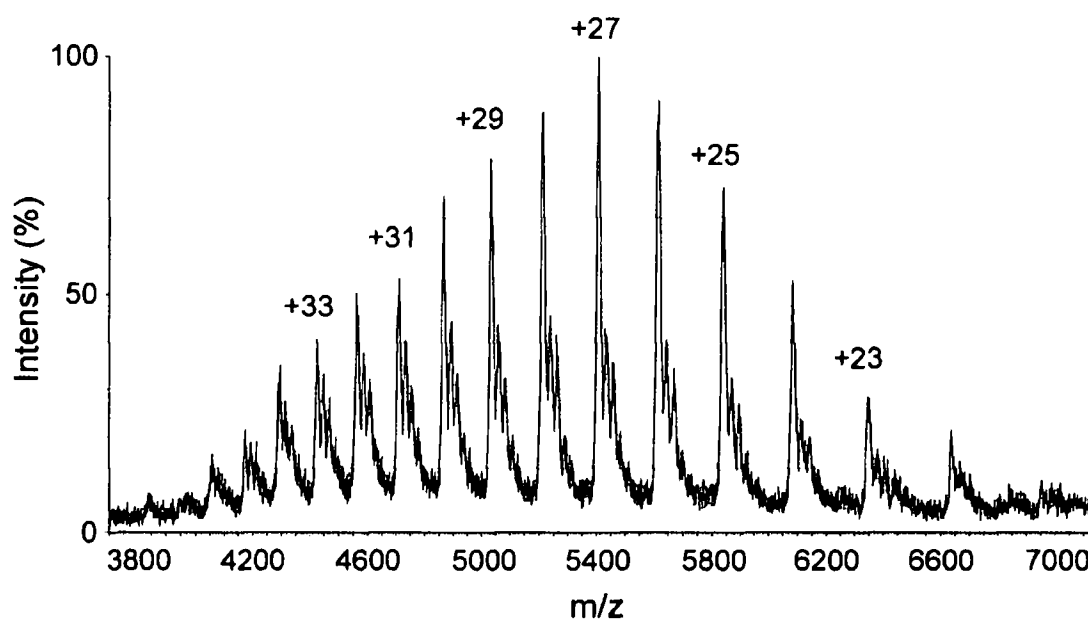
Figure 3.8 **Mass spectrum of MacB.** The charge states corresponding to the peaks are graphed.

3.7 AFM analysis of MacB

AFM analysis and data representation were carried out in collaboration with Dr. Nelson P. Barrera and Vassiliy N. Bavro at the University of Cambridge.

Using AFM larger particles could clearly be seen at high-resolution to consist of two protein domains that are highly suggestive of a dimer (Figure 3.9). Not surprisingly, in the presence of AMP-PNP, a non-hydrolysable analogue of ATP, the ratio of dimers to monomers on the AFM grids increased, which would be consistent with the nucleotide stabilizing the interaction between monomers (Figure 3.10).

Our findings are novel because detergent molecules tend to impair the resolution of AFM studies of detergent solubilized membrane proteins; so that in the case of MacB, we may be able to get information on the topology and stoichiometry of its assemblies with MacA and TolC. Indeed, when MacA, which was resolved as a single population of particles with a volume of 69 nm^3, was mixed with MacB, a number of particles with volumes far in excess of 238 nm^3 (e.g. MacB dimer volume) and 307 nm^3 (e.g. MacB dimer volume + MacA volume) were resolved, indicative not only of the interaction of MacA and MacB but also the formation of multi-subunit complexes (data not shown).

(a)

(b)
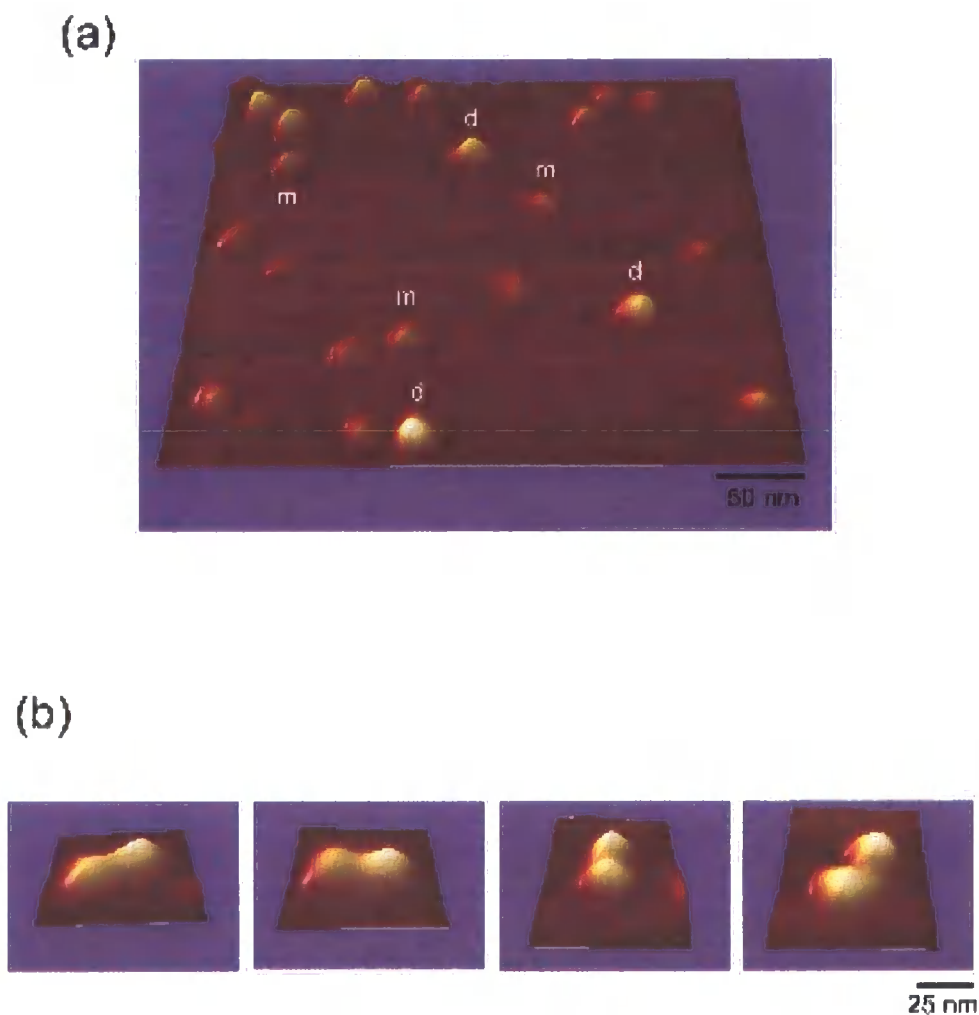
Figure 3.9   **AFM imaging of MacB**. (a) 3D picture of a low magnification image of MacB acquired in air in Tapping Mode with a diamond-like extratip of resonant frequency~300 kHz and spring constant of 40 N/m. Letters 'm' and 'd' represent MacB monomer and dimer, respectively. (b) High resolution images of structures where two small particles ('m'+'m') are attached to one another, clearly indicative of dimer formation.

(a)
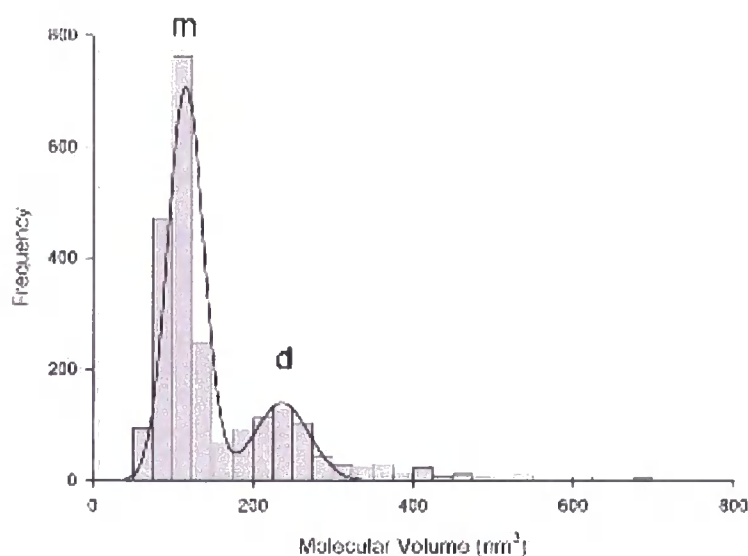
(b)
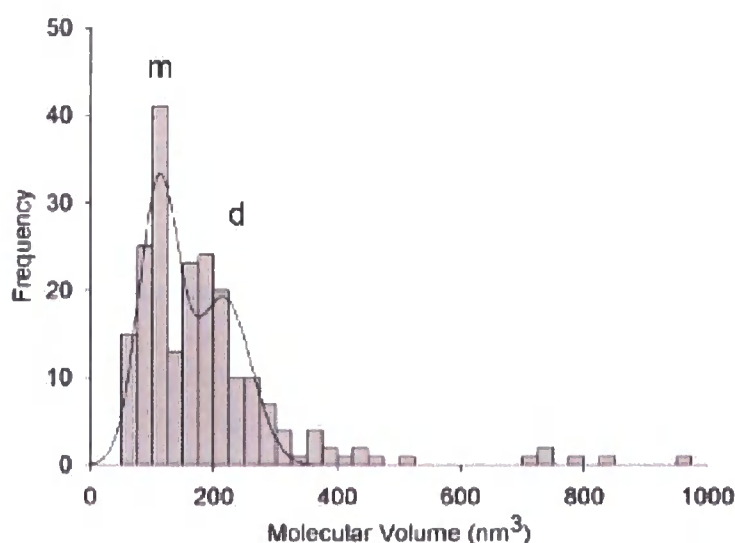
Figure 3.10 **Frequency distribution of molecular volumes of MacB**. (a) The curve indicates a fitted Gaussian function. The 'm' and 'd' peaks correspond to volumes of 118 ± 1 nm^3 (n= 1642) and 238 ± 5 nm^3 (n= 665). The data is consistent with the 'm' and 'd' peaks corresponding to the MacB monomer and dimer, respectively. (b) Frequency distribution of molecular volumes of MacB that had been incubated with the non-hydrolysable ATP analogue AMP-PNP. The peaks correspond to volumes of 112 ± 3 nm^3 (n= 94) and 218 ± 14 nm^3 (n= 116). This data indicates an increase in the dimer: monomer ratio in the presence of AMP-PNP.

3.8 Discussion

Membrane proteins are notoriously difficult to overexpress and manipulate due to their high hydrophobicity; and the integral membrane protein MacB, a ABC transporter from *E. coli*, is no exception. The *macB* gene was first cloned into the plasmid pQE80 (Qiagen) for overexpression in the *E. coli* strain M15/PREP4 (Qiagen), under the regulation of a T5 promoter. However, MacB tended to stop the cells from growing once induced and it degraded extensively using this expression system, resulting in an extremely low yield and stability (data not shown). The yield and stability of MacB protein was significantly improved using the T7 promoter regulated plasmid pET28a(+), along with the *E. coli* strain C43(DE3). Even so, using the latter expression system of the yield of pure MacB protein, after two purification steps, was only about 1 mg of protein from 2 L cells. MacB lost its ATPase activity when being extracted with 2% DDM, but retained activity when extracted with 5% Triton X-100 and subsequently switched into a buffer containing 0.2% DDM. This observation indicates that the activity of MacB is detergent-dependant, but the reason is unknown.

Our colorimetric analysis indicated that there were 171 molecules of DDM bound to one MacB molecule, which is consistent with the values found for other membrane proteins (Butler *et al.*, 2004; Ravaud *et al.*, 2006). EmrE, the best studied SMR protein, was found to be a dimer in the detergent-solubilized state, with a molar ratio of DDM/EmrE of 104.5 ± 6 (Butler *et al.*, 2004). BmrA was found to be dimeric in the detergent solubilized state and the molar ratio of DDM/BmrA was determined to be 194 (Ravaud *et al.*, 2006). However, our sedimentation velocity AUC analyses, where the detergent was taken into account, gave a DDM/MacB of molar ratio of 24. This difference might be due to using a DDM concentration of 0.006%, slightly below the CMC, in the buffer for AUC analysis.

In this study, ES-MS has been used to successfully identify MacB oligomeric state. ES-MS is now widely accepted as a powerful method to determine accurately the stoichiometry of intact protein complexes (Hernandez and Robinson, 2001; Sharon and Robinson, 2007). However, it has remained extremely difficult to analyze membrane proteins, solubilized in detergent due to their hydrophobicity, under similar conditions. So far, only a few studies have reported the observation of membrane proteins or their

complexes in MS (Hanson *et al.*, 2003; Ilag *et al.*, 2004; Lengqvist *et al.*, 2004; Meier *et al.*, 2007). In this study, using nanoflow ES (a miniaturized form of ES with reduced flow rates) and a high collision energy, which facilitates the desolvation process and induces dissociation of detergent-proteins clusters, we demonstrated for the first time the native dimeric state of MacB. Under our experimental conditions, it was possible to successfully maintain the non-covalent subunit interactions, determining the oligomeric state of the protein complex without ambiguity. The development of strategies to tackle this field is challenging, primarily since the large quantities of detergent suppress the protein signal while the highly hydrophobic membrane proteins in aqueous buffers often blocks electrospray needles.

Also of interest is the association between structural results provided by MS and AFM. AFM imaging has been applied previously to determine the stoichiometry of purified membrane proteins (Barrera *et al.*, 2005; Barrera *et al.*, 2008). Interestingly, using diamond-like extratips to scan the topography of isolated MacB, it was possible to identify both subunits forming the complex. Although AFM imaging cannot give very accurate measurements of molecular masses of particles, it provides a reasonable range for the MacB protein (approximately 130-140 kDa). The structure of each component of the AcrA/AcrB/TolC complex pump has been determined, giving some insight into how the complex is assembled; however, the stoichiometry of the whole tripartite complex pump is still controversial (Fernandez-Recio *et al.*, 2004; Higgins *et al.*, 2004). In this study, using AFM, each subunit of the MacB dimer can be identified, suggesting the possibility to extend such analyses to determine how the tripartite complex is assembled.

Chapter four: Defining the role of the membrane fusion protein MacA in MacB's ATP hydrolysis

Gram-negative bacteria such as *E. coli* employ membrane efflux systems to transport antibiotics, noxious chemicals and large protein toxins outside the cell (Koronakis *et al.*, 2004). Multidrug efflux pumps consist of three components: an energy-providing integral inner membrane protein, either an ABC transporter or a proton antiporter of the RND family or MFS (Borges-Walmsley *et al.*, 2003), cooperates with a protein of the TolC exit duct family. The third component of tripartite complex pumps is a membrane fusion protein, largely periplasmic and anchored to the inner membrane by a single transmembrane α-helix or an N-terminal lipid moiety. One of the best studied efflux pumps of *E. coli* is the AcrA/ArcB/TolC system, where the membrane fusion protein AcrA was proposed to provide a physical link between AcrB and TolC.

Kobayashi *et al* in 2001 showed that the MacAB complex confers TolC-dependent macrolide resistance via active drug efflux. In this chapter, the potential roles and domains of membrane fusion protein MacA to interact with MacB will be investigated.

4.1 MacA-His₆ construction and production

A construct was made to overexpress the MacA protein in this study. The details of the construction are described in section 3.1. In short, the forward primer, NcoI-macA, and reverse primer, XhoI-macA, were designed to incorporate the RE sites, *NcoI* and *XhoI*, at the 5' and 3' ends of the amplified *macA*, respectively. Successful PCR amplification of the *macA* sequence was shown to be consistent with the predicted size on an agarose gel (Figure 4.1a). Plasmid DNA purified from recombinant colonies was digested with *NcoI* and *XhoI* to confirm the presence of the inserted DNA (Figure 4.1b).

The pET21d-*macA* expression construct was transformed into the *E. coli* strain C43(DE3) for protein production. The cell membranes were dissolved in 20 mM Tris

buffer pH 7.5, 300 mM NaCl, 15 mM imidazole, 1 mM THP, 10% glycerol and 5% Triton X-100 on a rotary shaker overnight.

MacA-His$_6$ was purified by metal affinity chromatography using a HiTrap Ni^{2+} column (section 2.5.1). MacA-His$_6$ was eluted in buffer containing 20 mM Tris-HCl pH 7.5, 500 mM NaCl, 10% glycerol, 500 mM imidazole and 0.2% Triton X-100. The efficiency of expression and purification of MacA-His$_6$ was determined by gel electrophoresis (section 2.6.1) (Figure 4.2). The migration of the major protein band (lanes 2 to 10) between the 39 kDa and 51 kDa bands of the SeeBlue protein marker (lane 1) is consistent with the calculated molecular weight of 41.8 kDa MacA-His$_6$. Further identification of the MacA-His$_6$ protein was achieved by Western Blot, as shown in figure 4.2.
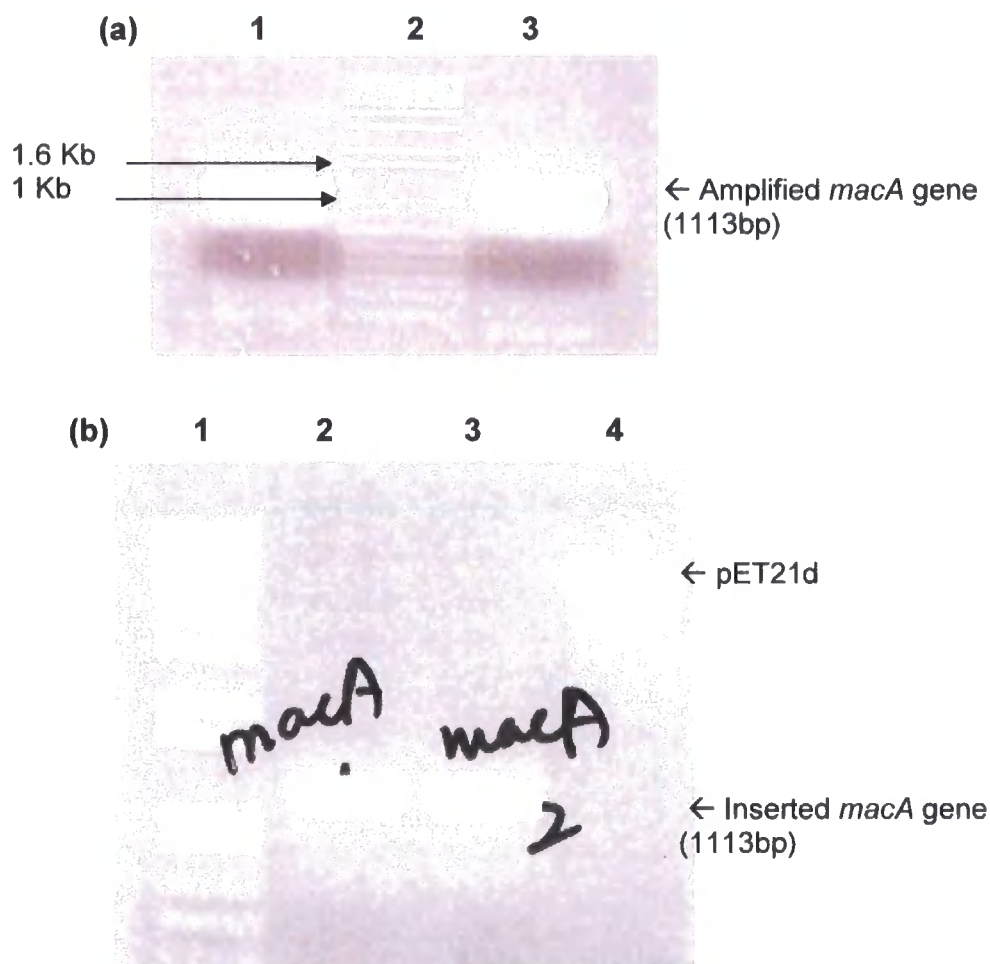
Figure 4.1 **pET21d/macA construction**. (a) PCR amplification of *macA* gene from *E.coli* K-12. Lane 2 = the DNA ladder. Lane 1 and 3 indicate the amplified *macA* gene. (b) Restriction enzyme digestion analysis of the pET21d/*macA* plasmid. Lane 1= DNA ladder. Lanes 2-3 indicate the presence of the *macA* gene.
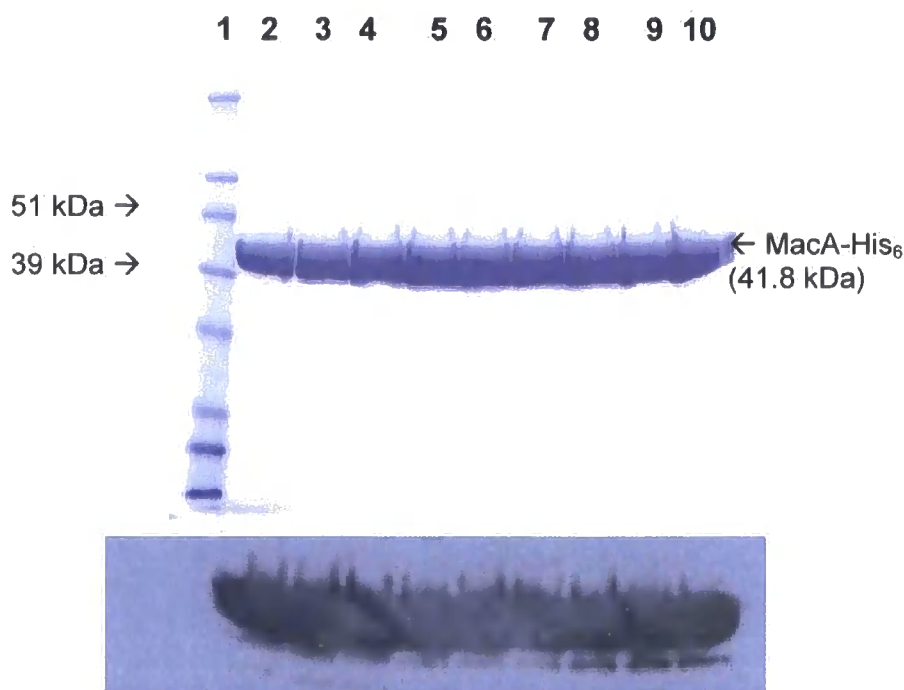
Figure 4.2   **SDS-PAGE of MacA-His$_6$.** Lane 1= the protein M_r marker. Lanes 2-10 indicate the MacA proteins. The signals of MacA-His$_6$ were shown on the X-ray film by using Western blot.

4.2 MacA regulates the ATPase activity of MacB

Although MacB belongs to the ABC superfamily it has an exceptional architecture. The presence of an NBD in MacB affords the opportunity to test for an interaction with, and modulation of its ATPase activity by, MacA, which can be carried out in solution. The MacB protein was purified as described in section 3.1. and shown to have its detergent-dependent ATPase activity, being active in Triton X-100 but not in a high concentration of DDM. In order to investigate the potential role of the membrane fusion protein MacA in the ATP hydrolysis by MacB, the dye 2-amino-6-mercapto-7-methylpurine riboside (MESG) was used to monitor the time course of ATP hydrolysis by detecting the production of inorganic phosphate (Pi) (section 2.7.1). A standard curve was generated, which illustrated the amount of Pi released in nanomoles (nmoles) plotted against the absorbance at 360 nm (Abs$_{360}$) and analyzed by linear regression. Points plotted were from an average of three independent experiments (Figure 4.3).
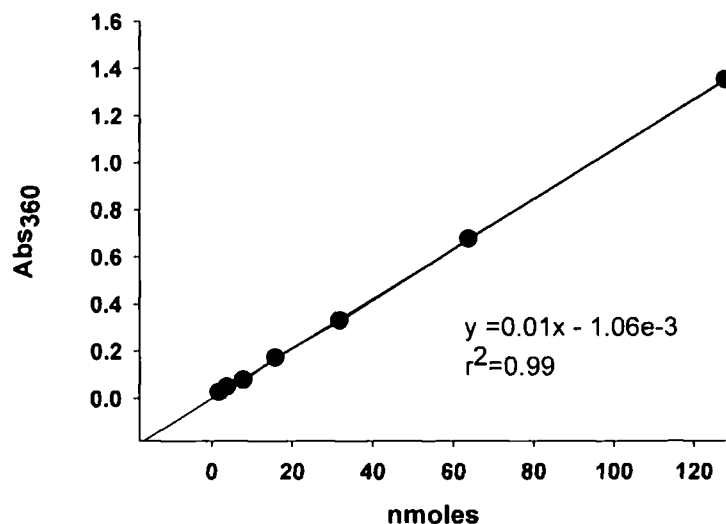
Figure 4.3 **Standard curve of inorganic phosphate (Pi).** Measurments were undertaken at absorbance 360 nm using the EnzChek phosphate assay.

The MacB ATPase activity was determined in the presence of $MgCl_2$ and various concentration of ATP. The amount of Pi released in each sample was measured by the change in A_{360} and was calculated by using the equation generated from the standard curve. The time course was characterized by a burst in Pi production, during the first 20 seconds, followed by a slower steady-state rate (Figure 4.4). This kinetic behavior indicated that the ATP was hydrolyzed rapidly in the burst phase of the trace, and further turnovers were rate limited by the slow release of product.

The amplitude of the burst phase, measured at eight different ATP concentrations, from 0.01 mM to 4 mM, ranged from 2.3-2.4 µM (Figure 4.4), which is equivalent to the MacB concentration (2.3 µM). When the MacB concentration was increased to 3.5 µM, the amplitude of the burst phase increased to 3.3 µM (Figure 4.5), indicating that the burst is approximately equivalent to the MacB concentration and that both NBDs within the MacB dimer are functional. The rate constant for the hydrolysis step was determined by fitting the burst phase to an exponential function, yielding a value of about 0.22 s^{-1}, which was independent of the ATP concentration.
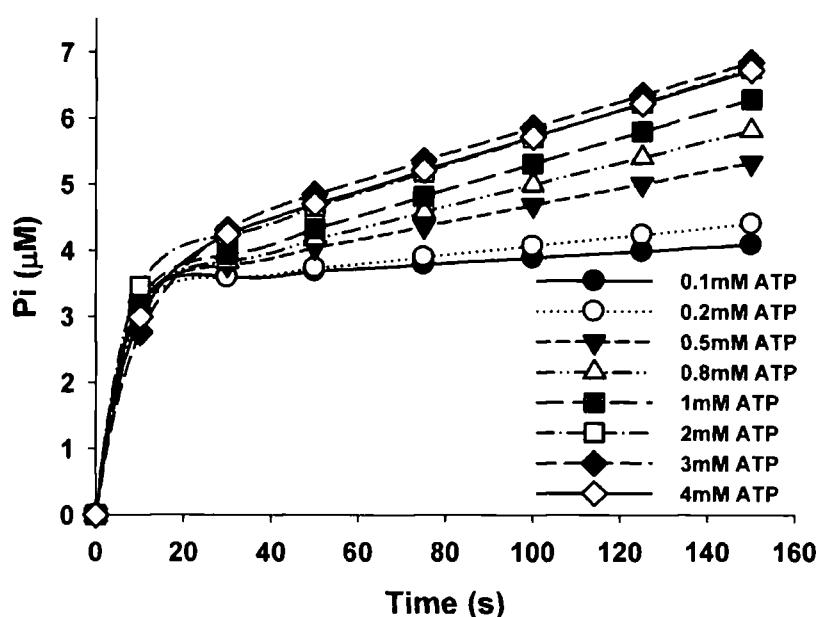
Figure 4.4   **A plot for Pi generation by MacB on concentration of ATP.** MacB's ATPase activity was measured by the time course for the change in Pi concentration. 2.3 µM MacB was used and the ATPase activity was measured in the presence of various concentration of Mg-ATP, from 0.1 mM to 4 mM.
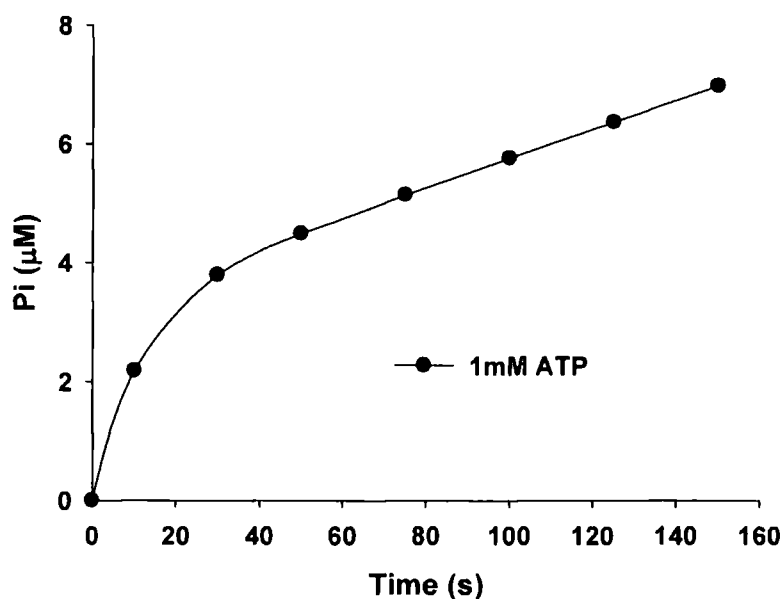
Figure 4.5   **A plot for Pi generation by MacB.** MacB's ATPase activity was measured by the time course for the change in Pi concentration. 3.5 µM MacB was used, and the ATPase activity was measured at Mg-ATP concentration of 1 mM.
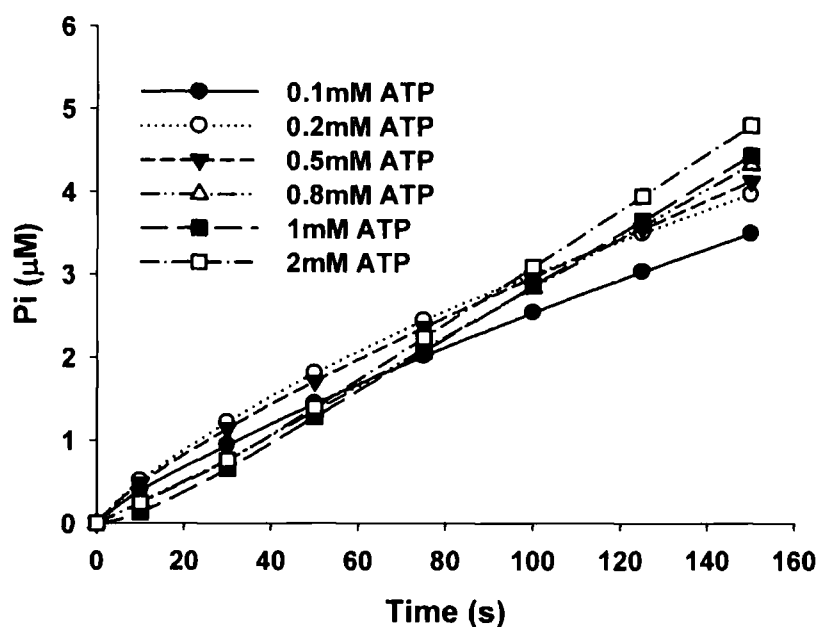
Figure 4.6   **A plot for Pi generation by MacAB on concentration of ATP.** 2.3 μM MacA and MacB were used, and the ATPase activity was measured in the presence of Mg-ATP.
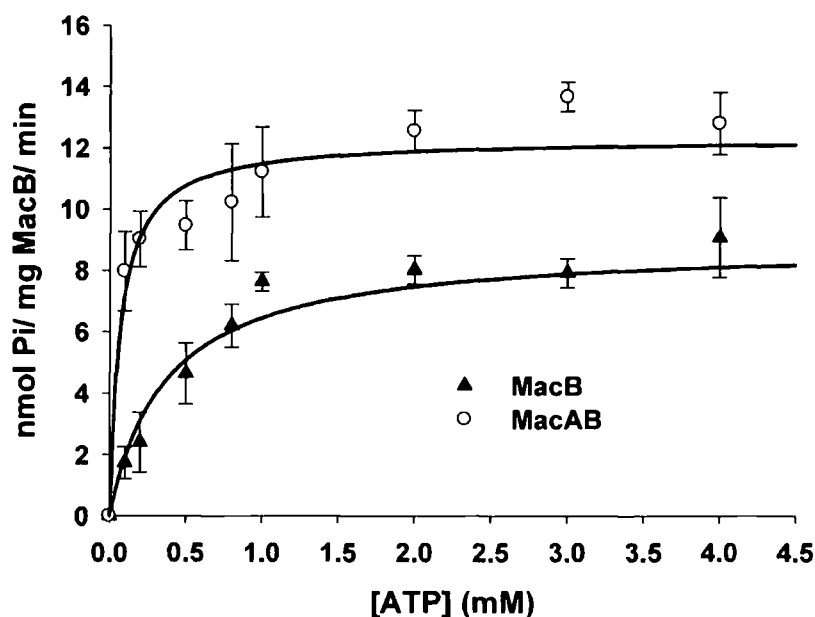
Figure 4.7   **The steady-state rate of Pi production by MacB** as a function of the ATP concentration in the absence (lower curve) and presence (upper-curve) of an equivalent concentration of MacA. The data are characterized by V_{max} and K_m values of 8.9 nmoles ATP/mg MacB/min and 374 μM, respectively, for MacB alone; and of 12.3 nmoles ATP/mg MacB/min and 72 μM, respectively, for MacB in the presence of an equivalent concentration of MacA.

The steady-state phase was characterized by a rate of Pi production that increased in a hyperbolic manner with the ATP concentration (Figure 4.7). A maximal specific activity of 8.9 nmoles ATP/mg MacB/min and a K_m of 374 μM were obtained by fitting the data to a hyperbolic function. The macrolides erythromycin and oleandomycin, substrates of MacB, were also added respectively in the reaction to investigate the possibility of a substrate-induced change in the ATPase activity; however, the presence of the macrolides did not affect ATP hydrolysis by MacB, which is consistent with a previous report on MacB (Tikhonova et al, 2007) but contrasts with the findings for Sav1866 (Dawson and Locher, 2006). The ATPase activity of Sav1866, reconstituted into liposomes, was stimulated by the anti-cancer drugs doxorubicin, vinblastine and the fluorescent dye Hoechst 33342.

An equivalent concentration of MacA was added to 2.3 μM MacB, the ATPase activity was determined in the presence of $MgCl_2$ and various concentration of ATP. Surprisingly, the Pi burst phase disappeared but the steady-state rate was enhanced (Figure 4.6). This behavior might suggest that MacA increased the rate of ADP dissociation from MacB, making this step is no longer rate-limiting. However, k_{cat} did not increase to a rate above that determined for the burst phase and so we must assume that the hydrolysis rate also decreases.

Figure 4.7 illustrated the steady state ATPase activity of MacB on various ATP concentrations. The non-linear regression line was obtained by fitting in a hyperbolic trace. The equation of the regression line is as follows:

$$y = a*x/(b+x)$$

In the equation, "a" represents V_{max} and "b" represents K_m. The k_{cat}/K_m ratio is often thought of as a measure of enzyme efficiency. Both a big value of K_{cat} (rapid turnover) or a small value of K_m (high affinity to substrate) can makes k_{cat}/K_m large.

Although MacA increased the specific activity of MacB from 8.9 to 12.3 nmoles ATP/mg MacB/min, which would correspond to an increase in k_{cat} from 0.011 to 0.015 s^{-1}, the steady-state rate did not exceed the rate for hydrolysis in the absence of MacA (e.g. 0.22 s^{-1}). Accordingly, the increase in the steady-state rate, which was attributed

to product release, would not be rapid enough to prevent the phosphate burst. Consequently our results suggest that MacA hinders the rate of ATP hydrolysis, so that this process is no longer rate limited by the product release. This finding contrasts with a previous report on MacB, where the presence of MacA had no affect on the ATPase activity of MacB in solution. However, they did find that MacA, when co-reconstituted with MacB, had the effect of increasing both k_{cat} (e.g. k_{cat} from 0.1 to 0.78 s^{-1}) and the affinity of MacB for ATP (e.g. K_m from 2.3 to 0.38 mM), which is similar to the effect of MacA on the steady-state kinetics of ATPase activity of MacB in a detergent solubilized state in our study.

4.3 The MacA periplasmic domain

The previous section indicated that MacA regulates the ATPase activity of MacB. MacA is a membrane fusion protein with an anchored transmembrane domain. To investigate the possibility that the transmembrane domain is involved in the interaction with MacB, soluble truncated MacA, in which the first N-terminal 20 residues were deleted, was generated based on the predication of its secondary structure, using the program Jpred at University of Dundee (Section 2.1). Figure 4.8 illustrates the short transmembrane α-helix (pink) and large periplasmic domain (blue).

```
-----HHHHHHHHHHHHHHH--------------EEEEEEEE----EEEEEEEEEEEEEEEEEEEE---
MKKRKTVKKRYVIALVIVIAGLITLWRILNAPVPTYQTLIVRPGDLQQSVLATGKLDALRKVDVGAQV

--EEEEEEEE--EE----EEEEE--HHHHHHHHHHHHHHHHHHHHHHHHHHHHHHHHHHHHHHHHHHH
SGQLKTLSVAIGDKVKKDQLLGVIDPEQAENQIKEVEATLMELRAQRQQAEAELKLARVTYSRQQRLA

----HHHHHHHHHHHHHHHHHHHHHHHHHHHHHHHHHHHHHHHH---EEEEE----EEEEEEE----E
QTKAVSQQDLDTAATEMAVKQAQIGTIDAQIKRNQASLDTAKTNLDYTRIVAPMAGEVTQITTLQGQT

EE------EEEEEE----EEEEEE--HHHHHHHH----EEEEE------EEEEEEEEE---------
VIAAQQAPNILTLADMSAMLVKAQVSEADVIHLKPGQKAWFTVLGDPLTRYEGQIKDVLPTPEKVNDA

EEEEEEEE------------EEEEEEE-------EE----EEEE-----EEEEEEEE---EEEEEEEEEE
IFYYARFEVPNPNGLLRLDMTAQVHIQLTDVKNVLTIPLSALGDPVGDNRYKVKLLRNGETREREVTIG

E----EEEEEE------EEEEE-------
ARNDTDVEIVKGLEAGDEVVIGEAKPGAAQ
```

Figure 4.8 **Secondary structure prediction of E. coli MacA.** The predicted secondary structure elements of MacA are drawn above the amino acid sequence with the α-helices and β-sheets depicted as **H** and **E** respectively. Horizontal arrows drawn above secondary structure describe predicted protein topology (**Green** arrow indicates cytoplasmic domain, **pink** arrow indicates membrane spanning domain and **blue** arrow indicates periplasmic domain).

4.3.1 Truncated MacA construction and production

A construct was made for the expression of the N-terminal truncated MacA. The details of the construction are described in section 3.1, indicating the changes in DNA template and primers. In short, the forward primer, NcoI-FD20macA, and reverse primer, XhoI-macA, were designed to incorporate the RE sites, *NcoI* and *XhoI*, at the 5' and 3' ends of the amplified *macA* sequence, respectively. Plasmid DNA purified from recombinant colonies was digested with *NcoI* and *XhoI* to confirm the presence of the inserted DNA (Figure 4.9a).

The pET21d-*Δ20macA* expression construct was transformed into the *E. coli* strain C43(DE3) for protein production. Δ20MacA-His$_6$ was purified by metal affinity chromatography using a HiTrap Ni^{2+} column (section 2.5.1). MacA-His$_6$ was eluted in buffer containing 20 mM Tris-HCl pH 7.5, 500 mM NaCl, 10% glycerol, and 500 mM imidazole. The efficiency of expression and purification of MacA-His$_6$ was determined by gel electrophoresis (section 2.6.1) (Figure 4.9b). The migration of the major protein band (lanes 2 to 10) is just above the 39 kDa SeeBlue protein marker (lane 1), which is consistent with a calculated molecular weight of 39.3 kDa for MacA-His$_6$.
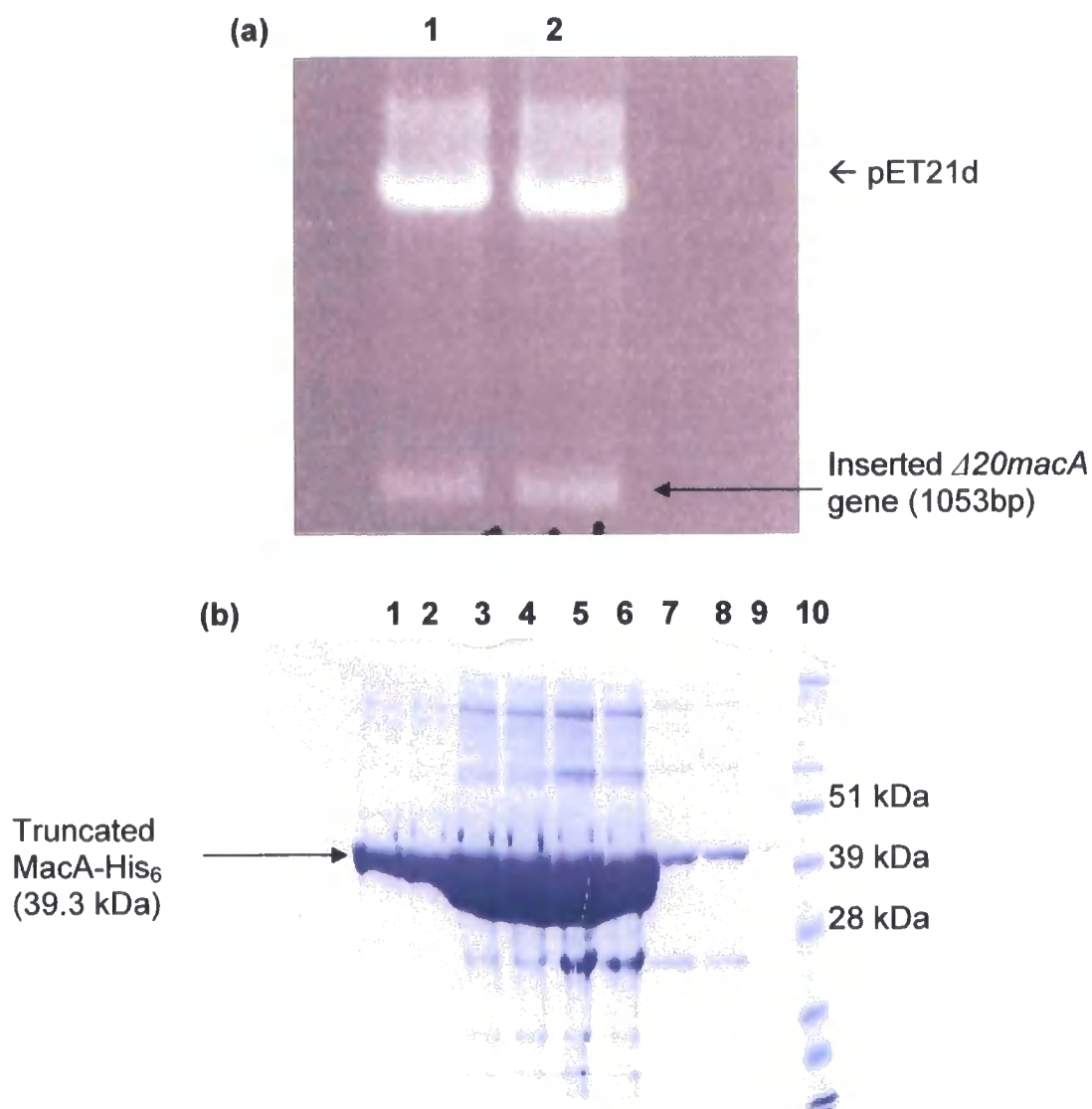
Figure 4.9 **pET21d/Δ20macA construction**. (a) Restriction enzyme digestion analysis of the pET21d/*ΔmacA* plasmid. Lanes 1-2 indicate the presence of the truncated *macA* gene. (b) SDS-PAGE of truncated MacA-His$_6$. Lanes 1-9 indicate the truncated Δ20MacA protein. Lane 10= the protein M_r marker.

4.3.2 N-terminal truncated MacA regulates the ATPase activity of MacB

When N-terminal truncated MacA was added to MacB, at an equivalent concentration, a similar behavior was observed as in the presence of full length MacA, which is different as observed in the absence of MacB (Figure 4.4), indicating that truncated MacA was equally capable of regulating the ATPase activity of MacB (Figure 4.10). Thus, we concluded that the N-terminal transmembrane domain is not required in the regulation of the ATPase of MacB. This finding is consistent with a report on the membrane fusion protein AcrA, in which, a lipid-deficient derivative of AcrA was shown to retain its ability to cooperate with AcrB and TolC to confer resistance to drugs (Zgurskahya and Nikaido, 1999).
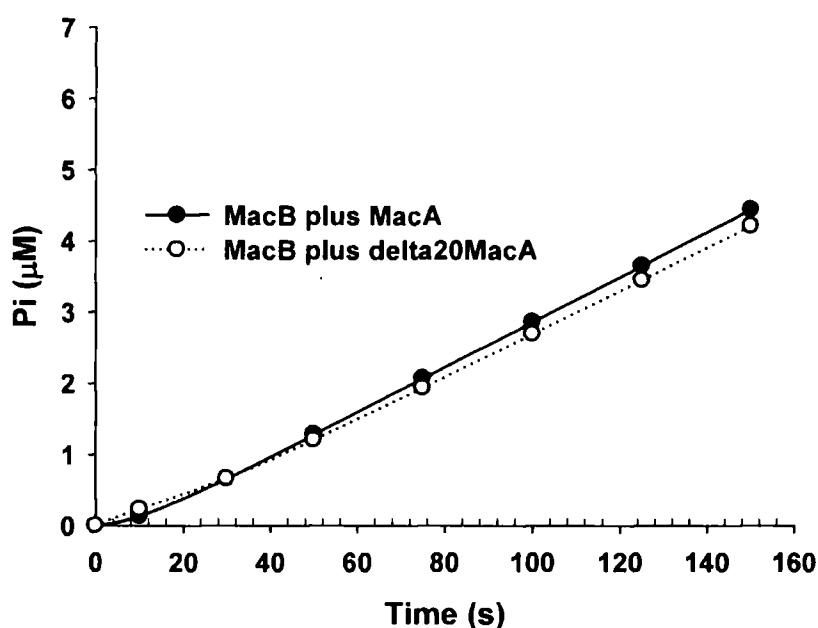
Figure 4.10 **Pi generation by MacAB and Δ20MacA plus MacB.** 2 μM MacB and Δ20 MacA were used, and the ATPase activity was measured at Mg-ATP concentration of 1 mM.

4.4 The α-helical hairpin of MacA is not required in the regulation of the ATPase activity of MacB

The measurements of the ATPase activity of *E. coli* MacB in the presence of *S. aureus* MacA was undertaken in collaboration with Mrs. Helen Frankish from our group.

Both gram-negative and gram-positive bacteria, such as *E.* coli and *S. aureus*, possess *macAB* genes encoding macrolide transporters; however, gram-positive bacteria would not be expected to require MacA to interact with an OMP due to the lack of an outer-membrane. We have noted that in some strains of *S. aureus*, MacA has a large deletion that corresponds to the coiled-coil hairpin which is the domain believed to interact with the outer membrane protein (Mikolosko *et al.*, 2006; Bavro *et al.*, 2008).

The genome sequence of *S. epidermidis* reveals three genes that putatively encode a macrolide efflux pump: *SE2405*, encoding a membrane translocase; *SE2406*, encoding an ATPase; and *SE2407*, encoding a membrane fusion protein. *SE2405* and *SE2406* have 46.5% and 55.4% sequence similarity, respectively, to the corresponding domains of *E. coli* MacB and *SE2407* has 26% sequence similarity to *E. coli* MacA (Figure 4.11). Furthermore, secondary structure predications suggest that SE2407 and *E. coli* MacA are arranged into similar domains, consisting of an N-terminal transmembrane α-helix and a pair of long helices between two β-strand containing domains. *S. aureus* possesses three homologous genes, with SAS0173 and SAS0174 having 76.8% and 72.1% amino acid sequence similarity to SE2405 and SE2406, respectively. Interestingly, the alignment of SAS0172 with SE2407 indicates that the *S. aureus* MFP MacA encoded by *SAS0172* has lost a large fragment, spanning residues 88-206 in the MFP encoded by *SE2407* (Figure 4.11). This is the region that incorporates the hairpin that interacts with TolC, suggesting that *S. aureus* MacA has lost this domain because of absence of an outer membrane in gram-positive bacteria. However, *S. aureus* still retains the other domains of the MFP, strongly suggesting that this plays an important functional role, such as activating its cognate ABC transporter composed of SAS0173 and SAS0174.

Figure 4.11 **MacA sequence alignment.** A sequence alignment of the MacA membrane fusion proteins from the gram-negative bacterium *E. coli* and gram-positive bacteria *S. epidermitis* and *S.aureus* was represented. This analysis indicates that while the proteins from *E. coli* and *S. epidermitis* have similar secondary structures, the large α-helical domain predicted to harbor the TolC interaction site is missing in the *S. aureus* protein. The illustration of MacA sequence alignment was undertaken in collaboration with Dr. Vassiliy N. Bavro at the University of Cambridge.

In order to test the hypothesis, the ATPase activity of MacB was determined in the presence *S. aureus* MacA (SAS0172). The addition of an excess of *S. aureus* MacA to *E. coli* MacB was able to abolish the Pi burst and this kinetic behavior was consistent with the effect of *E. coli* MacA on MacB (Figure 4.12), suggesting that the the α-helical hairpin of MacA is not required for activation of MacB. This finding is consistent with a report on AcrA (Elkins and Nikaido, 2003). In this report, several chimeric mutants of AcrA were created by replacing with the corresponding sequences from YhiU, a homolog does not function with the AcrB. Drug susceptibility tests of these chimeras revealed that N-terminal region of AcrA could be replaced with the corresponding domain of YhiU up to residue 290 and these mutants still retained functional as native AcrA. However, AcrA lost its ability to function with AcrB when the region between residues 290 and 357 was replaced with corresponding sequence of YhiU, indicating a small region of AcrA close to its C terminus is involved in the interaction with its cognate pump protein, AcrB.
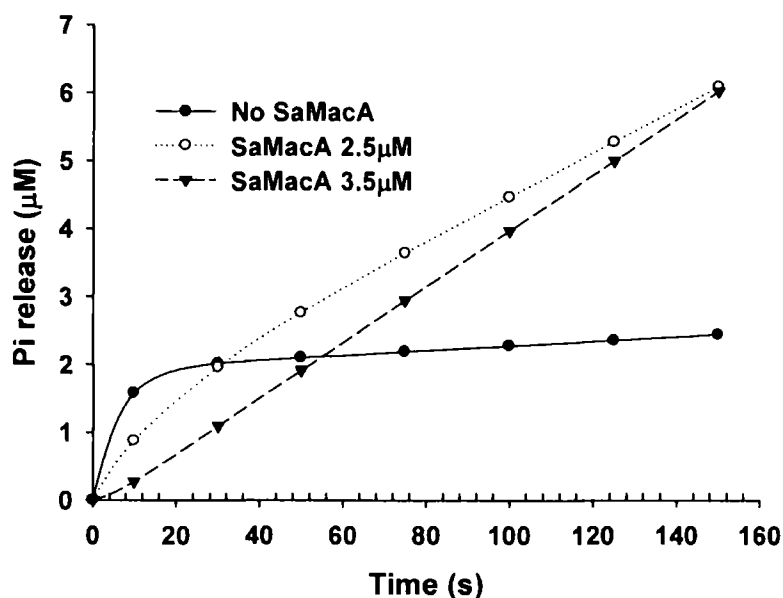
Figure 4.12 **Pi generation by *E. coli* MacB in the presence of *S. aureus* MacA.** 2 µM MacB was used, and the ATPase activity was measured at Mg-ATP concentration of 1 mM.

4.5 CD analysis

In the previous section, we predicted that *S. aureus* MacA encoded by *SAS0172* has lost the coiled coil hairpin structure found in *E. coli* MacA (Figure 4.11). In order to determine the secondary structure of the N-terminal truncated MacA from *E. coli*, CD spectrum analysis was applied. Protein samples were dialyzed against buffer containing NaF rather than NaCl, minimizing the strong absorbance from Cl⁻ in the far UV region. In order to estimate the best protein concentration for CD analysis, the absorbance of the sample was measured at in range of the wavelength (190 nm-260 nm), on the priority of keeping the strongest absorbance value within 0.8-1, generating a concentration for CD at around 0.09 mg/ml (2.25 μM). The spectrum of proteins in Tris buffer containing 20 mM NaF, pH 7.5 was recorded from 260 nm to 190 nm, for an average of six and subtracted by baseline spectrum of buffer itself to get the final spectrum. A quench and a peak can be seen at around 210 nm and 195 nm respectively (Figure 4.13). The High Tension voltage, the voltage applied to the photomultiplier, reached 700 when the wavelength went down to 195 nm during the measurement of the protein sample; however, this situation can also be observed in the measurements of buffer and H_2O respectively. Generally, for reliable data, the High Tension voltage should remain within 700 V, but this value will depend on the particular instrucment being used (Kelly *et al.*, 2005). The reason could be due to the combination of using a weak Xe arc light source and the strong absorbance of H_2O in the far UV region.
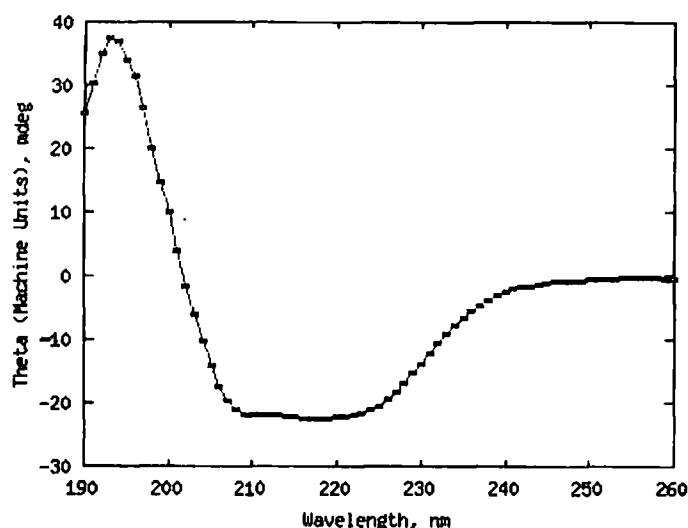
Figure 4.13   **The CD Spectrum of Δ20MacA.** Data was collected from 260 nm to 190 nm for a 2 mm pathlength, with a 2 sec rate constant, 10 nm/min scanning speed and 1 nm bandwidth.

(a)

NRMSD:0.105

Helix segments per 100 residues: 2.475 · Strand segments per 100 residues: 5.512

Ave helix length per segment: 7.168 · Ave strand length per segment: 5.664

Result	Helix1	Helix2	Strand1	Strand2	Turns	Unordered	Total
1	0.093	0.094	0.165	0.099	0.191	0.358	1
2	0.078	0.099	0.202	0.110	0.197	0.313	0.999

(b)

NRMSD:0.027

Helix segments per 100 residues: 1.332 · Strand segments per 100 residues: 4.628

Ave helix length per segment: 6.757 · Ave strand length per segment: 6.726

Helix1	Helix2	Strand1	Strand2	Turns	Unordered	Total
0.04	0.05	0.22	0.09	0.16	0.44	1

(c)

NRMSD:0.086   Rvalue: 0.279

All Matching Solutions

Stage	Helix1	Helix2	Strand1	Strand2	Turns	Unordered	Total
3	0.031	0.085	0.255	0.126	0.208	0.277	0.982
3	0.026	0.078	0.264	0.129	0.225	0.296	1.018
3	0.034	0.076	0.245	0.120	0.213	0.281	0.970
3	0.029	0.075	0.254	0.120	0.219	0.284	0.981
3	0.033	0.114	0.248	0.130	0.200	0.262	0.987
4	0.031	0.085	0.255	0.126	0.208	0.277	0.982
4	0.026	0.078	0.264	0.129	0.225	0.296	1.018
4	0.034	0.076	0.245	0.120	0.213	0.281	0.970
4	0.029	0.075	0.254	0.120	0.219	0.284	0.981
4	0.033	0.114	0.248	0.130	0.200	0.262	0.987

HELICES (Per 100 Residues) are: 2.103 · STRANDS (Per 100 Residues) are: 6.135

The AVERAGE LENGTH of HELICES : 5.608 · The AVERAGE LENGTH of STRANDS : 6.075

Figure 4.14   The secondary structure prediction of Δ20MacA. The data were analyzed by three algorithms (a) Contin-LL, (b) CDSSTR and (c) SELCON3.

Data was then input into the online server Dichroweb at Birbeck College, and analyzed by the algorithms SELCON3, CDSSTR and CONTIN-LL. The NRMSD (normalized root mean square deviation) values in the analyses generated from these three algorithms CONTIN-LL, CDSSTR, and SELCON3 are 0.105, 0.027 and 0.086 respectively (Figure 4.14). Generally speaking, a low value for the NRMSD is a necessary but not sufficient condition for concluding that an analysis has produced a good result (Brahms S and Brahms J, 1980) That is, if the NRMSD is high (> 0.1), the correspondence of the calculated secondary structure with the actual one is probably 'incorrect', but a low NRMSD does not necessarily indicate an accurate analysis. Among the three algorithms, CDSSTR gave the lowest NRMSD value; however, this algorithm tends, but not always, to give the lowest NRMSD values for a given reference database, but this does not mean that those results are the most significant. Apart from the NRMSD, the total sum of the secondary structure compositions must be ≥ 1. Based on these rules, the selected predicted compositions of α-helix were 18.7%, 9%, and 10.4% from CONTIL-LL, CDSSTR, and SELCON3 respectively (Figure 4.14). The membrane fusion protein AcrA in *E. coli* in its truncated form (Mikolosko *et al.*, 2006) has approximate 15% α-helix composition. Thus, our data is consistent with the prediction that the truncated MacA has the coiled coil hairpin structure.

4.6 Discussion

Membrane fusion proteins have been found to be essential components of tripartite pumps utilizing RND, MFS, and ABC transporters (Putman *et al.*, 2000). The ATPase domain of MacB supplies a good approach to study the interaction of MacA with MacB. At first, MacA was originally extracted from membranes using DDM, however, our EM analysis and gel filtration data (data now shown) indicated it aggregated immediately after purification. Oddly, both MacB and MacA lost stability when extracted with DDM, but they both retained activity when extracted with Triton X-100.

Our kinetic data indicated that MacB had a maximal specific activity of 8.9 nmoles ATP/min/mg MacB and a K_m of 374 μM Mg-ATP. During the course of our studies another investigation reported on the ATPase activity of MacB (Tikhonova *et al.*, 2007), in which it was found that MacB retained ATPase activity in Triton X-100 but was inhibited by DDM. In this report, MacB, solubilized in 0.2% Triton X-100, appeared to have a specific activity that was an order of magnitude higher than we had found; however, a discontinuous assay was used to determine the ATPase activity and this could have been exaggerated by the initial Pi burst in the reaction. Indeed, k_{cat} was marginally slower than the hydrolysis rate determined from the Pi burst phase in our experiments (e.g. 0.17 s^{-1} versus 0.22 s^{-1}). In this report, they found that MacA could stimulate the ATPase activity of MacB when both of them were co-reconstituted into proteoliposomes; however, MacA had no substantial effect on the modulation of the ATPase activity of MacB in the detergent-solubilized state, which contrasts with our findings in that MacA increases the rate of product release (k_{cat} from 0.011 to 0.015 s^{-1}), whilst decreasing the rate of hydrolysis to a similar rate to product release. The reason for this discrepancy could be because a discontinuous assay was used to determine the ATPase activity in the study undertaken by Tikhonova *et al* (Tikhonova *et al.*, 2007), and the initial Pi burst in the reaction could have gone unnoticed. However, they did find that co-reconstitution of MacB with MacA had the effect of increasing both k_{cat} (k_{cat} from 0.1 to 0.78 s^{-1}) and the affinity of MacB for ATP (K_m from 2.3 to 0.38 mM). This behaviour is similar to the effect of MacA on the steady-state kinetics of the ATPase activity of solubilized MacB in our study. To know if the reconstituted protein behaves in an identical manner to the solubilized protein would require the

reconstitution of sufficient amounts of MacB to define any Pi burst, which is technically demanding.

We found that the addition of a slightly sub-stoichiometric concentration of *E. coli* MacA to MacB was sufficient block the Pi burst catalysed by MacB, suggesting that the stoichiometry of binding of MacA:MacB is 1:2. This makes sense in the light of our finding that MacB forms dimers, which presumably bind a single MacA. Considering that TolC forms a trimer this would suggest that it binds at least three MacA molecules; implying that the minimal stoichiometry for the tripartite complex is a trimer of MacB dimers, each of which is connected to TolC via a single MacA (e.g. a MacA/MacB/TolC assembly of 3: 6: 3). Consistent with this proposal our AFM studies have identified particles larger than expected for a complex of a MacA monomer and MacB dimer (e.g. 307 nm^3) and with volumes sufficient to accommodate a trimer of MacB dimers and MacA trimer (e.g. > 900 nm^3).

The CD data is consistent with our prediction that MacA possess a coiled-coil hairpin structure. We predicted that *S. aureus* MacA has lost a large fragment, spanning residues 88-206 in the MFP encoded by *SAS0172*, and that this is the region that would incorporate the α-helical coiled-coil domain that interacts with the OMP (Lobedanz *et al.*, 2007). The addition of either *E. coli* MacA or *S. aureus* MacA can regulate the ATPase activity of MacB, suggesting that it is the β-strand domain of MacA, which is involved in the MacA-MacB interaction.

Chapter five: Tripartite pump: MacA, MacB and open state TolC

The membrane fusion protein AcrA, the RND transporter AcrB and the multi-functional outer membrane protein TolC can form a functional complex, and the latter can also function with MF and ABC transporters (Saier and Paulsen, 2001). Although the structure of an assembled tripartite complex structure has not been determined, the structure of each component has revealed how those components may assemble. The MacA/MacB/TolC complex was shown to confer resistance to macrolides in *E. coli* (Kobayashi *et al.*, 2001); in this study, our aim was to investigate how the complex is aeeembled and functions.

5.1 A functional tripartite complex

To evaluate the function of the tripartite complex, we adopted measurements of the growth of cells expressing various combinations of the *macA*, *macB* and *tolC* genes. The expression level of wild type TolC was not stable so the plasmid encoding the open-state TolC, which has a deletion of the last 43 amino acids and two mutation points, Y362F and R367E, was a courtesy from the lab of Dr. Ben Luisi at the University of Cambridge (Bavro *et al.*, 2008), has been used in this experiment. This served as the template for PCR amplifications in all TolC constructs.

5.1.1 Constructions

Constructs were made in a similar manner as described in section 3.1. In short, the chromosomal *macB* region of *E. coli* Novablue was amplified using PCR and cloned into *EcoRI* and *SalI* restriction sites in the first cloning site of pETDuet™-1 to yield the pETDuet™-1/*macB* plasmid. The amplified *tolC* gene was then cloned into *NdeI* and *XhoI* restriction sites in the second cloning site of the pETDuet™-1/*macB* plasmid to yield the pETDuet™-1/*macB-tolC* plasmid (Figure 5.1a). A Shine-Dalgarno (SD) sequence was added upstream of the full length *macA* gene during PCR amplification. The amplified *SD-macA* gene was cloned into the *SalI* and *NotI* sites in the first cloning site of the pETDuet™-1/*macB* and the pETDuet™-1/*macB-tolC* plasmids to yield pETDuet™-1/*macB-macA* and pETDuet™-1/*macB-macA-tolC* plasmids, respectively (Figure 5.1b). In order to test whether the N-terminus of MacA is required for the functional assembly of the complex, the plasmid pETDuet™-1/*macB-SS-Δ20macA-tolC* plasmid was constructed in a similar manner but with a slight modification. The signal sequence gIII from the vector pBAD/gIII was fused to the 5' end of the *SD-Δ20macA* sequence in order to lead truncated MacA to the periplasm (Figure 5.1c).
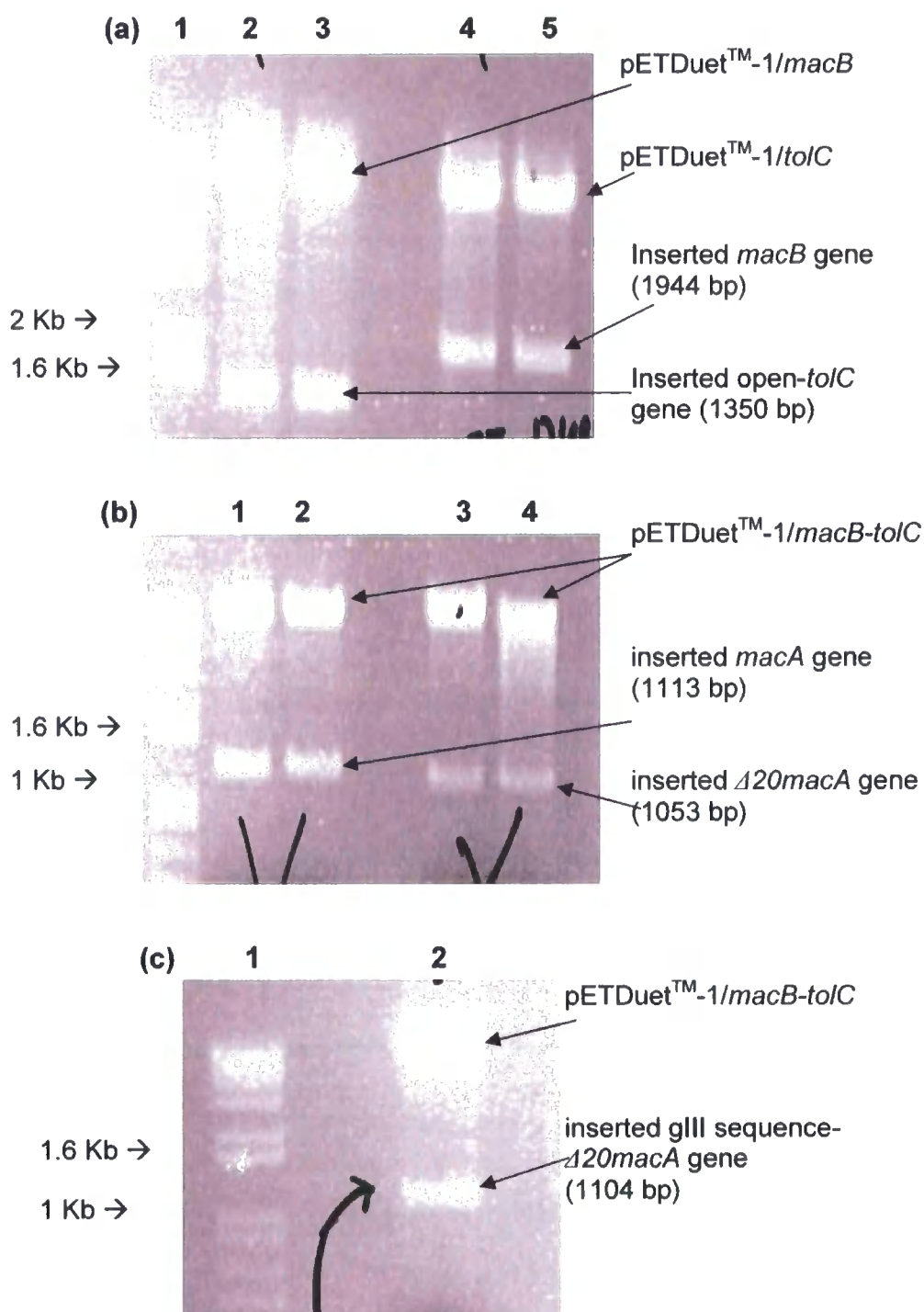
Figure 5.1 **Constructions for drug susceptibility tests.** (a) Restriction enzyme digestion analysis of pETDuet™-1/*macB-tolC* plasmid. Lane 1= the DNA ladder. Lanes 2-3 indicate the presence of the *tolC* gene. Lanes 4-5 indicate the presence of the *macB* gene. (b) Restriction enzyme digestion analysis of pETDuet™-1/*macB-macA-tolC* and pETDuet™-1/*macB-Δ20macA-tolC*. Lane 1= the DNA ladder. Lanes 2-3 indicate the presence of the *macA* gene. Lanes 4-5 indicate the presence of the *Δ20macA* gene. (c) Restriction enzyme digestion analysis of pETDuet™-1/*macB-gIII-Δ20macA-tolC*. Lane 1= the DNA ladder. Lane 2 indicates the presence of the *gIII-Δ20macA* gene.

5.1.2 Drug susceptibility test

Plasmids pETDuet™-1/*macB*, pETDuet™-1/*macB-macA*, pETDuet™-1/*macB-tolC*, pETDuet™-1/*macB-macA-tolC* and pETDuet™-1/*macB-Δ20macA-tolC* were transformed into the *E. coli* △*acrAB* strain Kam3(DE3), which is highly susceptible to a range of antibiotics (Morita *et al.*, 1998). The λDE3 lysogenisation of Kam3 was described in section 2.4.5.

The *macA*, *macB* and *tolC* genes were simultaneously expressed from pETDuet™-1 in the Kam3(DE3) strain, conferring elevated resistance to the macrolide erythromycin compared to the control Kam(DE3), harboring only the pETDuet™-1 vector, indicative of the formation of a functional complex (Figure 5.2).

Our previous data in section 4.3 suggested that the N-terminal transmembrane domain of MacA is not required in the regulation of the ATPase activity of MacB. In order to test whether the N-terminus of MacA is required for the functional assembly of the complex. A construct in which the gIII signal sequence was fused to truncated MacA, targetting it to the periplasm, was capable of conferring resistance to erythromycin (Figure 5.2), indicating that the N-terminal transmembrane domain is not essential for the assembly of the functional complex. This finding is consistent with two reports on membrane fusion proteins. Yoneyama *et al* (Yoneyama *et al.*, 2000) substituted cysteine 24 with phenylalanine or tyrosine and showed this mutant soluble MexA, without the lipid moiety, retained its function in the MexA/MexB/OprM complex pumps, retaining the antibiotic susceptibility. Membrane fusion protein AcrA, when being truncated the first 25 residues, still functional active in the AcrA/AcrB/TolC complex pumps, conferring erythromycin and novobiocin resistance in the *△acrA* deletion *E. coli* strain N43 (Zgurskaya and Nikaido, 1999).

Cells expressing *macB* with *tolC* conferred modest resistance to erythromycin in comparison to cells expressing *macB*, *tolC* and *macA*, indicating that MacA is required to couple MacB to TolC (Figure 5.2).
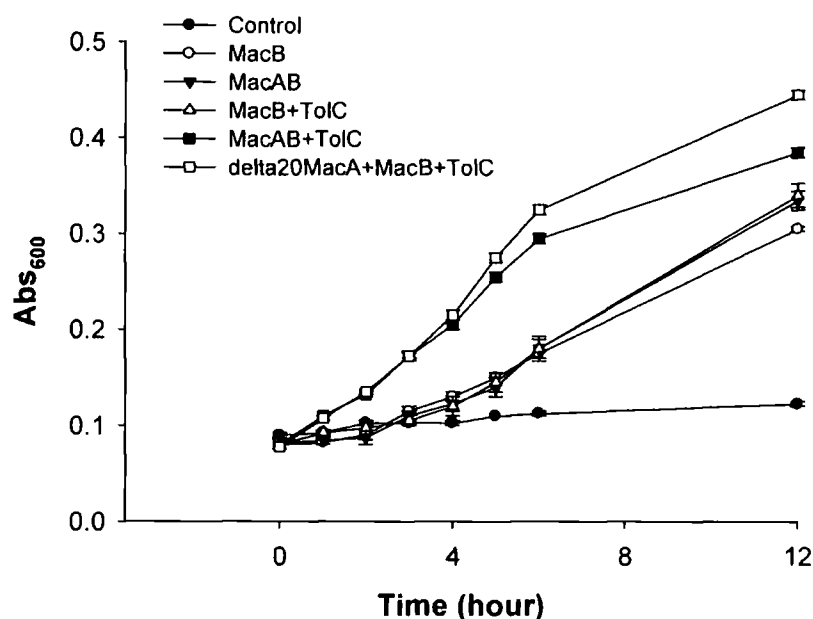
Figure 5.2 **Growth curve measurements.** The cell growth of Kam3 cells harboring plasmids were measured at absorbance 600 nm up to 12 hours in the presence of erythromycin at the concentration of 100 µg/ml.

MacB alone conferred elevated resistance to erythromycin, probably due to its ability to pump the antibiotic into the periplasm, but we consistently found that expressing *macB* with either *tolC* or *macA* conferred greater resistance. Consequently, we sought to test if MacA could enhance this ability. However, it is difficult to distinguish the slight difference in resistance since cells harboring different plasmids tend to grow at different rates. Consequently, we adopted an alternative procedure of monitoring the growth of cells in the presence and absence of erythromycin and determining the loss in growth due to the antibiotic. This procedure enable us to determine the susceptibility of the MacB and MacAB expressing cells to erythromycin, revealing a more significant loss in growth of the MacB expressing cells compared to the MacAB expressing cells and indicating that the simultaneous expression of MacA and MacB increases the resistance of the cells to erythromycin (Figure 5.3). This data suggests that MacA enhances the ability of MacB to confer antibiotic resistance. Similarly, a previous study reported that MacAB, but not MacB alone, conferred resistance to macrolides (Kobayashi *et al.*, 2001).
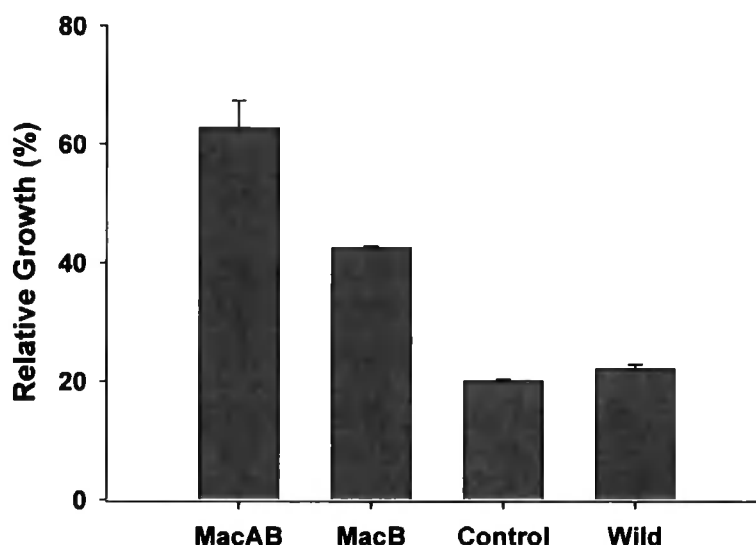
Figure 5.3 **Drug susceptibility histogram.** The cell growth of Kam3 cells harboring plasmids were measured at absorbance 600 nm up to 3 hours. Relative growth (%) was obtained by dividing the growth of cells in the presence of 50 µg/ml erythromycin by the growth of cells in the absence of erythromycin. MacAB represents the cells expressing MacAB proteins; MacB represents the cells expressing MacB protein; Control represents the cells harboring empty vector; and Wild represents the wild Kam3(DE3) *E. coli* strain.

5.2 MacA enhanced the erythromycin binding to MacB

The equilibrium binding of erythromhycin experiments were undertaken in collaboration with Dr. Saroj K. Velamakanni at the University of Cambridge.

From the previous section, we concluded that MacA, MacB and TolC can form a functional tripartite pump, conferring *E. coli* resistance to erythromycin. Furthermore, the cells harboring the plasmid encoding MacAB showed greater resistance than the plasmid encoding MacB itself. Our kinetics data has indicated that MacA regulates MacB ATPase activity; in this section, we detected the binding of [N-methyl-^{14}C]-erythromycin to purified MacB in the presence and absence of MacA (section 2.7.2). The experiments were divided into three groups containing 50 µg MacA, 50 µg MacB, and 25 µg MacB with 25 µg MacA respectively, where equal amount of protein was in each group. Interestingly, our data indicated that MacB bound more erythromycin in the presence of MacA, in a concentration dependent manner (Figure 5.4). However, it was not possible to increase the erythromycin to a concentration that saturated MacB to determine affinity due to erythromycin high hydrophobicity, leading erythromycin

to precipitate with proteins at higher concentration. The data indicate that MacA not only modulates the ATPase activity of MacB but also enhances its capacity to bind erythromycin.
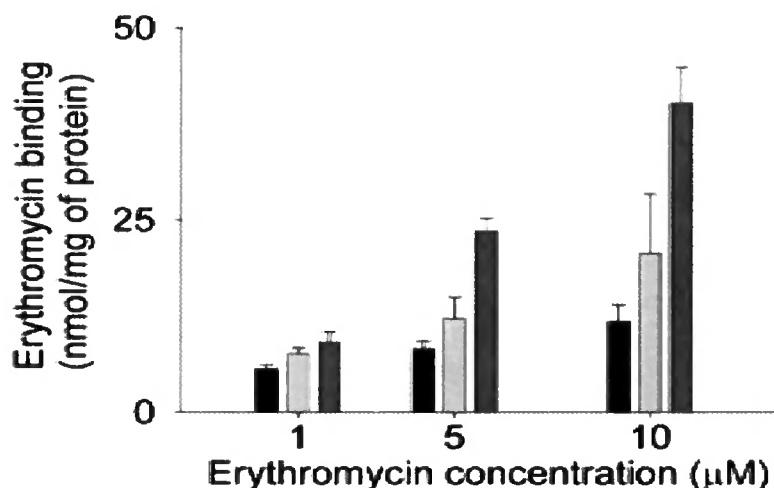
Figure 5.4 **Histogram of erythromycin equilibrium binding** to MacA, MacB and MacAB proteins. The bars represent the erythromycin bound by MacA (left, black), MacB (middle, light grey) and MacAB (right, dark grey).

5.3 *in vitro* crosslinking of MacA-MacB

The protein crosslinking experiments and data representation were undertaken in collaboration with Dr. Vassiliy N. Bavro at the University of Cambridge.

Our drug susceptibility tests indicated that MacA, MacB and TolC can form a functional complex pump *in vivo*; whilst our kinetics data indicate that purified MacA can regulate the ATPase activity of purified MacB in a detergent solubilized state. In this section, protein-protein crosslinking was adopted to gain more evidence that MacB can interact with MacA *in vitro*. Purified MacB and MacA were incubated with the crosslinker DMA and DMS for 1 hr at room temperature. Interestingly, additional bands (Lane 5, 6, 9 and 10) appeared with an Mr greater than the MacB monomer, and the one in the lane 5 was cut out along with the control bands in lane 3 for MALDI (Matrix-Assisted Laser Desorption/Ionization) analysis. MALDI in gel-digestion indicated that both MacA and MacB proteins were present in the cross-linked band (Figure 5.6); a miniscule amount of MacA could only be detected in the control band. This data suggested that MacB can interact directly with MacA.

Figure 5.5   **SDS-PAGE of the crosslinked MacA-MacB complexes** by using DMA and DMS. MacB-MacA complexes are framed in red boxes. Lane 1= MacA, Lane 2= MacB, Lane 3= MacA + 5 mM DMA, Lane 4= MacB + 5mM DMA, Lane 5= MacA + MacB + 5 mM DMA incubated for 1 h, Lane 6= MacB+ 5 mM DMA to be incubated for 30 min + MacA for another 30 min, Lane 7= MacA + 5 mM DMS, Lane 8= MacB + 5 mM DMS, Lane 9= MacA + MacB +5 mM DMS incubated for 1 h, Lane 10= MacB+ 5 mM DMS incubated for 30 min + MacA for another 30 min.

Figure 5.6   **MALDI analyses of the MacA-MacB complex fragment**. Fragments positively identified by MALDI are colored in red. (a) MacB protein has 42% sequence coverage of the peptide map. (b) MacA protein has 37% sequence coverage of the peptide map.

5.4 *in vitro* interaction between components in the complex

Interactions between *E. coli* MacA, MacB and TolC were tested for using detergent solubilized proteins for pull down assays. The strategy for the pull-down assay involved using a bait protein and a prey protein (section 2.7.3). MacB-His$_6$ served as the bait protein in the detection of MacA-MacB and MacB-TolC interaction, and TolC-His$_6$ served as the bait protein in the detection of TolC-MacA interaction.

5.4.1 Construction and overexpression of the bait proteins

Purifed MacB-His$_6$ protein was overexpressed and purified as previously described (section 3.1).

pET21a/*tolC* plasmid was constructed in a similar manner, to that described in section 3.1; and relevant primers, vector plasmids and *E. coli* strains can be found in section 2.3 and 2.4. In short, the amplified *tolC* gene was cloned into the *NdeI* and *XhoI* restriction sites of the pET21a(+) plasmid to yield the pET21a/*tolC* plasmid (Figure 5.7a). The pET21a/*tolC* expression construct was then transformed into the *E. coli* strain C43(DE3) for protein production. The protein expression and cell membranes harvest were manipulated as described in section 2.5. The cell membranes were dissolved in 20 mM Tris buffer pH 7.5, 300 mM NaCl, 10 mM imidazole, 1 mM THP, 10% glycerol and 5% Triton X-100 on a rotary shaker overnight.

TolC-His$_6$ was purified by metal affinity chromatography using a HiTrap Ni^{2+} column (section 2.5.1), and eluted in buffer containing 20 mM Tris-HCl pH 7.5, 500 mM NaCl, 10% glycerol, 500 mM imidazole and 0.2% Triton X-100. The yield and purify of the TolC-His$_6$ was determined by gel electrophoresis (section 2.6.1) (Figure 5.7b). The migration of the major protein band (lanes 2 to 6) is just above the 51 kDa protein marker band (lane 1), which is consistent with the Mr of the TolC-His$_6$, with a calculated molecular weight of 49.2 kDa.
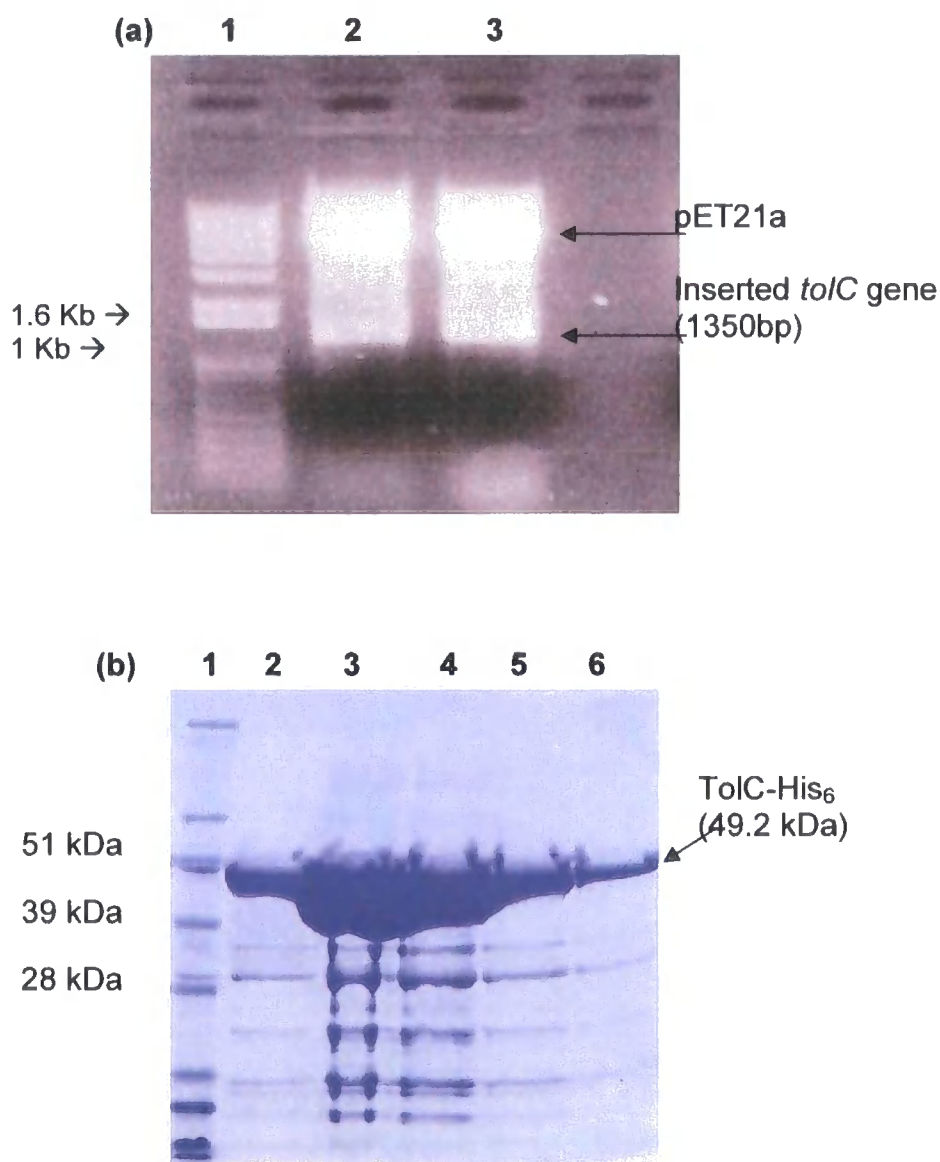
Figure 5.7 **pET21a/tolC construction and overexpression** (a) Restriction enzyme digestion analysis of pET21a/*tolC* plasmids. Lane 1= the DNA ladder. Lanes 2-3 indicate the presence of the *tolC* gene. (b) SDS-PAGE of TolC-His$_6$. Lane 1= the protein M_r marker. Lanes 2-6 indicate the TolC-His$_6$ proteins.

5.4.2 Construction of the prey proteins

Constructs were made in a similar manner to those described in the previous section. In short, the amplified *Δ20macA*, *macA* and *tolC* genes was cloned individually into the *NcoI* and *XhoI* restriction sites of the pET45b(+) plasmid to yield the pET45b/*Δ20macA*, pET45b/*macA* and pET45b/*tolC* plasmids (Figure 5.8a). Each of those expression constructs was transformed into the *E. coli* strain C43(DE3) for membrane slurry production.
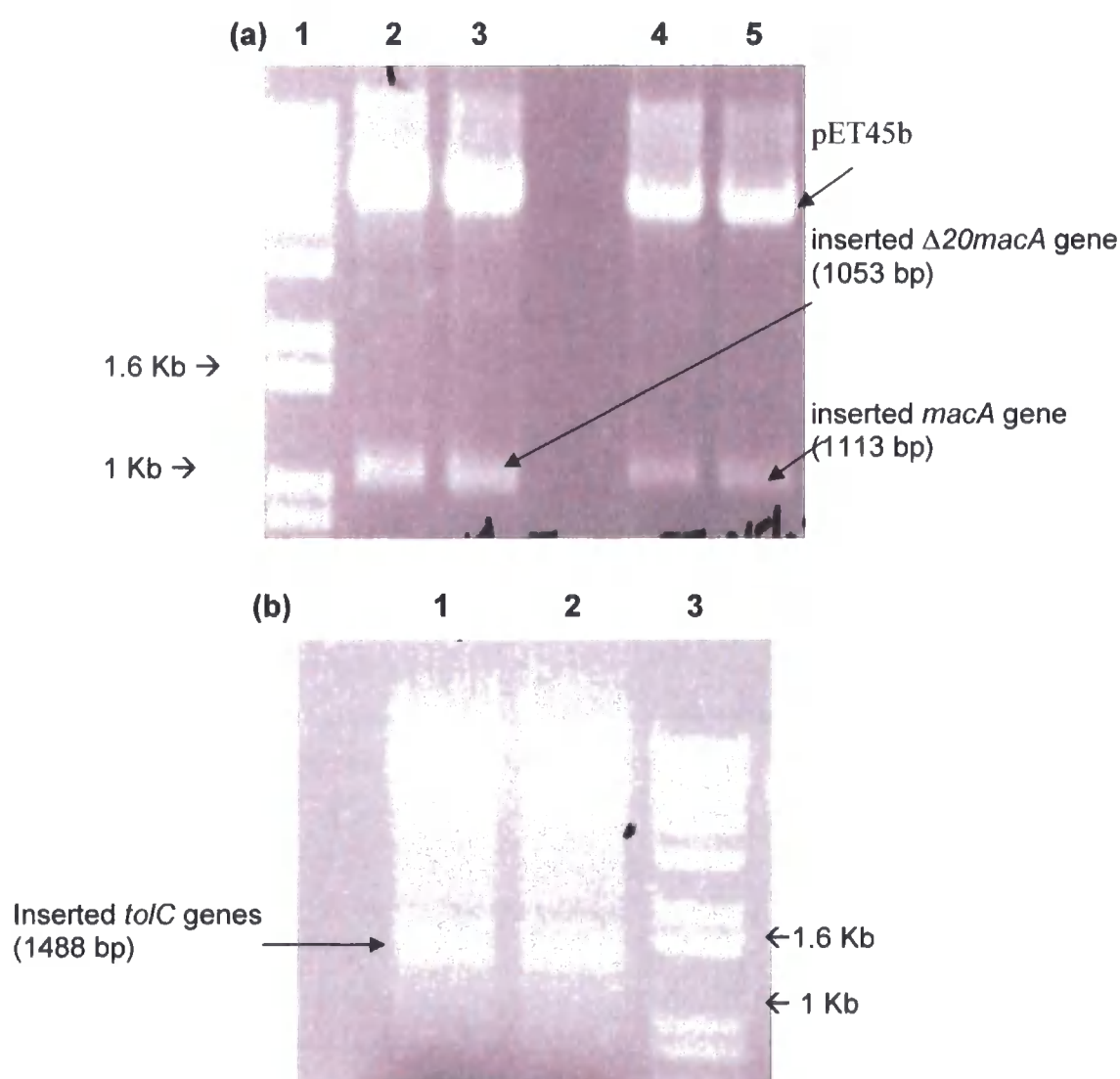
Figure 5.8   S-tagged protein construction for pull-down assay. (a) Restriction enzyme digestion analysis of pET45b/*macA* and pET45b/*Δ20macA* plasmid. Lane 1= the DNA ladder. Lanes 2-3 indicate the presence of the *Δ20macA* gene. Lanes 4-5 indicate the presence of the macA gene. (b) Restriction enzyme digestion analysis of the pET45b/*tolC* plasmid. Lane 3= the DNA ladder. Lanes 1-2 indicate the presence of the tolC gene.

5.4.3 Pull down Assay

In the AcrA/AcrB/TolC tripartite complex pump, calorimetry demonstrated energetically favourable interactions of AcrA with both purified AcrB and TolC proteins (Touzé *et al.*, 2004). We previously concluded that MacA, MacB and TolC form a functional complex on the basis of our drug susceptibility test data and our findings indicate that MacB directly interacts with MacA in crosslinking studies.

Using pull-down assay (section 2.7.3), in which MacB-His$_6$, served as the bait protein, we were able to capture the prey protein MacA-Stag (Figure 5.9). Membrane pellets containing MacA-Stag was dissolved in Triton X-100 and added to purified MacB-His$_6$. The mixture was loaded into a Ni^{2+} charged chelating column to immobilize the MacB-His$_6$, along with MacA-Stag. Unbound MacA-Stag can be seen in the flow-through (Figure 5.9 lane 6); the column was then given highly stringent wash to eliminate unbound MacA-Stag. A fraction was collected before the elution of the MacB-His$_6$-MacA-Stag complex and only a very tiny amount of MacA-Stag could be detected, indicating little or no unbound MacA-Stag suspending in the column (Figure 5.9 lane 5). The MacB-His$_6$ and MacA-Stag can be clearly observed in the elution (Figure 5.9 lane 4), revealing MacA could interact with MacB. No MacA-Stag was seen in the elution of the control group (Figure 5.9 lane 1), suggesting that there was no non-specific interaction between MacA and the column.

Using MacB-His$_6$ and N-terminal truncated MacA-Stag for the pull-down assay, Δ20MacA can be observed in the elution (Figure 5.10), indicating that there is interaction between the periplasmic domain of MacA and MacB. This behaviour is consistent with our previous data that indicated that truncated MacA can regulate the ATPase activity of MacB. Similarly, using TolC-His$_6$ and MacA-Stag, a strong interaction can be detected (Figure 5.11). Using MacB-His$_6$ and TolC-Stag, an interaction can be observed (Figure 5.12), but this interaction is apparently a lot weaker than those between MacA and MacB/TolC.
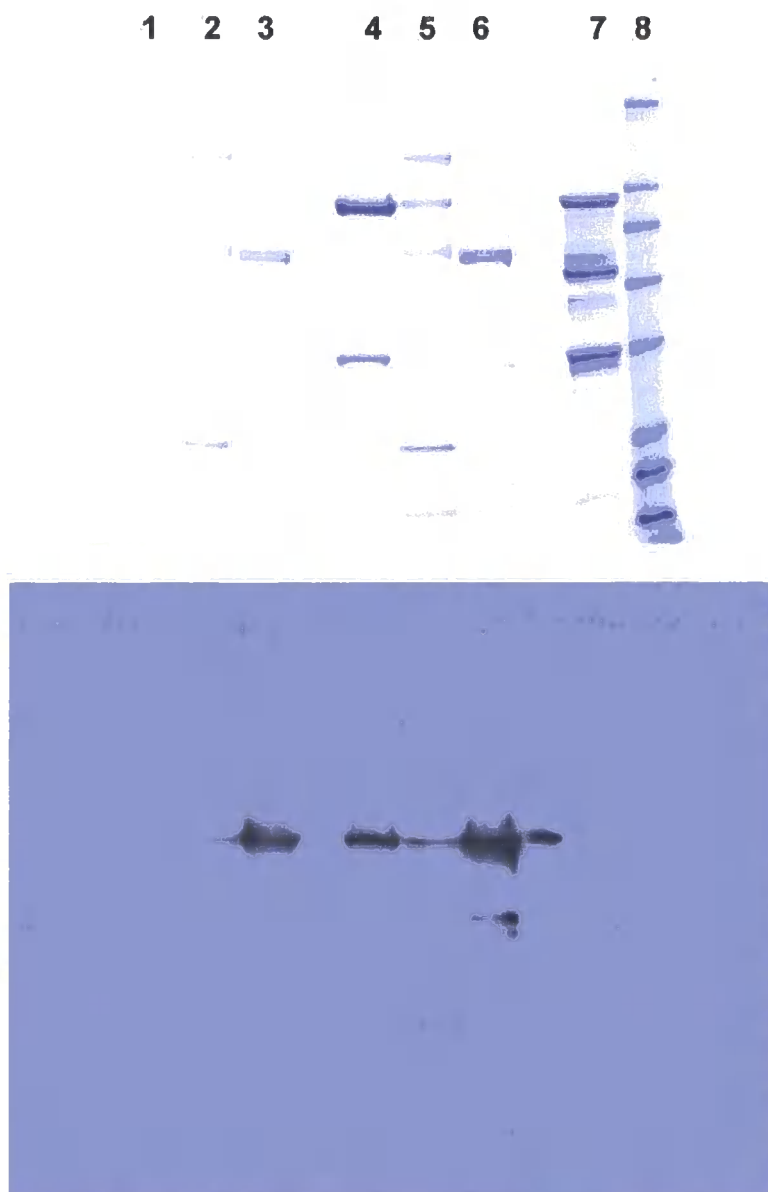
Figure 5.9 **MacA-Stag pulled down by MacB-His$_6$.** Lane1= elution, Lane 2= wash, Lane 3= flow-through (Lanes 1-3 were collected in the absence of the MacB-His$_6$ protein). Lane 4= elution, Lane 5= wash, Lane 6= FT (Lanes 4-6 were collected in the presence of the MacB-His$_6$ protein. Lane 7= the MacB-His$_6$ protein and Lane 8= the protein M$_r$ marker. The identity of the MacA-Stag protein was confirmed by Western blot using S-Tag monoclonal antibody.
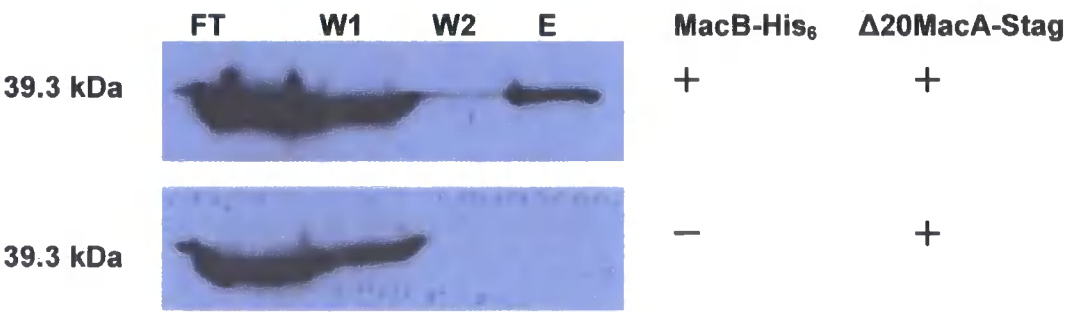
Figure 5.10   **Δ20MacA-Stag pulled down by MacB-His₆.** FT represents flow-through, W1 represents early stage of wash, W2 represents later stage of wash, and E represents elution. "+" indicates the presence of the protein, whereas "-" indicates the absence of the protein. In the film, the prey protein was detected by Western blot using S-Tag monoclonal antibody.
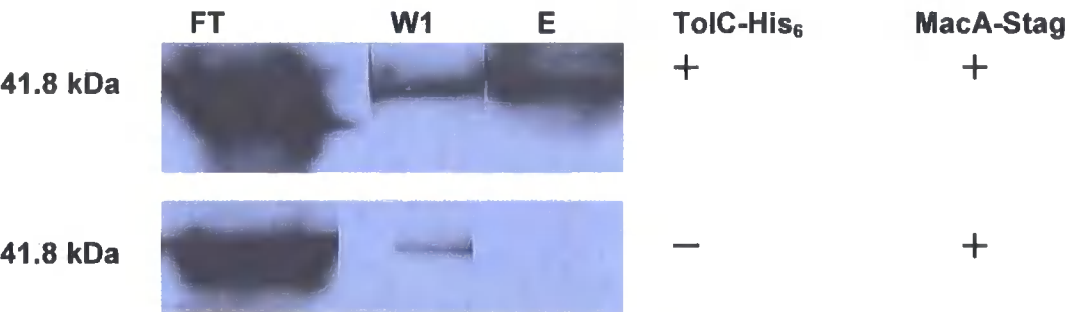
Figure 5.11   **MacA-Stag pulled down by TolC-His₆.** FT represents flow-through, W1 represents early stage of wash, and E represents elution. "+" indicates the presence of the protein, whereas "-" indicates the absence of the protein. In the film, the prey protein was detected by Western blot using S-Tag monoclonal antibody.
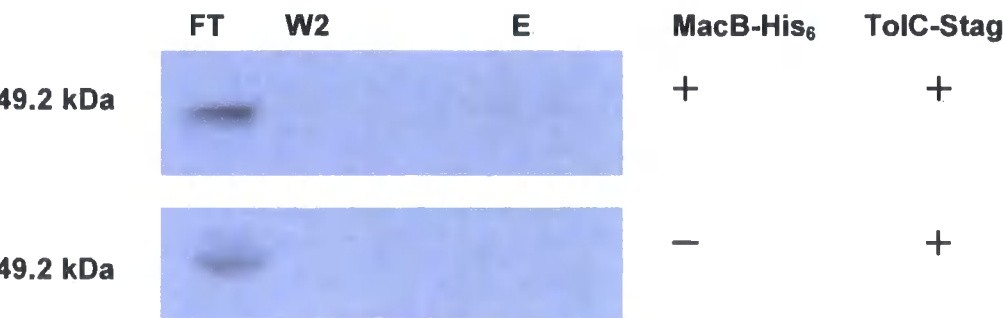
Figure 5.12   **TolC-Stag pulled down by MacB-His₆.** FT represents flow-through, W2 represents later stage of wash, and E represents elution. "+" indicates the presence of the protein, whereas "-" indicates the absence of the protein. In the film, the prey protein was detected by Western blot using S-Tag monoclonal antibody.

5.5 Discussion

Gram-negative bacteria possess tripartite pumps composed of an inner membrane protein, a periplasmic protein and an outer membrane protein, which work together to confer multidrug resistance. In order to determine the function of the MacA/MacB/TolC tripartite-complex pump, we undertook growth curve measurement to determine the drug susceptibility of the strains expressing different combinations of the MacA, MacB and TolC proteins.

Originally, minimum inhibitory concentration tests (MIC) were adopted to determine whether the MacA/MacB/TolC complex pump confers resistance to the macrolide erythromycin in bacteria. However, $E.$ $coli$ strain Kam3(DE3) harboring plasmids encoding MacA, MacB and TolC didn't have a substantial effect on the resistance of the cells to erythromycin (data not shown). It could be that although the proteins assembled together to translocate drugs successfully, the high toxicity of the three proteins had a detrimental effect on the host cells, leading to the insignificance of drug resistance. As an alternative, growth curve measurements were undertaken to determine the function of the tripartite complex pump. During the grow curve measurements, the tubes were put in an incubator with shaking to enable more O_2 to be dissolved into the media, allowing the host cells to grow more vigorously. The effect was that in the growth curve measurements, the minimum concentration that inhibited growth of erythromycin is a lot greater than the one in the MIC tests (e.g. 300 μM vs 16 μM erythromycin).

Our drug susceptibility tests revealed that MacB can confer elevated resistance in bacteria to erythromycin in the presence of MacA (Figure 5.3) and our equilibrium erythromycin binding experiments indicated that MacA increases the binding ability of MacB to erythromycin (Figure 5.4); besides, our kinetics data suggested that MacA increased the rate of product release from MacB, speeding up the turn over rate. We speculated that MacA increases the binding ability of MacB for erythromycin to catch up the faster conformation switch between the outward-facing and inward-facing conformation, speeding up the transportation of drugs.

In the AcrA/AcrB/TolC complex pump, AcrA can be crosslinked with AcrB and TolC individually *in vivo*, and microcalorimetry studies demonstrated energetically favourable interactions of AcrA with both purified AcrB and TolC *in vitro* (Touzé *et al.*, 2004). Our pull-down data indicated that any two components of the MacA/MacB/TolC complex pump can interact directly in the absence of the third component. However, the intensity of the band in Figures 5.10, 5.11 and 5.12 suggests that the interaction between MacB and TolC is weak compared to those between MacA and MacB/TolC. This may suggest that the dimerization of MacB can recruit TolC, via MacA, and simultaneous open TolC for translocation.

Chapter six: Crystallization trials

Integral membrane proteins such as transporters and receptors are critical components of many fundamental biological processes. Furthermore, integral membrane proteins are important in biomedical and biotechnological applications; whilst the majority of drug targets are integral membrane proteins. The macrolide ABC transporter MacB putatively has an exceptional structure comprising of four transmembrane helices, which is drastically different to the topology of the structure determined for ABC exporters Sav1866 and MsbA, which has six transmembrane helices, in bacteria. In this chapter, I report on how the MacB protein was to crystallization screens in order to acquire crystal for structure determination.

6.1 Dynamic light scattering of MacB

Purified MacB in buffer containing 20 mM Tris-HCl pH 7.5, 50 mM NaCl, 0.05% DDM and 10% glycerol was analyzed by dynamic light scattering to determine the size distribution profile of MacB. The DLS profiles of 1 mg/ml MacB and the buffer itself were measured at 16°C and 4°C. A good correlation between the traces suggested that measurements and data are reliable, and MacB showed its high homogeneity (> 97%) at both 16°C and 4°C (Figure 6.1ab), indicating that it is monodispersed in solution. The analysis of the buffer itself served as the control, compared to MacB, eliminating the chance of a false signal from the buffer (Figure 6.1c).

(a)
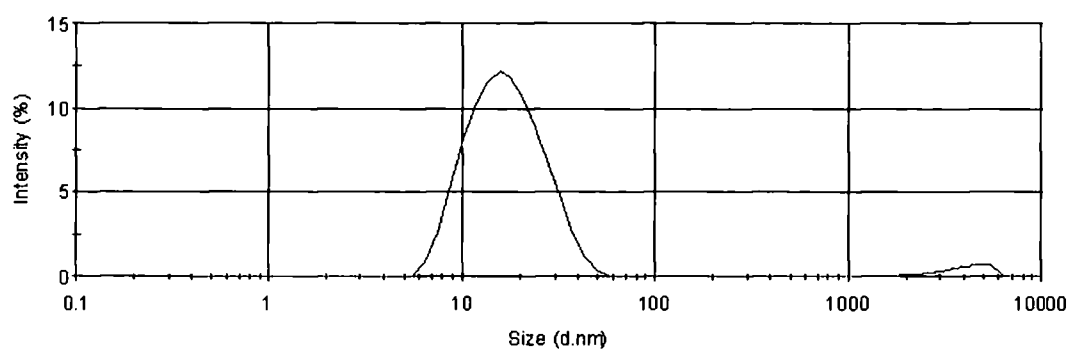
(b)
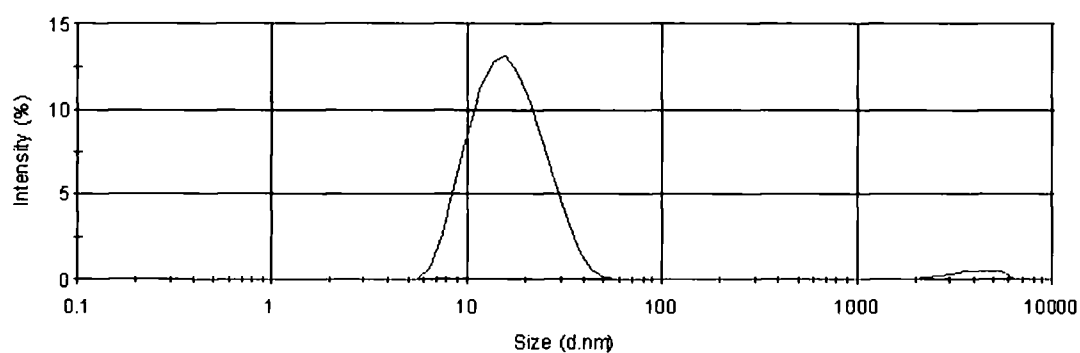
(c)
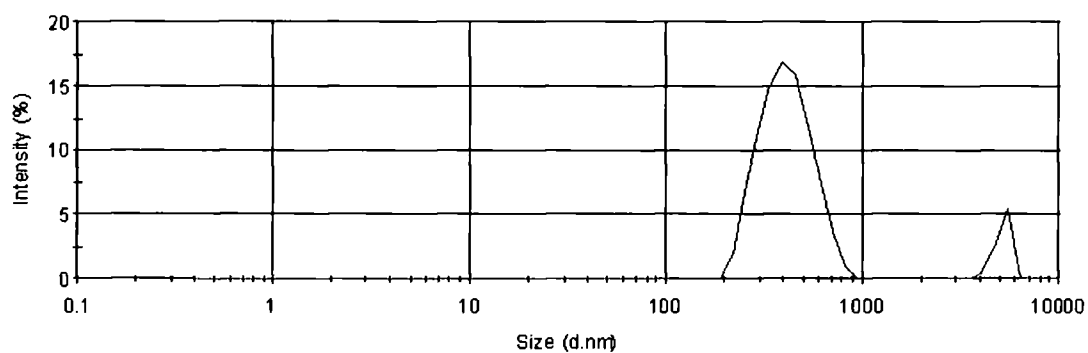
Figure 6.1   **Size distribution analysis of MacB.** The DLS profile of MacB was measured at 16°C (a) and at 4°C (b), and the DLS profile of the buffer was measured at 4°C (c).

6.2 Preliminary sparse matrix screen of MacB

The protein crystallization and data collection were undertaken in collaboration with Dr. Vassiliy N. Bavro and Mr. Zbigniew Pietras at the University of Cambridge.

The *macB* gene sequence was cloned on to the pET28a(+) plasmid vector, which introduces a thrombin digestion site between the N-terminal His tag and the cloning site, making it possible to make tag-free MacB proteins for crystallization trials. However, after being treated with thrombin enzyme (Novagen), a small proportion of MacB still retained the tags, detected by Western blot (section 2.6.3), causing heterogeneity in the protein prep (data not shown). To avoid heterogeneity, the tag and the cleavage sequence were left on the N-teminal on MacB when it was crystallized

Purified MacB in Triton X-100 (0.2%) (section 3.1) was exchanged and dialyzed against buffer containing 20 mM Tris-HCl pH 7.5, 50 mM NaCl, 0.05% DDM and with or without 10% glycerol before being used in crystallization trials. Preliminary crystallization trials of MacB were accomplished using sparse matrix screens to discover a suitable starting condition.

The commercial sparse matrix screens used were SM1, MbClass, MbClassII, Classics, Classics light, pHClear II (Qiagen), MembFac (Hampton Research), and MemSys (Molecular Dimensions). Crystallization trials were undertaken using 10 mg/ml MacB in the vapour diffusion sitting drop method on 96 well plates with round bottoms and automated screening by a Cartesian robot. The development was monitored intermittent by light microscopy.

As shown in Figure 6.2, a few putative micro-crystals could be observed in five conditions, but only one of them was from non-glycerol MacB samples (#57 Classics light), suggesting that MacB is more stable in the presence of glycerol. Among the five conditions, 28-30% PEG400 is found in three conditions (Classics 74 and 75, and MbClassII 39), suggesting that precipitant PEG 400 is suitable for MacB crystalization; however, no specific salt or pH value is preferable for the formation of MacB crystals (Table 6.1).

Having identified a promising starting condition, the condition can be further optimised to improve crystal quality through adjustments in precipitant and salt concentration, and pH ranges (Delucas *et al.*, 2005).
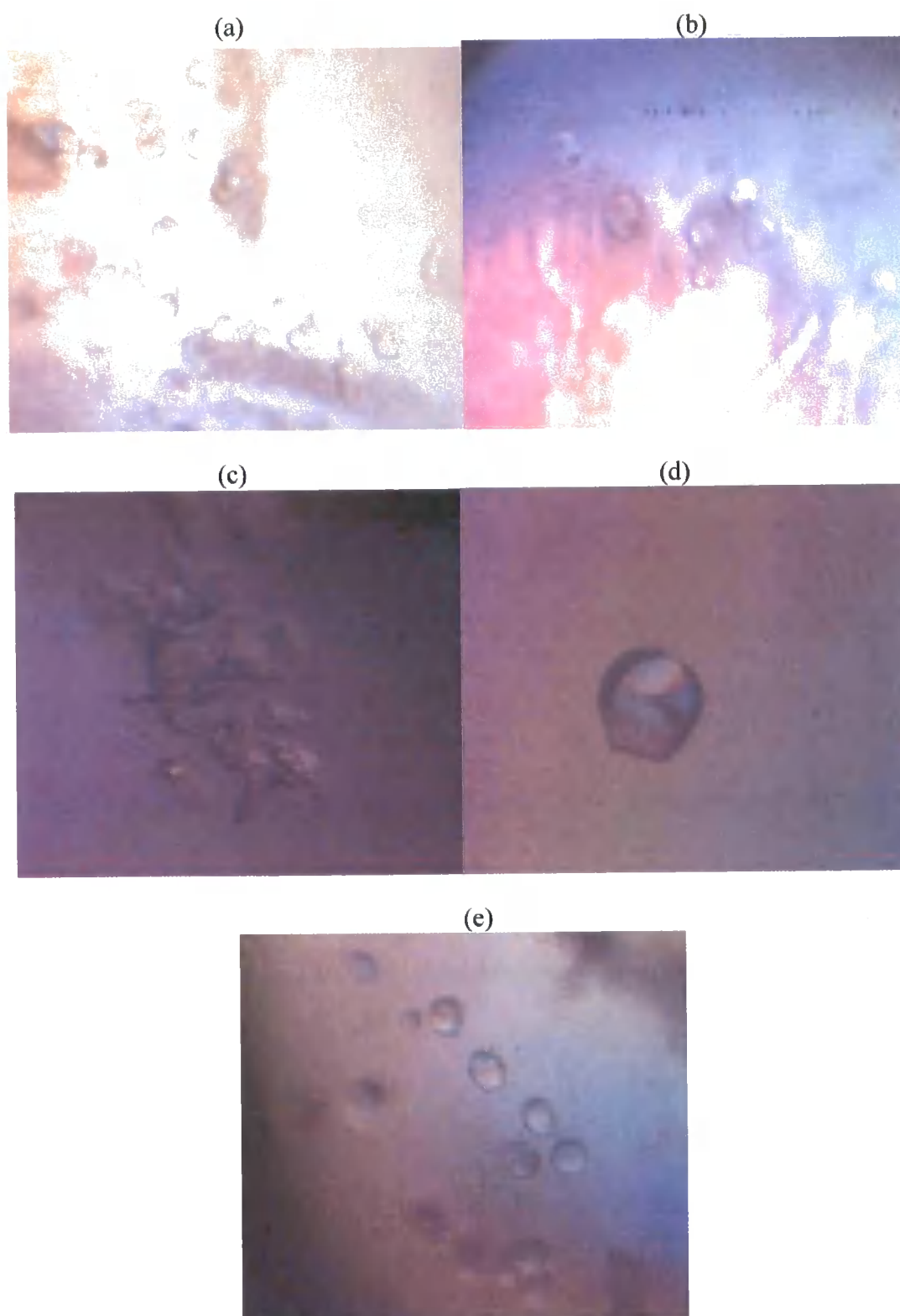
Figure 6.2 **Photographs of putative MacB micro-crystals** taken under light microscopy. Micro-crystals indicative of initial microcrystal development identified from (a) #74 Classics (b) #75 Classic (c) #57 Classics light (d) #39 MbClassII (e) #62 SM1 screen kits.

Kit	Salt	Buffer	Precipitant
Classics 74	0.2 M Calcium chloride	0.1 M HEPES sodium salt pH 7.5	28 %(v/v) PEG 400
Classics 75	0.1 M Cadmium chloride	0.1 M Sodium acetate pH 4.6	30 %(v/v) PEG 400
Classics Light 57	0.5 M Ammonium sulfate	0.1 M tri-Sodium citrate pH 5.6	0.5 M Lithium sulfate
MbClassII 39	0.1 M Magnesium chloride	0.1 M Sodium acetate pH 4.6	30 %(v/v) PEG 400
SM1 62	--	0,1 M sodium acetate anhydrous pH 4.5	20% (w/v) PEG3000

Table 6.1   **Compositions of conditions yielding putative micro-crystals.**

6.3 Preliminary sparse matrix screen of MacA/MacB/TolC complex

The protein crystallization and data collection were undertaken in collaboration with Dr. Vassiliy N. Bavro and Mr. Zbigniew Pietras at the University of Cambridge.

Purified MacA in Triton X-100 (0.2%) (section 4.1) and MacB (section 3.1) in Triton X-100 (0.2%) , and open state TolC (supplied by Dr. Bavro) were exchanged and dialyzed against buffer containing 20mM Tris-HCl pH 7.5, 150 mM NaCl, 0.05% DDM and with 10% glycerol. 40 μL of MacA (3 mg/ml), 60 μL of MacB (8 mg/ml) and 20 μL of TolC (10 mg/ml) were mixed together to make a final concentration of around 6.5 mg/ml, allowing the Molar ratio of MacA: MacB: TolC = 1: 2: 2. Preliminary crystallization trials of the MaA/MacB/TolC complex were accomplished using sparse matrix screens to discover a suitable starting condition.

The commercial sparse matrix screens used were SM1, MbClass, and MbClassII, Classics (Qiagen). Crystallization trials were undertaken using the mixture of the proteins in the vapour diffusion sitting drop method on 96 well plates with round bottoms and automated screening by a Cartesian robot. The development was monitored intermittent by light microscopy.

As shown in Figure 6.3a, a micro-crystal could be observed in the SM1 66 condition, 0.2 M MgCl$_2$, 0.1 M Tris pH 7.0, and 10% (w/v) PEG 8000. The crystal was frozen using cryo-agent 30% PEG 400 and taken to the European Synchrotron Radiation Facility (ESRF) to test for X-ray diffraction. The crystal generated a low diffraction of 20 Å in the lattice (Figure 6.3). Unfortunately, there was a technical problem to get a definitive result indicating either single protein or the protein complex within the crystal since the crystal was too small to tell.

The optimizations of the crystal condition of the complex proteins were undertaken by a gradient of PEG 8000 (5.5-13%, with an interval of 1.5%) versus pH (6.5-8, with an interval of 0.5) and of PEG 8000 (5-15%, with an interval of 2%) versus MgSO$_4$ (50-200 mM, with an interval of 50 mM). However, no crystal was observed in this optimization. The possible reason could be that we used proteins for crystallization from batch to batch, causing the crystal not reproducible.
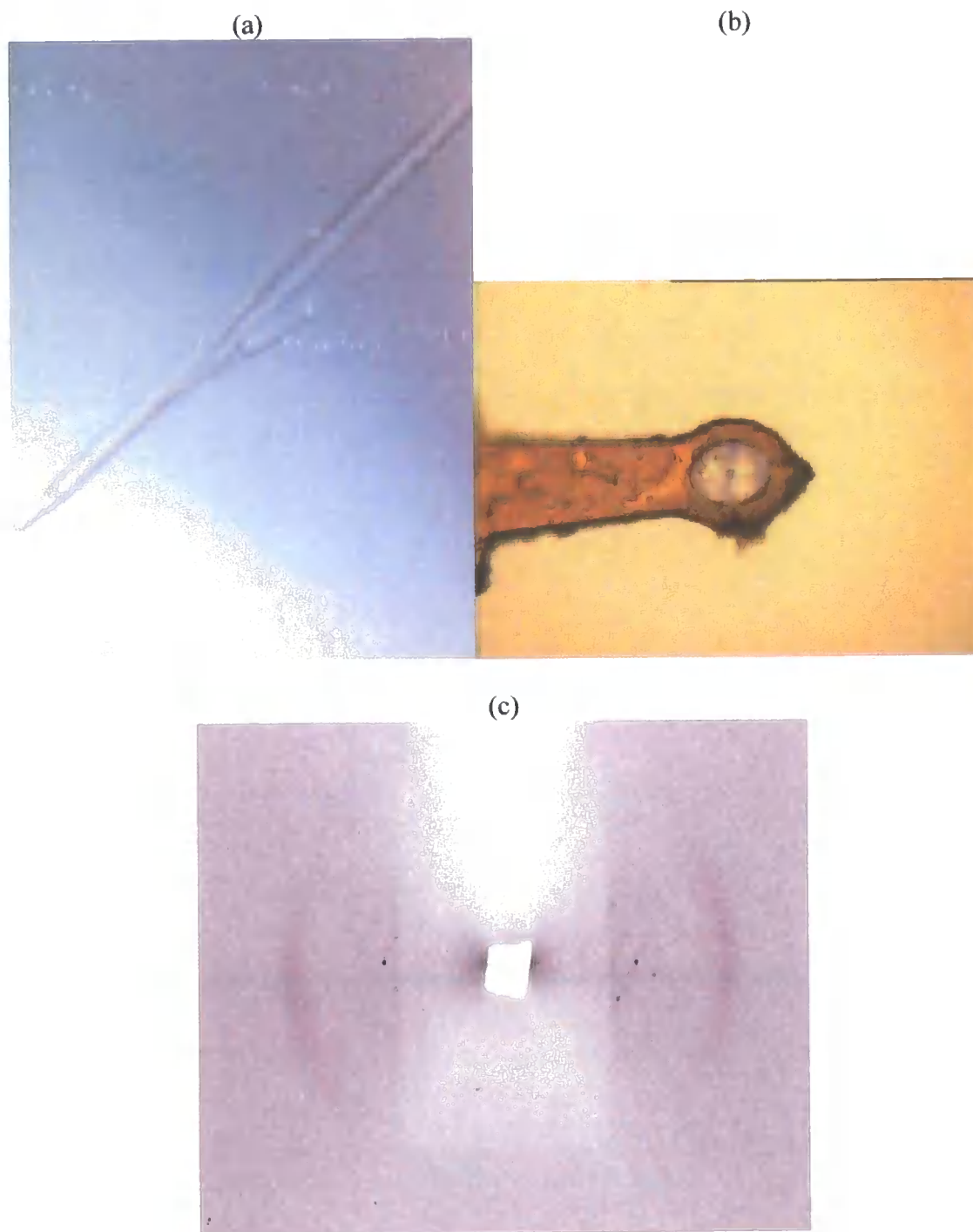
Figure 6.3 **Images of the crystal of the MacA/MacB/TolC complex.** (a) The image of the MacA/MacB/TolC crystal in the well of SM1 66. (b) The image of the loop and the crystal during scanning. (c) The complex diffraction image, with a diffraction of 20 Å limit.

6.4 Discussion

Membrane protein crystallography is a challenge. It is reasonable to state that from expression, purification to crystallization and structure determination of integral membrane proteins still remain non-trivial endeavors that require substantial time and resources (Caffrey, 2003; Wiener *et al.*, 2004). Even more, diffraction-quality crystals are particularly difficult to get when a membrane protein source is used. The reason could be current limited ability to manipulate proteins bearing hydrophobic/amphiphilic surfaces that are usually enveloped with membrane lipid. For this reason there are only around 160 structures for unique membrane proteins (White, 2008).

MacB retained ATPase activity when detergent solubilized but this was detergent dependent, being active in Triton X-100 but not in high DDM. MacB was first extracted using 2% DDM but didn't retain its ATPase activity under these conditions. However, interestingly, MacB remained functional when extracted with 5% Triton X-100 and then exchanged into low DDM concentrations (e.g. 0.05%). The reason why MacB does not remain functional when extracted by DDM is unknown. MacB went through two steps of purification before the crystallization trials; after which a DLS analysis showed that the MacB samples had reached 97% homogeneity. Figure 6.2 shows some putative micro-crystals of MacB but the majority of them do not have angles, indicating 10 mg/ml of MacB may be too high, resulting in shortage of time for crystal formation. Besides, MacB was extracted by 5% Triton X-100 to obtain the best yield, but excess detergent may result in excess delipidation, causing protein instability. (Boulter and Wang, 2001).

Another hindrance in MacB crystallization is that the tag and the cleavage sequence were left on the N-teminal on MacB when it was crystallized. This could be surmounted by taking a further step purification for affinity chromatography to isolate the tagged and tag-free MacB proteins. However, too many purification steps may lead to protein delipidation. Another suggestion is to put the His tag onto the C-terminal of

MacB; since the NBD is on the N-terminal of MacB, we speculated that a C-terminal tag on MacB may avoid a disordered hydrophilic contact.

Structure determination of ABC transporters has been challenging due to their dynamic nature in a detergent solubilized state, which often hinders formation of well-ordered, three-dimensional crystals. The addition of AMP-PNP may be helpful to fix the protein flexibility. Since MacB ATPase activity is detergent dependent, another approach to think about is to exchange into polyoxyethylene glycol detergents such as $C_{12}E_8$, which has a similar structure to Triton X-100 but without a benzene ring. Sav1866 and $ModB_2C_2A$ were both crystallized successfully in the presence of the detergent $C_{12}E_8$.

Chapter seven: Final discussion

Tripartite pumps in gram-negative bacteria can facilitate the extrusion of a wide variety of substrates from the cell. There three components assembled in the tripartite pumps are as follows: an inner membrane protein (IMP), an outer membrane protein (OMP) and a membrane fusion protein (MFP), making it possible to translocate substrates across both the inner and outer membranes. Interestingly, gram-positive bacteria that lack an outer membrane are also found to possess MFPs, suggesting an additional function on top of serving as a scaffold to stabilize the pump assembly. Murakami proposed that conformational changes in AcrB can be transmitted via AcrA to TolC, suggesting AcrA may play a role in addition to stabilize the interaction between AcrB and TolC (Mikolosko *et al.*, 2006). In order to verify this assumption, we chose the MacA/MacB/TolC tripartite complex pump in *E. coli* (Kobayashi *et al.*, 2001) since there are clearly homologous systems in gram-positive bacteria. The MFP MacA not only stabilizes the tripartite-assembly by interacting with both the IMP MacB and the OMP TolC but also has a role in regulating the function of MacB, apparently increasing its affinity for both erythromycin and ATP. Moreover, a better understanding of this complex will give us a better insight into type I secretion systems in bacteria, such as HlyB/HlyD/TolC, where HlyB is an ABC transporter (Thanabalu *et al.*, 1998).

Generally, the MFP is anchored to the inner membrane by either an α-helix or a lipid moiety, attached to a cysteine residue, located towards the N-terminus of the protein (Tikhonova *et al.*, 2004). This might suggest that there is only a requirement to anchor the MFP to the inner membrane, rather than a need for specific interactions between the IMP and MFP. Using pull-down assay, we showed that the anchor, N-terminal α-helix, of *E. coli* MacA was not required for complex formation with either MacB or TolC. This is consistent with a previous report that N-terminal truncated MacA could interact with MacB (Tikhonova *et al.*, 2007). However, using drug susceptibility tests, we showed that the transmembrane helix of MacA was required to target MacA to the periplasm, where the periplasmic domain of MacA could interact

with the periplasmic domains of MacB and TolC to form a functional tripartite complex. This is consistent with a report about the MFP AcrA in *E. coli*, which concluded that the truncated lipid-deficient AcrA derivative was as functional as full length AcrA, as judged by the resistance of the cells to erythromycin and novobiocin (Zgurskaya *et al.*, 1999). However, this behaviour is different from another report that the deletion of the N-terminal α-helix of MacA, whilst not blocking its interaction with MacB, yielded a derivative that when expressed with MacB didn't confer elevated resistance to erythromycin (Tikhonova *et al.*, 2007). The exact reason for the failure of this study to detect the elevated resistance of cells expressing N-terminal truncated MacA is unknown. One possibility is that we used different truncations; in our study we used Δ20MacA whilst Tikhonova *et al* used a Δ31MacA; alternatively maybe the Δ31MacA fused to the OmpA signal sequence failed to reach the periplasm?

The MFP component of the tripartite efflux systems of gram-negative bacteria is believed to act as a bridge between the outer and the inner membranes proteins. The MFP AcrA incorporates a pair of α-helices that form a coiled-coil, sandwiched between two β-strand domains, which have been shown to interact with the α-helical barrel of the OMP TolC (Lobedanz *et al.*, 2007; Bavro *et al.*, 2008). Furthermore by domain swapping experiments showed the β–strand domains are crucial for the interaction with AcrB, but the exact role of these domains remains obscure (Elkins and Nikaido, 2003). Here, we provided evidence that the β-strand domain activates the MacB ATPase. When excess *S. aureus* MacA was added to *E. coli* MacB, no phosphate burst was observed but the steady-state rate was enhanced (Figure 4.12), in direct analogy with the effect of *E. coli* MacA on *E. coli* MacB, indicating that this interaction is via the β-strand domains of the MFP MacA. We established that cells expressing only MacB were less resilient, in terms of their growth, than those expressing both MacA and B, when exposed to erythromycin, suggesting that the latter are more efficient in extruding the antibiotic (Figure 5.3). This may have acted as a selective pressure for gram-positive bacteria to retain the MFP. In the case of *S. aureus*, we speculate that there has been a selective pressure to retain MacA, but because there is no OMP with which it would interact, there has been no pressure to retain the coiled-coil domain that has been deleted from MacA. Recently, the role of the MFP

BesA in the fuction of the BesABC complex pump has been reported (Bunikis *et al.*, 2008). BesC, a TolC homologue, interacts with the putative inner membrane transporter BesB, an AcrB homologue, and the AcrA homologue BesA, a periplasmic adaptor protein. Interestly, in this system BesA lacks the α-helical hairpin. It could be that the interaction between IMP BesB and OMP BesC is suffient to trigger and stabilize the opening of BesC. The reason for the retention of BesA in the BesABC system is most likely associated with its function in the activation of the inner-membrane component, BesB, which could explain the preservation of the hairpin-lacking MFPs in gram-positive bacteria, such as *S. aureus*.

MacB has a nucleotide-binding domain that incorporates Walker A and B motifs and an ABC signature sequence, which are characteristic features of members of the ABC superfamily. Biochemical and structural data suggested the conserved motifs are involved in the binding and hydrolysis of ATP, which are believed to be the key steps in the transport mechanism of ABC transporters. The binding of ATP to both soluble ATPase subunits (Chen *et al.*, 2003) and to the NBDs within a complete ABC transporter (Dawson and Locher, 2007) have been shown to promote dimerisation as the ATP is bound at the interface of these nucleotide binding-sites, sandwiched between the Walker A motif of one NBD and the ABC signature motif of the other NBD. The ATP occlusion model in human p-gp, different from the ATP switch model as described previously, indicated that ATP-driven NBD dimerization was followed by a rapid, temperature-dependent occlusion of ATP at one of the ATP sites, which showed an asymmetry. The latter step is actually energetically driven, involves relatively large conformation changes, and may drive the conformational change in the TMDs (Sauna and Ambudkar, 2007).

In this chapter, using SEC, crosslinking, AUC, ES-Mass spectrometry, and AFM, MacB was proven to be dimeric in a DDM solubilized state. Although MacB has an exceptional four transmembrane helices, different from the six helices characteristics of ABC exporters such as Sav1866 and MsbA, its ability to form dimer suggests that MacB operates by a similar mechanism to ABC transporters.

Our AFM studies indicated that there are a higher proportion of MacB dimers in the presence of the non-hydrolysable nucleotide AMP-PNP. A proposed mechanism of

complete ABC transporters suggested that the binding of ATP triggers the transporter to adopt a conformation in which the substrate binding site is outward-facing, because ATP bridges the two NBDs, closing off the inward-facing substrate binding site (Hollenstein *et al.*, 2007). Conversely, the release of the hydrolysis products ADP and phosphate promotes an inward-facing conformation, as the structural constraint imposed by binding of the nucleotide is released. Consistent with this proposal, several studies indicate that NBD dimerisation cannot be induced by ADP (Zaitseva *et al.*, 2006), because interactions between the γ-phosphate of ATP and the signature sequence catalyse these events (Lu *et al.*, 2005; Oloo *et al.*, 2006). Our kinetic data indicated that MacA can increase the affinity of MacB for ATP and decrease the rate of ATP hydrolysis in the initial stage, so that MacA actually helps to stimulate and stabilize the ATP binding conformation of MacB, presumeably the outward-facing conformation. In this manner, MacA could play a direct role in driving antibiotic translocation between MacB and TolC. Our equilibrium erythromycin binding data pointed out that MacB bound more erythromycin in the presence of MacA and that the amount bound increased in a concentration dependent manner, suggesting that MacA not only modulate the ATPase activity of MacB but also its capacity to bind drugs.

Our studies established that the conformational changes of MacB can be propagated from the periplasmic domain of MacA to the cytoplasmic NBD of MacB, so it is possible that TolC, by interacting with MacA, can detect the nucleotide state of MacB. The binding of ATP to MacB could stimulate MacA to interact with TolC, possibly via the coiled coil hairpin of MacA, trigger the formation of the tripartite complex pump. Murakami (Murakami *et al.*, 2006) proposed the conformational change caused by proton translocation and drug binding may be transmitted, via AcrA, to TolC, thus causing opening of the TolC periplasmic channel. In this case, the AcrA α-helical hairpin may be involved in the opening TolC, via its conformational flexibility (Mikolosko *et al.*, 2006).

There is an anology in the mechanism of operation of ABC importer that works in conjunction with a periplasmic binding-protein (Daus *et al.*, 2007). In the *E. coli* maltose transporter, the binding of ATP to the ATPase subunit MalK induces conformational changes in the periplasmic loops of the membrane subunits MalF

and MalG (Daus *et al.*, 2006); whilst EPR studies revealed that ATP-binding, but not ADP-binding, caused an increase in affinity between the transporter and the maltose binding-protein (MBP), and opening of the MBP (Chen *et al.*, 2001). The binding of ATP to MacB could induce reorientation of the substrate binding-site of MacB and recruit TolC, via MacA, and simultaneous open the TolC to receive the translocated antiobiotic. The interaction between TolC and MacA would uncouple them from MacB, promoting reorientation of the substrate binding-site that would be assisted by the rapid hydrolysis of ATP to ADP.
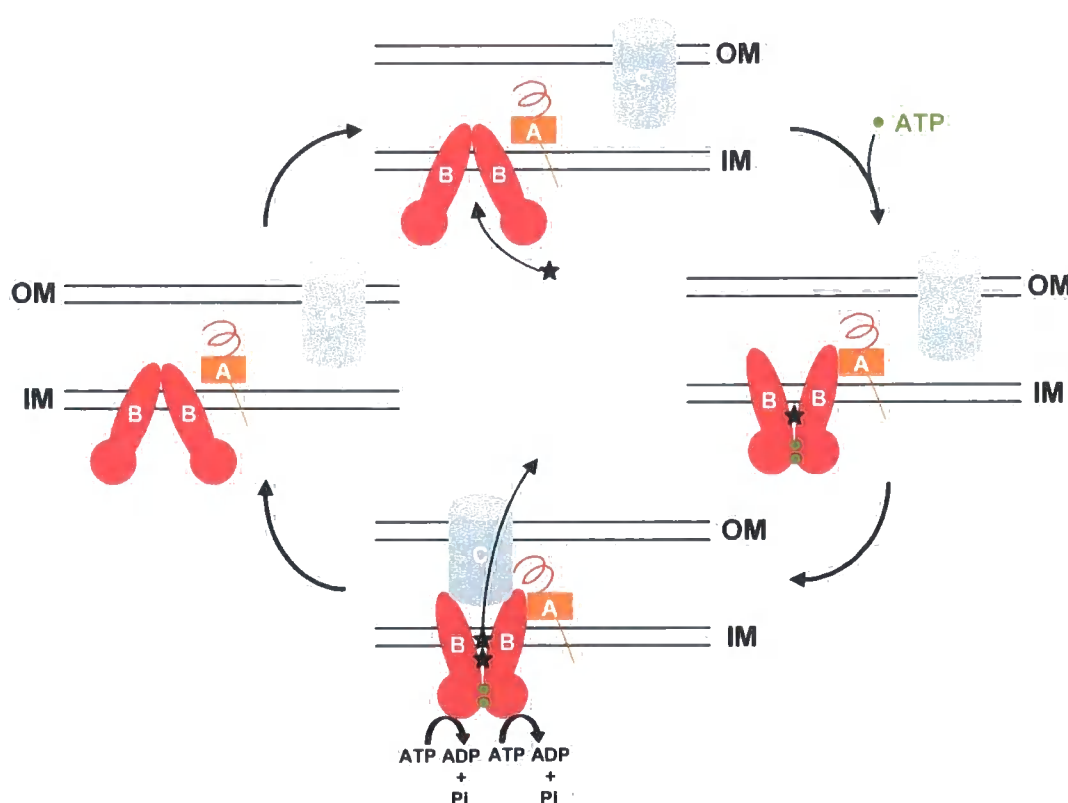
Figure 7.1 **Proposed mechanism of action for the MacA/MacB/TolC pump.** MacAs are represented by orange squares; MacBs are colored in red, in which NBDs are represented by circles and TMDs are represented by ovals; TolCs are represented by blue cylinders; substrates are represented by black stars; ATP molecules are represented by green spheres.

Based on our studies of MacB and knowledge of the structure and function of other ABC transporters we proposed the following mechanism of action for the MacA/MacB/TolC pump. MacB recruits the substrate from the inner leaflet of the membrane or the cytoplasm, triggering a conformational change of MacB, from the inward-facing conformation to the outward-facing conformation, and relocates the NBDs of MacB, allowing the formation of the ATP sandwich in the presence of nucleotide (Figure 7.1). Meanwhile, the MacA can interact with the MacB dimer, increasing the affinity of MacB for ATP, helping the formation of ATP sandwich and decreasing the initial ATPase activity of MacB to stabilize dimer formation. The recruitment of the TolC to the MacAB complex allows translocation of the substrate across the periplasm and leads to the ATP hydrolysis; at this stage, MacA helps to seal the channel across the periplasm and aids ATP hydrolysis by increasing the steady state ATPase activity of MacB due to an increase in the release rate of the products of ATP hydrolysis, allowing a faster conformational change of MacB, from the outward-facing to the inward-facing conformation, resetting the transporter in its original conformation.

Reference

Adler, J., and Bibi, E. (2002). Membrane topology of the multidrug transporter MdfA: complementary gene fusion studies reveal a nonessential C-terminal domain. J Bacteriol *184*, 3313-3320.

Adler, J., and Bibi, E. (2004). Determinants of substrate recognition by the Escherichia coli multidrug transporter MdfA identified on both sides of the membrane. J Biol Chem *279*, 8957-8965.

Adler, J., Lewinson, O., and Bibi, E. (2004). Role of a conserved membrane-embedded acidic residue in the multidrug transporter MdfA. Biochemistry *43*, 518-525.

Alanis, A.J. (2005). Resistance to antibiotics: are we in the post-antibiotic era? Arch Med Res *36*, 697-705.

Alekshun, M.N., and Levy, S.B. (2007). Molecular mechanisms of antibacterial multidrug resistance. Cell *128*, 1037-1050.

Ambudkar, S.V., Kim, I.W., Xia, D., and Sauna, Z.E. (2006). The A-loop, a novel conserved aromatic acid subdomain upstream of the Walker A motif in ABC transporters, is critical for ATP binding. FEBS Lett *580*, 1049-1055.

Andersen, C., Koronakis, E., Bokma, E., Eswaran, J., Humphreys, D., Hughes, C., and Koronakis, V. (2002). Transition to the open state of the TolC periplasmic tunnel entrance. Proc Natl Acad Sci U S A *99*, 11103-11108.

Arkin, I.T., and Brunger, A.T. (1998). Statistical analysis of predicted transmembrane alpha-helices. Biochim Biophys Acta *1429*, 113-128.

Arkin, I.T., Russ, W.P., Lebendiker, M., and Schuldiner, S. (1996). Determining the secondary structure and orientation of EmrE, a multi-drug transporter, indicates a transmembrane four-helix bundle. Biochemistry *35*, 7233-7238.

Augustus, A.M., Celaya, T., Husain, F., Humbard, M., and Misra, R. (2004). Antibiotic-sensitive TolC mutants and their suppressors. J Bacteriol *186*, 1851-1860.

Bakos, E., Klein, I., Welker, E., Szabo, K., Muller, M., Sarkadi, B., and Varadi, A. (1997). Characterization of the human multidrug resistance protein containing mutations in the ATP-binding cassette signature region. Biochem J *323 (Pt 3)*, 777-783.

Barrera, N.P., Ge, H., Henderson, R.M., Fitzgerald, W.J., and Edwardson, J.M. (2008). Automated analysis of the architecture of receptors, imaged by atomic force microscopy. Micron *39*, 101-110.

Barrera, N.P., Henderson, R.M., and Edwardson, J.M. (2008). Determination of the architecture of ionotropic receptors using AFM imaging. Pflugers Arch *456*, 199-209.

Barrera, N.P., Herbert, P., Henderson, R.M., Martin, I.L., and Edwardson, J.M. (2005). Atomic force microscopy reveals the stoichiometry and subunit arrangement of 5-HT3 receptors. Proc Natl Acad Sci U S A *102*, 12595-12600.

Bavro, V.N., Pietras, Z., Furnham, N., Perez-Cano, L., Fernandez-Recio, J., Pei, X.Y., Misra, R., and Luisi, B. (2008). Assembly and channel opening in a bacterial drug efflux machine. Mol Cell *30*, 114-121.

Borges-Walmsley, M.I., McKeegan, K.S., and Walmsley, A.R. (2003). Structure and function of efflux pumps that confer resistance to drugs. Biochem J *376*, 313-338.

Boulter, J.M., and Wang, D.N. (2001). Purification and characterization of human erythrocyte glucose transporter in decylmaltoside detergent solution. Protein Expr Purif *22*, 337-348.

Brahms, S., and Brahms, J. (1980). Determination of protein secondary structure in solution by vacuum ultraviolet circular dichroism. J Mol Biol *138*, 149-178.

Brodersen, D.E., Clemons, W.M., Jr., Carter, A.P., Morgan-Warren, R.J., Wimberly, B.T., and Ramakrishnan, V. (2000). The structural basis for the action of the antibiotics tetracycline, pactamycin, and hygromycin B on the 30S ribosomal subunit. Cell *103*, 1143-1154.

Brown, M.H., Paulsen, I.T., and Skurray, R.A. (1999). The multidrug efflux protein NorM is a prototype of a new family of transporters. Mol Microbiol *31*, 394-395.

Bunikis, I., Denker, K., Ostberg, Y., Andersen, C., Benz, R., and Bergstrom, S. (2008). An RND-type efflux system in Borrelia burgdorferi is involved in virulence and resistance to antimicrobial compounds. PLoS Pathog *4*, e1000009.

Butler, P.J., Ubarretxena-Belandia, I., Warne, T., and Tate, C.G. (2004). The Escherichia coli multidrug transporter EmrE is a dimer in the detergent-solubilised state. J Mol Biol *340*, 797-808.

Caffrey, M. (2003). Membrane protein crystallization. J Struct Biol *142*, 108-132.

Campbell, E.A., Korzheva, N., Mustaev, A., Murakami, K., Nair, S., Goldfarb, A., and Darst, S.A. (2001). Structural mechanism for rifampicin inhibition of bacterial rna polymerase. Cell *104*, 901-912.

Chen, H., Bjerknes, M., Kumar, R., and Jay, E. (1994). Determination of the optimal aligned spacing between the Shine-Dalgarno sequence and the translation initiation codon of Escherichia coli mRNAs. Nucleic Acids Res *22*, 4953-4957.

Chen, J., Lu, G., Lin, J., Davidson, A.L., and Quiocho, F.A. (2003). A tweezers-like motion of the ATP-binding cassette dimer in an ABC transport cycle. Mol Cell *12*, 651-661.

Chen, J., Sharma, S., Quiocho, F.A., and Davidson, A.L. (2001). Trapping the transition state of an ATP-binding cassette transporter: evidence for a concerted mechanism of maltose transport. Proc Natl Acad Sci U S A *98*, 1525-1530.

Chen, Y.J., Pornillos, O., Lieu, S., Ma, C., Chen, A.P., and Chang, G. (2007). X-ray structure of EmrE supports dual topology model. Proc Natl Acad Sci U S A *104*, 18999-19004.

Choo, E.F., Leake, B., Wandel, C., Imamura, H., Wood, A.J., Wilkinson, G.R., and Kim, R.B. (2000). Pharmacological inhibition of P-glycoprotein transport enhances the distribution of HIV-1 protease inhibitors into brain and testes. Drug Metab Dispos *28*, 655-660.

Cole, S.P., Sparks, K.E., Fraser, K., Loe, D.W., Grant, C.E., Wilson, G.M., and Deeley, R.G. (1994). Pharmacological characterization of multidrug resistant MRP-transfected human tumor cells. Cancer Res *54*, 5902-5910.

Compton, S.J., and Jones, C.G. (1985). Mechanism of dye response and interference in the Bradford protein assay. Anal Biochem *151*, 369-374.

Das, D., Xu, Q.S., Lee, J.Y., Ankoudinova, I., Huang, C., Lou, Y., DeGiovanni, A., Kim, R., and Kim, S.H. (2007). Crystal structure of the multidrug efflux transporter AcrB at 3.1A resolution reveals the N-terminal region with conserved amino acids. J Struct Biol *158*, 494-502.

Daus, M.L., Grote, M., Muller, P., Doebber, M., Herrmann, A., Steinhoff, H.J., Dassa, E., and Schneider, E. (2007). ATP-driven MalK dimer closure and reopening and conformational changes of the "EAA" motifs are crucial for function of the maltose ATP-binding cassette transporter (MalFGK2). J Biol Chem *282*, 22387-22396.

Daus, M.L., Landmesser, H., Schlosser, A., Muller, P., Herrmann, A., and Schneider, E. (2006). ATP induces conformational changes of periplasmic loop regions of the maltose ATP-binding cassette transporter. J Biol Chem *281*, 3856-3865.

Davidson, A.L. (2002). Structural biology. Not just another ABC transporter. Science *296*, 1038-1040.

Davidson, A.L., and Chen, J. (2004). ATP-binding cassette transporters in bacteria. Annu Rev Biochem *73*, 241-268.

Davidson, A.L., and Sharma, S. (1997). Mutation of a single MalK subunit severely impairs maltose transport activity in Escherichia coli. J Bacteriol *179*, 5458-5464.

Dawson, R.J., and Locher, K.P. (2006). Structure of a bacterial multidrug ABC transporter. Nature *443*, 180-185.

Dawson, R.J., and Locher, K.P. (2007). Structure of the multidrug ABC transporter Sav1866 from Staphylococcus aureus in complex with AMP-PNP. FEBS Lett *581*, 935-938.

Delucas, L.J., Hamrick, D., Cosenza, L., Nagy, L., McCombs, D., Bray, T., Chait, A., Stoops, B., Belgovskiy, A., William Wilson, W., et al. (2005). Protein crystallization: virtual screening and optimization. Prog Biophys Mol Biol *88*, 285-309.

Diederichs, K., Diez, J., Greller, G., Muller, C., Breed, J., Schnell, C., Vonrhein, C., Boos, W., and Welte, W. (2000). Crystal structure of MalK, the ATPase subunit of the

trehalose/maltose ABC transporter of the archaeon Thermococcus litoralis. EMBO J 19, 5951-5961.

Eda, S., Maseda, H., Yoshihara, E., and Nakae, T. (2006). Assignment of the outer-membrane-subunit-selective domain of the membrane fusion protein in the tripartite xenobiotic efflux pump of Pseudomonas aeruginosa. FEMS Microbiol Lett 254, 101-107.

Edgar, R., and Bibi, E. (1997). MdfA, an Escherichia coli multidrug resistance protein with an extraordinarily broad spectrum of drug recognition. J Bacteriol 179, 2274-2280.

Edgar, R., and Bibi, E. (1999). A single membrane-embedded negative charge is critical for recognizing positively charged drugs by the Escherichia coli multidrug resistance protein MdfA. EMBO J 18, 822-832.

Elbaz, Y., Tayer, N., Steinfels, E., Steiner-Mordoch, S., and Schuldiner, S. (2005). Substrate-induced tryptophan fluorescence changes in EmrE, the smallest ion-coupled multidrug transporter. Biochemistry 44, 7369-7377.

Elkins, C.A., and Nikaido, H. (2003). Chimeric analysis of AcrA function reveals the importance of its C-terminal domain in its interaction with the AcrB multidrug efflux pump. J Bacteriol 185, 5349-5356.

Eswaran, J., Hughes, C., and Koronakis, V. (2003). Locking TolC entrance helices to prevent protein translocation by the bacterial type I export apparatus. J Mol Biol 327, 309-315.

Eswaran, J., Koronakis, E., Higgins, M.K., Hughes, C., and Koronakis, V. (2004). Three's company: component structures bring a closer view of tripartite drug efflux pumps. Curr Opin Struct Biol 14, 741-747.

Evers, R., Zaman, G.J., van Deemter, L., Jansen, H., Calafat, J., Oomen, L.C., Oude Elferink, R.P., Borst, P., and Schinkel, A.H. (1996). Basolateral localization and export activity of the human multidrug resistance-associated protein in polarized pig kidney cells. J Clin Invest 97, 1211-1218.

Fernandez-Recio, J., Walas, F., Federici, L., Venkatesh Pratap, J., Bavro, V.N., Miguel, R.N., Mizuguchi, K., and Luisi, B. (2004). A model of a transmembrane drug-efflux pump from Gram-negative bacteria. FEBS Lett 578, 5-9.

Gerlach, R.G., and Hensel, M. (2007). Protein secretion systems and adhesins: the molecular armory of Gram-negative pathogens. Int J Med Microbiol 297, 401-415.

Ginn, S.L., Brown, M.H., and Skurray, R.A. (1997). Membrane topology of the metal-tetracycline/H+ antiporter TetA(K) from Staphylococcus aureus. J Bacteriol 179, 3786-3789.

Gottesman, M.M., and Ambudkar, S.V. (2001). Overview: ABC transporters and human disease. J Bioenerg Biomembr 33, 453-458.

Grant, E.H. (1957). The dielectric method of estimating protein hydration. Phys Med

Biol *2*, 17-28.

Hancock, R.E., and Chapple, D.S. (1999). Peptide antibiotics. Antimicrob Agents Chemother *43*, 1317-1323.

Hannun, Y.A. (1997). Apoptosis and the dilemma of cancer chemotherapy. Blood 89, 1845-1853.

Hanson, C.L., Fucini, P., Ilag, L.L., Nierhaus, K.H., and Robinson, C.V. (2003). Dissociation of intact Escherichia coli ribosomes in a mass spectrometer. Evidence for conformational change in a ribosome elongation factor G complex. J Biol Chem *278*, 1259-1267.

Henderson, P.J.F. (1998). Function and structure of membrane transport proteins. In The transporter FactsBook, J.K. Griffith, and Sansom, C. E., ed. (London: Academic Press Publishers), pp. 3-29.

Hernandez, H., and Robinson, C.V. (2001). Dynamic protein complexes: insights from mass spectrometry. J Biol Chem *276*, 46685-46688.

Higgins, C.F. (1992). ABC transporters: from microorganisms to man. Annu Rev Cell Biol *8*, 67-113.

Higgins, M.K., Bokma, E., Koronakis, E., Hughes, C., and Koronakis, V. (2004). Structure of the periplasmic component of a bacterial drug efflux pump. Proc Natl Acad Sci U S A *101*, 9994-9999.

Hollenstein, K., Dawson, R.J., and Locher, K.P. (2007). Structure and mechanism of ABC transporter proteins. Curr Opin Struct Biol *17*, 412-418.

Hollenstein, K., Frei, D.C., and Locher, K.P. (2007). Structure of an ABC transporter in complex with its binding protein. Nature *446*, 213-216.

Howlett, G.J., Minton, A.P., and Rivas, G. (2006). Analytical ultracentrifugation for the study of protein association and assembly. Curr Opin Chem Biol *10*, 430-436.

Huisman, M.T., Smit, J.W., and Schinkel, A.H. (2000). Significance of P-glycoprotein for the pharmacology and clinical use of HIV protease inhibitors. AIDS *14*, 237-242.

Hunke, S., Mourez, M., Jehanno, M., Dassa, E., and Schneider, E. (2000). ATP modulates subunit-subunit interactions in an ATP-binding cassette transporter (MalFGK2) determined by site-directed chemical cross-linking. J Biol Chem *275*, 15526-15534.

Huovinen, P. (2001). Resistance to trimethoprim-sulfamethoxazole. Clin Infect Dis *32*, 1608-1614.

Ilag, L.L., Westblade, L.F., Deshayes, C., Kolb, A., Busby, S.J., and Robinson, C.V. (2004). Mass spectrometry of Escherichia coli RNA polymerase: interactions of the core enzyme with sigma70 and Rsd protein. Structure *12*, 269-275.

Jack, D.L., Yang, N.M., and Saier, M.H., Jr. (2001). The drug/metabolite transporter

superfamily. Eur J Biochem *268*, 3620-3639.

Katz, L., and Ashley, G.W. (2005). Translation and protein synthesis: macrolides. Chem Rev *105*, 499-528.

Kelly, S.M., Jess, T.J., and Price, N.C. (2005). How to study proteins by circular dichroism. Biochim Biophys Acta *1751*, 119-139.

Kobayashi, N., Nishino, K., Hirata, T., and Yamaguchi, A. (2003). Membrane topology of ABC-type macrolide antibiotic exporter MacB in Escherichia coli. FEBS Lett *546*, 241-246.

Kobayashi, N., Nishino, K., and Yamaguchi, A. (2001). Novel macrolide-specific ABC-type efflux transporter in Escherichia coli. J Bacteriol *183*, 5639-5644.

Koronakis, V., Eswaran, J., and Hughes, C. (2004). Structure and function of TolC: the bacterial exit duct for proteins and drugs. Annu Rev Biochem *73*, 467-489.

Koronakis, V., Sharff, A., Koronakis, E., Luisi, B., and Hughes, C. (2000). Crystal structure of the bacterial membrane protein TolC central to multidrug efflux and protein export. Nature *405*, 914-919.

Lage, H. (2003). ABC-transporters: implications on drug resistance from microorganisms to human cancers. Int J Antimicrob Agents *22*, 188-199.

Laue, T., Shah, B., Ridgeway, T., and Pelletier, S. (1992). Computer-aided interpretation of analytical sedimentation data for proteins. In Analytical Ultracentrifugation in Biochemistry and Polymer Science, S. Harding, Rowe, A., and Horton, J., ed. (Cambridge: The Royal Society of Chemistry), pp. 90-125.

Lengqvist, J., Svensson, R., Evergren, E., Morgenstern, R., and Griffiths, W.J. (2004). Observation of an intact noncovalent homotrimer of detergent-solubilized rat microsomal glutathione transferase-1 by electrospray mass spectrometry. J Biol Chem *279*, 13311-13316.

Lewinson, O., Adler, J., Sigal, N., and Bibi, E. (2006). Promiscuity in multidrug recognition and transport: the bacterial MFS Mdr transporters. Mol Microbiol *61*, 277-284.

Lewinson, O., and Bibi, E. (2001). Evidence for simultaneous binding of dissimilar substrates by the Escherichia coli multidrug transporter MdfA. Biochemistry *40*, 12612-12618.

Lowe, S.W., Ruley, H.E., Jacks, T., and Housman, D.E. (1993). p53-dependent apoptosis modulates the cytotoxicity of anticancer agents. Cell *74*, 957-967.

Li, X.Z. (2005). Quinolone resistance in bacteria: emphasis on plasmid-mediated mechanisms. Int J Antimicrob Agents *25*, 453-463.

Lobedanz, S., Bokma, E., Symmons, M.F., Koronakis, E., Hughes, C., and Koronakis, V. (2007). A periplasmic coiled-coil interface underlying TolC recruitment and the assembly of bacterial drug efflux pumps. Proc Natl Acad Sci U S A *104*, 4612-4617.

Locher, K.P., Lee, A.T., and Rees, D.C. (2002). The E. coli BtuCD structure: a framework for ABC transporter architecture and mechanism. Science *296*, 1091-1098.

Loo, T.W., and Clarke, D.M. (1995). P-glycoprotein. Associations between domains and between domains and molecular chaperones. J Biol Chem *270*, 21839-21844.

Loo, T.W., and Clarke, D.M. (2005). Recent progress in understanding the mechanism of P-glycoprotein-mediated drug efflux. J Membr Biol *206*, 173-185.

Lu, G., Westbrooks, J.M., Davidson, A.L., and Chen, J. (2005). ATP hydrolysis is required to reset the ATP-binding cassette dimer into the resting-state conformation. Proc Natl Acad Sci U S A *102*, 17969-17974.

Mannering, D.E., Sharma, S., and Davidson, A.L. (2001). Demonstration of conformational changes associated with activation of the maltose transport complex. J Biol Chem *276*, 12362-12368.

Martin, J.M., Green, M., Barbadora, K.A., and Wald, E.R. (2002). Erythromycin-resistant group A streptococci in schoolchildren in Pittsburgh. N Engl J Med *346*, 1200-1206.

Meier, T., Morgner, N., Matthies, D., Pogoryelov, D., Keis, S., Cook, G.M., Dimroth, P., and Brutschy, B. (2007). A tridecameric c ring of the adenosine triphosphate (ATP) synthase from the thermoalkaliphilic Bacillus sp. strain TA2.A1 facilitates ATP synthesis at low electrochemical proton potential. Mol Microbiol *65*, 1181-1192.

Michel, H. (2006). Membrane proteins of known structure. pp. Retrieved June 25, 2008, from http://www.mpibp-frankfurt.mpg.de/michel/public/memprotstruct.

Mikolosko, J., Bobyk, K., Zgurskaya, H.I., and Ghosh, P. (2006). Conformational flexibility in the multidrug efflux system protein AcrA. Structure *14*, 577-587.

Miroux, B., and Walker, J.E. (1996). Over-production of proteins in Escherichia coli: mutant hosts that allow synthesis of some membrane proteins and globular proteins at high levels. J Mol Biol *260*, 289-298.

Moody, J.E., Millen, L., Binns, D., Hunt, J.F., and Thomas, P.J. (2002). Cooperative, ATP-dependent association of the nucleotide binding cassettes during the catalytic cycle of ATP-binding cassette transporters. J Biol Chem *277*, 21111-21114.

Mordoch, S.S., Granot, D., Lebendiker, M., and Schuldiner, S. (1999). Scanning cysteine accessibility of EmrE, an H+-coupled multidrug transporter from Escherichia coli, reveals a hydrophobic pathway for solutes. J Biol Chem *274*, 19480-19486.

Morita, Y., Kodama, K., Shiota, S., Mine, T., Kataoka, A., Mizushima, T., and Tsuchiya, T. (1998). NorM, a putative multidrug efflux protein, of Vibrio parahaemolyticus and its homolog in Escherichia coli. Antimicrob Agents Chemother *42*, 1778-1782.

Murakami, S., Nakashima, R., Yamashita, E., Matsumoto, T., and Yamaguchi, A. (2006). Crystal structures of a multidrug transporter reveal a functionally rotating mechanism. Nature *443*, 173-179.

Murakami, S., Nakashima, R., Yamashita, E., and Yamaguchi, A. (2002). Crystal structure of bacterial multidrug efflux transporter AcrB. Nature *419*, 587-593.

Muth, T.R., and Schuldiner, S. (2000). A membrane-embedded glutamate is required for ligand binding to the multidrug transporter EmrE. EMBO J *19*, 234-240.

Narita, S., Eda, S., Yoshihara, E., and Nakae, T. (2003). Linkage of the efflux-pump expression level with substrate extrusion rate in the MexAB-OprM efflux pump of Pseudomonas aeruginosa. Biochem Biophys Res Commun *308*, 922-926.

Naroditskaya, V., Schlosser, M.J., Fang, N.Y., and Lewis, K. (1993). An E. coli gene emrD is involved in adaptation to low energy shock. Biochem Biophys Res Commun *196*, 803-809.

Ninio, S., Elbaz, Y., and Schuldiner, S. (2004). The membrane topology of EmrE - a small multidrug transporter from Escherichia coli. FEBS Lett *562*, 193-196.

Nishino, K., and Yamaguchi, A. (2001). Analysis of a complete library of putative drug transporter genes in Escherichia coli. J Bacteriol *183*, 5803-5812.

Oldham, M.L., Khare, D., Quiocho, F.A., Davidson, A.L., and Chen, J. (2007). Crystal structure of a catalytic intermediate of the maltose transporter. Nature *450*, 515-521.

Oloo, E.O., Kandt, C., O'Mara, M.L., and Tieleman, D.P. (2006). Computer simulations of ABC transporter components. Biochem Cell Biol *84*, 900-911.

Otsuka, M., Yasuda, M., Morita, Y., Otsuka, C., Tsuchiya, T., Omote, H., and Moriyama, Y. (2005). Identification of essential amino acid residues of the NorM Na+/multidrug antiporter in Vibrio parahaemolyticus. J Bacteriol *187*, 1552-1558.

Owen, A., Chandler, B., and Back, D.J. (2005). The implications of P-glycoprotein in HIV: friend or foe? Fundam Clin Pharmacol *19*, 283-296.

Pao, S.S., Paulsen, I.T., and Saier, M.H., Jr. (1998). Major facilitator superfamily. Microbiol Mol Biol Rev 62, 1-34.

Paulsen, I.T., Brown, M.H., Littlejohn, T.G., Mitchell, B.A., and Skurray, R.A. (1996). Multidrug resistance proteins QacA and QacB from Staphylococcus aureus: membrane topology and identification of residues involved in substrate specificity. Proc Natl Acad Sci U S A *93*, 3630-3635.

Peterson, G.L., Rosenbaum, L.C., and Schimerlik, M.I. (1988). Solubilization and hydrodynamic properties of pig atrial muscarinic acetylcholine receptor in dodecyl beta-D-maltoside. Biochem J *255*, 553-560.

Pinkett, H.W., Lee, A.T., Lum, P., Locher, K.P., and Rees, D.C. (2007). An inward-facing conformation of a putative metal-chelate-type ABC transporter. Science *315*, 373-377.

Poole, K. (2001). Multidrug resistance in Gram-negative bacteria. Curr Opin Microbiol *4*, 500-508.

Putman, M., van Veen, H.W., and Konings, W.N. (2000). Molecular properties of bacterial multidrug transporters. Microbiol Mol Biol Rev *64*, 672-693.

Rapoza, M.P., and Webster, R.E. (1993). The filamentous bacteriophage assembly proteins require the bacterial SecA protein for correct localization to the membrane. J Bacteriol *175*, 1856-1859.

Ravaud, S., Do Cao, M.A., Jidenko, M., Ebel, C., Le Maire, M., Jault, J.M., Di Pietro, A., Haser, R., and Aghajari, N. (2006). The ABC transporter BmrA from Bacillus subtilis is a functional dimer when in a detergent-solubilized state. Biochem J *395*, 345-353.

Raviv, Y., Puri, A., and Blumenthal, R. (2000). P-glycoprotein-overexpressing multidrug-resistant cells are resistant to infection by enveloped viruses that enter via the plasma membrane. FASEB J *14*, 511-515.

Rouquette-Loughlin, C.E., Balthazar, J.T., and Shafer, W.M. (2005). Characterization of the MacA-MacB efflux system in Neisseria gonorrhoeae. J Antimicrob Chemother *56*, 856-860.

Saidijam, M., Benedetti, G., Ren, Q., Xu, Z., Hoyle, C.J., Palmer, S.L., Ward, A., Bettaney, K.E., Szakonyi, G., Meuller, J., et al. (2006). Microbial drug efflux proteins of the major facilitator superfamily. Curr Drug Targets *7*, 793-811.

Saier, M.H., Jr., Beatty, J.T., Goffeau, A., Harley, K.T., Heijne, W.H., Huang, S.C., Jack, D.L., Jahn, P.S., Lew, K., Liu, J., et al. (1999). The major facilitator superfamily. J Mol Microbiol Biotechnol *1*, 257-279.

Saier, M.H., Jr., and Paulsen, I.T. (2001). Phylogeny of multidrug transporters. Semin Cell Dev Biol *12*, 205-213.

Sauna, Z.E., and Ambudkar, S.V. (2007). About a switch: how P-glycoprotein (ABCB1) harnesses the energy of ATP binding and hydrolysis to do mechanical work. Mol Cancer Ther 6, 13-23.

Schmees, G., Stein, A., Hunke, S., Landmesser, H., and Schneider, E. (1999). Functional consequences of mutations in the conserved 'signature sequence' of the ATP-binding-cassette protein MalK. Eur J Biochem *266*, 420-430.

Schneider, E., and Hunke, S. (1998). ATP-binding-cassette (ABC) transport systems: functional and structural aspects of the ATP-hydrolyzing subunits/domains. FEMS Microbiol Rev *22*, 1-20.

Schuldiner, S. (2006). Structural biology: the ins and outs of drug transport. Nature *443*, 156-157.

Schuldiner, S., Granot, D., Mordoch, S.S., Ninio, S., Rotem, D., Soskin, M., Tate, C.G., and Yerushalmi, H. (2001). Small is mighty: EmrE, a multidrug transporter as an experimental paradigm. News Physiol Sci *16*, 130-134.

Seeger, M.A., Schiefner, A., Eicher, T., Verrey, F., Diederichs, K., and Pos, K.M. (2006). Structural asymmetry of AcrB trimer suggests a peristaltic pump mechanism.

Science *313*, 1295-1298.

Seeger, M.A., von Ballmoos, C., Eicher, T., Brandstatter, L., Verrey, F., Diederichs, K., and Pos, K.M. (2008). Engineered disulfide bonds support the functional rotation mechanism of multidrug efflux pump AcrB. Nat Struct Mol Biol *15*, 199-205.

Sennhauser, G., Amstutz, P., Briand, C., Storchenegger, O., and Grutter, M.G. (2007). Drug export pathway of multidrug exporter AcrB revealed by DARPin inhibitors. PLoS Biol *5*, e7.

Sharon, M., and Robinson, C.V. (2007). The role of mass spectrometry in structure elucidation of dynamic protein complexes. Annu Rev Biochem *76*, 167-193.

Sharoni, M., Steiner-Mordoch, S., and Schuldiner, S. (2005). Exploring the binding domain of EmrE, the smallest multidrug transporter. J Biol Chem *280*, 32849-32855.

Sheppard, D.N., and Welsh, M.J. (1999). Structure and function of the CFTR chloride channel. Physiol Rev *79*, S23-45.

Shyamala, V., Baichwal, V., Beall, E., and Ames, G.F. (1991). Structure-function analysis of the histidine permease and comparison with cystic fibrosis mutations. J Biol Chem *266*, 18714-18719.

Singh, A.K., Haldar, R., Mandal, D., and Kundu, M. (2006). Analysis of the topology of Vibrio cholerae NorM and identification of amino acid residues involved in norfloxacin resistance. Antimicrob Agents Chemother *50*, 3717-3723.

Smith, P.C., Karpowich, N., Millen, L., Moody, J.E., Rosen, J., Thomas, P.J., and Hunt, J.F. (2002). ATP binding to the motor domain from an ABC transporter drives formation of a nucleotide sandwich dimer. Mol Cell *10*, 139-149.

Sobott, F., Hernandez, H., McCammon, M.G., Tito, M.A., and Robinson, C.V. (2002). A tandem mass spectrometer for improved transmission and analysis of large macromolecular assemblies. Anal Chem *74*, 1402-1407.

Soskine, M., Adam, Y., and Schuldiner, S. (2004). Direct evidence for substrate-induced proton release in detergent-solubilized EmrE, a multidrug transporter. J Biol Chem *279*, 9951-9955.

Spratt, B.G., and Cromie, K.D. (1988). Penicillin-binding proteins of gram-negative bacteria. Rev Infect Dis *10*, 699-711.

Stegmeier, J.F., Polleichtner, G., Brandes, N., Hotz, C., and Andersen, C. (2006). Importance of the adaptor (membrane fusion) protein hairpin domain for the functionality of multidrug efflux pumps. Biochemistry *45*, 10303-10312.

Takatsuka, Y., and Nikaido, H. (2006). Threonine-978 in the transmembrane segment of the multidrug efflux pump AcrB of Escherichia coli is crucial for drug transport as a probable component of the proton relay network. J Bacteriol *188*, 7284-7289.

Takatsuka, Y., and Nikaido, H. (2007). Site-directed disulfide cross-linking shows that cleft flexibility in the periplasmic domain is needed for the multidrug efflux pump

AcrB of Escherichia coli. J Bacteriol *189*, 8677-8684.

Tamura, N., Murakami, S., Oyama, Y., Ishiguro, M., and Yamaguchi, A. (2005). Direct interaction of multidrug efflux transporter AcrB and outer membrane channel TolC detected via site-directed disulfide cross-linking. Biochemistry *44*, 11115-11121.

Tate, C.G., Kunji, E.R., Lebendiker, M., and Schuldiner, S. (2001). The projection structure of EmrE, a proton-linked multidrug transporter from Escherichia coli, at 7 A resolution. EMBO J *20*, 77-81.

Tate, C.G., Ubarretxena-Belandia, I., and Baldwin, J.M. (2003). Conformational changes in the multidrug transporter EmrE associated with substrate binding. J Mol Biol *332*, 229-242.

Tatusov, R.L., Koonin, E.V., and Lipman, D.J. (1997). A genomic perspective on protein families. Science *278*, 631-637.

Thanabalu, T., Koronakis, E., Hughes, C., and Koronakis, V. (1998). Substrate-induced assembly of a contiguous channel for protein export from E.coli: reversible bridging of an inner-membrane translocase to an outer membrane exit pore. EMBO J *17*, 6487-6496.

Tikhonova, E.B., Devroy, V.K., Lau, S.Y., and Zgurskaya, H.I. (2007). Reconstitution of the Escherichia coli macrolide transporter: the periplasmic membrane fusion protein MacA stimulates the ATPase activity of MacB. Mol Microbiol *63*, 895-910.

Tikhonova, E.B., and Zgurskaya, H.I. (2004). AcrA, AcrB, and TolC of Escherichia coli Form a Stable Intermembrane Multidrug Efflux Complex. J Biol Chem *279*, 32116-32124.

Touze, T., Eswaran, J., Bokma, E., Koronakis, E., Hughes, C., and Koronakis, V. (2004). Interactions underlying assembly of the Escherichia coli AcrAB-TolC multidrug efflux system. Mol Microbiol *53*, 697-706.

Ubarretxena-Belandia, I., Baldwin, J.M., Schuldiner, S., and Tate, C.G. (2003). Three-dimensional structure of the bacterial multidrug transporter EmrE shows it is an asymmetric homodimer. EMBO J *22*, 6175-6181.

Urbani, A., and Warne, T. (2005). A colorimetric determination for glycosidic and bile salt-based detergents: applications in membrane protein research. Anal Biochem *336*, 117-124.

van Veen, H.W., Callaghan, R., Soceneantu, L., Sardini, A., Konings, W.N., and Higgins, C.F. (1998). A bacterial antibiotic-resistance gene that complements the human multidrug-resistance P-glycoprotein gene. Nature *391*, 291-295.

Vazquez-Ibar, J.L., Guan, L., Svrakic, M., and Kaback, H.R. (2003). Exploiting luminescence spectroscopy to elucidate the interaction between sugar and a tryptophan residue in the lactose permease of Escherichia coli. Proc Natl Acad Sci U S A *100*, 12706-12711.

Velamakanni, S., Janvilisri, T., Shahi, S., and van Veen, H.W. (2007). A functional

steroid-binding element in an ATP-binding cassette multidrug transporter. Mol Pharmacol.

Verdon, G., Albers, S.V., Dijkstra, B.W., Driessen, A.J., and Thunnissen, A.M. (2003). Crystal structures of the ATPase subunit of the glucose ABC transporter from Sulfolobus solfataricus: nucleotide-free and nucleotide-bound conformations. J Mol Biol *330*, 343-358.

Verkman, A.S., Lukacs, G.L., and Galietta, L.J. (2006). CFTR chloride channel drug discovery--inhibitors as antidiarrheals and activators for therapy of cystic fibrosis. Curr Pharm Des *12*, 2235-2247.

Vistica, J., Dam, J., Balbo, A., Yikilmaz, E., Mariuzza, R.A., Rouault, T.A., and Schuck, P. (2004). Sedimentation equilibrium analysis of protein interactions with global implicit mass conservation constraints and systematic noise decomposition. Anal Biochem *326*, 234-256.

Walker, J.E., Saraste, M., Runswick, M.J., and Gay, N.J. (1982). Distantly related sequences in the alpha- and beta-subunits of ATP synthase, myosin, kinases and other ATP-requiring enzymes and a common nucleotide binding fold. EMBO J *1*, 945-951.

Walsh, C. (2000). Molecular mechanisms that confer antibacterial drug resistance. Nature *406*, 775-781.

Ward, A., Reyes, C.L., Yu, J., Roth, C.B., and Chang, G. (2007). Flexibility in the ABC transporter MsbA: Alternating access with a twist. Proc Natl Acad Sci U S A *104*, 19005-19010.

Washington, C.B., Wiltshire, H.R., Man, M., Moy, T., Harris, S.R., Worth, E., Weigl, P., Liang, Z., Hall, D., Marriott, L., and Blaschke, T.F. (2000). The disposition of saquinavir in normal and P-glycoprotein deficient mice, rats, and in cultured cells. Drug Metab Dispos *28*, 1058-1062.

Webb, M.R. (1992). A continuous spectrophotometric assay for inorganic phosphate and for measuring phosphate release kinetics in biological systems. Proc Natl Acad Sci U S A *89*, 4884-4887.

White, S. (n. d.). Membrane proteins of known 3D structure. pp. Retrieved June 25, 2008, from http://blanco.biomol.uci.edu/Membrane_Proteins_xtal.html.

Whitmore, L., and Wallace, B.A. (2004). DICHROWEB, an online server for protein secondary structure analyses from circular dichroism spectroscopic data. Nucleic Acids Res *32*, W668-673.

Wiener, M.C. (2004). A pedestrian guide to membrane protein crystallization. Methods *34*, 364-372.

Ye, J., Osborne, A.R., Groll, M., and Rapoport, T.A. (2004). RecA-like motor ATPases--lessons from structures. Biochim Biophys Acta *1659*, 1-18.

Yerushalmi, H., Lebendiker, M., and Schuldiner, S. (1995). EmrE, an Escherichia coli 12-kDa multidrug transporter, exchanges toxic cations and H+ and is soluble in

organic solvents. J Biol Chem *270*, 6856-6863.

Yerushalmi, H., and Schuldiner, S. (2000). An essential glutamyl residue in EmrE, a multidrug antiporter from Escherichia coli. J Biol Chem *275*, 5264-5269.

Yin, Y., He, X., Szewczyk, P., Nguyen, T., and Chang, G. (2006). Structure of the multidrug transporter EmrD from Escherichia coli. Science *312*, 741-744.

Yoneyama, H., Maseda, H., Kamiguchi, H., and Nakae, T. (2000). Function of the membrane fusion protein, MexA, of the MexA, B-OprM efflux pump in Pseudomonas aeruginosa without an anchoring membrane. J Biol Chem *275*, 4628-4634.

Zacharias, N., and Dougherty, D.A. (2002). Cation-pi interactions in ligand recognition and catalysis. Trends Pharmacol Sci *23*, 281-287.

Zaitseva, J., Holland, I.B., and Schmitt, L. (2004). The role of CAPS buffer in expanding the crystallization space of the nucleotide-binding domain of the ABC transporter haemolysin B from Escherichia coli. Acta Crystallogr D Biol Crystallogr *60*, 1076-1084.

Zaitseva, J., Jenewein, S., Jumpertz, T., Holland, I.B., and Schmitt, L. (2005). H662 is the linchpin of ATP hydrolysis in the nucleotide-binding domain of the ABC transporter HlyB. EMBO J *24*, 1901-1910.

Zaitseva, J., Oswald, C., Jumpertz, T., Jenewein, S., Wiedenmann, A., Holland, I.B., and Schmitt, L. (2006). A structural analysis of asymmetry required for catalytic activity of an ABC-ATPase domain dimer. EMBO J *25*, 3432-3443.

Zgurskaya, H.I., and Nikaido, H. (1999). Bypassing the periplasm: reconstitution of the AcrAB multidrug efflux pump of Escherichia coli. Proc Natl Acad Sci U S A *96*, 7190-7195.

Zgurskaya, H.I., and Nikaido, H. (2000). Cross-linked complex between oligomeric periplasmic lipoprotein AcrA and the inner-membrane-associated multidrug efflux pump AcrB from Escherichia coli. J Bacteriol *182*, 4264-4267.

MacB ABC Transporter Is a Dimer Whose ATPase Activity and Macrolide-binding Capacity Are Regulated by the Membrane Fusion Protein MacA*⑤

Hong Ting Lin[‡1], Vassiliy N. Bavro[§1,2], Nelson P. Barrera[¶1,3], Helen M. Frankish[‡], Saroj Velamakanni[‖], Hendrik W. van Veen[‖], Carol V. Robinson[¶3], M. Inês Borges-Walmsley[‡4,5], and Adrian R. Walmsley[‡4,6]

From the ‡School of Biological and Biomedical Sciences, Durham University, Stockton-on-Tees, TS17 6BH, the §Department of Physics, University of Oxford, Clarendon Laboratory, Parks Road, Oxford OX1 3PU, the ¶Department of Chemistry, University of Cambridge, Lensfield Road, Cambridge CB2 1EW, and the ‖Department of Pharmacology, University of Cambridge, Tennis Court Road, Cambridge CB2 1PD, United Kingdom

Gram-negative bacteria utilize specialized machinery to translocate drugs and protein toxins across the inner and outer membranes, consisting of a tripartite complex composed of an inner membrane secondary or primary active transporter (IMP), a periplasmic membrane fusion protein, and an outer membrane channel. We have investigated the assembly and function of the MacAB/TolC system that confers resistance to macrolides in *Escherichia coli*. The membrane fusion protein MacA not only stabilizes the tripartite assembly by interacting with both the inner membrane protein MacB and the outer membrane protein TolC, but also has a role in regulating the function of MacB, apparently increasing its affinity for both erythromycin and ATP. Analysis of the kinetic behavior of ATP hydrolysis indicated that MacA promotes and stabilizes the ATP-binding form of the MacB transporter. For the first time, we have established unambiguously the dimeric nature of a noncanonic ABC transporter, MacB, that has an N-terminal nucleotide binding domain, by means of nondissociating mass spectrometry, analytical ultracentrifugation, and atomic force microscopy. Structural studies of ABC transporters indicate that ATP is bound between a pair of nucleotide binding domains to stabilize a conformation in which the substrate-binding site is outward-facing. Consequently, our data suggest that in the presence of ATP the same conformation of MacB is promoted and stabilized by MacA. Thus, MacA would facilitate the delivery of drugs by MacB to TolC by enhancing the binding of drugs to it and inducing a conformation of MacB that is primed and competent for binding TolC. Our structural studies are an important first step in understanding how the tripartite complex is assembled.

Gram-negative bacteria utilize transport systems composed of a tripartite assembly of proteins that span both the inner and outer membranes to pump cytotoxic compounds, such as antibiotics (1), and protein toxins (2), such as α-hemolysin, from the cell. These assemblies are composed of inner (IMP)[7] and outer (OMP) membrane proteins that are connected by a periplasmic membrane fusion protein (MFP), which is anchored to the inner membrane. The systems responsible for toxin extrusion invariably utilize an ABC transporter as the IMP (2), whereas those involved in antibiotic extrusion largely utilize proton antiporters (1), but there are some that utilize ABC transporters (3). The same OMP can be utilized for both drug and toxin extrusion; for example, TolC functions with antibiotic H^+ antiporters, such as AcrB that belongs to the regulation nodulation cell division family of transporters (4, 5), with ABC transporters, such as the macrolide transporter MacB (3), and with HlyB that extrudes the protein toxin α-hemolysin (2).

Although the structure of an assembled tripartite complex has not yet been determined, the structures of a few individual components have been elucidated. Most significantly, the structure of the RND transporter AcrB (6, 7) and of its cognate MFP, AcrA (8), and OMP, TolC (9), have been determined. Both AcrB and TolC are organized as homotrimers. The AcrB trimer has a periplasmic headpiece formed by the loops between helices 1 and 2 and helices 7 and 8. The headpiece has a funnel-shaped internal cavity that is connected by a pore to a large central cavity formed between the periplasmic and membrane domains. The trimeric TolC forms a cylindrical channel with a structure that is arranged into two major domains as follows: a β-barrel in the outer membrane and a periplasmic α-helical barrel. It has been proposed, and is supported by cross-linking studies (10), that the six hairpins from the upper headpiece of the AcrB trimer contact the tips of the six helical pairs of the TolC trimer (11) to form a continuous path across

---

MacB Dimer Is Regulated by MacA

the periplasmic space. The structure of AcrA revealed an elongated monomer that is composed of three subdomains as follows: a β-barrel, a lipoyl domain, and a 58-Å-long α-helical hairpin (8). AcrA has been reported to interact with both TolC, via the α-helical hairpin (12), and AcrB, via the β-domains (13), to stabilize the tripartite complex (4, 5).

Several lines of evidence suggest that assembly of the tripartite complex is a dynamic process that induces conformational changes in the protein components. The structures of a number of OMPs indicate that the channel is closed at one or both sides, requiring conformational changes to allow passage of the substrate (11–14). Several studies support the hypothesis that a small number of key interactions between adjacent coiled-coils of the OMP are broken to allow the inner coils to untwist and realign with the outer coils, thereby opening the OMP entrance aperture (11, 15–17). The conformational flexibility of AcrA may enable realignment of the coiled-coil to stabilize the open state of TolC (8, 11, 15). Recently, the structures of a number of different conformations of AcrB have been determined that support a mechanistic model in which there is a functional rotation in the periplasmic domains driving transfer of drugs into the OMP (18–21). The conformational asymmetry in the IMP is also reflected in the asymmetry in the open state of the OMP TolC (11). Such conformational changes in AcrB could be transmitted to TolC via AcrA. Furthermore, studies of the RND transporter AcrD from *Escherichia coli*, whose typical substrates, aminoglycosides, are not expected to diffuse spontaneously across the lipid bilayer, revealed that only when AcrD was reconstituted with AcrA was it able to take up aminoglycosides, implying that AcrA is needed to "activate" AcrD (22). Collectively, these findings suggest that the MFP supports conformational changes in both the IMP and OMP.

We have sought to further investigate the assembly of the tripartite complex using the MacABTolC system responsible for the extrusion of macrolides from *E. coli* (3). To date this is the only tripartite pump for antibiotics that has been shown to utilize an ABC transporter, MacB, which has a novel architecture, consisting of a four-helix transmembrane domain, an N-terminal cytoplasmic nucleotide binding domain (NBD), and a large periplasmic domain formed by the loops connecting helices 1 and 2 (3, 23). The fact that the ATPase activity of the transporter can be monitored, using purified proteins, provides an additional tool for elucidating how its activity is modulated by assembly and disassembly of the tripartite complex. Indeed, recent studies, reported while this work was in progress, established that the MFP MacA modulates the steady-state ATPase activity of the IMP MacB (24). Our studies have confirmed these findings and, by undertaking pre-steady-state analysis of the kinetics, extended them by identifying how MacA modulates the ATPase mechanism of MacB. In addition, we have established that MacA also increases the capacity of MacB for binding erythromycin. This behavior provides a rationale for the retention of MacA by related systems from Gram-positive bacteria, such as *Staphylococcus aureus*, which lack an outer membrane and OMP (supplemental Fig. 1). Such analyses will not only have a bearing on understanding the function of tripartite drug-pumps but also of related toxin transporters.

EXPERIMENTAL PROCEDURES

Strains and Plasmids—The *E. coli* strains and plasmids used are described in supplemental Table 1, and the primers used for construction of plasmid vectors are described in supplemental Table 2.

Protein Overexpression and Purification—All the proteins used in this study were purified as fusion proteins with a six-histidine tag from *E. coli* overexpressing strains according to the protocols given in the supplemental material.

Pulldown Assays—For pulldown assays, proteins were overexpressed with a C-terminal S-tag for use with the cognate protein that was His-tagged. Membrane pellets, dissolved in detergent, or cell supernatant containing the S-tagged prey protein were mixed with 2 mg of purified His-tagged bait-protein. The mixture was loaded onto a Ni^{2+}-charged Hitrap chelating column (GE Healthcare), so that the bait-protein could be immobilized on the column along with the prey-protein if they interact. The column was then washed with 15–20 column volumes of Tris buffer containing 75–100 mM imidazole and Triton X-100 (0.2% (v/v)) to eliminate any false-positive results because of nonspecific interactions. The bait-prey protein complex was eluted with 500 mM imidazole Tris buffer, containing Triton X-100 (0.2% (v/v)), and SDS-PAGE was used to visualize the bait- and prey-proteins. A Western blot was performed with anti-S-tag antibodies to confirm the presence of the S-tagged prey-protein.

Growth Curve Analyses—*E. coli* cells, of strain Kam3(DE3), harboring plasmids were grown at 37 °C, with shaking at 200 rpm, until the cell density gave an A_{600} of 0.5, when 0.05–0.1 mM isopropyl 1-thio-β-D-galactopyranoside was added to the cells. The cells were grown for a further 3 h, when the cells were diluted with 2× YT media containing 50 or 100 μg/ml erythromycin, and the growth curve was recorded over the next 3 h. For experiments to measure the loss in growth because of erythromycin, cells were grown for 3 h in the absence and presence of 50 or 100 μg/ml erythromycin, and the growth loss is the ratio of the A_{600} values.

Analytical Ultracentrifugation—Sedimentation equilibrium measurements were performed using a Beckman Optima XL-A analytical ultracentrifuge equipped with both absorbance and interference optics. 100 μl of MacB in buffer 1 (20 mM Tris, pH 8.0, 150 mM NaCl, 1% w/v glycerol, and 0.006% (w/v) βDDM) supplemented with 10, 25, or 50% D_2O was placed in the sample compartment of a Epon double-sector centerpiece, and 110 μl of buffer 1 was placed in the reference compartment. The final protein concentrations used in the runs were between 0.5 and 1.0 mg/ml. The D_2O was used to match the density of the solvent to the density of the detergent as described previously (25) The samples were centrifuged at 283 K (10 °C) and 10,000, 15,000, and 25,000 rpm using an An60-Ti rotor. Scans were acquired using the absorbance optical system 15 h after the start of the experiment and in 1-h intervals until equilibrium was attained. Sedimentation velocity measurements were performed using the same hardware at 55,000 rpm at 10 °C in buffer 1. The details of the data analysis are given as supplemental material.

Mass Spectrometry—Analyses were performed in a nanoflow ES mass spectrometer Q-ToF2 (Micromass). The following
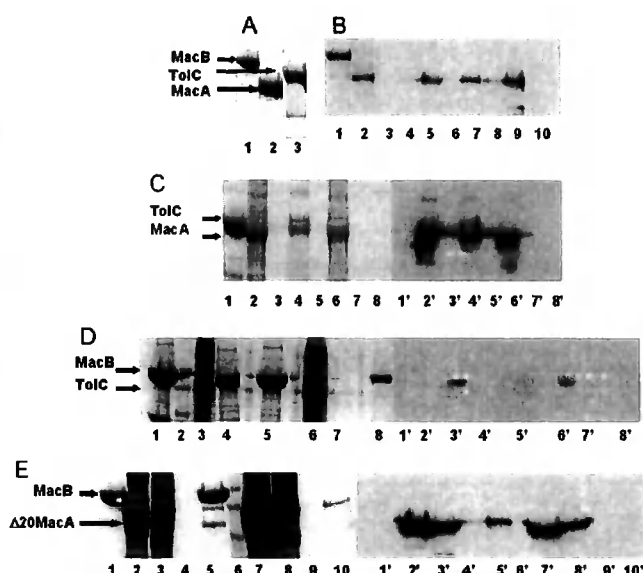
FIGURE 1. **MacA interacts with both MacB and TolC.** *A,* overexpression and purification of MacA, MacB, and TolC. An SDS-polyacrylamide gel of purified MacB (*lane 1*), MacA (*lane 2*), and TolC (*lane 3*) is shown. The purified His-tagged MacB and TolC proteins were used as bait, immobilized on a Ni²⁺-agarose column, over which a slurry of either detergent-solubilized membranes (*e.g.* from strains overexpressing S-tagged MacA or TolC) or soluble proteins (*e.g.* from strains overexpressing S-tagged Δ20MacA) was passed to test whether the cognate proteins from the tripartite pump could be pulled out of this complex mixture of proteins. *B,* pulldown of MacA by MacB. *1st* and *2nd lanes,* SDS-polyacrylamide gel of immobilized His-tagged MacB (*1st lane*) and the detergent-solubilized membranes from cells overexpressing the S-tagged MacA (*2nd lane*). *3rd* to *11th lanes,* Western blot using antibodies to the S-tag (1:5000 dilution) on MacA. The pulldown assay was performed with His-tagged MacB immobilized on a Ni²⁺-agarose column, over which a slurry of detergent-solubilized membranes from cells overexpressing S-tagged MacA was passed (*7th* to *9th lanes*). The flow-through (*9th lane*), 100 mM imidazole wash (*8th lane*), and the 500 mM imidazole elution (*7th lane*) were tested for the presence of MacA, which was now also detected in the elution fraction, indicating that it was bound to MacB. A negative control experiment was performed in the absence of immobilized MacB in which MacA was passed through a Ni²⁺-agarose column (*3rd* to *5th lanes*), and the flow-through (*5th lane*), 100 mM imidazole wash (*4th lane*), and the 500 mM imidazole elution (*3rd lane*) were tested for the presence of MacA, which was only found in the flow-through (*5th lane*), establishing that S-tagged MacA does not bind to the column. These results indicate that MacB can pull MacA from a complex mixture of membrane proteins. Purified His-tagged MacB did not cross-react with the antibodies to the S-tag (*10th lane*). *C,* pulldown of MacA by TolC. An SDS-polyacrylamide gel (*lanes 1–8*) for the pulldown of S-tagged MacA by His-tagged TolC and the corresponding Western blot (*lanes 1′–8′*) probed with antibodies (1:5000 dilution) to the S-tag on MacA. Purified His-tagged TolC was immobilized on a Ni²⁺-agarose column (*lanes 1* and *1′*); a slurry of detergent-solubilized membranes from cells overexpressing S-tagged MacA was passed through the column and the proteins in the flow-through (*lane 2* and *2′*), released by washing the column with 100 mM imidazole (*lanes 3* and *3′*) and eluted with 500 mM imidazole (*lanes 4* and *4′*), were detected. As a negative control, S-tagged MacA was passed through the column (*lanes 5* and *6′*), in the absence of immobilized TolC, and the column was washed with 100 mM (*lanes 7* and *7′*) and 500 mM (*lanes 8* and *8′*). Comparing *lane 4′* and *8′* demonstrates that MacA is only bound to the column in the presence of TolC, indicative of its interaction with TolC. *D,* pulldown of TolC by MacB. An SDS-polyacrylamide gel (*lanes 1–4*) for the pulldown of S-tagged TolC by His-tagged MacB and the corresponding Western blot (*lanes 1′–4′*) probed with antibodies (1:5000 dilution) to the S-tag on TolC. Purified His-tagged MacB was immobilized on a Ni²⁺-agarose column (*lanes 1* and *1′*), and a slurry of detergent-solubilized membranes from cells overexpressing S-tagged TolC was passed through the column (*lane 3* and *3′*), which was then washed with 75 mM imidazole (*lanes 4* and *4′*), and bound proteins were eluted with 500 mM imidazole (*lanes 5* and *5′*). A weak band, which was not present in the absence of immobilized MacB, was apparent in *lane 5′*, indicative of a weak interaction between MacB and TolC. A control experiment was performed in the absence of immobilized MacB in which TolC was passed through a Ni²⁺-agarose column and the flow-through (*lane 6*), the 100 mM imidazole wash (*lane 7*), and the 500 mM imidazole elution (*lane 8*) were tested for the presence

of TolC, which was only found in the flow-through (*lane 6′*), establishing that S-tagged TolC does not bind to the column. A protein *M*ᵣ marker was run in *lane 2*. *E,* pulldown of N-terminal truncated MacA by MacB. An SDS-polyacrylamide gel shows the His-tagged MacB (*lane 1*) that was immobilized on a Ni²⁺-agarose column (*lane 1*), a slurry of cytoplasmic proteins released by disruption of cells overexpressing S-tagged Δ20-MacA (*lane 2*), which was passed through the column, over immobilized MacB, and the proteins in the flow-through detected (*lane 3*); the proteins were released by washing the column with 100 mM imidazole (*lane 4*); and the proteins were eluted with 500 mM imidazole (*lane 5*). A Western blot was performed on each of the corresponding protein fractions (indicated with *1′–5′*) using antibodies to the S-tag (1:5000 dilution) to detect S-tagged MacA. The elution of MacB yields an extra, low *M*ᵣ band on the SDS-polyacrylamide gel that corresponds to that expected for MacA (*lane 5*) and was identified as such by Western blotting (*lane 5′*). A control experiment was performed in the absence of immobilized MacB in which Δ20MacA was passed through a Ni²⁺-agarose column and the flow-through (*lane 7*), the first and second washes with 100 mM imidazole (*lanes 8* and 9, respectively), and the 500 mM imidazole elution (*lane 10*) were tested for the presence of MacA, which was only found in the flow-through and first wash (*lane 7′* and *8′*, respectively), establishing that S-tagged MacA does not bind to the column. These results indicate that MacA does not require the N-terminal α-helix, which anchors it to the inner membrane, to interact with MacB. A protein *M*ᵣ marker was run in *lane 6*.

experimental parameters were used to record mass spectra of 2 mg/ml MacB in the Q-ToF2 instrument: needle voltage of 1.5 kV and MCP 2350 V.

Atomic Force Microscopy—MacB was diluted to a final concentration of 1 μg/ml, and 45 μl of the sample was allowed to adsorb to freshly cleaved mica. Imaging in air was performed with a Multimode atomic force microscope (Digital Instruments, Santa Barbara, CA) in tapping mode. The silicon cantilevers containing a diamond-like extratip had a drive frequency of ≈300 kHz and a specified spring constant of 40 newtons/m (MikroMasch, Portland, OR), and the applied imaging force was kept as low as possible (target amplitude ≈1.6–1.8 V and amplitude set-point ≈1.3–1.5 V). The molecular volumes of the protein particles were determined from particle dimensions based on AFM images (see supplemental material).

ATPase Assays—An EnzChek phosphate assay kit (Invitrogen) was used to determine the ATPase activity of MacB hydrolyzing MgATP to release phosphate, when the reactants were mixed in a stopped-flow device (see supplemental material). Generally, 2.3 μM protein was mixed with varying concentrations of ATP, up to 4 mM, in the presence of 6 mM MgCl₂, to ensure that all the ATP was complexed with Mg²⁺. In control experiments, no ATPase activity was apparent in the absence of Mg²⁺. Generally, for MacB alone, the hydrolysis of ATP was characterized by a P_i burst, which was of near equivalence to the MacB concentration, consistent with the ATPase activity being attributable to MacB, rather than any contaminant proteins.

Quantification of Erythromycin Binding to Affinity-purified Mac Proteins—The equilibrium binding of [*N*-methyl-¹⁴C]erythromycin to purified Mac proteins was determined by rapid filtration and quantification of the radioactivity remaining on 0.2-μm filters as outlined in the supplemental material.

RESULTS

MacA Interacts with Both MacB and TolC via Its Periplasmic Domain—Interactions between *E. coli* MacA, MacB, and TolC were tested using detergent-solubilized proteins for pulldown assays (Fig. 1). MacA interacted with MacB (Fig. 1*B*), which we confirmed by cross-linking the proteins (supplemental Fig. 2*A*),
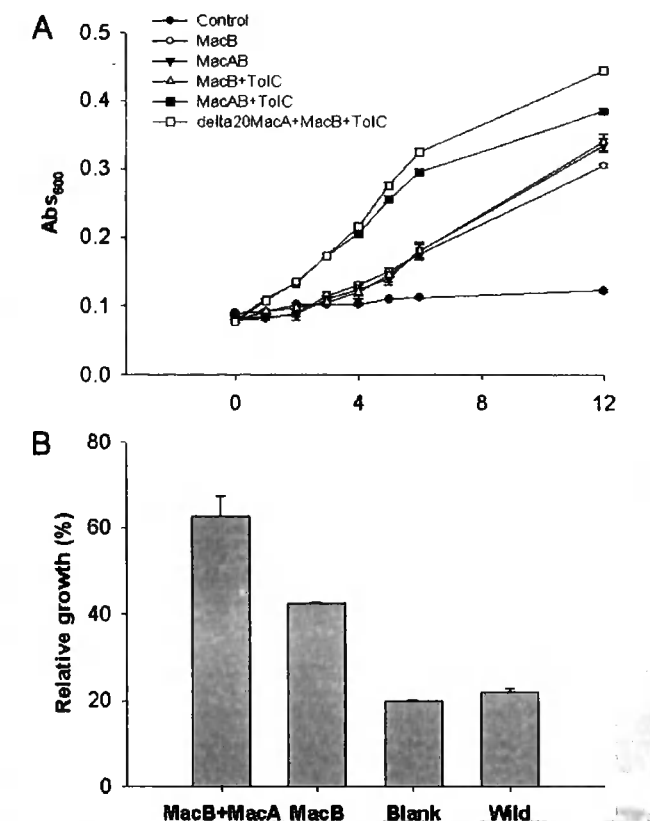
MacB Dimer Is Regulated by MacA

FIGURE 2. **MacAB-TolC form a tripartite complex that confers resistance to erythromycin.** A, growth curves for E. coli cells, of strain Kam(DE3), harboring the plasmids pETDuet (●), pETDuet-MacB (O), pETDuet-MacB/MacA (▼), pETDuet-MacB/TolC (△), pETDuet-MacB/MacA/TolC (■), and pETDuet-MacB/gIII-SS-Δ20MacA/TolC (□) grown in the presence of 100 μg/ml erythromycin. B, bar chart showing the extent of inhibition of the growth of E. coli cells in response to 50 μg/ml erythromycin, of strain Kam3(DE3), harboring the plasmids pETDuet (blank), pETDuet-MacB (MacB), pETDuet-MacB/MacA (MacAB) or no plasmid (Wild). For each strain the A_{600} was determined after growth for 3 h in the absence and presence of erythromycin, and the growth inhibition was determined as the ratio of these measurements. Cells expressing both MacA and MacB suffered less from erythromycin growth inhibition than those expressing only MacB, suggesting that MacA confers elevated resistance to erythromycin on the MacB strain.

and TolC (Fig. 1C). Although we detected an interaction between TolC and MacB (Fig. 1D), the intensity of the band suggested a weak interaction. N-terminal truncated MacA (Δ20-MacA) interacted with MacB (Fig. 1E), indicating that it is the periplasmic domains of these proteins that interact. The fact that in each case the cognate pump protein could be pulled out of a complex mixture of detergent-solubilized proteins from membranes or cells indicated that the interactions are specific.

E. coli MacA and MacB Form a Functional Complex with TolC—The simultaneous expression of *macA*, *macB*, and *tolC* in the *E. coli* Δ*acrB* strain Kam3 (26) conferred resistance to erythromycin, indicative of the formation of a functional complex (Fig. 2A). Cells expressing *macB* with *tolC* conferred modest resistance to erythromycin in comparison with cells expressing *macB*, *tolC*, and *macA*, indicating that MacA is required to couple MacB to TolC (Fig. 2A). We sought to test whether the N terminus of MacA, which incorporates an α-helix that could interact with MacB, is required for the functional assembly of the complex. A construct in which the gIII-signal

sequence was fused to truncated MacA, targeting it to the periplasm, was capable of conferring resistance to erythromycin (Fig. 2A), indicating that the N-terminal domain is not essential for the assembly of the functional complex. This is consistent with a report that a truncated lipid-deficient AcrA derivative was functional as judged by resistance of the cells to erythromycin (27). MacB alone conferred elevated resistance to erythromycin, probably because of its ability to pump the antibiotic into the periplasm, but we consistently found that expressing *macB* with either *tolC* or *macA* conferred greater resistance. Consequently, we sought to test if MacA could enhance this ability. To overcome the difficulty in comparing the growth of cells overexpressing multiple proteins that tend to grow at different rates, we monitored the growth of cells in the presence and absence of erythromycin and determined the growth loss (for cells growing in the presence of erythromycin in comparison with cells growing in the absence of erythromycin) (Fig. 2B). This revealed a significant loss in growth of the cells expressing MacB compared with those expressing MacAB, indicating that the simultaneous expression of MacA and MacB increases the resistance of the cells to erythromycin (Fig. 2B), suggesting that MacA enhances the ability of MacB to confer antibiotic resistance. Similarly, a previous study reported that MacAB, but not MacB alone, conferred resistance to macrolides (3).

MacB Forms Dimers—MacB has an atypical structure for an ABC transporter as it is predicted to have an N-terminal cytoplasmic NBD, which is connected to a four-helix transmembrane domain, with a large periplasmic domain formed by the loops connecting helices 1 and 2 (3, 23). If MacB resembles other ABC transporters that use a pair of NBDs to bind ATP, then it should function as a dimer. However, many transporters, including ABC transporters, have 12 membrane-spanning helices; MacB could adopt a similar topology by forming trimers. Furthermore, AcrB (4, 5) and TolC (9), which assemble into a tripartite complex with AcrA, clearly form trimers. If the trimeric arrangement of the periplasmic domains in AcrB forms a necessary scaffold for binding of AcrA, so that it can effectively interact with TolC, then by analogy the periplasmic domain of MacB might also be forced into forming trimers when interacting with MacA and TolC.

Therefore, we sought to determine the oligomeric state of MacB. Size-exclusion chromatography indicated that it forms higher order oligomers consistent with a dimer (data not shown), but such measurements are not only dependent upon the molecular weight but also the shape of the protein. Furthermore, there is a need to determine the number of detergent molecules complexed by the protein. Consequently, to determine whether the detergent-solubilized MacB was dimeric, we added a cross-linker to trap the oligomers; when we ran the cross-linked protein on an SDS-polyacrylamide gel, the most predominant band ran between the 120- and 160-kDa markers, indicative of a dimer, which has a calculated molecular mass of 145.8 kDa (supplemental Fig. 2B). [ZSl]

To further confirm the basic oligomeric unit as a dimer, we used two other techniques, analytical ultracentrifugation (AUC) and electrospray mass spectrometry (ES-MS). For the AUC experiments, we reduced the βDDM concentration to
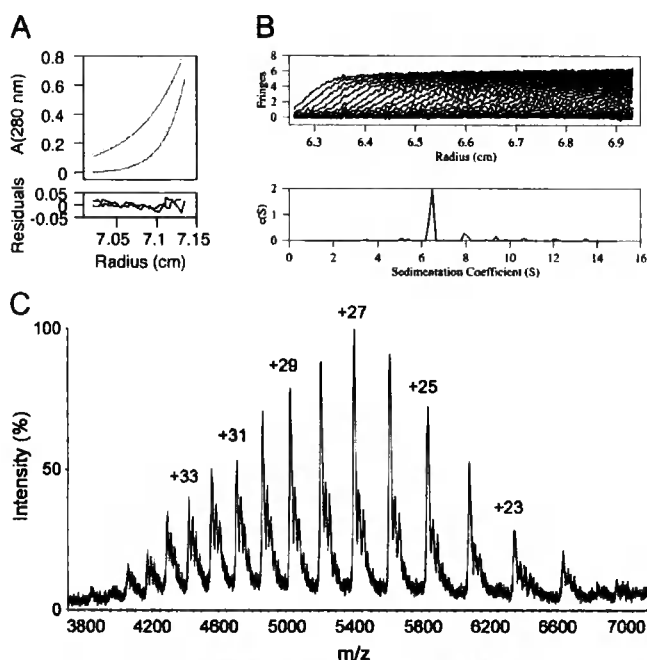
FIGURE 3. **Biophysical evidence for MacB dimer formation.** *A*, AUC sedimentation equilibrium profiles of MacB. A representative sedimentation equilibrium profile from one of the runs (two different velocities of the same sample) is shown. Experimental data (*dots*) and fitted model for a 162.6-kDa particle (*solid line*) is shown for each. The *bottom panel* represents the residuals after fitting. *B*, AUC sedimentation velocity profiles of MacB are consistent with the formation of a stable dimer. The *upper panel* shows sedimentation profile curves at different time points, and the *lower panel* presents a $c(s)$ size distribution analysis with solutions of the Lamm equation. The sedimentation coefficient is 6.8 S corresponding to an apparent molecular mass of 160 kDa, consistent with a dimer with about 16 detergent molecules bound. *C*, mass spectrum of MacB. The charge states corresponding to the peaks are graphed. The mass spectrum indicated a molecular mass for MacB of 145.96 kDa, which is consistent with a dimer.

just below the critical micelle concentration to avoid the formation of micelles. To determine the detergent contribution in the buoyant mass of the protein-detergent complex, we used a series of different density buffers prepared using a range of D_2O concentrations. The apparent molecular mass for MacB was determined from sedimentation equilibrium measurements to be 162.6 kDa (Fig. 3*A*) and from sedimentation velocity measurements to have a sedimentation coefficient of 6.8 S, corresponding to a molecular mass of 160.0 kDa (Fig. 3*B*). This molecular mass is greater than expected for monomeric and less than expected for trimeric MacB, complexed with bound detergent, but it is highly consistent with a MacB dimer to which about 16 βDDM molecules are bound. Although the amount of detergent bound to the MacB dimer appears to be lower than reported for RND (28) and MF (29) transporters, this reflects the fact that in our experimental set-up the detergent contribution was actively suppressed using a solvent density matching technique (25). Our independent measurement of bound detergent using a calorimetric assay (30) indicated that, when the detergent concentration was close to the critical micelle concentration, the amount of bound detergent was similar to that of other membrane proteins (*e.g.* MacB solubilized in 0.05% w/v βDDM bound 1.2 g of βDDM/g of MacB, which is equivalent to a βDDM:MacB molar ratio of 164:1). Electrospray-mass spectrometry (ES-MS) was used in nontandem con-

figuration to determine accurately the molecular mass of the protein, under conditions that would dissociate the βDDM, revealing a peak with a molecular mass of 145,961.25 $\pm$ 20.57 Da that is consistent with a MacB dimer (Fig. 3*C*).

We also sought to visualize single particles of MacB by AFM (Fig. 4, *A* and *D*). Two populations were revealed with average molecular volumes of 118 and 238 nm³ (Fig. 4*B*). These would accommodate proteins of about 60–70 and 130–140 kDa, respectively. Furthermore, the larger particles could clearly be seen at higher resolution to consist of two protein domains that are highly suggestive of a dimer. We found that in the presence of AMP-PNP, a nonhydrolysable analogue of ATP, the ratio of dimers to monomers on the AFM grids increased (Fig. 4*C*), which would be consistent with the nucleotide stabilizing the interaction between monomers. Our findings are novel because detergent molecules tend to impair the resolution of AFM studies of detergent-solubilized membrane proteins; this implies that for MacB, we may be able to get information on the topology and stoichiometry of its assemblies with MacA and TolC. Indeed, under coincubation of MacA and MacB, we could clearly distinguish a significant distribution of particles with molecular volumes larger than those corresponding to MacB dimers, which is consistent with multiprotein complexes formed between both proteins (data not shown). Such promising data paves the way toward further characterization of membrane multiprotein complexes and could prove a powerful instrument for determining the stoichiometry of the tripartite assembly.

MacA Regulates the ATPase Activity of MacB—MacB retained ATPase activity when detergent-solubilized, but this was detergent-dependent, being active in Triton X-100 but not in βDDM (data not shown). The time course for hydrolysis of MgATP by MacB was determined in a stopped-flow spectrophotometer, using the dye 2-amino-6-mercapto-7-methylpurine riboside to monitor the production of inorganic phosphate (P_i). The time course was characterized by a burst in P_i production, during the first 20 s, followed by a slower steady-state rate (Fig. 5*A*). This kinetic behavior is consistent with the ATP being rapidly hydrolyzed, to produce P_i and ADP, but further turnovers are rate-limited either by a subsequent conformational change or the slow release of products. Because previous studies have established that the ATPase activity of MacB is inhibited by vanadate (24), which stabilizes bound ADP, this indicates that P_i is released before ADP, suggesting that ADP release is rate-limiting. The rate constant for the hydrolysis step was determined by fitting the burst phase to an exponential function, yielding a k_{cat} value of 0.24 s^{-1}, whereas the amplitude of the burst phase was 2.2 μM for 1 mM ATP (Fig. 5*A*). When the MacA and MacB concentrations were increased to 3.5 μM, the amplitude of the burst phase increased to 3.3 μM (data not shown), indicating that the burst is approximately equivalent to the MacB concentration and that both NBDs within the MacB dimer are functional. We did not notice any deviation from a single exponential that would indicate that these NBDs turn over ATP differentially. The steady-state phase was characterized by a rate of P_i production that increased in a hyperbolic manner with the ATP concentration (Fig. 5*B*); fitting the steady-state rate data to a hyperbolic function yielded a maxi-
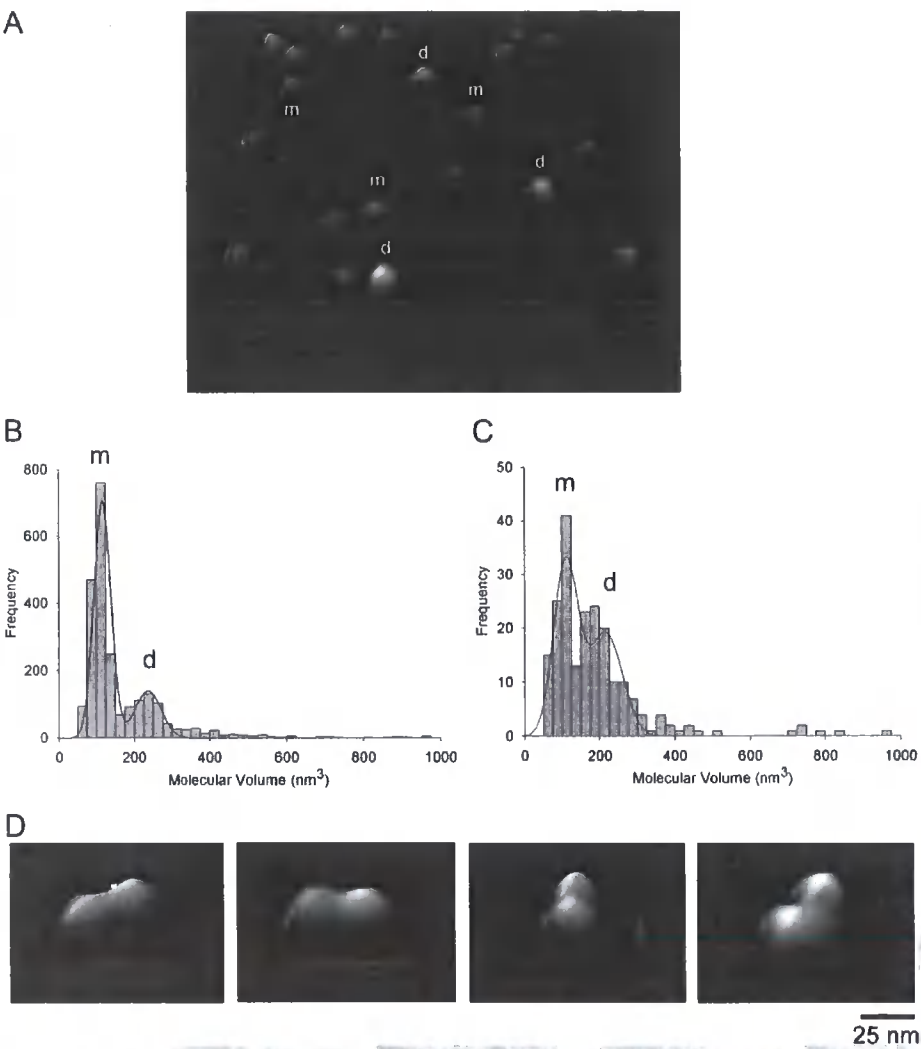
MacB Dimer Is Regulated by MacA

FIGURE 4. **AFM analyses, AFM imaging of MacB.** *A*, three-dimensional picture of a low magnification image of MacB acquired in air in Tapping Mode with a diamond-like extra tip of resonant frequency ~300 kHz and spring constant of 40 newtons/m. *m* and *d* show particles that belong to the first and second peak in *B*, respectively. *B*, frequency distribution of molecular volumes of MacB. The curve indicates a fitted Gaussian function. The *m* and *d* peaks correspond to volumes of 118 ± 1 nm³ (*n* = 1642) and 238 ± 5 nm³ (*n* = 665), consistent with the monomer and dimer, respectively. *C*, frequency distribution of molecular volumes of MacB that had been incubated with the nonhydrolysable ATP analogue AMP-PNP. The peaks correspond to volumes of 112 ± 3 nm³ (*n* = 94) and 218 ± 14 nm³ (*n* = 116). These data indicate an increase in the dimer:monomer ratio in the presence of AMP-PNP. *D*, high resolution images of structures where two small particles (*m*+*m*) are attached to one another, clearly indicative of dimer formation.

cannot be attributed to the detergent modifying the behavior of MacB. Interestingly, although there was no P_i burst by MacB in the presence of MacA, there was a lag in P_i production; this could signify that a conformational change that precedes the hydrolysis step becomes rate-limiting for the first turnover. The steady-state rate of ATP hydrolysis by MacB, in the presence of MacA, was enhanced (Fig. 5*B*). At first glance, this behavior might appear consistent with MacA increasing the rate of ADP dissociation from MacB, so that this step was no longer rate-limiting. However, although MacA increased the specific activity of MacB from 8.9 to 12.3 nmol of ATP/mg MacB/min, which would correspond to an increase in k_{cat} from 0.011 to 0.015 s^{-1}, the steady-state rate did not exceed the rate for hydrolysis in the absence of MacA (*e.g.* 0.24 s^{-1}) (Fig. 5*B*). Accordingly, the increase in the steady-state rate, which we attribute to product release, or a conformational change preceding this, would not be rapid enough to prevent the phosphate burst. It seems more likely that MacA also retards the rate of ATP hydrolysis, so that this process becomes slower than the rate of product release. Indeed, we found that the affinity of MacB for ATP was increased by more than 5-fold, from 374 to 72 μM, in the presence of MacA (Fig. 5*B*). If the effect of MacA was simply to enhance product release to a rate faster than that for nucleotide hydrolysis, then we would have expected a decrease in affinity for ATP. On the other hand, if MacA simply retarded nucleotide hydrolysis to a rate slower than product release, then the maximal steady-state rate would have decreased. Our data are consistent with MacA increasing the rate of product release, while decreasing the rate of hydrolysis to a similar rate to product release.

In contrast to a previous study, which indicated that the ATPase activity of reconstituted MacB was not activated by N-terminal truncated MacA (24), we found that when MacB was mixed with Δ20-MacA no P_i burst was apparent (data not shown). In the same study, and consistent with our findings, N-terminal truncated MacA was shown to interact with MacB; however, in contrast to our findings, when MacB was expressed with N-terminal truncated MacA in erythromycin-susceptible

mal specific activity of 8.9 nmol of ATP/min/mg MacB and a K_m of 374 μM. A progressive reduction in the amplitude of the burst phase for ATP concentrations below the steady-state K_m value hindered analyses because the pre-steady-state phase tended to merge with the steady-state phase; consequently, we only used the steady-state rates determined at ATP concentrations of 0.1 mM and above. For comparison, the lipid A transporter MsbA, an half-ABC transporter, was characterized by a V_{max} of 37 nmol of ATP/min/mg and a K_m of 878 μM (31).

When MacA was added to MacB, at an equivalent or higher concentration, with both proteins in detergent, no phosphate burst was observed (Fig. 5*A*). Considering that the detergent was present for both the ATPase assays with MacB and MacAB suggests that the burst phase is mechanistically important and
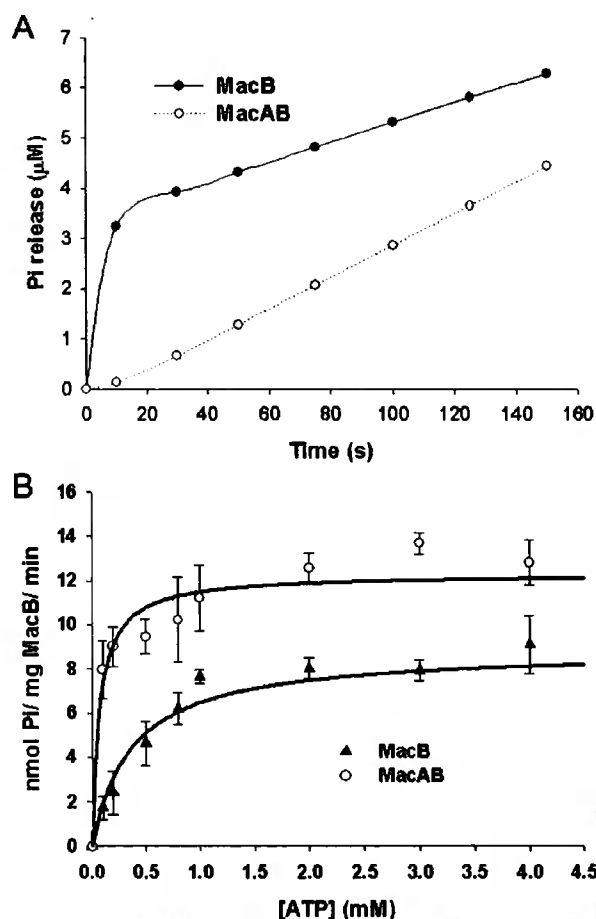
MacB Dimer Is Regulated by MacA

FIGURE 5. **MacA regulates the ATPase activity of MacB.** *A,* time course for the change in P_i concentration, corresponding to the absorbance change of the 2-amino-6-mercapto-7-methylpurine riboside in *A,* where 2.3 μM MacB was mixed with 1 mM ATP in the absence (*upper trace*) and presence (*lower trace*) of an equivalent concentration of MacA. In the absence of MacA, MacB produced a phosphate (P_i) burst, with a rate and amplitude of 0.235 ($\pm$0.001) s^{-1} and 2.20 ($\pm$0.01) μM, respectively. MacB did not produce a P_i burst in the presence of MacA. *B,* steady-state rate of P_i production by MacB as a function of the ATP concentration in the absence (*lower curve*) and presence (*upper curve*) of an equivalent concentration of MacA. The data are characterized by V_{max} and K_m values of 8.9 ($\pm$0.7) nmol of ATP/mg MacB/min and 374 ($\pm$126) μM, respectively, for MacB alone; and of 12.3 ($\pm$0.5) nmol of ATP/mg MacB/min and 72 ($\pm$22) μM, respectively, for MacB in the presence of an equivalent concentration of MacA.
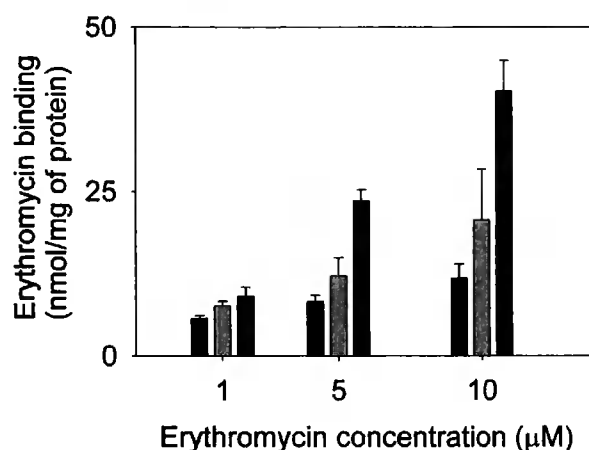
FIGURE 6. **MacA increases the capacity of MacB to bind erythromycin.** Purified proteins (50 μg of MacA or MacB, or 25 μg of MacA plus 25 μg of MacB) were incubated in the presence of [*N-methyl-*[14]*C*]erythromycin at concentrations as indicated (1, 5, or 10 μM), after which drug binding was measured by rapid filtration. The *bars* represent the erythromycin bound by MacA (*left, black*), MacB (*middle, light gray*), and MacAB (*right, dark gray*). The data indicate that MacA enhances the binding of erythromycin to MacB.

cells, there was no increase in erythromycin resistance (24). The reason for the difference with our own findings is unclear; however, in the previous study the signal sequence of OmpA was used to target MacA, truncated at position 32, to the periplasm (24), raising the possibility that the shorter MacA sequence and/or the OmpA signal sequence interfered with the ability of MacA to affect the ATPase activity of MacB.

In accord with previous studies (24), we could not detect an effect of erythromycin on the kinetics of MacB ATPase either in the absence or presence of MacA (data not shown). Recent studies have established that the ATPase activity of Pdr5 is uncoupled from substrate binding; this basal ATPase activity might be required to constantly cycle the transporter between conformations, so as to maintain the accessibility of the cytosolic substrate-binding site (32). In the case of MacB, its ATPase

activity might instead be stimulated by TolC, to reset its conformation following drug transfer to TolC.

MacA Increases the Capacity of MacB to Bind Erythromycin—Although we could not detect any effect of erythromycin on the ATPase activity of MacB, we could detect the binding of [14C]erythromycin to detergent-solubilized MacB (Fig. 6). Importantly, we found that the MacAB complex bound more erythromycin than MacB alone (which binds considerably more than MacA alone) and that the amount bound increased in a concentration-dependent manner, as would be expected if MacA increased the affinity of MacB for erythromycin. However, because of the insolubility of the antibiotic in aqueous solutions, it was not possible to test a full range of erythromycin concentrations that might saturate MacAB. Consequently, we cannot exclude the possibility of the formation of additional sites within the MacAB complex that are not apparent in either MacB or MacA alone. Our data indicate that MacA not only modulates the ATPase activity of MacB but also enhances its capacity to bind erythromycin (be this due to an increase in affinity of MacB for drugs or the formation of additional drug-binding sites within the MacAB complex).

DISCUSSION

Gram-negative bacteria possess tripartite pumps that facilitate the extrusion of protein toxins and cytotoxic compounds, such as antibiotics, from the cell. In these tripartite assemblies the IMP is coupled to an OMP by a periplasmic MFP, forming a pump that can translocate molecules across both the inner and outer membranes. Intriguingly, Gram-positive bacteria that lack an outer membrane also possess MFPs, suggesting that they play a role in addition to stabilizing the interaction of the IMP with the OMP. Indeed, we have noted in some of these MFPs a large deletion corresponding to the coiled-coil hairpin that would interact with the OMP (supplemental Fig. 1). To investigate this possibility, we sought to determine the role of MacA, the MFP that couples the IMP MacB, an ATP-driven transporter, with the OMP TolC in *E. coli* to extrude macrolide

MacB Dimer Is Regulated by MacA

antibiotics (3). We established that MacA interacts with both MacB and TolC (Fig. 1) to form a functional tripartite complex (Fig. 2). However, we also found that MacA enhanced the resistance to erythromycin conferred by MacB alone (Fig. 2B), suggesting that it modulated the transport activity of MacB, which is consistent with our data demonstrating that MacA regulates the drug binding and ATPase activity of MacB (Figs. 5 and 6). The role of the MFP BesA in the activity of the BesABC pump in *Borrelia burgdorferi*, the causative agent of Lyme disease, has recently been highlighted (33). It is quite remarkable that in this system BesA also lacks the α-helical hairpin. As such this periplasmic protein is unable to unlock the periplasmic entry site of the OMP, a function that is attributed to the hairpin (11). To compensate, the OMP has evolved to be constitutively leaky. The reason for the retention of BesA in the *Borrelia* system is most likely associated with its function in the activation of the inner membrane component, in that case an RND transporter. It is conceivable then, that a similar role is also present in the ABC transporters and their associated MFPs, and it could explain the preservation of the hairpin-lacking MFPs in Gram-positive bacteria, such as *S. aureus* (supplemental Fig. 1).

Although *E. coli* MacB has an NBD, which incorporates Walker A and B motifs and an ABC signature sequence that are characteristic features of members of the ABC superfamily, it is not a classic ABC transporter. It has a large periplasmic domain, reminiscent of that found in RND transporters, which form trimers in which these domains form substantive sites of contact between the protomers. Consequently, we sought to determine the oligomeric state of MacB and in doing so have developed a novel ES-MS approach to unambiguously establish that MacB forms dimers (Fig. 3C). ES-MS is now widely accepted as a powerful method to determine accurately the stoichiometry of intact protein complexes (34). However membrane proteins, solubilized by detergent or adsorbed in micelles, have remained difficult to analyze under similar MS conditions. The development of strategies to tackle this field is challenging, primarily because the large quantities of detergent suppress the protein signal, whereas the poor solubility of membrane proteins in aqueous buffers often causes the electrospray needle to block. To date only a few MS studies have reported the observation of membrane proteins or their complexes by MS (35–39). Here we report on the use of a miniaturized form of ES with reduced flow rates (nano-ES), and a high collision energy that facilitates the desolvation process and induces dissociation of detergent-proteins clusters, to determine the oligomeric state of an integral homomeric membrane protein. In our protocol we used lower quantities of βDDM, than have been reported previously, without apparent detrimental effects on the stability of the protein. Under our experimental conditions, we have successfully maintained the noncovalent subunit interactions, such that the oligomeric state of the protein complex could be determined without ambiguity. As would be expected for an ABC transporter in which the NBDs interact, our biophysical studies of MacB indicate that it forms dimers (Figs. 3 and 4 and supplemental Fig. 3). This is an interesting observation because it raises the following question. How does dimeric MacB interact with trimeric TolC and the number of MacA molecules needed to stabilize the tripartite complex? Extension of our AFM studies will be vital for determining the stoichiometry of the interactions to provide an understanding of the assembly of the tripartite complex, which may be difficult to address by other methods, such as crystallization of the complex.

Our findings and previous studies, which have shown that disruption of the Walker A and B motifs not only inhibits the ATPase activity but also blocks the capacity of MacB to confer macrolide resistance (24), suggest that MacB operates by a similar mechanism to typical ABC transporters. Our understanding of how ABC transporters couple ATP hydrolysis to transport is still rudimentary, but the determination of the crystal structures of several ATPase subunits and complete ABC transporters has suggested conservation of key steps in the molecular mechanism. The binding of ATP to both soluble ATPase subunits (40), solubilized NBDs from ABC transporters (41, 42), and to the NBDs within a complete ABC transporter (43, 44) has been shown to promote dimerization as the ATP is bound at the interface of these nucleotide-binding sites, sandwiched between the Walker A motif of one NBD and the ABC signature motif of the other NBD. Our AFM studies indicated that there is a higher proportion of MacB dimers in the presence of the nonhydrolysable nucleotide AMP-PNP (Fig. 4). In complete ABC transporters, the binding of ATP causes the transporter to adopt a conformation in which the substrate-binding site is outward-facing, because ATP bridges the two NBDs, closing off the inward-facing substrate-binding site (45). Conversely, the release of the hydrolysis products ADP and phosphate is thought to promote an inward-facing conformation, as the structural constraint imposed by binding of the nucleotide is released. Consistent with this proposal, several studies indicate that NBD dimerization cannot be induced by ADP (46), because interactions between the γ-phosphate of ATP and the signature sequence catalyze these events (47). We found that MacA modulates these processes in MacB (Fig. 5), and so our kinetic data have clear implications in terms of such a mechanism. Most significantly, MacA increases the apparent affinity of MacB for ATP, while decreasing the rate of ATP hydrolysis, so as to promote and stabilize the ATP binding conformation, which we presume to be the conformation in which the antibiotic-binding site is outward-facing. In this manner, MacA would play a direct role in driving antibiotic translocation between MacB and TolC.

During the course of our studies another investigation reported on the effect of MacA on the steady-state ATPase activity of MacB (24). In this study, MacB, solubilized in Triton X-100, appeared to have a specific activity that was an order of magnitude higher than we had found; however, a discontinuous assay was used to determine the ATPase activity, and this could well have been influenced by pooling the time points from both the burst and steady-state phases. Indeed, k_{cat} was marginally slower than the hydrolysis rate determined from the P_i burst phase in our experiments (*e.g.* 0.17 *versus* 0.24 s^{-1}). Possibly for similar reasons, this assay did not detect the effect of MacA on MacB solubilized in Triton X-100. However, they did find that MacB reconstituted into liposomes was characterized by a reduced k_{cat} (*e.g.* $k_{cat} = 0.10$ s^{-1}) and decreased affinity of MacB for ATP (*e.g.* $K_m = 2.30$ mM). Co-reconstitution of MacB with MacA had the effect of increasing both k_{cat} (*e.g.* $k_{cat} = 0.78$ s^{-1})

MacB Dimer Is Regulated by MacA

and the affinity of MacB for ATP (*e.g.* K_m = 0.38 mM). This behavior is similar to the effect of MacA on the steady-state kinetics of the ATPase activity of solubilized MacB in our study. To know if the reconstituted protein behaves in an identical manner to the solubilized protein would require the reconstitution of sufficient amounts of MacB to define any P_i burst, which is technically demanding. Consequently, although these earlier studies support our conclusion that MacA affects the ATPase activity of MacB, they do not give the detailed insight into the ATPase mechanism provided by our pre-steady-state analyses.

Our studies established that conformational changes can be propagated from the periplasmic domain of MacA to the cytoplasmic NBD of MacB (Figs. 1 and 2), and consequently, it is plausible that TolC, by interacting with MacA, can detect the nucleotide state of MacB. The binding of ATP to MacB would stimulate MacA to interact with TolC, inducing the latter to adopt the open state. Because ATP and MacA stabilize in the outward-facing conformation of MacB, drug transfer from MacB to TolC would be facilitated. TolC would then communicate with the NBD of MacB (again, such communication is probably conveyed via MacA) to stimulate ATP hydrolysis, which would be required to reset MacB in the inward-facing conformation. If ATP hydrolysis is controlled by TolC, so that the MacB conformation is only reset after the interaction with TolC and productive transfer of drugs, this would provide an explanation of the apparent insensitivity of the ATPase activity of MacB to drugs. Indeed, without such a feedback control mechanism of drug export, it would appear that drug stimulation of the ATPase activity of MacB would be counter-productive because the MacB conformation could be reset before drug transfer to TolC. There is an analogy in the mechanism of operation of ABC transporters that work in conjunction with a periplasmic binding protein (47). In the *E. coli* maltose transporter, the binding of ATP to the ATPase subunit MalK induces conformational changes, detected by tryptic digestion, in the periplasmic loops of the membrane subunits MalF and MalG (48), although EPR studies revealed that ATP binding, but not ADP binding, caused an increase in affinity between the transporter and the maltose-binding protein (MBP), and "forcing open" the bound MBP to release its substrate (49). The transporter is reset in its original inward-facing conformation by ATP hydrolysis, which is stimulated by the MBP (50). In our model TolC replaces the MBP and, because the open state requires disruption of the second selectivity filter and subsequent twisting of the helices of the TolC channel to keep it fully open, there is a need for the MacA hairpins to stabilize this conformation, which could not be achieved by interaction with MacB alone. Although we have interpreted our findings in terms of an alternating conformation model for MacB, in which the drug-binding sites are inwardly and outwardly exposed, such a model could easily be refined to account for drug binding to a fixed periplasmic site, in analogy to AcrB, with ATP binding and hydrolysis coupled to conformational changes that induce TolC association and dissociation. Clearly the work presented here provides an important framework for further studies that will enable the elucidation of the mechanism underlying the dynamics of assembly of the MacABTolC tripartite pump in the future.

REFERENCES

1. Borges-Walmsley, M. I., McKeegan, K. S., and Walmsley, A. R. (2003) *Biochem. J.* **376**, 313–338   AQ: C
2. Holland, I. B., Schmitt, L., and Young, J. (2005) *Mol. Membr. Biol.* **22**, 29–39
3. Kobayashi, N., Nishino, K., and Yamaguchi, A. (2001) *J. Bacteriol.* **183**, 5639–5644
4. Touze, T., Eswaran, J., Bokma, E., Koronakis, E., Hughes, C., and Koronakis, V. (2004) *Mol. Microbiol.* **53**, 697–706
5. Tikhonova, E. B., and Zgurskaya, H. I. (2004) *J. Biol. Chem.* **279**, 32116–32124
6. Murakami, S., Nakashima, R., Yamashita, E., and Yamaguchi, A. (2002) *Nature* **419**, 587–593
7. Yu, E. W., McDermott, G., Zgurskaya, H. I., Nikaido, H., and Koshland, D. E., Jr. (2003) *Science* **300**, 976–980
8. Mikolosko, J., Bobyk, K., Zgurskaya, H. I., and Ghosh, P. (2006) *Structure (Lond.)* **14**, 577–587
9. Koronakis, V., Sharff, A., Koronakis, E., Luisi, B., and Hughes, C. (2000) *Nature* **405**, 914–919
10. Tamura, N., Murakami, S., Oyama, Y., Ishiguro, M., and Yamaguchi, A. (2005) *Biochemistry* **44**, 11115–11121
11. Bavro, V. N., Pietras, Z., Furnham, N., Pérez-Cano, L., Fernández-Recio, Pei, X. Y., Misra, R., and Luisi, B. (2008) *Mol. Cell* **30**, 114–121
12. Lobedanz, S., Bokma, E., Symmons, M. F., Koronakis, E., Hughes, C., and Koronakis, V. (2007) *Proc. Natl. Acad. Sci. U. S. A.* **104**, 4612–4617
13. Elkins, C. A., and Nikaido, H. (2003) *J. Bacteriol.* **185**, 5349–5356
14. Federici, L., Du, D., Walas, F., Matsumura, H., Fernandez-Recio, J., McKeegan, K. S., Borges-Walmsley, M. I., Luisi, B. F., and Walmsley, A. R. (2005) *J. Biol. Chem.* **280**, 15307–15314
15. Andersen, C., Koronakis, E., Bokma, E., Eswaran, J., Humphreys, D., Hughes, C., and Koronakis, V. (2002) *Proc. Natl. Acad. Sci. U. S. A.* **99**, 11103–11108
16. Bokma, E., Koronakis, E., Lobedanz, S., Hughes, C., and Koronakis, V. (2006) *FEBS Lett.* **580**, 5339–5343
17. Vediyappan, G., Borisova, T., and Fralick, J. A. (2006) *J. Bacteriol.* **188**, 3757–3762
18. Murakami, S., Nakashima, R., Yamashita, E., Matsumoto, T., and Yamaguchi, A. (2006) *Nature* **443**, 173–179
19. Seeger, M. A., Schiefner, A., Eicher, T., Verrey, F., Diederichs, K., and Pos, K. M. (2006) *Science* **313**, 1295–1298
20. Sennhauser, G., Amstutz, P., Briand, C., Storchenegger, O., and Grutter, M. G. (2007) *PLoS Biol.* **5**, e7
21. Seeger, M. A., von Ballmoos, C., Eicher, T., Brandstätter, L., Verrey, F., Diederichs, K., and Pos, K. M. (2008) *Nat. Struct. Mol. Biol.* **15**, 199–205
22. Aires, J. R., and Nikaido, H. (2005) *J. Bacteriol.* **187**, 1923–1929
23. Kobayashi, N., Nishino, K., Hirata, T., and Yamaguchi, A. (2003) *FEBS Lett.* **546**, 241–246
24. Tikhonova, E. B., Devroy, V. K., Lau, S. Y., and Zgurskaya, H. I. (2007) *Mol. Microbiol.* **63**, 895–910
25. Reynolds, J. A., and Tanford, C. (1976) *Proc. Natl. Acad. Sci. U. S. A.* **73**, 4467–4470
26. Morita, Y., Kodama, K., Shiota, S., Mine, T., Kataoka, A., Mizushima, T., and Tsuchiya, T. (1998) *Antimicrob. Agents Chemother.* **42**, 1778–1782
27. Zgurskaya, H. I., and Nikaido, H. (1999) *J. Mol. Biol.* **285**, 409–420
28. Stroebel, D., Sendra, V., Cannella, D., Helbig, K., Nies, D. H., and Covès, J. (2007) *Biochim. Biophys. Acta* **1768**, 1567–1573
29. Heuberger, E. H., Veenhoff, L. M., Duurkens, R. H., Friesen, R. H., and Poolman, B. (2002) *J. Mol. Biol.* **317**, 591–600
30. Butler, P. J., Ubarretxena-Belandia, I., Warne, T., and Tate, C. G (2004) *J. Mol. Biol.* **340**, 797–808
31. Doerrler, W. T., and Raetz, C. R. (2002) *J. Biol. Chem.* **277**, 36697–36705

MacB Dimer Is Regulated by MacA

32. Ernst, R., Kueppers, P., Klein, C. M., Schwarzmueller, T., Kuchel, K., and Schmitt, L. (2008) *Proc. Natl. Acad. Sci. U. S. A.* **105,** 5069–5074
33. Bunikis, I., Denker, K., Ostberg, Y., Andersen, C., Benz, R., and Bergstrom, S. (2008) *PLoS Pathog.* **4,** e1000009
34. Sharon, M., and Robinson, C. V. (2007) *Annu. Rev. Biochem.* **76,** 167–193
35. Hanson, C. L., Ilag, L. L., Malo, J., Hatters, D. M., Howlett, G. J., and Robinson, C. V. (2003) *Biophys. J.* **85,** 3802–3812
36. Ilag, L. L., Ubarretxena-Belandia, I., Tate, C. G., and Robinson, C. V. (2004) *J. Am. Chem. Soc.* **126,** 14362–14363
37. Lengqvist, J., Svensson, R., Evergren, E., Morgenstern, R., and Griffiths, W. J. (2004) *J. Biol. Chem.* **279,** 13311–13316
38. Meier, T., Morgner, N., Matthies, D., Pogoryelov, D., Keis, S., Cook, G. M., Dimroth, P., and Brutschy, B. (2007) *Mol. Microbiol.* **65,** 1181–1192
39. Barrera, N. P., Di Bartolo, N., Booth, P. J., and Robinson, C. V. (2008) *Science* **321,** 243–246
40. Chen, J., Lu, G., Lin, J., Davidson, A. L., and Quiocho, F. A. (2003) *Mol. Cell* **12,** 651–661
41. Smith, P. C., Karpowich, N., Millen, L., Moody, J. E., Rosen, J., Thomas, P. J., and Hunt, J. F. (2002) *Mol. Cell* **10,** 139–149
42. Zaitseva, J., Oswald, C., Jumpertz, T., Jenewein, S., Wiedenmann, A., Holland, I. B., and Schmitt, L. (2006) *EMBO J.* **25,** 3432–3443
43. Dawson, R. J., and Locher, K. P. (2007) *FEBS Lett.* **581,** 935–938
44. Ward, A., Reyes, C. L., Yu, J., Roth, C. B., and Chang, G. (2007) *Proc. Natl. Acad. Sci. U. S. A.* **104,** 19005–19010
45. Dawson, R. J., Hollenstein, K., and Locher, K. P. (2007) *Mol. Microbiol.* **65,** 250–257
46. Lu, G., Westbrooks, J. M., Davidson, A. L., and Chen, J. (2005) *Proc. Natl. Acad. Sci. U. S. A.* **102,** 17969–17974
47. Oloo, E. O., Fung, E. Y., and Tieleman, D. P. (2006) *J. Biol. Chem.* **281,** 28397–28407
48. Daus, M. L., Landmesser, H., Schlosser, A., Muller, P., Herrmann, A., and Schneider, E. (2006) *J. Biol. Chem.* **281,** 3856–3865
49. Chen, J., Sharma, S., Quiocho, F. A., and Davidson, A. L. (2001) *Proc. Natl. Acad. Sci. U. S. A.* **98,** 1525–1530
50. Oldham, M. L., Khare, D., Quiocho, F. A., Davidson, A. L., and Chen, J. (2007) *Nature* **450,** 515–521